

**INVESTIGATION OF THE ROLE OF THE *LEISHMANIA MEXICANA* A600  
PROTEINS IN AMASTIGOTES DEVELOPMENT**

by

Maryvonne Rosamont-Ursulet

MSc, Henri Poincaré University, Nancy, 2004

A THESIS SUBMITTED IN PARTIAL FULFILLMENT OF  
THE REQUIREMENTS FOR THE DEGREE OF

DOCTOR OF PHILOSOPHY

in

THE FACULTY OF GRADUATE AND POSTDOCTORAL STUDIES  
(Microbiology and Immunology)

THE UNIVERSITY OF BRITISH COLUMBIA

(Vancouver)

August 2018

© Maryvonne Rosamont-Ursulet, 2018

The following individuals certify that they have read, and recommend to the Faculty of Graduate and Postdoctoral Studies for acceptance, the dissertation entitled:

Investigation of the role of the *Leishmania mexicana* A600 proteins in amastigotes development

---

submitted by Maryvonne Rosamont-Ursulet in partial fulfillment of the requirements

the degree of Doctor of Philosophy

in Microbiology and Immunology

---

**Examining Committee:**

Dr Robert McMaster

---

Supervisor

Dr Erin Gaynor

---

Supervisory Committee Member

Dr David Granville

---

University Examiner

Dr Wilfred Jefferies

---

University Examiner

**Additional Supervisory Committee Members:**

Dr Rachel Fernandez

---

Supervisory Committee Member

Dr Laura Sly

---

Supervisory Committee Member

## Abstract

Protozoan parasites of the genus *Leishmania* are responsible for the disease leishmaniasis, one of the major parasitic diseases in humans. The *Leishmania* life cycle alternates between promastigotes, present in the digestive tract of the sand fly, and amastigotes that reside in the phagolysosome of macrophages after transmission of the parasite to a mammalian host. Because the amastigote is the form under which the parasite can survive and multiply in the human host while evading the immune system and leading to the disease, *Leishmania* genes that are preferentially expressed in amastigotes have been investigated.

Previous studies in our laboratory identified a family of four tandemly linked genes in *L. mexicana*, the *A600* locus, which members show upregulation in amastigotes. Targeted gene deletion studies showed that these genes are essential for the successful replication of amastigotes. The aim of the present work was to elucidate the role of the A600 proteins, A600.1 and A600.4 in amastigotes development.

Western blot analysis of *L. mexicana* promastigotes and amastigotes found that the A600.1 protein was constitutively expressed throughout the parasite life cycle, and localized to the mitochondria of amastigotes. *A600*<sup>-/-</sup> amastigotes exhibited impaired mitochondrial functions, characterized by low cellular ATP levels and mitochondrial membrane potential in comparison to the wild type amastigotes. This correlated with a decrease in the activity of Complexes III and IV of the oxidative phosphorylation (OXPHOS) pathway, while Complexes II and V activities were not affected by the absence of the A600 proteins. This data suggest an involvement of the A600 proteins in the optimisation of the OXPHOS pathway function in amastigotes, either by

mediating interactions between Complexes III and IV or by contributing to the mitochondrial inner membrane architecture.

A GST protein-protein affinity chromatography technology and a co-immunoprecipitation approach were applied to isolate and identify potential A600.1 interacting proteins. The co-immunoprecipitation approach used was successful in immunoprecipitating the A600.1 protein and identified a number of potential interacting proteins. Due to variability between replicates, the data obtained was not conclusive as to whether A600.1 was part of a protein complex and what mitochondrial process it may be associated to.

## Lay Summary

*Leishmania* represent a genus of protozoan parasites that are transmitted to mammals by infected sand flies. The parasite is responsible for the disease leishmaniasis, a major public health issue in many tropical and subtropical regions of the world. There is an urgent need for new therapies as there is currently no effective vaccine available and the current drug treatments are often toxic, costly and becoming ineffective. The *A600* genes were previously found to be essential for the development of amastigotes, the form of the parasite present in mammals. The present study identified the A600.1 protein as a mitochondrial inner membrane protein and found the A600 proteins to be important for the maintenance of the mitochondrial function in amastigotes, via optimization of the respiration chain activity. These data confirm the importance of this pathway for the parasite development *in vivo*, making it an interesting target for novel drug therapies.

## **Preface**

### **Chapter 3**

For the work presented in Chapter 3, the research was designed by me with supervision by Dr Robert McMaster and in collaboration with Dr Anton Horvath. Dr Miriam Lynn performed the cloning of the *A600.1* gene into the pGEX-6P1 vector. The rest of the experiments and analysis of the data were conducted by me.

### **Chapter 4**

Part of the research presented in Chapter 4 was designed in collaboration with Dr Alexandra Marr and Dr Anton Horvath. Technical guidance was provided by Dr Anton Horvath and Dr Alena Zikova. I was responsible for the execution and analysis of the data, under the supervision of Dr Robert McMaster.

### **Chapter 5**

Experiments conducted in Chapter 5 were designed in collaboration with Dr Robert McMaster, Dr Miriam Lynn and Dr Charlotte Morrison. Cloning of the *ANA600.1* gene in the pGEX-6P1 vector was performed by Dr Miriam Lynn. Technical guidance was provided by Dr Leonard Foster and Jenny Moon. I performed all the experiments and all the mass spectrometry was conducted by Jenny Moon in Dr Leonard Foster laboratory. I realized the analysis and interpretation of the data under the guidance of Dr Robert McMaster and Dr Leonard Foster.

All animal work was conducted following protocols approved by University of British Columbia Animal Care Committee (Project #: A10-0222 and A12-0293, Gene Expression in

*Leishmania*) and under strict accordance with the guidelines from the Canadian Council for Animal Care. Cell culture work was performed following approval by the University of British Columbia Biosafety Committee (Certificate #: B12-0105, Studies in Molecular Parasitology).

# Table of Contents

<b>Abstract.....</b>	<b>iii</b>
<b>Lay Summary .....</b>	<b>v</b>
<b>Preface.....</b>	<b>vi</b>
<b>Table of Contents .....</b>	<b>viii</b>
<b>List of Tables .....</b>	<b>xiv</b>
<b>List of Figures.....</b>	<b>xv</b>
<b>List of Abbreviations .....</b>	<b>xix</b>
<b>Acknowledgements .....</b>	<b>xxiii</b>
<b>Dedication .....</b>	<b>xxiv</b>
<b>Chapter 1: Introduction .....</b>	<b>1</b>
1.1    The parasite <i>Leishmania</i> and leishmaniasis .....	1
1.1.1    Taxonomy .....	1
1.1.2    Clinical forms of the disease.....	2
1.1.3    Global impact.....	3
1.1.4    Current therapies against leishmaniasis .....	4
1.1.5 <i>Leishmania</i> life cycle .....	9
1.2 <i>Leishmania</i> metabolism .....	12
1.2.1    Carbohydrate metabolism .....	15
1.2.2    The pentose phosphate pathway .....	17
1.2.3    Amino acid metabolism .....	18
1.2.4    Fatty acid metabolism .....	20

1.2.5	The tricarboxylic acid (TCA) cycle .....	21
1.2.6	The electron transport chain.....	23
1.2.7	Mitochondrial ATP metabolism .....	25
1.3	<i>Leishmania</i> gene and protein expression throughout the life cycle .....	26
1.3.1	<i>Leishmania</i> experiences profound changes throughout its life cycle .....	26
1.3.2	<i>Leishmania</i> gene expression .....	26
1.3.3	Variation of gene expression during <i>Leishmania</i> development.....	27
1.3.4	Biological function of the stage-specific proteins .....	29
1.3.5	Mechanisms involved in developmental gene regulation.....	30
1.4	Genomic analysis in <i>Leishmania</i> .....	33
1.4.1	Comparative genomic analysis .....	33
1.4.2	Analysis of <i>Leishmania</i> gene function.....	37
1.5	The <i>L. mexicana</i> A600 gene family .....	39
1.6	Thesis hypothesis and specific aims .....	44
1.6.1	Objective 1 .....	45
1.6.2	Objective 2 .....	45
1.6.3	Objective 3 .....	45
<b>Chapter 2: Material and methods .....</b>		<b>47</b>
2.1	<i>Leishmania</i> strains .....	47
2.2	<i>Leishmania</i> culture.....	47
2.3	Isolation of <i>L. mexicana</i> genomic DNA .....	47
2.4	Cloning of the A600.1 and A600.4 genes into the pGEX vector .....	48
2.4.1	Polymerase Chain Reaction amplification of the A600 genes .....	48

2.4.2	Insertion of the <i>A600</i> ORFs in the pGEX vector .....	50
2.5	Purification of the GST fusion proteins .....	52
2.5.1	Production of the GST fusion proteins .....	52
2.5.2	Purification of the GST tagged proteins .....	54
2.5.3	Purification of the recombinant A600.1 and A600.4 proteins .....	54
2.6	Generation of polyclonal antibodies .....	55
2.6.1	Generation of anti-A600.1 antibodies.....	55
2.6.2	Generation of an anti-A600.4 antibody .....	55
2.7	ELISA .....	56
2.8	Western Blot .....	57
2.8.1	Preparation of bacterial samples .....	57
2.8.2	Preparation of <i>Leishmania</i> whole cell lysates.....	58
2.8.3	SDS-PAGE .....	58
2.8.4	Immunodetection .....	58
2.9	Differential digitonin permeabilization.....	60
2.10	Measurement of cellular ATP content .....	61
2.11	Assessment of the mitochondrial redox activity.....	62
2.12	Measurement of the mitochondrial membrane potential .....	62
2.13	Native PAGE .....	63
2.13.1	Isolation of crude organellar fractions .....	63
2.13.2	Lysis of the organellar fractions .....	64
2.13.3	Electrophoresis.....	65
2.13.4	Blue-silver gel staining .....	66

2.13.5 In-gel activity staining .....	66
2.13.6 Western blot .....	67
2.14 Measurement of the enzymatic activities of the mitochondrial oxidative phosphorylation complexes .....	68
2.15 Statistical analysis .....	72
2.16 GST pull-down assay .....	72
2.16.1 Isolation of amastigotes mitochondria-enriched fractions .....	72
2.16.2 Pull-down .....	73
2.17 Co-immunoprecipitation .....	74
2.17.1 Antibody-coupling to magnetic beads .....	74
2.17.2 Preparation of whole cell lysate .....	75
2.17.3 Proteins pull-down .....	75
2.18 Mass spectrometry analysis .....	76

**Chapter 3: The A600.1 protein is expressed in both promastigotes and amastigotes and**

**localized to the mitochondria of amastigotes..... 78**

3.1 Introduction .....	78
3.2 Results .....	80
3.2.1 Production of recombinant A600.1 and A600.4 proteins .....	80
3.2.2 Characterization of the anti-A600.1 antibodies .....	84
3.2.3 Characterization of the anti-A600.4 antibody .....	94
3.2.4 Characterization of the A600.1 protein expression profile during the <i>L. mexicana</i> life cycle .....	99
3.2.5 Subcellular localization of the endogenous A600.1 protein in amastigotes .....	101

3.2.6	Summary of bioinformatic analysis of the <i>L. mexicana</i> A600.1 and A600.4 proteins.....	104
3.3	Discussion.....	110
<b>Chapter 4: The A600 genes and the <i>Leishmania</i> mitochondrial metabolism .....</b>		<b>115</b>
4.1	Introduction.....	115
4.2	Results.....	116
4.2.1	Measurement of the ATP levels in <i>L mexicana</i> WT and A600 <sup>-/-</sup> amastigotes.....	116
4.2.2	Comparison of the mitochondrial redox activity of <i>L. mexicana</i> WT and A600 <sup>-/-</sup> amastigotes.....	118
4.2.3	Comparison of the mitochondrial membrane potential $\Delta\Psi_m$ in <i>L mexicana</i> WT and A600 <sup>-/-</sup> amastigotes.....	119
4.2.4	Native PAGE analysis of the mitochondrial OXPHOS complexes in <i>L mexicana</i> WT and A600 <sup>-/-</sup> amastigotes .....	122
4.2.5	Comparison of the enzymatic activities of the mitochondrial OXPHOS complexes in <i>L. mexicana</i> WT and A600 <sup>-/-</sup> amastigotes.....	134
4.3	Discussion.....	145
<b>Chapter 5: Investigation of the potential A600.1 interacting proteins .....</b>		<b>154</b>
5.1	Introduction.....	154
5.2	Results.....	155
5.2.1	Investigation of the A600.1 binding partners by native PAGE .....	155
5.2.2	Identification of the A600.1 binding partners by GST pull-down.....	167
5.2.3	Identification of A600.1 binding partners by co-immunoprecipitation .....	184
5.2.4	Summary regarding the identification of potential A600.1 interacting proteins	197

5.3	Discussion .....	199
<b>Chapter 6: Conclusion .....</b>		<b>205</b>
6.1	Overall analysis and conclusion of the research .....	205
6.2	Contribution to the field.....	207
6.3	Strengths and limitations of the research .....	209
6.4	Possible future directions .....	210
6.4.1	Identification of the A600-associated mitochondrial pathway .....	210
6.4.2	Characterization of the A600.4 protein function .....	211
6.4.3	Analysis and comparison of the subunit composition of the OXPHOS complexes of <i>Leishmania</i> amastigotes and promastigotes .....	212
<b>References .....</b>		<b>214</b>
<b>Appendices.....</b>		<b>238</b>
	Appendix A Nucleotide coding sequence of the <i>A600</i> genes .....	238
	Appendix B Comparison of the enzymatic activities of <i>L. mexicana</i> WT and <i>A600</i> <sup>-/-</sup> amastigotes .....	239
	Appendix C Mass spectrometry results of the GST pull-down assays .....	243

## List of Tables

Table 2.1: List of primary antibodies used for Western blot analysis after SDS-PAGE.....	60
Table 2.2: List of primary antibodies used for Western blot after native PAGE separation of mitochondrial proteins. ....	68
Table 4.1: Enzymatic activities of the mitochondrial electron transport chain complexes. ....	145
Table 5.1: List of proteins identified by MS from the 300 kDa native PAGE band detected by Western blot with the anti-A600.1 antibody.....	166
Table 5.2: List of potential $\Delta$ N.A600.1 interacting partners.....	180
Table 5.3: List of potential contaminants .....	182
Table 5.4: List of potential A600.1 binding partners identified by co-IP.....	194
Table 5.5: List of proteins identified in second co-IP.....	196
Table 5.6: List of proteins identified in the GST pull-downs and co-IP assays .....	197
Table C.1: List of proteins isolated from GST pull-down assay 1 with a heavy to light ratio above 1.2.....	243
Table C.2: List of proteins identified in GST pull-down assay 2 with a H/L ratio above 1.2....	244
Table C.3: List of proteins identified in GST pull-down assay 3 with a H/L ratio above 1.2...	248

## List of Figures

Figure 1.1: Clinical manifestations of leishmaniasis. ....	3
Figure 1.2: The <i>Leishmania</i> life cycle. ....	12
Figure 1.3: Overview of carbon metabolism in <i>Leishmania</i> . ....	14
Figure 1.4: Map of the <i>A600</i> locus. ....	41
Figure 1.5: Alignment of the four <i>L. mexicana</i> <i>A600</i> predicted protein sequences. ....	41
Figure 1.6: Predicted membrane topology of the <i>L. mexicana</i> <i>A600.1</i> and <i>A600.4</i> proteins. ....	42
Figure 2.1: Map of the glutathione S-transferase fusion vector, pGEX-6P-1. ....	51
Figure 2.2: Alignment of the <i>L. mexicana</i> <i>A600.1</i> and <i>A600.4</i> protein sequences. ....	56
Figure 3.1: Production and purification of the <i>A600.1</i> and <i>A600.4</i> proteins from BL21(de3) <i>E. coli</i> clones transformed with the pGEX vector containing the <i>A600.1</i> gene (BL21+pGST- <i>A600.1</i> ) or the <i>A600.4</i> gene (BL21+pGST- <i>A600.4</i> ) respectively. ....	84
Figure 3.2: ELISA analysis of the GenScript anti- <i>A600.1</i> antibodies 1 and 2 specificity for the recombinant <i>A600.1</i> protein. ....	87
Figure 3.3: Western Blot analysis of the GenScript anti- <i>A600.1</i> antibodies 1 and 2 specificity for the recombinant <i>A600.1</i> protein. ....	89
Figure 3.4: Western Blot analysis of the GenScript anti- <i>A600.1</i> antibodies 1 and 2 specificity for the endogenous <i>L. mexicana</i> <i>A600.1</i> protein. ....	91
Figure 3.5: Western Blot testing of the GenScript anti- <i>A600.1</i> antibody 1 specificity for the endogenous <i>L. mexicana</i> <i>A600.1</i> protein. ....	93
Figure 3.6: ELISA analysis of the GenScript anti- <i>A600.4</i> antibody specificity for the <i>A600.4</i> protein. ....	95

Figure 3.7: Western Blot analysis of the GenScript anti-A600.4 antibody specificity for the recombinant A600.4 protein produced from <i>E. coli</i> clones.....	96
Figure 3.8: Western Blot analysis of the GenScript anti-A600.4 antibody specificity for the <i>L. mexicana</i> endogenous A600.4 protein.....	98
Figure 3.9: Western Blot analysis of the A600.1 protein expression profile in <i>L. mexicana</i> WT and <i>A600<sup>-/-</sup></i> promastigotes and amastigotes. ....	101
Figure 3.10: Western Blot analysis of supernatants of <i>L. mexicana</i> WT amastigotes lysates after digitonin titration. ....	104
Figure 3.11: Diagram representation of the <i>L. mexicana</i> A600.1 (a) and A600.4 (b) protein secondary structures as determined by the PSIPRED program. ....	106
Figure 3.12: Graphic representation of the topology of the <i>L. mexicana</i> A600.1 (a) and A600.4 (b) proteins as predicted by the PHOBIUS program. ....	108
Figure 3.13: Graphic representation of the intrinsic disorder profile of the <i>L. mexicana</i> A600.1 (a) and A600.4 (b) proteins as predicted by the DISOPRED program.....	110
Figure 4.1: Measurement of ATP concentrations in <i>L. mexicana</i> WT and <i>A600<sup>-/-</sup></i> amastigotes. ....	117
Figure 4.2: Measurement of the mitochondrial redox activity in <i>L. mexicana</i> WT and <i>A600<sup>-/-</sup></i> amastigotes.....	119
Figure 4.3: Diagram of the mitochondrial OXPHOS complexes. ....	120
Figure 4.4: Measurement of mitochondrial membrane potential $\Delta\Psi_m$ in <i>L mexicana</i> WT and <i>A600<sup>-/-</sup></i> amastigotes. ....	122
Figure 4.5: Blue-native PAGE analysis of <i>L. mexicana</i> WT promastigote mitochondrial membrane complexes.....	125

Figure 4.6: High resolution clear native PAGE analysis of <i>L. mexicana</i> WT promastigote mitochondrial OXPHOS complexes. ....	127
Figure 4.7: High resolution clear native PAGE analysis of <i>L. mexicana</i> WT amastigote mitochondrial complexes. ....	129
Figure 4.8: High resolution clear native PAGE analysis of <i>L mexicana</i> WT and <i>A600<sup>-/-</sup></i> amastigote mitochondrial OXPHOS complexes. ....	133
Figure 4.9: Analysis of Complex I NADH dehydrogenase activity in <i>L. mexicana</i> WT and <i>A600<sup>-/-</sup></i> amastigotes. ....	136
Figure 4.10: Analysis of the Complex II succinate dehydrogenase activity in <i>L. mexicana</i> WT and <i>A600<sup>-/-</sup></i> amastigotes. ....	138
Figure 4.11: Analysis of the Complex III cytochrome c reductase activity in <i>L. mexicana</i> WT and <i>A600<sup>-/-</sup></i> amastigotes. ....	140
Figure 4.12: Analysis of Complex IV cytochrome c oxidase activity in <i>L. mexicana</i> WT and <i>A600<sup>-/-</sup></i> amastigotes. ....	142
Figure 4.13: Analysis of Complex V ATPase activity assay in <i>L mexicana</i> WT and <i>A600<sup>-/-</sup></i> amastigotes. ....	144
Figure 5.1: Western blot analysis of SDS-PAGE of <i>L. mexicana</i> WT promastigotes and amastigotes fractions after hypotonic cell lysis and mitochondrial digitonin lysis. ....	157
Figure 5.2: Western blot detection of A600.1 in the <i>L. mexicana</i> WT promastigotes and amastigotes fractions isolated in presence of protease inhibitors. ....	158
Figure 5.3: High resolution clear native PAGE of <i>L. mexicana</i> WT amastigotes mitochondrial membrane complexes isolated in presence of protease inhibitors. ....	160

Figure 5.4: Western blot analysis after high resolution clear native PAGE of <i>L. mexicana</i> WT amastigotes organellar lysates isolated in presence of protease inhibitors. ....	161
Figure 5.5: High resolution clear native PAGE analysis of <i>L. mexicana</i> WT amastigotes organellar lysate. ....	162
Figure 5.6: Western blot analysis of <i>L. mexicana</i> WT amastigotes whole cell lysates obtained by hypotonic lysis in presence of different combination of protease inhibitors. ....	164
Figure 5.7: Western blot analysis of GST-ΔN.A600.1-bound Glutathione Sepharose 4B beads after incubation with 8 U of PreScission Protease. ....	170
Figure 5.8: Western blot analysis of GST-ΔN.A600.1-bound Glutathione Sepharose 4B beads after incubation with different amounts of PreScission Protease. ....	172
Figure 5.9: Western blot analysis of GST-ΔN.A600.1-bound Glutathione Sepharose 4B beads after incubation with 16 U of PreScission Protease. ....	176
Figure 5.10: Western Blot analysis of <i>L. mexicana</i> WT amastigotes digitonin fractions. ....	178
Figure 5.11: Western blot detection of the A600.1 protein in <i>L. mexicana</i> WT amastigotes fractions after lysis with RIPA or IP buffer. ....	185
Figure 5.12: Western blot analysis of <i>L. mexicana</i> WT and A600 <sup>-/-</sup> amastigotes samples before and after incubation with the anti-A600.1-coupled magnetic beads. ....	187
Figure 5.13: Western blot analysis of washes of the anti-A600.1 antibody-coupled beads. ....	190
Figure 5.14: Western blot analysis of <i>L. mexicana</i> WT and A600 <sup>-/-</sup> amastigotes samples after immunoprecipitation with the anti-A600.1 antibody coupled to magnetic beads and elution. ..	192
Figure 5.15: Blue silver staining of SDS-PAGE of co-immunoprecipitated proteins from 45 x 10 <sup>9</sup> <i>L. mexicana</i> WT and A600 <sup>-/-</sup> amastigotes lysates. ....	195
Figure 6.1: Schematic summarizing the possible functions of A600.1. ....	207

## List of Abbreviations

ADP	adenosine diphosphate
AMP	antimicrobial peptide
APRT	adenine phosphoribosyltransferase
ASCT	acetate: succinate CoA transferase / succinyl-CoA synthetase cycle
ATP	adenosine triphosphate
BCA	bicinchoninic acid
BiP	binding protein
BSA	bovine serum albumin
Cas9	CRISPR-associated gene 9
CRISPR	clustered regularly interspaced short palindromic repeat
Cyt c	cytochrome c
DAB	diamino benzidine
DCPIP	2,6-dichlorophenolindophenol
DDM	dodecyl maltoside
DNA	deoxyribonucleic acid
DSB	double stranded DNA break
DTT	dithiothreitol
E-64	<i>trans</i> -Epoxy succinyl-L-leucylamido(4-guanidino)butane
<i>E. coli</i>	<i>Escherichia coli</i>
EDTA	ethylenediaminetetraacetic acid
FCCP	carbonyl cyanide-4-(trifluoromethoxy)phenylhydrazone

FDA	food and drug administration
GFP	green fluorescent protein
gGAPDH	glycosomal glyceraldehyde 3-phosphate dehydrogenase
GSF	glycosomal succinate fermentation
GST	glutathione S-transferase
GTP	guanosine 5'-triphosphate
HGPRT	hypoxanthine-guanine phosphoribosyltransferase
hrCN-PAGE	high resolution clear native PAGE
ID	identity
IgG	immunoglobulin
IPTG	isopropyl $\beta$ -D-1-thiogalactopyranoside
iTRAQ	isobaric tagging for relative and absolute quantifications
KCN	potassium cyanide
kDa	kilodaltons
<i>L. mexicana</i>	<i>Leishmania mexicana</i>
<i>LmX</i>	<i>Leishmania mexicana</i>
LB	Luria-Bertani
M	molar
mg	milligram
mM	millimolar
mtHSP70	mitochondrial heat-shock protein 70
NADH	$\beta$ -nicotinamide adenine dinucleotide
NADPH	nicotinamide adenine dinucleotide phosphate

NaCl	sodium chloride
NH <sub>4</sub> HCO <sub>3</sub>	ammonium bicarbonate
NBT	nitrotetrazolium blue
ORF	open reading frame
OXPHOS	oxidative phosphorylation
PAGE	polyacrylamide gel electrophoresis
PBS	phosphate-buffered saline
PCR	polymerase chain reaction
PMS	phenazine methosulfate
PMSF	phenylmethylsulfonyl fluoride
PVDF	polyvinylidene fluoride
RNA	ribonucleic acid
RNAi	RNA interference
SCoAS	succinyl-CoA synthetase
SDS	sodium dodecyl Sulfate
SOC	super optimal broth
TBS	tris buffered saline
TBS-T	tris buffered saline with 0.1% Tween-20
<i>T. brucei</i>	<i>Trypanosoma brucei</i>
TCA	tricarboxylic acid
TMB	3,3',5,5'-tetramethylbenzidine
TMRM	tetramethylrhodamine methyl ester
WT	wild-type

U            unit  
UTR        untranslated region

## Acknowledgements

I would like to thank my supervisor, Dr Robert McMaster for welcoming me in his lab and for his support and guidance throughout these years. One of my aims in starting this PhD was to specialize in the research on neglected tropical diseases and under his supervision, I have developed a passion for the field.

I also wish to thank the members of my supervisory committee, Dr Rachel Fernandez, Dr Laura Sly and Dr Erin Gaynor, for their time and their valuable input regarding my research.

My immense gratitude goes to Dr Alena Zikova and Dr Anton Horvath for their guidance and tremendous help and advice. To Dr Leonard Foster and Jenny Moon, thank you for your help and guidance and for answering my constant mass spectrometry questions. A special thank you goes to Darlene Birkenhead for her constant encouragement and support.

I would also like to thank the past and present members of the McMaster lab: Dr Miriam Lynn, Dr Eva Horakova, Dr Alexandra Marr, Dr Charlotte Morrison, Adriana Airo, Sarah Kam.

To my friends, Stephanie, Doris, Lucia, Peter, Sneha, Jenn, Solace, Veronica, Mary-Jane and David, with you I learned the meaning of “if you want to go far, go together”. Thank you for your continuous support throughout those years, I wouldn’t have made it without your encouragements.

Finally, I would like to thank my parents and my sister for their love and support, for continuously encouraging me in the pursuit of my dreams and for inspiring the adventurous side in me.

**Dedication**

***A mes parents,***

***Ginette et Alfassa***

***Et à la mémoire de mon oncle,***

***Dr Octave Céry***

# Chapter 1: Introduction

## 1.1 The parasite *Leishmania* and leishmaniasis

*Leishmania* is a genus of protozoan parasites responsible for the disease leishmaniasis. This parasite is transmitted to humans and other mammals during a blood meal by infected female sand flies.

### 1.1.1 Taxonomy

Parasites of the *Leishmania* genus belong to the order of *Kinetoplastida* and the family of *Trypanosomatidae*. The Kinetoplastids are characterized by a unique DNA-containing structure, the kinetoplast, which is associated with the flagellar basal body in the single mitochondrion. Other characteristics of the order include the editing of mitochondrial precursor mRNAs into functional and translatable mRNAs, the absence of tRNAs encoded by the mitochondrial DNA - which requires the import of tRNAs from the cytosol for mitochondrial protein synthesis - and the compartmentalization of most of the glycolytic enzymes into a specialized organelle called the glycosome (Simpson et al, 2006). The Trypanosomatidae family includes parasites of vertebrates, invertebrates and plants and constitutes the most studied Kinetoplastid group. This group comprises parasites of medical and veterinary importance, such as *Trypanosoma brucei*, which is responsible for human African trypanosomiasis (also known as sleeping sickness) and transmitted by tsetse flies; *Trypanosoma cruzi*, the causative agent of American trypanosomiasis or Chagas disease, transmitted by triatomine bugs (commonly known as “kissing bugs”) and the *Leishmania* species, transmitted by sand flies. Approximately 21 species of the *Leishmania* genus are pathogenic to humans (Jhingran et al, 2008).

### 1.1.2 Clinical forms of the disease

The leishmaniasis constitute a group of diseases which range in severity, from causing a cutaneous lesion through disfiguration to death. There are three major forms of leishmaniasis in humans, depending on the species of the parasite and on the immune response of the host (Figure 1.1). In the cutaneous form, which is the most common form of the disease, a skin lesion develops at the site of the sand fly bite, starting as a papule that often evolves into an ulcer. The lesion generally self-heals after several months, leaving atrophic scars. This disease is usually caused in the Old World by *L. major*, *L. tropica* and *L. aethiopica* and in the New World by the *L. mexicana* complex and the *L. Vianna* subgenus (Reithinger et al, 2007). In the mucocutaneous form, the parasite metastasizes via haematogenous or lymphatic dissemination, from the skin to the mucous membrane of the naso-oropharyngeal region leading to its destruction and severe disfiguration. This form of the disease is usually the result of infection by *L. amazonensis* and species of the *Viannia* subgenus, such as *L. braziliensis*, *L. guyanensis*, *L. panamensis* (Handler et al, 2015). Visceral leishmaniasis, commonly referred to as kala-azar in the Old World, is the most serious form and is often fatal if left untreated. In this disease, the parasite migrates to the internal organs, such as the liver, the spleen or the bone marrow, resulting in hepatosplenomegaly, bouts of fever, substantial weight loss and pancytopenia. It is caused by *L. donovani*, *L. infantum* in the Old World and *L. chagasi* in the New World (Jhingran et al, 2008).

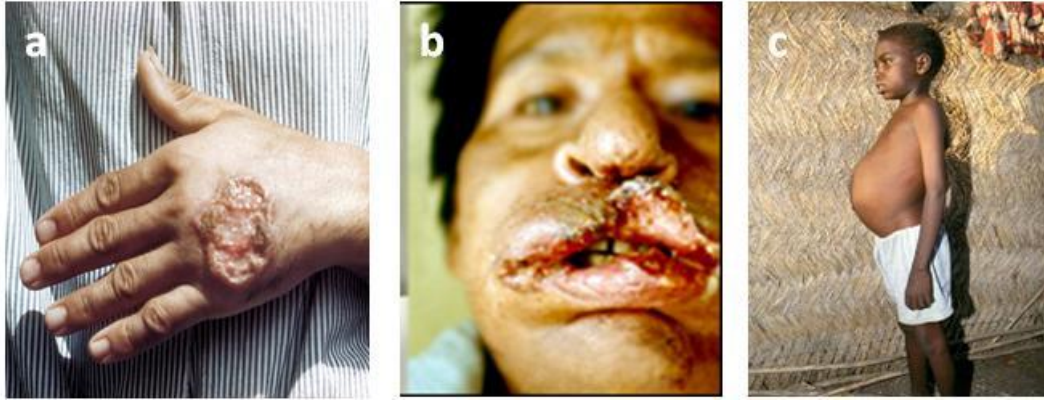


**Figure 1.1: Clinical manifestations of leishmaniasis.**

a) Cutaneous leishmaniasis lesion. Retrieved 7 August 2018 from [https://commons.wikimedia.org/w/index.php?title=File:Skin\\_ulcer\\_due\\_to\\_leishmaniasis,\\_hand\\_of\\_Central\\_American\\_adult\\_3MG0037\\_lores.jpg&oldid=151784631](https://commons.wikimedia.org/w/index.php?title=File:Skin_ulcer_due_to_leishmaniasis,_hand_of_Central_American_adult_3MG0037_lores.jpg&oldid=151784631). b) Mucocutaneous leishmaniasis. Retrieved 7 August 2018, from [http://www.who.int/neglected\\_diseases/integrated\\_media\\_leishmaniasis/en/](http://www.who.int/neglected_diseases/integrated_media_leishmaniasis/en/). c) Child with visceral leishmaniasis, characterized by an enlarged abdomen due to swollen liver and spleen (Retrieved 7 August 2018, 2018, from <http://www.who.int/tdr/news/2016/visceral-leishmaniasis-research/en/>).

### 1.1.3 Global impact

Leishmaniasis represent the second largest cause of deaths due to parasitic infection in the world, after malaria (WHO, 2010) and in terms of disease burden, is considered one of the most important neglected tropical diseases in the world (Alvar et al, 2012; Hotez et al, 2006). It is present in 98 predominantly developing countries on four continents, mainly in the tropical and subtropical regions of the world and Southern Europe, and affects about 12 million people worldwide. It is estimated that approximately 1.3 million new cases occur each year, among which 300,000 are of the visceral form (over 90% of them being in Bangladesh, Brazil, Ethiopia, India, Nepal, Sudan and South Sudan) and 1 million are of the cutaneous (mostly in Afghanistan, Algeria, Brazil, Colombia, Iran, Pakistan, Peru, Saudi Arabia, Syria and Tunisia) or mucocutaneous form (mainly in Brazil, Peru and Bolivia). The number of deaths attributable to visceral leishmaniasis annually ranges between 20,000 to 40,000 (Alvar et al, 2012). However,

those numbers are likely to be an underestimation of the true incidence of the diseases. Data related to the number of deaths generally account for hospital-based deaths only, with a significant proportion of cases going unreported as they may occur outside of health facilities or because the disease was not recognized. Furthermore, notification of cases is mandatory in only 34% of endemic countries and many patients may be misdiagnosed or undiagnosed due to the absence of symptoms or to a lack of access to health facilities (Desjeux, 2004). In recent years, a series of factors, such as co-infection with *Leishmania* and HIV, movements of populations, notably close to vector-breeding sites, and the deterioration of the socio-economic conditions, have contributed to the spread of the disease (Aagaard-Hansen et al, 2010; Desjeux, 2004; WHO, 2015).

Leishmaniasis represents a major public health problem in developing countries where, in addition to the cost in human lives, it also constitutes an enormous economic burden. In endemic regions, this disease causes significant loss in the labour force, which negatively impacts the overall economic development of a region. Moreover, the disease predominantly affects people of the lowest socio-economic category of society who are unable to afford treatment, thus sustaining a vicious circle of disease and poverty (Desjeux, 2004; Meheus et al, 2006; Rijal et al, 2006).

#### **1.1.4 Current therapies against leishmaniasis**

##### ***1.1.4.1 Current treatments***

In the absence of an effective vaccine, drug therapies constitute the main method for control of leishmaniasis. There is a great need for novel therapies for the treatment of the disease. The number of drugs currently in use is limited and they present significant disadvantages associated to their toxicity, the long duration of treatment which often leads to

patient poor adherence, their cost and their increasing inefficacy due to the development of drug resistance.

Pentavalent antimonials have been the standard first-line of treatment for all leishmaniasis for the past six decades. Two of them are currently in use: sodium stibogluconate and meglumine antimoniate. They are administered intramuscularly or intravenously for visceral leishmaniasis treatment, or intralesionally in the case of cutaneous leishmaniasis (WHO, 2010). Although easily available and low in cost, the long duration of treatment (daily for 28 to 30 days) often results in patients abandoning treatment before completion, contributing to the emergence of parasite strains resistant to those drugs (>65% in Bihar, India) (de Menezes et al, 2015). The serious side effects of those drugs require close monitoring of the patients and their efficacy is variable (30-95% depending on the geographical region).

For patients that do not respond to pentavalent antimonials treatment, amphotericin B and pentamidine are used as second-line therapies. Amphotericin B was first isolated from *Streptomyces nodosus* in 1953 and was originally developed against fungal infections (Gallis et al, 1990). It was introduced as a leishmanicidal drug in the 1960s (Ponte-Sucre et al, 2017). It is administered intravenously. Although it is more efficacious than the pentavalent antimonials, its high toxicity has limited its use for treatment. It is the treatment of choice against visceral leishmaniasis in India where the prevalence of resistance to pentavalent antimonials is high. New formulations of amphotericin B, such as liposomal amphotericin B, amphotericin B colloidal dispersion and amphotericin B lipid complex, have been developed to improve its pharmacokinetics and decrease its toxicity by improving its delivery to the target cells (macrophages) while maintaining the compound efficacy (Berman, 1997). Liposomal amphotericin B is currently the most efficacious of the antileishmanial drugs. It is also less toxic

than the conventional amphotericin B deoxycholate or the amphotericin B lipid complex and reduces the length of treatment (from 30-40 days with amphotericin B deoxycholate to 3-5 days or a single dose) (Singh et al, 2016). However, its use as first-line of treatment is hampered by its high cost and its instability at temperatures above 25°C (de Menezes et al, 2015; Meheus et al, 2010).

Due to its serious toxicity and its lower efficacy in comparison to amphoterin B, pentamidine is only used in combination therapies or in cases where it is proved to be less toxic, involving fewer injections or be as effective as pentavalent antimonials. It is mainly used for specific forms of cutaneous leishmaniasis in South America (Croft & Olliaro, 2011; Jha & Sharma, 1984).

Paromomycin is an antibiotic that was originally isolated from *Streptomyces krestomuceticus*. It was first tested in humans against visceral leishmaniasis in the 1980s (Singh et al, 2016). It is administered intramuscularly for the treatment of visceral leishmaniasis or topically for cutaneous leishmaniasis. Although highly efficacious for the treatment of visceral leishmaniasis in India, it is less so in East Africa. It is inexpensive but reversible ototoxicity and nephrotoxicity have been reported, along with occasional hepatotoxicity (Croft & Olliaro, 2011; de Menezes et al, 2015).

Miltefosine was originally developed as an anti-cancer drug (Sundar & Olliaro, 2007). In 2014, it was approved by the US FDA, under the name Impavido, as an oral treatment against visceral, cutaneous and muco-cutaneous leishmaniasis (Yao, 2014). It is the first and only oral leishmanicidal drug currently available. Its adverse effects are mainly gastrointestinal but its teratogenic effect in rats makes it a contraindication in pregnant women (Sundar & Olliaro, 2007). The other disadvantages of this drug are the duration of treatment (28 days) which can

lead to poor patient adherence and its long half-life (7 days) which increases the risk of drug resistance (Singh et al, 2016).

Due largely to the serious side effects of the current drugs and the development of drug resistance, new and safer therapies are needed. Examples of new treatment approaches include combination therapies. The advantage of such approach is that it shortens the duration of treatment improving patients compliance, reduces the cost of treatment and toxicity as lower doses of the drugs are used and it delays the development of drug resistance (Kimutai et al, 2017; Meheus et al, 2010; WHO, 2010).

Another alternative approach to improve drug efficacy is the use of drug-delivery systems, in which the drug is attached to the surface or encapsulated in a carrier, such as liposomes, nanoparticles or carbon nanotubes for delivery to the targeted tissue or cells. Targeting of the drug delivery may be passive (such as relying on the leakage of the vasculature at the diseased site) or it may be achieved through the presence at the surface of the nanocarrier of ligands specific to receptors at the targeted site or at the surface of the targeted cells (Jain et al, 2013). Such system presents several benefits: a decrease of the risk of toxicity associated with the drug off-target effects, an extension of the drug half-life by providing protection from potential degradation during transit to the targeted site, a control of the drug release, a reduction of the drug therapeutic dose. Different delivery systems for amphotericin B are being developed for the treatment of visceral leishmaniasis (Nahar et al, 2010; Prajapati et al, 2011; Pruthi et al, 2012; Ribeiro et al, 2014; Sánchez-Brunete et al, 2004; Wasan et al, 2010).

Another strategy in the development of leishmanicidal treatments is the use of antimicrobial peptides (AMPs). AMPs are cationic amphiphilic peptides that are part of the innate immune system and are found in virtually all organisms ranging from bacteria, fungi,

plants to invertebrates and vertebrates, including humans (Bulet et al, 2004). They are relatively short, generally between 12 and 50 amino-acid long, have an overall positive charge and a significant proportion of hydrophobic residues. They, or their synthetic analogs, have been considered as potential novel therapies due to their potent activities against bacteria, enveloped viruses, fungi and sometimes cancerous cells. Their mode of actions can be direct, via disruption of the plasmic membrane or interactions with intracellular targets, or indirect via modulation of the host immune system (chemoattraction of immune cells, modulation of gene expression, induction of chemokines) (Hancock & Sahl, 2006; Marr et al, 2012). Some AMPs have been shown to exhibit leishmanicidal activities *in vitro* (Dabirian et al, 2013; do Nascimento et al, 2015; Marr et al, 2016; Marr et al, 2012) and *in vivo* (Alberola et al, 2004; Kulkarni et al, 2011).

The development of new effective drugs against leishmaniasis also encompasses the identification of new drug targets in the parasite and/or in the host. As research regarding the biology of intracellular amastigotes progresses and the mechanisms that allow the parasite to evade killing by the host immune system are better understood, new potential drug targets are being identified. Of particular interest are proteins or cellular pathways that are trypanosomatid-specific or differ significantly from their mammalian homologs, as drugs targeted to those are less likely to find a target in the mammalian host (Chen et al, 2001; Singh et al, 2012). One example of such potential targets is the acetate:succinate CoA transferase (ASCT) / succinyl CoA synthetase cycle (or ASCT cycle), which has only been identified in trypanosomatids, some parasitic helminths and in the hydrogenosome of trichomonads and some fungi (Van Hellemond et al, 1998).

Another approach involves the use of high-throughput screening (HTS), which consists in testing the anti-leishmanial activities of large libraries of chemically diverse compounds in an

automated setting. This method has proven to be effective for the discovery of new leishmanicidal chemotypes (Nühs et al, 2015; Sharlow et al, 2009; Siqueira-Neto et al, 2010).

Since the endemicity of leishmaniasis is primarily in developing countries often with limited financial resources and the fact that the disease tend to affect people at the lowest socio-economic level, it is also important that the cost of the novel therapies is kept low (Meheus et al, 2006; Rijal et al, 2006).

#### **1.1.4.2 Vaccines**

Natural infection by *Leishmania* provides lifelong immunity as many patients who recover from the disease do not develop clinical symptoms if re-infected. Moreover, the ancient practice of leishmanization, which consists in inoculating individuals with live *L. major* parasites at unexposed parts of the body, offered long term immunity. Although successful, this practice was abandoned due to issues related to the risks of development of serious form of the disease in immune compromised individuals and to the ethics of injecting healthy humans with live pathogens. The success of this practice however, attests of the feasibility of developing a protective vaccine against the leishmaniases (Gillespie et al, 2016).

To date, leishmanization remains the only successful vaccination strategy to be used in humans. Despite many endeavors, there is still no effective vaccine currently available as most vaccine candidates so far have failed in providing sufficient protection in humans (Gillespie et al, 2016; Srivastava et al, 2016).

#### **1.1.5 *Leishmania* life cycle**

The parasite *Leishmania* is transmitted to humans and other mammals after the bite of an infected female sand fly of the genus *Phlebotomus* in the Old World or of the genus *Lutzomyia* in

the New World. It is estimated that among the 800 species of sand flies, approximately 98 are known or potential vectors of the parasite (Maroli et al, 2013).

*Leishmania* has a two-stage life cycle that alternates between the promastigote stage in the insect vector and the amastigote stage in mammals, including humans, rodents and dogs. When an infected sand fly takes a bloodmeal from a mammal, the infective metacyclic promastigotes present in the insect salivary glands are released in the bloodstream where they are taken up by professional (macrophages, monocytes, dendritic cells, neutrophils) and non-professional (eosinophils, fibroblasts, erythrocytes) phagocytic cells (McConville & Naderer, 2011). The parasite is eventually phagocytised by macrophages, the predominant cell type for *Leishmania* infection. There, it establishes residence in the phagolysosome and the changes in environmental conditions (increase in temperature, acidic pH) trigger the differentiation of promastigotes into amastigotes. Under the amastigote form, *Leishmania* can survive, multiply and infect new cells. *Leishmania* has developed several mechanisms to evade the host immune response that allow it to persist in the mammalian host and to trigger the symptoms of the disease (Handman & Bullen, 2002). When an infected mammal is bitten by a sand fly, the infected cells are ingested by the insect and lysed in the abdominal midgut, releasing the amastigotes. Under the new conditions (lower temperature, neutral pH), between 6 and 12 hours after the insect meal, amastigotes begin to differentiate into actively multiplying procyclic promastigotes. Within 36 to 48 hours, the short, ovoid procyclic promastigotes start to transform into long, slender, non-dividing promastigotes, designated nectomonads. These parasite forms migrate forward to the thoracic midgut where they transform into multiplying leptomonads. The leptomonads differentiate into non-dividing, unattached, infective metacyclic promastigotes that migrate to the

foregut, where they can be ejected into a new mammalian host during a new bloodmeal (Gossage et al, 2003; Sacks et al, 2008).

The development of cell culture protocols has allowed the *in vitro* replication of the life cycle of some *Leishmania* species (Bates, 1994; Zilberstein, 2008). Morphological, metabolic and biochemical comparison of axenic promastigotes and amastigotes grown in culture to promastigotes isolated from sand flies and amastigotes isolated from *in vivo* lesions have showed that logarithmic phase (LP) axenic promastigotes resemble non-infective procyclic promastigotes that reside in the sand fly mid-gut, whereas stationary phase (SP) axenic promastigotes resemble the infective, non-dividing metacyclic promastigotes present in the sand fly salivary glands (Bates & Tetley, 1993; Sacks et al, 1985; Zakai et al, 1998).

Replicating the conditions inside the phagolysosome (increase of temperature and acidic pH) was found to trigger the differentiation of SP promastigotes into axenic amastigotes. Amastigotes were considered to be fully mature after 5 to 6 days in culture and were found to be comparable to lesion-derived amastigotes (Bates et al, 1992; Debrabant et al, 2004; Gupta et al, 1996; Saunders et al, 2014).

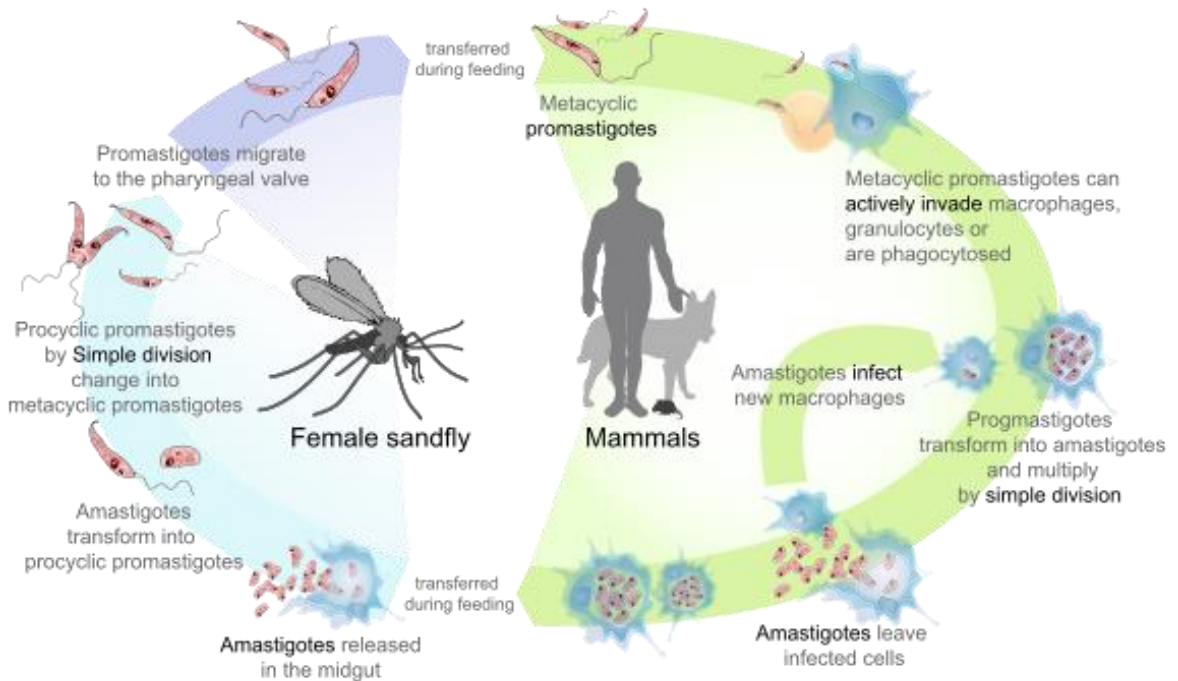


**Figure 1.2: The *Leishmania* life cycle.**

In the insect vector, *Leishmania* exists as flagellated promastigotes. In the mammalian host, the parasite is present as aflagellated amastigotes and reside in the phagolysosome of macrophages (Retrieved 1 June 2016 from

[https://commons.wikimedia.org/w/index.php?title=File:Leishmaniasis\\_life\\_cycle\\_diagram\\_en.svg&oldid=166425481](https://commons.wikimedia.org/w/index.php?title=File:Leishmaniasis_life_cycle_diagram_en.svg&oldid=166425481))

## 1.2 *Leishmania* metabolism

During its life cycle, the *Leishmania* parasite evolves in very different niches, which may vary in terms of nutrients availability and composition. The procyclic promastigotes reside in the sand fly midgut which is likely to be rich in nutrients from the bloodmeal and the sugar-rich meals from plant juices (Sacks et al, 2008). The infective metacyclic promastigotes which are present in the insect salivary glands may be exposed to nutrient-poor conditions (McConville & Naderer, 2011). In the mammalian host, the parasite can infect professional (macrophages, monocytes, dendritic cells, neutrophils) and non-professional phagocytic cells (fibroblasts, erythrocytes, eosinophils), with some being more permissive (macrophages) than others

(neutrophils) to *Leishmania* development. This difference of permissiveness reflects a difference in the conditions encountered by the parasite in those different cells (McConville & Naderer, 2011; McConville et al, 2015). Recent data indicate that the mature phagolysosome environment of macrophages is very dynamic as the phagolysosome continuously merges with phagosomes, endosomes, autophagosomes and vesicles from the endoplasmic reticulum, which may expose the intracellular parasites to a variety of carbon sources and nutrients (Ndjamen et al, 2010; Real & Mortara, 2012).

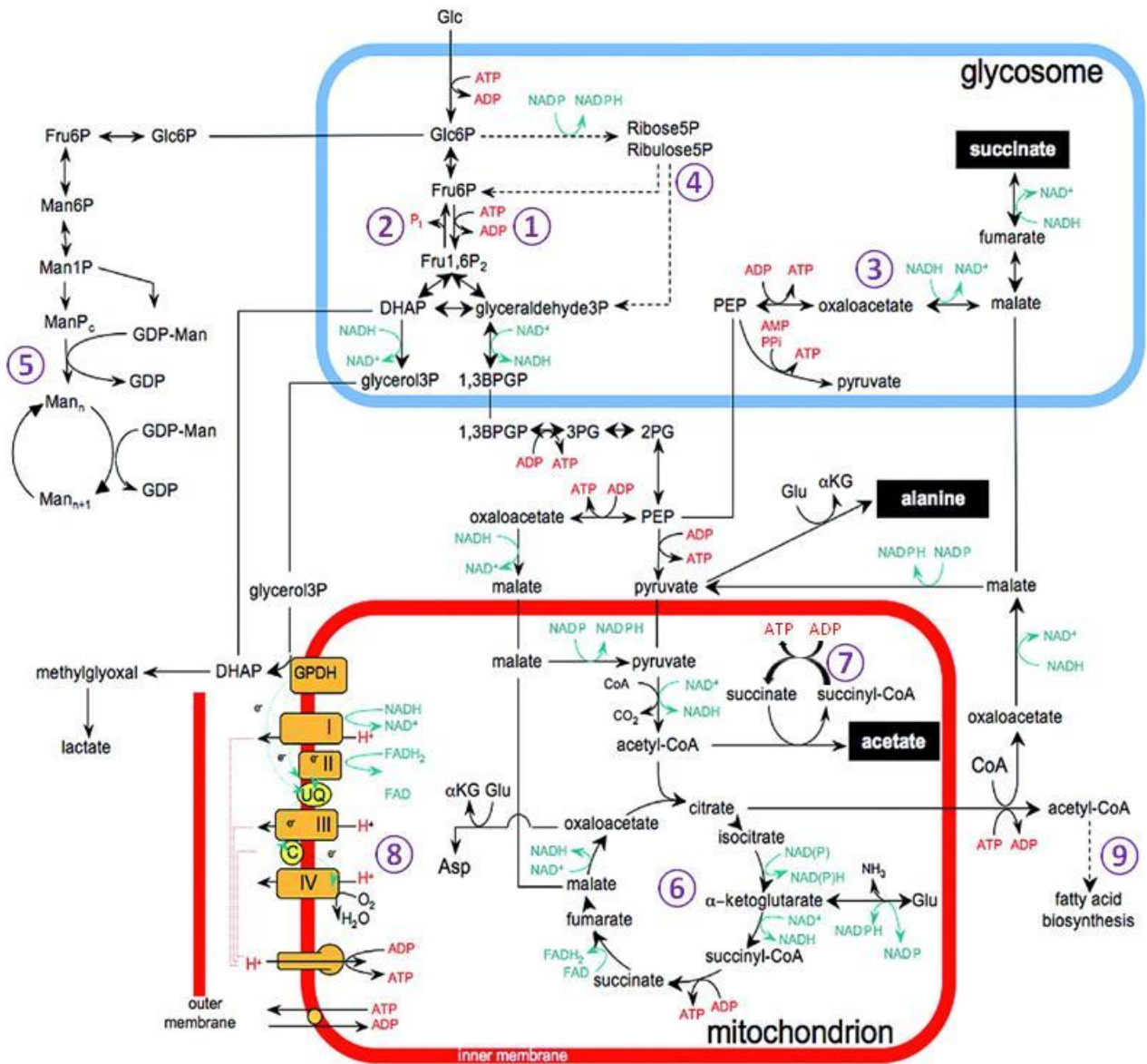


**Figure 1.3: Overview of carbon metabolism in *Leishmania*.**

The numbers in circle represent the major pathways that are mentioned here (1: glycolysis; 2: gluconeogenesis; 3: glycosomal succinate fermentation; 4: pentose phosphate pathway; 5: mannogen synthesis; 6: TCA cycle; 7: ASCT cycle; 8: electron transport chain, 9: fatty acid biosynthesis). Products on a black background represent the major secreted metabolites in promastigotes (acetate, alanine, succinate). The dotted arrows correspond to pathways with multiple steps that are not represented.

Abbreviations: I-IV: complexes of the electron transport chain;  $\alpha$ KG:  $\alpha$ -ketoglutarate; 1,3BPGP: 1,3-bisphosphoglycerate; DHAP: dihydroxyacetone phosphate; Fru1,6P<sub>2</sub>: fructose-1,6-bisphosphatase; Glu: glutamate; GPDH: FAD-dependent glycerol 3-phosphate dehydrogenase; Glc6P: glucose-6-phosphate; Man6P: mannose-6-phosphate; ManP<sub>c</sub>: Man1,4-cyclic-phosphate; Mann: mannogen oligomers; PEP: phosphoenolpyruvate; 2PG: 2-phosphoglycerate; 3PG: 3 phosphoglycerate. Modified from (Saunders et al, 2010). Re-used with permission.

### 1.2.1 Carbohydrate metabolism

Both *Leishmania* promastigotes and amastigotes use glucose as carbon source. The three isoforms of the *L. mexicana* glucose transporter encoded by the *lmg*t gene family were found to be constitutively expressed throughout the parasite life cycle. *L. mexicana* promastigotes show limited growth in the absence of glucose or after deletion of all three genes of the *lmg*t locus. Those same conditions resulted in the loss of viability of amastigotes, inferring that glucose is essential for amastigotes survival (Burchmore et al, 2003). Promastigotes and amastigotes are capable of taking up other hexoses such as fructose, mannose and galactose, which, with the exception of galactose, are able to support the growth of both stages of the parasite in the absence of glucose (Rodriguez-Contreras et al, 2007). Deletion of *L. major* glucosamine 6-phosphate deaminase that catalyzes the conversion of the amino sugars N-acetylglucosamine and glucosamine to fructose 6-phosphate was found to affect the survival of the parasite in macrophages both *in vitro* and *in vivo* in mice (Naderer et al, 2010). This reflects the importance of amino sugar catabolism as a source of sugars for amastigotes. These amino sugars may be present in significant proportion in the phagolysosome as a result of glycoproteins degradation (McConville et al, 2015).

After uptake by *Leishmania*, the sugars are transported into the glycosomes where they are phosphorylated (Figure 1.3, pathway 1). This organelle contain many of the enzymes involved in carbohydrate metabolism (glycolysis, pentose phosphate pathway, gluconeogenesis) (Haanstra et al, 2016). The first seven steps of glycolysis occur in the glycosomes, while the final steps occur in the cytosol, where the ATP-generating enzymes, phosphoglycerate kinase and pyruvate kinase are located (Haanstra et al, 2016; Saunders et al, 2010). The glycosomal ATP and NAD<sup>+</sup> (nicotinamide adenine dinucleotide) consumed in the first steps of glycolysis may be

regenerated by import of the phosphoenolpyruvate (PEP) produced in the cytosol into the glycosome, where it is converted to pyruvate by decarboxylation (producing one molecule of ATP per molecule of PEP) or to succinate via the glycosomal succinate fermentation (GSF) pathway (Figure 1.3, pathway 3). The GSF pathway produces one molecule of ATP (catalysed by PEP carboxykinase) and 2 molecules of  $\text{NAD}^+$  (catalysed by malate dehydrogenase and fumarate reductase) per molecule of PEP (Saunders et al, 2010). Another pathway that regenerates the glycosomal  $\text{NAD}^+$  is the glycerol 3-phosphate (G3P) / dihydroxyacetone phosphate (DHAP) shuttle between the glycosome and the mitochondria, during which one molecule of  $\text{NAD}^+$  is produced during conversion of DHAP into G3P by the glycosomal NADH-dependent glycerol 3-phosphate dehydrogenase (Guerra et al, 2006).

The excess of carbohydrates may be used for the synthesis of mannogen, a carbohydrate reserve material in *Leishmania*, and the alternative to glycogen or starch present in other eukaryotes (Figure 1.3, pathway 5). It is composed of chains of  $\beta$ -1,2-linked mannose (4-40 residues) and accumulates in stationary phase promastigotes and amastigotes. In this case, the phosphorylated hexoses present in the glycosome are exported to the cytosol where mannogen is synthesized and accumulates (up to 10 mM). This reserve is degraded and used in conditions of poor sugar supply (Ralton et al, 2003).

Metabolite profiling and  $^{13}\text{C}$ -stable isotope labeling of different stages of *L. mexicana* in culture showed that actively multiplying logarithmic-phase (LP) promastigotes and non-dividing stationary-phase (SP) promastigotes exhibited high rates of glucose uptake, associated with the secretion of partially oxidized end-products of glucose catabolism such as acetate, succinate and alanine (termed overflow metabolism). In comparison, amastigotes displayed lower levels of glucose uptake and undetectable secretion of overflow metabolites, suggesting the complete

oxidation of glucose as carbon source and/or its utilization for biomass increase (Saunders et al, 2014). In both promastigote and amastigote stages, products of glucose catabolism could be traced in glycolysis, the pentose phosphate pathway, the glycosomal succinate fermentation (GSF) pathway, the mitochondrial TCA cycle, and in oligosaccharide-derived mannogen (Saunders et al, 2014).

Gluconeogenesis was also found to be essential for the successful growth of intracellular amastigotes (Figure 1.3, pathway 2). An *L. major* mutant lacking the gluconeogenic enzyme fructose-1,6-bisphosphatase failed to multiply in macrophages although it remained viable. This led to the idea that the supply of hexoses in the phagolysosome was limited and could not sustain amastigotes growth which may rely on the production of sugars via gluconeogenesis resulting from amino acids catabolism (Naderer et al, 2006). This correlates with the upregulation of enzymes involved in gluconeogenesis during *L. donovani* amastigotes differentiation (Rosenzweig et al, 2008b). However, it contrasts with the observation of a loss of viability of amastigotes deficient in hexose transporters or sugar catabolism (Burchmore et al, 2003), as it would suggest that amastigotes growth would require both hexose uptake from the environment and *de novo* synthesis. This may reflect a switch of the parasite metabolism from sugar catabolism in the early stages of differentiation to gluconeogenesis once infection is established in the phagolysosome and amastigote maturation is complete (McConville & Naderer, 2011; Naderer et al, 2006; Naderer et al, 2010).

### **1.2.2 The pentose phosphate pathway**

The hexoses phosphorylated in the glycosome are also catabolised in the pentose phosphate pathway (PPP) (Figure 1.3, pathway 4) (Haanstra et al, 2016). This pathway consists of two branches. The first three steps which constitute the oxidative branch, uses glucose 6-

phosphate for the generation of nicotinamide adenine dinucleotide phosphate (NADPH), an essential reducing agent in biosynthetic reactions such as lipid synthesis, and in oxido-reductive reactions involved in the defense against oxidative stress. The subsequent reactions form the non-oxidative branch and result in the production of ribose 5-phosphate, which serves in the synthesis of nucleotides, and of erythrose 4-phosphate, a precursor for the synthesis of aromatic amino acids and of some vitamins. The presence of the enzymes of both branches in *Leishmania* has been characterized (Kovářová & Barrett, 2016; Maugeri et al, 2003). Although some of the enzymes have been identified in the glycosomes, most of the PPP activities are located in the cytosol. <sup>13</sup>C-stable isotope labeling studies found a downregulation of the non-oxidative part in amastigotes, characterized by a marked decrease of seduheptulose 7-phosphate labeling in comparison to ribulose 5-phosphate (Saunders et al, 2014), which coincides with a downregulation of the PPP enzymes during differentiation of promastigotes into amastigotes (Rosenzweig et al, 2008b). In comparison to LP promastigotes, SP promastigotes exhibited a decrease in the labeling of PPP intermediates, suggesting a reduction in the synthesis of nucleotides in those non-dividing cells (Saunders et al, 2014).

### **1.2.3 Amino acid metabolism**

*Leishmania* possess several amino acid permeases, among which some were found to be upregulated in amastigotes (Akerman et al, 2004; Geraldo et al, 2005; Inbar et al, 2012; Marchese et al, 2018; Shaked-Mishan et al, 2006). Both stages of the parasite are able to scavenge amino acids (Burchmore et al, 2003; Saunders et al, 2014). In comparison to LP promastigotes, SP promastigotes showed a reduced uptake and catabolism of amino acids. This decrease was even more pronounced in amastigotes, in correlation with the nutrient-sparing metabolism of this latter stage. The uptake of amino acids by promastigotes was associated with

the secretion of partially oxidized organic acids, such as succinate and alanine (Saunders et al, 2014). The catabolic pathways of many amino acids feed into the TCA cycle (glutamate, proline, alanine, serine, cysteine, threonine, methionine, valine, isoleucine, aspartate/asparagine, glycine) (Figure 1.3, pathway 7) (Opperdoes & Coombs, 2007). Gluconeogenesis appears to be essential for intracellular amastigote development. In the absence of the enzymes of the glyoxylate pathway for the conversion of acetyl-CoA (the main product of fatty acid  $\beta$ -oxidation) to sugars through the TCA cycle and gluconeogenesis, amastigotes may rely on amino acid catabolism for gluconeogenesis (Naderer et al, 2006). This correlates with an upregulation of enzymes involved in amino acid catabolism observed during *L. donovani* amastigote differentiation (Rosenzweig et al, 2008b).

*Leishmania* has the capacity to synthesize a number of amino acids: cysteine, glycine, serine, alanine, aspartate, asparagine, proline, glutamate, glutamine, methionine and threonine (Opperdoes & Coombs, 2007; Saunders et al, 2014). However, in culture, some amino acids (glycine, serine, threonine and proline) were found to be preferentially taken up from the medium (Saunders et al, 2011; Saunders et al, 2014). Bioinformatic analysis predicted that other amino acids cannot be synthesized by *Leishmania* and therefore need to be supplied by the parasite environment: arginine, histidine, isoleucine, leucine, lysine, phenylalanine, tryptophan, tyrosine, valine (Opperdoes & Coombs, 2007). Six of them were confirmed to be essential for promastigotes survival in culture: arginine, leucine, lysine, phenylalanine, tryptophan, and valine (Nayak et al, 2018). Although the cells could survive in the absence of isoleucine or histidine, their growth was significantly affected, while synthesis of tyrosine can be ensured by conversion of phenylalanine by a phenylalanine hydroxylase.

#### 1.2.4 Fatty acid metabolism

*Leishmania* has the capacity of taking up free fatty acids from its environment as well as the capacity to synthesize them *de novo*. The scavenged fatty acids can be catabolised by  $\beta$ -oxidation in the glycosome and in the mitochondria or used for lipid biosynthesis (McConville et al, 2008). The catabolism of fatty acids by  $\beta$ -oxidation appears to be repressed in *Leishmania* promastigotes in the presence of glucose, and induced in conditions of glucose starvation (Naderer et al, 2006; Saunders et al, 2014). In comparison,  $\beta$ -oxidation occurred in axenic amastigotes even when glucose was present in the culture medium and increased when glucose was depleted (Hart & Coombs, 1982; Rosenzweig et al, 2008b; Saunders et al, 2014). The acetyl-CoA produced by the  $\beta$ -oxidation of fatty acids in the mitochondria is used in the TCA cycle (McConville et al, 2008; Saunders et al, 2014). The glyoxylate cycle enzymes, isocitrate lyase and malate synthase which mediate the use of acetyl-CoA for the generation of carbohydrates via gluconeogenesis, are absent in *Leishmania* (Ivens et al, 2005). This makes the use of fatty acids as the sole carbon source of *Leishmania* unlikely, since gluconeogenesis appears to be essential for the development of intracellular amastigotes (Naderer et al, 2006).

In eukaryotic and prokaryotic cells, the biosynthesis of fatty acids involves repeats of a cycle of four enzymatic reactions that result in the addition of two carbons to the growing acyl chain at the end of each cycle. The two carbons are provided by a malonyl group after transfer from malonyl-CoA to the acyl carrier protein (ACP) (Uttaro, 2014). Conventionally, fatty acids biosynthesis is ensured by a type I or a type II synthase. The type I synthase is found in the cytosol of animal and fungal cells and consists of a complex of one or two large enzymes that contain the different catalytic domains for the four enzymatic reactions. The type II synthase is present in plants, bacteria and mitochondria and is formed by a complex of individual enzymes,

each catalyzing one of the four reactions. No gene encoding a type I synthase was found in the trypanosomatids genomes. Genes encoding components of a type II synthase and ACP were identified and the proteins localized to the mitochondria. It is estimated that this pathway ensures only 10% of the fatty acid biosynthesis and mainly provides the lipids essential for the mitochondria, such as the mitochondrial phospholipid cardiolipin (Lee et al, 2007; Uttaro, 2014).

In trypanosomatids, the majority of the fatty acids are synthesized by a pathway involving integral membrane proteins of the endoplasmic reticulum designated ELOs (endoplasmic reticulum-based elongases). These elongases catalyse similar reactions as the type I and II synthases, with the differences that the fatty acyl and malonyl groups are esterified to CoA instead of ACP and each reaction is carried out by a different enzyme. In addition to the synthesis of saturated fatty acids, the ELO pathway also contributes to the synthesis of large polyunsaturated fatty acids. Desaturases, which are integral membranes proteins of the endoplasmic reticulum are responsible for the synthesis of unsaturated fatty acids while long polyunsaturated fatty acids require both desaturases and ELOs (Lee et al, 2007; Uttaro, 2014).

The fatty acids taken up from the environment or synthesized *de novo* are used to produce glycerol-phospholipids, sphingolipids and triacylglycerols (TAG), which serve as the parasite reserve of fatty acids (Lee et al, 2007; McConville et al, 2008). Intracellular amastigotes are also able to scavenge complex lipids from their hosts as a source of fatty acids and to synthesize their sphingolipids and phospholipids (Zhang & Beverley, 2010).

### **1.2.5 The tricarboxylic acid (TCA) cycle**

Pyruvate, the end product of glycolysis can either be converted by transamination into alanine and secreted, or transported to the mitochondria. In the mitochondria, pyruvate is converted into acetyl-CoA which can be oxidized either into CO<sub>2</sub> via the TCA cycle (Figure 1.3,

pathway 6) or into acetate via the acetate:succinate CoA transferase / succinyl-CoA synthetase (ASCT) cycle (Figure 1.3, pathway 7) (Van Hellemond et al, 1998).

Acetyl-CoA resulting from pyruvate oxidation or fatty acid  $\beta$ -oxidation can be further oxidized in the TCA cycle. The generation of CO<sub>2</sub> as one of the major end products of *Leishmania* metabolism is an indication of the presence of a functional TCA cycle (Hart & Coombs, 1982; Saunders et al, 2011). <sup>13</sup>C-stable isotope labeling studies found that in both stages of the parasite, products of glucose breakdown are further processed in the TCA cycle. Analysis of the isotopomer labeling of different TCA metabolites reveal the operation of the TCA cycle in a highly cyclic mode in SP promastigotes, while in LP promastigotes and amastigotes, the TCA cycle intermediates are extracted for the synthesis of other metabolites, such as glutamate (Saunders et al, 2011; Saunders et al, 2014). This depletion of the TCA cycle components is compensated by the supply of substrates such as malate and succinate from the GSF pathway, that replenish the stock of TCA cycle intermediates. The sensitivity of the parasite, particularly the amastigote stage, to inhibition of the TCA cycle infers its dependency on the TCA cycle for *de novo* synthesis of glutamate and glutamine and its poor ability to salvage those amino acids. Inhibition of the TCA enzyme aconitase that mediates the generation of  $\alpha$ -ketoglutarate from citrate via isocitrate, results in growth arrest in promastigotes that could be reversed by supplementation with exogenous glutamate (Saunders et al, 2011). In amastigotes, this inhibition induced a loss of viability that could only be rescued partially in the presence of exogenous glutamate. Similar results were observed when glutamine synthetase which converts glutamate to glutamine was inhibited. However, in this case, supplementation with glutamine did not rescue the inhibition of intracellular amastigotes proliferation (Saunders et al, 2014).

### 1.2.6 The electron transport chain

The genes encoding the components of the mitochondrial electron transport chain Complexes I, II, III and IV have been identified in the *Leishmania* genome (Berriman et al, 2005) (Figure 1.3, pathway 8). In a conventional electron transport chain, there are four multi-protein complexes that are embedded in the inner mitochondrial membrane. Electrons from the NADH and succinate produced during the TCA cycle are donated to the electron transport chain via Complex I (also designated NADH dehydrogenase or NADH:ubiquinone reductase or NADH:CoQ reductase) and Complex II (succinate dehydrogenase or succinate:ubiquinone reductase), respectively. Those two complexes then donate their electrons to Complex III via reduction of ubiquinone (also designated coenzyme Q). Complex II also participates in the TCA cycle, catalyzing the sixth step of the cycle that converts succinate to fumarate, which is coupled to the reduction of ubiquinone to ubiquinol. The latter then transfers electrons to Complex III (cytochrome  $bc_1$  complex) which uses them to reduce cytochrome c. Electrons are then carried by cytochrome c to Complex IV (cytochrome c oxidase) which passes them on to oxygen ( $O_2$ ), the final electron acceptor, leading to the production of  $H_2O$ . This transfer of electrons is associated with the translocation of protons from the mitochondrial matrix to the mitochondrial intermembrane space, by the proton pumps of Complexes I, III and IV, creating an electrochemical proton gradient across the inner mitochondrial membrane. This gradient has two components: a pH gradient and a voltage gradient (also referred to as the  $\Delta\Psi_m$  membrane potential). This gradient is essential for the regulation of many mitochondrial activities, such as the synthesis of ATP via oxidative phosphorylation, ion homeostasis or the import of proteins or substrates into the mitochondria (Hauser et al, 1996; Perry et al, 2011).

In *Leishmania*, the presence of Complexes II to IV have been characterized either by visualization of the protein complexes after separation by Blue Native PAGE, by Western blot detection of their protein subunits (Horváth et al, 2000; Maslov et al, 1999; Nebohacova et al, 2009; Verner et al, 2014) or by characterization of their activities (Chen et al, 2001; Dey et al, 2010; Santhamma & Bhaduri, 1995; Uboldi et al, 2006; Van Hellemond & Tielens, 1997; Verner et al, 2014; Zikova et al, 2008). However, the presence of a functional Complex I in *Leishmania* remains unclear (Duarte & Tomas, 2014; Opperdoes & Michels, 2008). The nuclear and mitochondrial genes that encode the proteins of Complex I have been identified in *Leishmania*. While some inhibition studies have characterized the presence of the complex in *L. mexicana* using the Complex I inhibitor rotenone, no inhibitory effect was seen in *L. donovani* (Benaim et al, 1990; Bermúdez et al, 1997; Santhamma & Bhaduri, 1995). Furthermore, the complex is not detected after Blue Native PAGE separation of mitochondrial lysates from *L. tarentolae*, *L. amazonensis* and *L. donovani* (Horváth et al, 2000; Maslov et al, 1999; Nebohacova et al, 2009; Verner et al, 2014) and the level of its enzymatic activity in *L. tarentolae* mitochondrial preparations was negligible (Verner et al, 2014). The relevance of the Complex I function in the parasite survival is further questioned by the lack of growth defect observed in promastigotes of the UC strain of *L. tarentolae*. Those cells have lost regions of their kinetoplast minicircle which encode guide RNAs (gRNAs). These gRNAs mediate the editing of mitochondrial precursor mRNAs into translatable mRNAs, some of which encode for subunits of Complex I (Sloof et al, 1994; Thiemann et al, 1994). This has led to the hypothesis that Complex I may not be essential, at least in the promastigote form of the parasite studied in culture but may have a more significant role in different stages of the life cycle or *in vivo*, such as in the mammalian host or in some stages in the insect vector. Moreover, identification of the complex subunits

composition in the closely related *T. brucei* found that it also contains proteins involved in fatty acid synthesis, suggesting that it may be involved in functions other than electron transport (Acestor et al, 2011; Panigrahi et al, 2008a).

### **1.2.7 Mitochondrial ATP metabolism**

In *Leishmania* mitochondria, as in other trypanosomatids, ATP is produced via three different pathways that are designated types I, II and III (Bochud-Allemann & Schneider, 2002; Bringaud et al, 2006). The type I pathway corresponds to the synthesis of ATP via oxidative phosphorylation, as found in other eukaryotes (Figure 1.3, pathway 8). The  $F_0F_1$  ATP synthase or Complex V utilizes the mitochondrial membrane potential  $\Delta\Psi_m$  created during the transport of electrons through the electron transport chain, to synthesize ATP from ADP and inorganic phosphate. Type II and III corresponds to the synthesis of ATP by substrate level phosphorylation. In the type II pathway, ATP is produced during oxidation of succinyl-CoA to succinate by the succinyl-CoA synthetase of the TCA cycle, a step that in higher eukaryotes produces GTP (Figure 1.3, pathway 6). In the type III pathway, ATP production occurs in the acetate:succinate CoA transferase (ASCT) / succinyl CoA synthetase cycle (also referred to as the ASCT cycle). This cycle has been identified mainly in trypanosomatids, some parasitic helminths and in the hydrogenosome of trichomonads and some fungi (Van Hellemond et al, 1998) (Figure 1.3, pathway 7). It combines the activities of two enzymes, acetate:succinate CoA transferase and succinyl-CoA synthetase. Acetate:succinate CoA transferase catalysed the transfer of the CoA of acetyl-CoA to succinate, resulting in the production of acetate and succinyl-CoA. Succinyl-CoA is then oxidized to succinate by the succinyl-CoA synthetase, a step that, as in the TCA cycle, produces ATP.

### **1.3 *Leishmania* gene and protein expression throughout the life cycle**

#### **1.3.1 *Leishmania* experiences profound changes throughout its life cycle**

During its life cycle, *Leishmania* alternates between considerably different environments. In the insect vector, the parasite is present as extracellular promastigotes, residing in the digestive tract where it encounters near neutral pH and temperatures varying around 25°C (Sacks, 2001). When the parasite is transmitted to a mammalian host during an infected sand fly blood meal, it is released into the bloodstream and takes up residence in the phagolysosomes of macrophages. It encounters first a significant increase in temperature, followed by a decrease in pH, an exposure to oxygen and nitrogen reactive species and a change in the nutrient supply. These new environmental conditions trigger the differentiation of the promastigotes into amastigotes, which is characterized by changes in the morphology and the metabolism of the parasite. This allows *Leishmania* to survive and thrive in the new environment and to resist the host immune system, which subsequently leads to development of the disease (McConville & Naderer, 2011; Olivier et al, 2005). Such changes were expected to be associated with the differential expression of a variety of genes. Identification of genes that are differentially expressed during *Leishmania* life cycle may provide a better understanding of the parasite biology. Furthermore, the genes that are preferentially expressed at the amastigote stage may be involved in the parasite survival and multiplication in the mammalian host and/or in its ability to evade killing by the host immune system. Those genes may be involved in the pathogenesis of the disease and therefore could represent potential targets for the development of new therapies.

#### **1.3.2 *Leishmania* gene expression**

Analysis of the *L. major* genome found that most of the protein-coding genes are grouped in clusters of 10 to 100 genes of unrelated predicted functions, in the same 5'-3' direction, on the

same chromosome DNA strand, separated by short (0.9-14 kb) non-coding strand-switch regions (Ivens et al, 2005; Myler et al, 1999; Worthey et al, 2003). They are co-transcribed into polycistronic pre-mRNAs by the RNA polymerase II. However, the mechanisms of regulation of transcription initiation in *Leishmania*, as in the closely related parasites *T. brucei* and *T. cruzi*, appear to be different than in other eukaryotes. There are no consensus promoter sequences and very few potential homologs of the basal transcription factors found in other eukaryotes were identified in its genome. Regulation factors such as the TATA-box-binding protein-associated factors are missing (Berriman et al, 2005; El-Sayed et al, 2005; Ivens et al, 2005). This suggested that the control of gene expression in *Leishmania* may occur at the post-transcriptional level. In absence of defined RNA polymerase II promoters and of identified transcription factors, initiation of transcription has been proposed to occur at the strand-switch regions (Haile & Papadopoulou, 2007).

The generation of mature, monocistronic mRNAs from the pre-polycistronic transcripts occurs by *trans*-splicing, at the 5' end and cleavage and polyadenylation at the 3' end. Trans-splicing involves the addition of a small capped RNA of 39 to 41 nucleotides, the splice leader RNA (SL RNA) at the 5' end of each monocistronic mRNA. It occurs at an AG splice acceptor located downstream of a U-rich polypyrimidine tract situated about 50-100 nucleotides upstream of the translational ATG start codon. No consensus polyadenylation signal was identified in *Leishmania* (Papadopoulou et al, 2008).

### **1.3.3 Variation of gene expression during *Leishmania* development**

Comparison of the transcriptome and of protein expression profiles between promastigotes and amastigotes detected a modest proportion of genes differentially expressed (Cohen-Freue et al, 2007). The percentage of genes whose mRNAs abundance exhibited

significant differences between the two life stages was found to represent an average of 1 - 3.5% of the total genes (Akopyants et al, 2004; Holzer et al, 2006; Leifso et al, 2007; Saxena et al, 2007). Two-dimensional (2D) PAGE analysis of whole cell lysates of promastigotes and amastigotes of *L. infantum*, *L. donovani*, *L. mexicana* and *L. panamensis* identified, on average 10% of proteins differentially expressed between the two stages (Bente et al, 2003; El Fakhry et al, 2002; Leifso et al, 2007; McNicoll et al, 2006; Nugent et al, 2004; Walker et al, 2006).

However, some more recent studies have reported the detection of higher percentages of differentially expressed genes during differentiation of promastigotes into amastigotes (De Pablos et al, 2016). Comparison of mRNA abundance of promastigotes and intracellular amastigotes isolated at early stage of infection (between 0 and 24 hours) revealed changes in mRNA abundance for 30-40% of the transcriptome (Dillon et al, 2015; Fernandes et al, 2016; Fiebig et al, 2015). A study of the variation of mRNA and protein levels in axenic amastigotes at different timepoints after initiation of differentiation found that about half of the identified genes (445/902) exhibited at least a 2-fold change in mRNA or protein levels during differentiation. 23% of those genes were differentially expressed at the mRNA level, while 32% were differentially expressed at the protein level (Lahav et al, 2011).

These studies are difficult to compare directly since various factors may account for the discrepancy in their results, such as the source of amastigotes and the stage of differentiation (logarithmic or stationary-phase or metacyclic promastigotes versus axenic or lesion-derived or macrophage-isolated amastigotes), the age of the axenic culture, the method used to evaluate gene expression (RNA-sequencing, DNA microarrays, 2D PAGE, iTRAQ LC-MS/MS), the criteria employed to define differential expression (fold-change, statistical cut-off). Indeed, while 41% of transcripts were determined to be statistically differentially expressed between *L.*

*mexicana* logarithmic-phase promastigotes and intracellular amastigotes isolated from macrophages 24 hours post-infection, that percentage fell to 14% when only transcripts that exhibit at least a 2-fold change were considered (Fiebig et al, 2015). In the same study, the proportion of transcripts with a significant change in abundance between the promastigotes and the axenic amastigotes was 23% but only 4% showed at least a 2-fold difference.

Interestingly, little correlation was found when comparing the expression profile of mRNAs and the expression of the corresponding proteins (Lahav et al, 2011; McNicoll et al, 2006). Among the *L.infantum* proteins found to be upregulated in amastigotes, only 53% had an mRNA with a similar expression pattern. For the remaining proteins, the corresponding mRNAs were constitutively expressed. In the former group, the level of mRNA abundance remained modest: only 35% of mRNAs exhibited over a two-fold increase and 10% had a three-fold increase. In comparison, no correlation was found between the expression of promastigotes-specific proteins and the levels of the corresponding mRNAs. 60% of those mRNAs displayed similar expression levels in amastigotes and 35% were upregulated in amastigotes (McNicoll et al, 2006). These findings provide further evidence of the paucity of regulation of transcription initiation in *Leishmania* and that the regulation of gene expression during differentiation is likely to occur at the translational and post-translational level.

#### **1.3.4 Biological function of the stage-specific proteins**

Since many of the protein-coding genes in the *Leishmania* genomes encode for proteins of unknown function, it is not surprising that a large number of the differentially-expressed proteins identified are of unknown functions (Ivens et al, 2005; Leifso et al, 2007; Papadopoulou et al, 2008). The rest of the proteins can be classified in different functional categories, including:

- Stress response and protein folding, such as the heat-shock proteins HSP70 and HSP60, which were found to be upregulated in amastigotes (Bente et al, 2003; McNicoll et al, 2006; Nugent et al, 2004).
- Energy metabolism, examples include the amastigote-specific Complex IV subunit p27, the glycolytic enzyme enolase and the Complex III Rieske iron-sulfur protein which are upregulated in amastigotes (Bente et al, 2003; Dey et al, 2010; Nugent et al, 2004; Rosenzweig et al, 2008b). Glycolytic enzymes localized to the cytosol appear to be downregulated in amastigotes, while the glycosomal enzymes are upregulated (Rosenzweig et al, 2008b).
- Cell structure, cytoskeleton: while some isoforms of  $\alpha$  tubulin were downregulated, one isoform of  $\alpha$  and  $\beta$  tubulin were upregulated (Bellatin et al, 2002; Bente et al, 2003);
- Proteolysis, such as the cysteine proteinases CPB 1 and 2 which are mainly present in metacyclic promastigotes while the cystein proteinases CPB3 to CPB18 were upregulated in amastigotes (Brooks et al, 2001). iTRAQ analysis of the changes in proteins levels during *L. donovani* differentiation to amastigotes identified 10 calpains (out of the 33 predicted to be encoded in *L. infantum*), among which 5 were downregulated in amastigotes and 3 had an increased expression (Rosenzweig et al, 2008b).

### **1.3.5 Mechanisms involved in developmental gene regulation**

The mechanisms involved in regulating gene expression in *Leishmania* are largely unknown. Many developmentally regulated genes are polycistronically co-transcribed along with

genes that are constitutively expressed (Brooks et al, 2001) and for many differentially expressed proteins the corresponding mRNAs are constitutively expressed (McNicoll et al, 2006), which indicates a control of gene expression at the post-translational level.

Sequences within the 3'UTR of mRNAs were found to be involved in the stage-specific expression of some genes, while no such evidence has been found for the 5'UTR. A sequence located between the 1500 and 1750 nucleotides from the 5' end of the 2.9-kb 3'UTR of the *L. mexicana* amastigote-specific *A600.4* gene was found to mediate the stage-specific expression of a *luciferase* reporter gene, integrated at the *A600* locus (Murray et al, 2007). Moreover, analysis of the *L. major* genome revealed the presence of two new families of short DNA sequences, averaging 500 bp, bearing the characteristics of extinct trypanosomatids retroposons, designated small interspersed degenerate retroposons or SIDER within the 3'UTR of mRNAs (Bringaud et al, 2007). Identified by the presence in their 5' end of a 79 nucleotide sequence that is highly conserved in other retroposons, the SIDERs were also characterized in other *Leishmania* species and shown to play a role in the post-transcriptional regulation of gene expression (Smith et al, 2009). Members of the SIDER1 subfamily were found to be predominantly present in amastigotes-specific mRNAs and appear to regulate stage-specific translation by increasing the association of SIDER1-containing mRNAs with heavy polysomes, a characteristic of highly translated mRNAs (Bringaud et al, 2008). On the other hand, the SIDER2 retroposons appear to have a negative regulatory effect on gene expression, by promoting mRNA degradation. SIDER2-containing mRNAs are generally less abundant than non-SIDER2-containing mRNAs and in the presence of SIDER2, the mRNA half-life is decreased (Bringaud et al, 2007).

Protein expression and function can also be affected by post-translational modifications, such as phosphorylation, methylation, acetylation, glycosylation and ubiquitination. In *L.*

*infantum*, a difference in glycosylation appears to be involved in the differential expression of two isoforms of the surface protease GP63 in promastigotes (González-Aseguinolaza et al, 1997). Monitoring of variations in post-translational modifications by iTRAQ analysis during *L. donovani* differentiation from stationary-phase (SP) promastigotes to mature amastigotes over the course of 144 hours found significant changes in the amount of protein phosphorylation/dephosphorylation, methylation and glycosylation, between SP promastigotes and mature amastigotes, whereas the changes in acetylation were more discrete (Rosenzweig et al, 2008a).

Overall, the polycistronic transcription and paucity of RNA polymerase II promoters and basal transcription factors suggest that gene expression in *Leishmania* is poorly regulated at the transcription initiation. The control of gene expression appears to occur predominantly at the level of translation, including a mechanism involving sequences within the mRNAs 3'UTRs, and of post-translation, through post-translational modifications, which determine the developmental expression of genes throughout the parasite life cycle. Exposure to environmental changes, such as temperature changes have been shown to influence transcription (McNicoll et al, 2005; Quijada et al, 2000). The molecular mechanisms that mediate such regulation remain to be elucidated. The regulation of gene expression at the level of translation or post-translation rather than at the transcriptional level may offer the parasite the capacity to rapidly adapt and increase their chance of survival when switching between environments that are extremely different.

## 1.4 Genomic analysis in *Leishmania*

### 1.4.1 Comparative genomic analysis

*Leishmania* infection can result in different clinical outcomes that can be attributed to factors such as the host immune responses, genetic variations but predominantly, to the species of the infecting parasite (Smith et al, 2007). To understand how different *Leishmania* species contribute to different forms of leishmaniasis, the genome of different species has been sequenced and compared (Peacock et al, 2007; Rogers et al, 2011). The genome of Old World species were found to consist of 36 chromosomes: *L. major*, the causative agent of cutaneous leishmaniasis, *L. infantum* and *L. donovani*, both responsible for visceral leishmaniasis, and *L. tarentolae*, a lizard parasite non-pathogenic to humans (Peacock et al, 2007; Raymond et al, 2012; Rogers et al, 2011). In comparison, the New World species, *L. braziliensis* and *L. panamensis*, that cause mucocutaneous leishmaniasis, contain 35 chromosomes, with one chromosome resulting from a fusion event between chromosomes 20 and 34, whereas *L. mexicana* and *L. amazonensis*, the causative agents of cutaneous lesions, contained 34 chromosomes, as a result of two fusion events between chromosomes 8 and 29 and between chromosomes 20 and 36 (Llanes et al, 2015; Rogers et al, 2011; Tschoeke et al, 2014).

Surprisingly, the different genomes were found to display a high degree of conservation. Within the coding sequences, the average sequence identity at the amino acid level was calculated to be 92% between *L. major* and *L. infantum* and 77% between *L. major* and *L. braziliensis* and between *L. infantum* and *L. braziliensis*. The average nucleotide identity was found to be 94% between *L. major* and *L. infantum*, 82% between *L. major* and *L. braziliensis* and 81% between *L. infantum* and *L. braziliensis* (Peacock et al, 2007). Less than 1% of the genes were found to be species-specific. Comparison of the *L. mexicana*, *L. major*, *L. infantum*

and *L. braziliensis* genomes revealed that among ~8,000 genes, only two were specific to *L. mexicana*, 14 were unique to *L. major*, 19 were unique to *L. infantum* and 67 were unique to *L. braziliensis*, and to *L. panamensis* (Llanes et al, 2015; Peacock et al, 2007; Rogers et al, 2011). The majority of species-specific genes encode for proteins of unknown functions, with approximately 80% of which correspond to a degeneration of existing genes due to in-frame stop codons or frame shifts that result in a possible loss of function (Peacock et al, 2007; Smith et al, 2007). Comparison of the *L. tarentolae* genome to *L. major*, *L. infantum* and *L. braziliensis*, identified 95 predicted protein coding genes specific to *L. tarentolae* and 250 genes that are absent from *L. tarentolae*, many of which were genes found to be upregulated in the amastigote stage of species that are pathogenic (Raymond et al, 2012).

Analysis of two strains of *L. mexicana*, *L. major* and *L. donovani*, in addition to one strain each of *L. infantum* and *L. braziliensis* revealed variations in chromosome copy number and distribution of multicopy genes within each chromosome, between different strains of the same species and between different species (Rogers et al, 2011). Variations in chromosome copy number were also detected between two strains of *L. donovani* from Sri Lanka, one isolated from a cutaneous leishmaniasis patient (designated CL-SL) and the other from a patient with visceral leishmaniasis (VL-SL). However, there was no correlation between the number of chromosomes and the corresponding mRNA levels. In comparison to an *L. donovani* reference strain, no genes appeared to be deleted in the genome of those two Sri Lankan isolates but variations in the gene copy number were detected in nine regions of their genome (Zhang et al, 2014).

Other species differences detected included the presence of transposable elements. Transposons are mobile elements of DNA capable of moving to different chromosomal locations, resulting in the creation or modification of existing genes or regulatory elements.

Retroelements are sequences which proliferation occurs via reverse transcription from an RNA intermediate. No active transposable elements were identified in *L. major* and *L. infantum* genomes, contrary to the *L. braziliensis* and *L. panamensis* genomes, in which potentially active retroposons were detected (Llanes et al, 2015; Peacock et al, 2007). However, remnants of retroelements were found in different *Leishmania* genomes, such as the DIREs retroposons (degenerate ingi/L1Tc-related elements) detected in *L. major*, *L. infantum* and *L. braziliensis* genomes, or the SIDER (short interspersed degenerated retroposon) elements which in *L. major* and *L. donovani* were found to localize predominantly in the 3'UTR where they regulate the mRNA levels of certain genes during differentiation (Bringaud et al, 2007; Fernandes et al, 2014; Smith et al, 2007).

One of the consequences of retrotransposable elements is the silencing of gene expression through RNA interference (RNAi) in which double-stranded RNAs (dsRNAs) are cleaved by the endonuclease dicer into small dsRNAs, allowing the association of one of the RNA strands (designated the guide RNA) to the RISC (RNA-induced silencing) complex. Pairing of the guide RNA with a complementary mRNA sequence leads to cleavage by the catalytic component of the RISC complex, the endonuclease argonaute, inhibiting expression of the corresponding gene. In trypanosomatids, the dicer activity is suggested to be carried by independent proteins. The genes encoding for such nucleases have been identified in the *L. braziliensis* and *L. panamensis* but not in the *L. major* or *L. infantum* genomes (Llanes et al, 2015; Peacock et al, 2007). Similarly, while a functional argonaute gene was detected in the *L. braziliensis* genome, only remnants of this gene was contained in *L. major* and *L. infantum* genomes, suggesting that the genes encoding for the RNAi machinery were lost in those species. The presence of the

potentially active retroposons and RNAi machinery in *L. braziliensis* suggest a greater ability of this parasite to rearrange its genome.

Among the genes originally identified as *L. donovani* specific, one multigene family, A2, was characterized as being involved in the parasite visceralization. The A2 genes were originally identified in *L. donovani* due to their amastigote-specific expression and were found to be present as pseudogenes in *L. major* (Charest & Matlashewski, 1994; Zhang et al, 2003). Downregulation of their expression was associated with a decrease in *L. donovani* amastigotes proliferation in macrophages and in their survival in the liver of infected mice (Zhang & Matlashewski, 1997). Transfection of the *L. donovani* A2 genes in *L. major* and *L. tarentolae* resulted in an increase of those parasites survival in mice visceral organs after intravenous infection, which represents the murine model of visceral leishmaniasis (Mizbani et al, 2011; Zhang & Matlashewski, 2001). Furthermore, A2 expression in *L. major* correlated with an impairment in the development of murine cutaneous leishmaniasis, a phenotype seen with *L. donovani* (Zhang et al, 2003). The number of copies of this gene, the corresponding mRNA levels as well as the protein abundance were found to be higher in the *L. donovani* VL-SL isolate than in the CL-SL isolate. Transfection of the CL-SL cells with a plasmid containing the A2 gene was associated with an increase in the CL-SL cells survival in the spleen of infected mice, while downregulation of the gene in VL-SL cells correlated with a decrease of the parasite burden in the spleen (Zhang et al, 2014). These results indicate a role of this gene family in the visceralization of the parasite and in its inability to develop the cutaneous form of the disease.

Other *L. donovani* specific genes were investigated for their visceralization potential. Some were found to increase *L. major* survival in visceral organs of infected mice, such as *LinJ.28.0340* encoding a cytosolic protein of unknown function or *LinJ.15.0900*, which encodes

a nucleotide sugar transporter of the Golgi apparatus, and/or their deletion in *L. donovani* resulted in a loss of virulence in the murine model of visceral leishmaniasis (*LinJ.28.0340* or *LinJ.36.2480*, encoding a cytosolic glyceraldehyde 3-phosphate dehydrogenase). However, the majority of the *L. donovani* specific genes did not result in an increase of parasite survival in visceral organs of infected mice when individually transfected in *L. major*, which suggest that visceralization may require the presence of a combination of those genes (Fernandes et al, 2014).

Overall, these observations lead to the hypothesis that some species-specific genes as well as differences in protein levels may play a role in the tissue tropism of the parasite and the ensuing clinical outcome.

#### **1.4.2 Analysis of *Leishmania* gene function**

Many of the approximately 8,000 protein-coding genes in *Leishmania* and the majority of those identified as species-specific encode for proteins of unknown function (Ivens et al, 2005; Rogers et al, 2011). The functional analysis of a particular gene involves the generation of cell lines in which the gene expression is inhibited and characterization of the mutant phenotype. This characterization is performed by studying its proliferation rate in culture as promastigotes and/or amastigotes, its survival in macrophages and its virulence in the appropriate animal model of infection. One approach used to delete gene expression, RNA interference, is often used in the closely related *T. brucei* but as discussed above, with the exception of species of the *Leishmania* subgenus *Viannia*, including *L. braziliensis* and *L. panamensis*, a functional RNAi machinery appears to have been lost in most *Leishmania* species (Llanes et al, 2015; Lye et al, 2010; Peacock et al, 2007).

Therefore, gene replacement by homologous recombination has been the main approach used in *Leishmania* to create null mutants of a gene of interest. Gene deletion is achieved after

two rounds of homologous recombination, in which each allele is replaced by a gene of antibiotic resistance. Each round requires transfection of the cells containing the gene of interest with a vector containing a gene of antibiotic resistance, such as the hygromycin phosphotransferase HYG gene or neomycin phosphotransferase NEO gene, flanked by fragments of the 5' and 3' sequences of the targeted gene or locus. The transfected cells are selected in presence of the drug for which they carry a resistance gene, such as hygromycin B for the HYG gene and G418 for the NEO gene. The final null mutants in which both alleles are replaced by two different resistance genes are selected in presence of the two drugs (Cruz et al, 1991).

The recently discovered CRISPR (clustered regularly interspaced short palindromic repeat)-Cas 9 (CRISPR-associated gene 9) genome editing system has been proved to be applicable to *Leishmania* and may provide an alternative approach to double targeted gene replacement to generate deletion mutants (Beneke et al, 2017; Martel et al, 2017; Sollelis et al, 2015; Zhang et al, 2017; Zhang & Matlashewski, 2015). The CRISPR-Cas 9 system was originally discovered as an adaptive defense system in bacteria and archaea against invasion by foreign DNA such as plasmids or viruses and has been developed as a molecular genetic tool (Doudna & Charpentier, 2014). It consists of a guide RNA (gRNA) that targets the nuclease activity of the Cas 9 protein to a specific DNA site in the target genome, resulting in double stranded DNA breaks (DSBs). The subsequent DSBs repair can be harnessed to modify the target DNA region (such as mutation, deletion, addition of an epitope tag).

In the first published study using the CRISPR-Cas9 system in *Leishmania*, an *L. major* PFR2 null mutant was generated in which the PFR2 locus, composed of three tandemly linked genes was replaced by a puromycin resistant gene. The approach employed two plasmids, subsequently transfected in *L. major* promastigotes: the first plasmid bore the Cas9 gene and the

hygromycin resistance gene, while the second one contained the sequences coding for the gRNA and the puromycin resistance gene flanked by two fragments corresponding to sequences flanking the PFR2 locus (Sollelis et al, 2015). A similar approach was used successfully to induce deletions in the *L. donovani* miltefosine transporter gene (*LdMT*) or to delete the entire gene, in absence of a DNA template, or to insert specific mutations, a drug resistance gene or an epitope tag such as GFP in specific sites of the *L. donovani* genome (Zhang & Matlashewski, 2015). Furthermore, the CRISPR-Cas 9 system allowed the specific deletion of the A2 gene family, which had been impossible to achieve with the conventional gene replacement method due to the alternance of the multiple copies of the A2 gene with the A2rel gene (Zhang et al, 2017). The technique was further optimized with the generation of a single vector co-expressing the Cas9 gene and the gRNA, which up until then were expressed on two different plasmids requiring two rounds of transfection (Zhang et al, 2017). Moreover, a library of plasmids was created to facilitate the PCR amplification of cassettes expressing gRNAs and of DNA donor cassettes for high-throughput deletion or tagging of genes in *Leishmania* (Beneke et al, 2017).

The on-going optimization of the new CRISPR-Cas9 system makes it more advantageous than the double gene target replacement technique, such as being less time-consuming and labour-intensive, in addition to offering a variety of options to manipulate the *Leishmania* genome. It is likely to become the method of choice and dramatically help our understanding of *Leishmania* biology.

### **1.5 The *L. mexicana* A600 gene family**

Since amastigotes constitute the form of the parasite that contributes to the disease, the study of amastigote-specific genes may provide better understanding of the mechanisms that

cause leishmaniasis and therefore lead to the identification of novel targets for potential therapies.

In the search for amastigote-specific genes, our laboratory used a suppression-subtraction PCR (SS-PCR) method, using cDNA from *L. mexicana* axenic promastigotes (driver) and amastigotes (tester) (Bellatin et al, 2002). This technique allows the PCR amplification of only cDNA fragments of the tester sample (amastigotes) that differ from the driver sample (promastigotes). Among the fragments identified, eight were found to be more abundant in amastigotes than in promastigotes. Further analysis of the four more abundant bands found that they corresponded to 3' untranslated region (UTR) sequences. One of them was part of the 3'UTR of a gene encoding for a  $\beta$ -tubulin. Two of them were non-contiguous sequences of the same 3'UTR and the identification of the corresponding transcript led to the discovery of an open reading frame (ORF) of 282 bp which was named *A600* that encodes a novel protein predicted to contain 93 amino acids with a molecular mass of 10.46 kDa (Bellatin et al, 2002).

Southern blot analysis of *L. mexicana* genomic DNA using the *A600* coding region or one of the 3'UTR cDNA fragments as probes indicated that the *A600* gene was present in multiple copies that were all contained in a single XhoI DNA fragment of about 14 kb (Bellatin et al, 2002). Further restriction digestion of the *A600* locus found that it contained four coding sequences that were named based on their relative position to the 5' end of the locus: the most proximal gene is referred to as *A600.1*, followed by the *A600.2* and *A600.3* genes, positioned in the middle of the locus. The most distal gene, *A600.4*, corresponds to the 282-bp ORF identified initially due to the abundance of its 3'UTR cDNA fragment in amastigotes (Figure 1.4) (Murray et al, 2010).

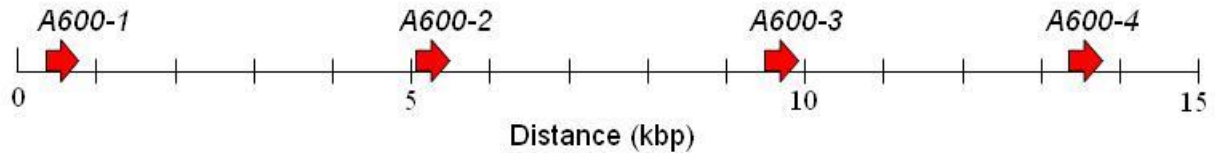


**Figure 1.4: Map of the *A600* locus.**

The four *A600* ORFs are represented by the red arrows (Murray et al, 2007).

The complete sequence of the *A600.1* and *A600.4* genes as well as the 3' UTR and downstream intergenic regions were determined. The *A600.1* and *A600.4* ORFs were found to share 78% nucleotide sequence identity but no significant sequence identity was seen between their 3'UTR sequences. The predicted *A600.1* and *A600.4* proteins shared only 55% sequence identity. Alignment of the predicted amino acid sequences of the proteins encoded by the *A600.1*, *A600.2* and *A600.3* genes indicate that the *A600.1* and *A600.2* proteins are 100% identical, while the *A600.3* protein share 99% sequence identity (Figure 1.5) (Murray et al, 2010).

```

A600.1  MPSMLNLVPATAIAVGAIALPAAATTTTAAAPVPVNLRLNIITAVLILGVS LVLTLVYTLWKLLPRIRSG 70
A600.2  MPSMLNLVPATAIAVGAIALPAAATTTTAAAPVPVNLRLNIITAVLILGVS LVLTLVYTLWKLLPRIRSG 70
A600.3  MPSMLNLVPATAIAVGAIALPAAATTTMTAAPVPVNLRLNIITAVLILGVS LVLTLVYTLWKLLPRIRSG 70
A600.4  MPSMLNLVPAV-----ET TMT RT P MY V EVR VNAV PLMMVF GVS LVLALVYTLWKLLPRIRSG 57
*****.          ** * :*: *::*: * . . ::::*****:*****

A600.1  ELSFSKFEFDWRAELLNQTPKKEKARRATEKARREEMASGCNRDNDGRVQYAHTQPRVEVGEEDAAAA 140
A600.2  ELSFSKFEFDWRAELLNQTPKKEKARRATEKARREEMASGCNRDNDGRVQYAHTQPRVEVGEEDAAAA 140
A600.3  ELSFSKFEFDWRAELLNQTPKKEKARRATEKARREEMASGCNRDNDGRVQYAHTQPRVEVGEEDAAAA 140
A600.4  ELSSNTEANFRAGLLNRKLRKREKVRSEDDSS----- 89
*** *: * ::** ***:. *::** * :.:

A600.1  RSQRKGQRHVEADVSVAVTVPRE 163
A600.2  RSQRKGQRHVEADVSVAVTVPRE 163
A600.3  RSQRKGQRHVEADVSVAVTVPRE 163
A600.4  -----AD-----MV--- 93
          **      *

```

**Figure 1.5: Alignment of the four *L. mexicana* *A600* predicted protein sequences.**

The alignment was performed using the T-Coffee multiple sequence alignment. Highly conserved amino acids are indicated in black and signaled by an asterisk. Less conserved amino acids are indicated in red.

Blastp searches based on the predicted amino acid sequences of the A600 proteins were conducted in the three *Leishmania* genomes: *L. infantum*, *L. major* and *L. braziliensis*. In all three species, two ORFs were identified: a longer sequence corresponding to the A600.1 protein and a shorter one corresponding to the A600.4 protein. The A600 genes in those three species are arranged in the same order as in the *L. mexicana* genome. Further analysis of the predicted amino acid sequences indicated that the A600.1 and A600.4 proteins do not contain any regions with conserved motifs or functional domains. However, it was predicted that the A600.1, A600.2 and A600.3 proteins contain two potential hydrophobic transmembrane domains, whereas the A600.4 protein has a single transmembrane domain (Figure 1.6). Two orthologs of A600.1, annotated as hypothetical proteins, were found in two species of the *Leptomonas* genus, *Leptomonas seymouri* and *Leptomonas pyrrocoris*, which are monoxenous insect trypanosomatids, which, along with the genera *Crithidia*, *Lotmaria* and *Leishmania*, belong to the subfamily Leishmaniinae. No orthologs of the A600 gene family was identified in the closely related trypanosomatids, *T. brucei* and *T. cruzi*, or in other species outside of the *Trypanosomatidae* family (Flegontov et al, 2016; Murray et al, 2010). In the absence of a conserved domain or motif and of a characterized homolog, the function of this novel gene family could not be inferred.

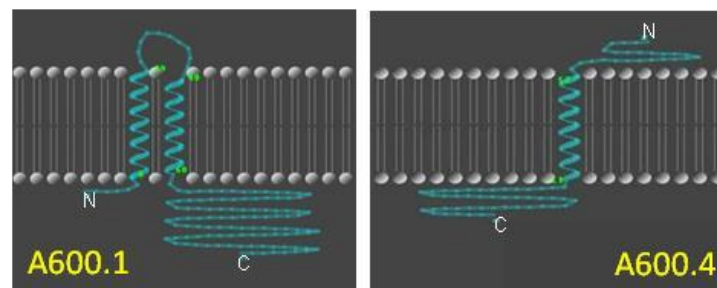


**Figure 1.6: Predicted membrane topology of the *L. mexicana* A600.1 and A600.4 proteins.**

Northern blot analysis of total RNA from promastigotes and lesion and axenic amastigotes found that the *A600.1* gene expression was about 1.5-fold upregulated in amastigotes, whereas the *A600.4* transcript was about 6-fold more abundant in amastigotes (Murray, 2005). In order to elucidate their function, a targeted deletion of this gene family was performed by homologous recombination. The deletion did not affect the *in vitro* proliferation of the promastigotes, as the *A600<sup>-/-</sup>* deficient mutants proliferate at the same rate as the wild-type (*WT*) promastigotes. However, five days after induction of promastigotes differentiation into amastigotes, the *A600<sup>-/-</sup>* amastigotes stopped multiplying, while the *WT* amastigotes continue to proliferate. Re-introduction of the *A600.1* gene in the *A600<sup>-/-</sup>* mutants (the cells were designated *A600<sup>-/-</sup>+A600.1*) partially restored the ability of the amastigotes to proliferate, but at a lower rate than the *WT*. The re-introduction of the *A600.4* gene (the cells were designated *A600<sup>-/-</sup>+A600.4*) however, did not complement the proliferation defect of the mutant amastigotes (Murray et al, 2010). When macrophages were infected with the *WT* and *A600<sup>-/-</sup>* parasites, the intra-macrophage parasite burden was initially similar in both groups but after 120h post-infection, the parasite burden of macrophages infected with the *A600<sup>-/-</sup>* parasites was much lower than for those infected with the *WT* parasites. This suggests that the *A600<sup>-/-</sup>* infective promastigotes infect macrophages at the same rate as the *WT*, but then cease to replicate as intracellular amastigotes. *A600<sup>-/-</sup>+A600.1* amastigotes were able to proliferate in macrophages, although at a lower rate than the *WT*. Re-introduction of the *A600.4* gene in the null mutants did not restore their ability to replicate. Taken together, these results indicate that the *A600* gene family is involved in a pathway that is important for the development of the mammalian stage of the parasite and that the presence of at least the *A600.1* gene is necessary for their successful replication. Such

pathway may not be essential or can be by-passed in the promastigote stage, since promastigotes are not affected by the deletion of the *A600* genes (Murray et al, 2010). Northern blot analysis of the *A600*<sup>-/-</sup>+*A600.4* mutants revealed that transcription of the *A600.4* gene from the episomal *pLexNeo-A600.4* plasmid resulted in an mRNA that was larger than expected, which suggests that the *A600.4* gene may not be translated efficiently in those cells (Murray, 2005). This may account for the absence of rescue of the knock-out phenotype in those cells, which could also be due to the *A600.4* protein requiring the presence of the other *A600* proteins or at least *A600.1* to function.

## **1.6 Thesis hypothesis and specific aims**

Research in our laboratory identified an *L. mexicana* family of four tandemly linked genes, the *A600* locus, that exhibit an upregulated expression in amastigotes. Targeted gene deletion studies showed that those genes are important for amastigotes replication, both *in vitro* and in macrophages (Murray et al, 2010). These findings make this novel gene family an interesting target for further investigation into understanding amastigote biology and virulence.

The objective of my thesis was to further the characterization of this gene family, by investigating the function of the *L. mexicana* *A600.1* and *A600.4* proteins in amastigotes development. Since the *A600.2* and *A600.3* proteins are predicted to share 100% and 99% sequence identity respectively with the *A600.1* protein, while the *A600.4* protein share 55% sequence identity with *A600.1*, my research focused on the study of the latter two proteins. I hypothesized that the *A600* proteins are part of a multi-protein complex or pathway that is involved in amastigotes development.

### **1.6.1 Objective 1**

The expression of the *A600.1* and *A600.4* genes has been characterized at the mRNA level. However, evidence suggests that gene expression in *Leishmania* is predominantly regulated at the translational and post-translational level and mRNA abundance may not reflect the expression profile of the corresponding protein. Since the *A600*<sup>-/-</sup> phenotype was observed in amastigotes, I hypothesized that the A600 proteins may be upregulated in amastigotes compared to promastigotes. Therefore, antibodies were produced against the *L. mexicana* A600.1 and A600.4 proteins to characterize their expression profile at different stages of the parasite life cycle and to determine their subcellular localization.

### **1.6.2 Objective 2**

Since amastigotes exhibited a proliferation defect in the absence of the *A600* genes, and this phenotype appeared in the late stage of differentiation of the parasite into amastigotes, I hypothesized that the A600 proteins may be involved in a metabolic process that is essential for the survival of the parasite in the phagolysosome. The metabolic activities of the *A600*<sup>-/-</sup> amastigotes were assayed and compared to the *WT* amastigotes to determine the cellular pathway in which the A600 proteins are involved.

### **1.6.3 Objective 3**

Most of the cellular proteins are predicted to function in collaboration with other proteins, either within a complex or through protein-protein interactions. Due to the small sizes of the A600.1 and A600.4 protein (17.8 and 10.4 kDa, respectively) and the fact that they are predicted to be transmembrane proteins, I hypothesized that the A600 proteins may serve as membrane

anchors for a multi-protein complex. Therefore, two pull-down assay approaches were employed to isolate and identify potential A600 interacting proteins.

## Chapter 2: Material and methods

### 2.1 *Leishmania* strains

Experiments were performed using the *Leishmania mexicana* WT strain MNYC/BZ/62/M379 and the derived *Leishmania mexicana* A600<sup>-/-</sup> mutants generated by A. Murray, as described in (Murray et al, 2010).

### 2.2 *Leishmania* culture

Promastigotes were cultivated at 26°C in M199 medium (Hyclone, Thermo Fisher Scientific, USA) supplemented with 10% heat inactivated (30 min at 56°C) fetal calf serum (Hyclone, Thermo Fisher Scientific, USA), 25 mM HEPES (Cellgro, Corning, USA), 10 mM hemin (Millipore Sigma, USA) and 10 U/mL penicillin + 10 µg/mL streptomycin (Hyclone, Thermo Fisher Scientific, USA).

Axenic amastigotes cultures were obtained by subculturing stationary-phase promastigotes (day 5) at  $5 \times 10^5$  cells/ml, in Schneider's *Drosophila* medium (Gibco, Thermo Fisher Scientific, USA) at pH 5.5, supplemented with 20% heat inactivated fetal calf serum, 20 mM 2-(N-Morpholino)ethanesulfonic acid (MES) (Millipore Sigma, USA) and 10 U/mL penicillin + 10 µg/mL streptomycin. Parasites were considered to be fully differentiated into amastigotes after 6 days at 32°C in that medium.

### 2.3 Isolation of *L. mexicana* genomic DNA

*L. mexicana* genomic DNA was isolated as described in (Medina-Acosta & Cross, 1993). All the steps were carried out at room temperature. Briefly, *L. mexicana* WT promastigotes at

logarithmic phase ( $1 \times 10^7$  to  $1 \times 10^8$  cells) were collected and centrifuged at  $3,000 \times g$  for 10 minutes. The cell pellet was resuspended in 150  $\mu\text{L}$  of lysis buffer (50 mM Tris-HCl, pH 8; 62.5 mM EDTA, pH 8; 2.5 M LiCl; 4% (v/v) Triton X-100). After a five-minute incubation, an equal volume of a water-equilibrated phenol/chloroform (1:1 v/v) solution was added. The lysate was then centrifuged at  $12,000 \times g$  for 5 minutes. The upper clear phase was collected into a new tube and the genomic DNA it contained was precipitated by addition of 300  $\mu\text{L}$  of absolute ethanol. The mixture was gently mixed for 15 seconds and incubated for 5 minutes. The nucleic acids were sedimented by centrifugation at  $12,000 \times g$  for 10 minutes. After removal of the supernatant, the DNA pellet was washed with 1 mL of absolute ethanol and centrifuged for 5 minutes at  $12,000 \times g$ . After vacuum-drying for 10 minutes, the DNA was dissolved in 50  $\mu\text{L}$  of EB Buffer (10 mM Tris-HCl, pH 8.5) (Qiagen, USA). The concentration of DNA in solution was determined with a NanoDrop 1000 spectrophotometer (Thermo Fisher Scientific, USA).

## **2.4 Cloning of the *A600.1* and *A600.4* genes into the pGEX vector**

### **2.4.1 Polymerase Chain Reaction amplification of the *A600* genes**

The *A600.1* and *A600.4* genes were respectively amplified from the *L. mexicana* WT genomic DNA by Polymerase Chain Reaction (PCR) using the following primers. The primers were designed so that the amplicon contained the *A600.1* or *A600.4* open reading frame (ORF) flanked by an EcoRI restriction site in its 5' end and an XhoI restriction site in its 3' end (cf. Appendix A and B for the *L. mexicana* *A600.1* and *A600.4* genes coding sequences).

- For the *A600.1* ORF:

Forward primer – CCGCGAATTCATGCCCTCTATGCTCAACC (the EcoRI restriction site is underlined)

Reverse primer – ATGCTCGAGCTACTCGCGGGGCACCGT (the XhoI restriction site is underlined)

- For the *A600.4* ORF:

Forward primer - GCTGAATTCATGCCCTCTATGCTCAACC

Reverse primer - ATGCTCGAGTTACACCATGTCCGCAGA

A third set of primers was designed to amplify the *A600.1* sequence that encodes the C-terminal region of the *A600.1* protein without the N-terminal portion predicted to contain two transmembrane domains (region between amino acids 1-64) (Figure 2.2). The resulting amplicon was designated  $\Delta N.A600.1$ :

Forward primer – TAGCGAATTCATGCCGAGGATCCGCAGTGG

Reverse primer – ATGCTCGAGCTACTCGCGGGGCACCGT (same reverse primer as for the entire *A600.1* coding region amplification).

The PCR reactions were set up with the following conditions: 25 ng genomic DNA, 1x PCR buffer (Qiagen, USA), 0.5 mM MgCl<sub>2</sub> (1 mM for the *A600.1* ORF amplification), 0.2 mM dNTP mix (dATP, dCTP, dGTP, dTTP), 1 μM forward primer, 1 μM reverse primer, 2.5 units HotStarTaq DNA polymerase (Qiagen, USA) in a 50 μL final volume. The reactions were carried out in the Veriti 96-well Thermal cycler (Applied Biosystems, USA). For the amplification of the *A600.1* ORF, the reaction started with an initialisation step at 95°C for 5 minutes, followed by denaturation at 94°C for 40 seconds, annealing at 55°C for 40 seconds and elongation at 72°C for 60 seconds. The denaturation, annealing and elongation steps were repeated for 39 cycles. The final elongation step was performed at 72°C for 10 minutes. In the

reaction with the  $\Delta N.A600.1$  primers, the annealing step was carried out for 60 seconds. For the amplification of the *A600.4* ORF, the denaturation and annealing steps were performed for 30 seconds each. The denaturation, annealing and elongation steps were repeated for 35 cycles. The PCR products were purified using the Qiagen MinElute PCR purification Kit (Qiagen, USA), following the manufacturer's instructions.

#### **2.4.2 Insertion of the *A600* ORFs in the pGEX vector**

In order to generate the GST-A600.1, GST-A600.4 and GST- $\Delta N.A600.1$  fusion proteins, the corresponding coding regions were each inserted into the multiple cloning site of a pGEX vector, pGEX-6P-1 (GE Healthcare, USA), downstream of and in frame with the GST (glutathione S-transferase) gene and the PreScission Protease cleavage site (Figure 2.1).

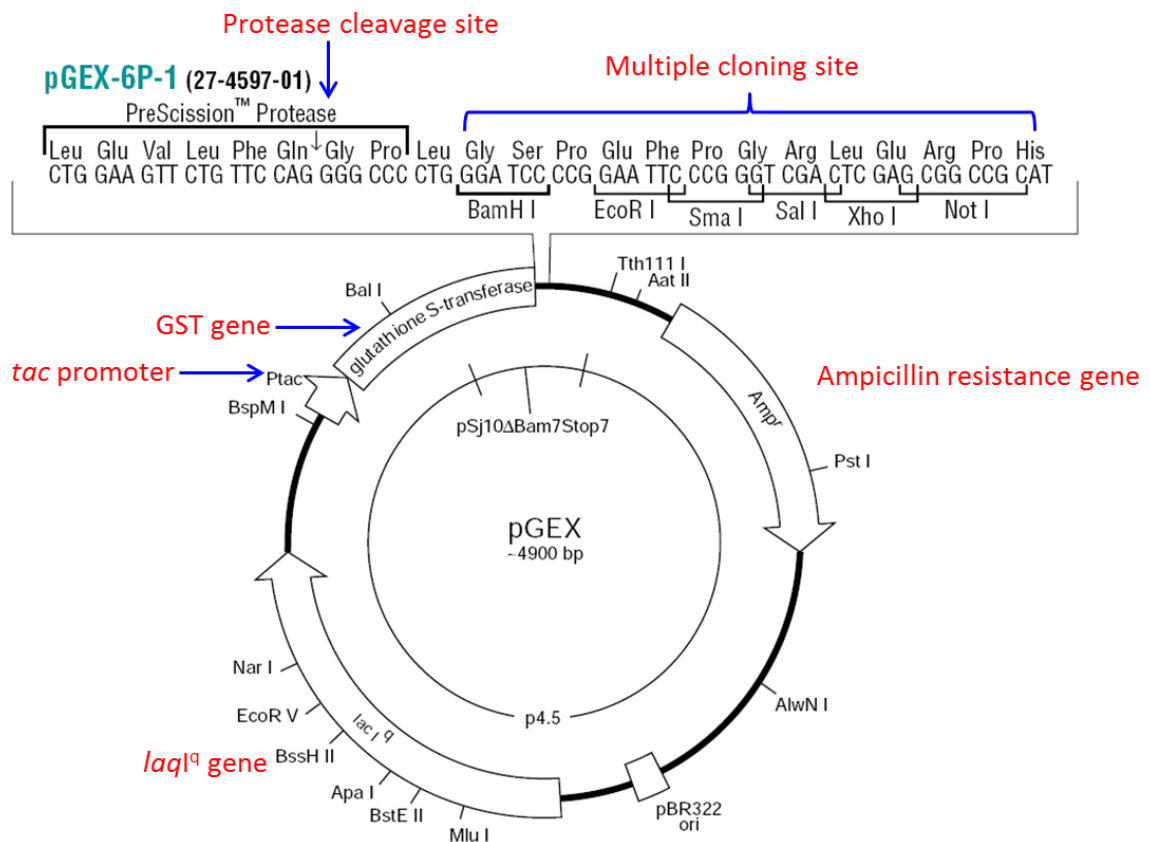


**Figure 2.1: Map of the glutathione S-transferase fusion vector, pGEX-6P-1.**

The vector contains a GST gene which expression is under the control of the inducible *tac* promoter, followed by a PreScission Protease cleavage site and a multiple cloning site. The *lacI<sup>q</sup>* gene encodes for a repressor protein that binds to the *tac* promoter, preventing expression of the GST gene. In presence of IPTG, the repressor protein binding to the *tac* promoter is inhibited, allowing expression of the GST gene (Adapted from the *GST Gene Fusion System* handbook, GE Healthcare).

The purified PCR products and the pGEX vector (~2 µg) were each digested at 37°C overnight by incubation with 40 U of each of the restriction enzymes EcoRI and XhoI (New England Biolabs, USA), in presence of 0.1 mg/ml BSA and 1x NEB EcoRI buffer (100 mM Tris-HCl, 50 mM NaCl, 10 mM MgCl<sub>2</sub>, 0.025% Triton X-100, pH 7.5) in a final volume of 20 µL.

After purification of the digestion products using the Qiagen MinElute PCR Purification Kit (Qiagen, USA), each digested PCR amplicon was ligated into the pGEX vector, using a vector to insert ratio of 1:3 moles of ends; 0.03 pmoles of ends (50 ng) of digested pGEX vector was mixed with 0.09 pmoles of ends of either of the digested *A600* amplicons (8 ng of *A600.4*, 14 ng of *A600.1* or 3 ng of *ΔN.A600.1*), in presence of 3 U of T4 DNA Ligase (Promega, USA) in 2x Rapid Ligation Buffer (Promega, USA) in a final volume of 10 μL. The reaction was incubated overnight at 4°C. Each ligation reaction was diluted 5-fold in 10 mM Tris-HCl, pH 7.5 + 1 mM EDTA and 1 μl of this dilution was used to transform by heat-shock 100 μl of CaCl<sub>2</sub>-competent *E. coli* cells of the DH5α strain (Invitrogen, USA), following the manufacturer's instructions. Briefly, after addition of the DNA, the cells were incubated on ice for 30 minutes, heat-shocked for 45 seconds in a 42°C water bath and placed on ice for 2 minutes. Following the addition of 0.9 mL of SOC medium, the cells were incubated for 1 hour at 37°C with shaking. Successfully transformed clones were selected on LB Agar plates containing 100 μg/ml ampicillin after overnight incubation at 37°C. Plasmid DNA from the positive clones was isolated using the QIAprep Spin Miniprep Kit (Qiagen, USA) and screened by PCR or double digestion with EcoRI and XhoI for the presence of the appropriate *A600* insert.

## **2.5 Purification of the GST fusion proteins**

### **2.5.1 Production of the GST fusion proteins**

The *E. coli* BL21(DE3) strain is protease-deficient, and therefore is the recommended strain for expression of recombinant fusion proteins in *E. coli*. Isolated plasmids found to contain the desired insert were used to transform CaCl<sub>2</sub>-competent BL21 cells, as described for the

transformation of the DH5 $\alpha$  cells. The plasmid DNA from the BL21 clones selected on LB Agar plates containing ampicillin were isolated as before by miniprep and were screened by DNA sequencing to check the correct insertion of the *A600* ORF into the pGEX vector (Macrogen, USA). The BL21(DE3) clones found to contain the pGEX vector with the *A600.1*, the *A600.4* or the  $\Delta N.A600.1$  insert were designated as BL21+pGST-A600.1, BL21+pGST-A600.4 and BL21+pGST- $\Delta N.A600.1$ , respectively. Clones transformed with the pGEX vector only were designated BL21+pGST.

The GST fusion proteins were produced as described in (Cherkasov et al, 2011). A single colony from the chosen BL21 clone (BL21+pGST-A600.1, BL21+pGST-A600.4, BL21+pGST- $\Delta N.A600.1$  or BL21+pGST) was used to grow an overnight culture in 2x YT medium (16 g/L tryptone, 10 g/L yeast extract, 5 g/L NaCl) containing 100  $\mu$ g/mL of ampicillin. The culture was then diluted at 1:100 in 2x YT medium with 100  $\mu$ g/mL of ampicillin and grown at 37°C with agitation until an OD600 of 0.5-1 was reached. For the production of the GST fusion proteins GST-A600.1, GST-A600.4 and GST- $\Delta N.A600.1$ , the culture was left to cool down without shaking for one hour at room temperature. The expression of the proteins was induced by addition of 0.3 mM Isopropyl  $\beta$ -D-1-thiogalactopyranoside (IPTG) and incubation of the culture for 4-5 hours at room temperature with shaking. For the production of the GST protein, once an OD600 of 0.5-1 was reached, the protein expression was induced with 0.5 mM of IPTG and incubation was carried out at 37°C. The bacteria were sedimented by centrifugation at 6,000 x g for 20 minutes at 4°C and lysed in 10 mL lysis buffer per 100 ml of culture (20 mM Hepes pH 7.6, 100 mM KCl, 0.2 mM EDTA, 100  $\mu$ g/mL lysozyme, 20% (v/v) glycerol, 0.5% (v/v) Nonidet-40 and 2 mM DTT) containing Complete EDTA-Free protease inhibitor cocktail

(Roche, USA). After a 30-minute incubation on ice, the lysate was sonicated. To help the solubilisation of the fusion protein, 1% Triton X-100 was added to the lysate, followed by gentle mixing for 30 minutes at 4°C and centrifugation at 48,400 x g for 20 minutes at 4°C. The lysate supernatant (soluble fraction) was collected and used for the purification of the GST tagged proteins or of the recombinant A600.1 and A600.4 proteins.

### **2.5.2 Purification of the GST tagged proteins**

For the purification of the GST and of the GST fusion proteins, the appropriate bacterial soluble fraction was incubated for 5 minutes at room temperature with 2 mM ATP and 10 mM MgCl<sub>2</sub> to reduce non-specific binding. Glutathione Sepharose 4B beads (GE Healthcare, Sweden) were added to the lysate soluble fraction at 1 mL per 200 mL of lysate. The mixture was incubated overnight at 4°C with end-to-end rotation. After collection of the unbound fraction, the beads were washed four times with 10 mL of PBS per mL of beads volume. The GST or GST fusion proteins were eluted after incubation at 4°C for at least 1 hour with end-to-end rotation in presence of 1 mL of 30 mM reduced glutathione (in 50 mM Tris-HCl, pH 8) per mL of beads volume. The elution step was repeated twice more and the three eluates were pooled. The eluted proteins were dialysed against PBS, using the Pierce Slide-A-Lyzer Dialysis Cassettes (Thermo Fisher Scientific, USA), according to the manufacturer's instructions.

### **2.5.3 Purification of the recombinant A600.1 and A600.4 proteins**

After overnight incubation of the BL21+pGST-A600.1 or BL21+pGST-A600.4 bacterial soluble fraction with the Glutathione Sepharose 4B beads, the beads were washed three times with 10 mL of PBS per mL of beads volume and twice with cleavage buffer (50 mM Tris-HCl, pH 7.0; 150 mM NaCl; 1 mM EDTA; 2 mM DTT; 0.05% Triton X-100; 2 mM DTT). The

A600.1 or A600.4 proteins were eluted from the beads after incubation for 5 hours at 4°C with 160 U of PreScission Protease (GE Healthcare, USA) per mL of beads volume in 1 mL of cleavage buffer per mL of beads volume.

Protein production and purification was monitored by analysis of the different bacterial fractions and eluates by SDS-PAGE and Western Blot with the rabbit anti-GST antibody (Millipore Sigma, USA). Protein concentration was determined with the Pierce BCA Protein Assay Kit (Thermo Fisher Scientific, USA).

## **2.6 Generation of polyclonal antibodies**

### **2.6.1 Generation of anti-A600.1 antibodies**

The expertise of the biotechnology company GenScript was used to design an antigenic peptide and generate an antibody specific for the A600.1 protein. Using their antigen design program and based on the alignment of the A600.1 and A600.4 protein sequences, they identified two antigenic sequences from the A600.1 sequence susceptible to produce antibodies unlikely to cross-react with the A600.4 protein (Figure 2.2). Antigens synthesis and conjugation to Keyhole Limpet Hemocyanin (KLH), immunization of rabbits (n=2) using a proprietary immunization adjuvant, and affinity-purification of the antibodies from the rabbit sera were performed by GenScript. The specificity of the isolated antibodies for the A600.1 protein was tested by ELISA and Western Blot.

### **2.6.2 Generation of an anti-A600.4 antibody**

An A600.4 antigen peptide was designed following the same method used to design antigens to generate anti-A600.1 specific antibodies. Only one antigenic sequence could be



stock solution was diluted at 1:1,000, followed by seven five-fold serial dilutions in PBS with 0.5% BSA. After three washes with PBS + 0.05% Tween-20, the wells were incubated with 100  $\mu$ L of the serial dilutions of the antibody for one hour at room temperature. After washing with PBS + 0.05% Tween-20, 100  $\mu$ L of anti-rabbit IgG horseradish peroxidase (HRP)-conjugated antibody diluted at 1:1,000 in PBS + 0.5% BSA were added. The plate was incubated for one hour at room temperature then washed as before. Detection was performed by the addition of 100  $\mu$ L of 3,3',5,5'-Tetramethylbenzidine (TMB) substrate, diluted at 1:20 in citrate buffer (36 mM citric acid anhydrous, pH 4.1) in presence of 0.018% of hydrogen peroxide. During a 20-minute incubation in the dark, the oxidation of TMB by the HRP in presence of hydrogen peroxide led to the formation of a blue-green color. The reaction was stopped by adding 50  $\mu$ L of 1 M HCl. The absorbance in each well was measured at 450 nm, using an Epoch Microplate Spectrophotometer (BioTek Instruments, USA).

## **2.8 Western Blot**

### **2.8.1 Preparation of bacterial samples**

Aliquots of the different bacterial fractions were collected during production and purification of the recombinant proteins from the transformed BL21 *E.coli* clones. 5-mL aliquots of the bacterial cultures were collected before and at the end of the induction of protein expression (following addition of IPTG). After centrifugation at 6,000 x g for 20 minutes at 4°C, the pelleted bacteria were resuspended in 0.5 mL of 5x sample buffer (250 mM Tris-HCl pH 6.8; 10% SDS; 50% (v/v) glycerol; 0.1% bromophenol blue; 0.1 M DTT). Aliquots of the lysates and eluates were supplemented with an equivalent volume of 5x sample buffer. The protein concentration of the bacterial fractions could not be determined due to interference of the Hepes

lysis buffer with the Pierce BCA Protein Assay Kit assay used (Thermo Fisher Scientific, USA). Therefore, the amount of samples to load on SDS PAGE gels was determined empirically.

### **2.8.2 Preparation of *Leishmania* whole cell lysates**

Protein lysates were prepared from promastigotes and axenic amastigotes of the different *L. mexicana* strains. The cells were collected and washed twice in PBS by centrifugation at 3,000 x g for 10 minutes. They were resuspended at 4–5 x 10<sup>8</sup> cells/ml in 5% SDS and boiled at 95°C for 5 minutes. The samples were left to cool down at room temperature before being stored at -80°C until analysis. The Pierce BCA Protein Assay Kit (Thermo Fisher Scientific, USA) was used to determine the samples protein concentration. Samples were supplemented with 5x sample buffer.

### **2.8.3 SDS-PAGE**

For the detection of proteins with a molecular mass above 30 kDa, the Laemmli-SDS-PAGE buffer system was used (Laemmli, 1970). For the detection of proteins smaller than 30 kDa, samples were separated by Tricine-SDS-PAGE (Schagger, 2006). Unless otherwise specified, 30 µg of proteins were loaded per lane on 12% SDS-PAGE gels, using the mini-Protean system (Biorad, USA). The electrophoresis was started at 30 V. Once all the samples had completely entered the stacking gel, the voltage was increased to 50 V and then to 90 V once all samples were in the resolving gel.

### **2.8.4 Immunodetection**

Proteins were transferred to a polyvinylidene fluoride (PVDF) membrane (Biorad, USA) for one hour at 100 V on ice or overnight at 30 V at 4°C, by wet transfer (48 mM Tris-HCl; 39 mM glycine; 20% methanol, 0.0375% SDS; pH 9) with stirring. The membrane was then

blocked for one hour in Odyssey blocking buffer (Licor, USA), before being incubated overnight at 4°C or for at least one hour at room temperature with the appropriate primary antibody diluted in Odyssey blocking buffer (Table 2.1). After three 10-minute washes in TBS-T (0.1% Tween in TBS), the membrane was incubated for one hour with the Alexa Fluor 680 goat anti-rabbit (Life Technologies, USA) or with the IRDye 800CW goat anti-mouse secondary antibody (Licor, USA) diluted at 1:10,000 in the Odyssey blocking buffer. The membrane was then washed three times in TBS-T and proteins were detected by scanning the blot with the Odyssey CLx Imager (Licor, USA). The primary antibodies used are listed in Table 2.1.

**Table 2.1: List of primary antibodies used for Western blot analysis after SDS-PAGE**

<b>Protein target</b>	<b>Target host</b>	<b>Antibody Host</b>	<b>Source</b>	<b>Reference</b>
<b>GST</b>	Protein from the pGEX expression vector	Rabbit	Upstate Biotechnology (MilliporeSigma, USA)	(Kivens et al, 1998)
<b>A600.1</b>	<i>L. mexicana</i>	Rabbit	GenScript, USA	NA
<b>A600.4</b>	<i>L. mexicana</i>	Rabbit	GenScript, USA	NA
<b><math>\alpha</math>-tubulin</b>	bovine	Mouse	Thermo Fisher Scientific, USA	(Foucher et al, 2006)
<b>APRT*</b>	<i>L. donovani</i>	Rabbit	Dr J. Boitz	(Zarella-Boitz et al, 2004)
<b>BiP**</b>	<i>T. brucei</i>	Rabbit	Dr J. Bangs	(Bangs et al, 1993)
<b>COIV***</b>	<i>L. tarentolae</i>	Rabbit	Dr E. Horakova	(Maslov et al, 2002)
<b>Cyt c****</b>	<i>L. major</i>	Rabbit	Dr A. Debrabant	(Gannavaram et al, 2008)
<b>HGPRT*****</b>	<i>L. donovani</i>	Rabbit	Dr J. Boitz	(Shih et al, 1998)
<b>Enolase</b>	<i>T. brucei</i>	Rabbit	Dr E. Horakova	(Hannaert et al, 2003)
<b>mtHSP70*****</b>	<i>T. brucei</i>	Mouse	Dr S. McDermott	(Panigrahi et al, 2008a)
<b>p27</b>	<i>L. donovani</i>	Rabbit	Dr R. Duncan	(Dey et al, 2010)

\*APRT: adenine phosphoribosyltransferase

\*\*BiP: binding protein

\*\*\* COIV: cytochrome c oxidase subunit IV

\*\*\*\*Cyt c: cytochrome c

\*\*\*\*\*HGPRT: hypoxanthine-guanine phosphoribosyltransferase

\*\*\*\*\*mtHSP70: mitochondrial heat-shock protein 70

## **2.9 Differential digitonin permeabilization**

*L. mexicana* WT amastigotes were lysed with different amounts of digitonin, as described by Skodova *et al* (Škodová et al, 2013) with some modifications. The cells were collected and centrifuged at 3,000 x g for 10 minutes at room temperature, then washed twice in STE wash buffer (250 mM sucrose; 10 mM Tris-HCl, pH 7.4; 1 mM EDTA). The protein concentration in

the final cell suspension was determined with the Pierce BCA Protein Assay Kit (Thermo Fisher Scientific, USA). Aliquots of the cell suspension corresponding to 375 µg of proteins were distributed in microcentrifuge tubes and the cells were pelleted by centrifugation at 3,000 x g for 10 minutes at room temperature. Each cell pellet was resuspended to a final concentration of 3 mg/ml with 125 µl of STE lysis buffer (250 mM sucrose; 25 mM Tris, pH 7.4; 1 mM EDTA) supplemented with protease inhibitors (10 mM 1,10-Phenanthroline, 10 µM E-64, 1x Roche Complete EDTA-free protease inhibitor cocktail, 100 µM iodoacetamide, 100 µM leupeptin, 1 mM Pefabloc). An equivalent volume of STE lysis buffer containing different concentrations of digitonin (at a final concentration of 0 - 6 mg/ml) and supplemented with protease inhibitors was added to each aliquot. The cell suspensions were incubated on ice for 5 minutes, and then centrifuged at 16,000 x g for 2 minutes at 4°C. The supernatants were collected, supplemented with 5x sample buffer to a 1x final concentration and analysed by Western blot. The anti-A600.1 peptide 2 antibody was used to detect the A600.1 protein.

## **2.10 Measurement of cellular ATP content**

Cellular ATP levels were measured in amastigotes cell lysates following the manufacturer's instructions of the ATP Bioluminescence Assay Kit CLS II (Roche, Germany). The cells were collected and centrifuged at 3,000 x g for 10 minutes. They were resuspended at  $2 \times 10^8$  cells/ml in TE buffer (100 mM Tris-HCl, 4 mM EDTA, pH 7.75). An aliquot was used to set up a  $2 \times 10^7$  cells/ml suspension in TE buffer. The cell suspensions were boiled at 100°C for 5 minutes. After being left to cool down at room temperature, the lysates were centrifuged at 1,000 x g for 5 minutes. The supernatants were collected in new tubes and placed on ice until analysis. ATP standards ( $10^{-11}$  to  $10^{-4}$  M ATP) were set up by serial dilutions in TE buffer. Each standard

and lysate was distributed in triplicates of 50  $\mu$ l per well on a Costar 96-well white clear bottom plate (Corning, Thermo Fisher Scientific, USA). 50  $\mu$ l of the reconstituted luciferase reagent was added to each sample and standard. The samples bioluminescence was measured with a Tecan Infinite 200 Pro luminescence plate reader (Tecan, Switzerland). The samples ATP concentrations were calculated from a log-log plot of the standards data, after subtracting the blank value (reading from the wells containing TE only) from all samples and standards readings.

### **2.11 Assessment of the mitochondrial redox activity**

The mitochondrial redox activity of the cells was evaluated using the Alamar Blue assay, following the manufacturer's instructions (Thermo Fisher Scientific, USA).  $1 \times 10^6$  cells resuspended at  $1 \times 10^7$  cells/ml were distributed in triplicates in a black 96-well polypropylene microplate (Greiner bio-one, VWR, Canada). After addition of 10  $\mu$ l of the Alamar Blue reagent, they were incubated at 32°C in the dark for 2.5 hours. The heat-killed samples, which served as negative controls, were incubated at 65°C for 40 minutes prior to incubation with Alamar Blue. The samples fluorescence was measured with the Infinite M200 plate reader (Tecan, Switzerland), using an excitation wavelength of 550 nm and an emission wavelength of 600 nm.

### **2.12 Measurement of the mitochondrial membrane potential**

The fluorescent dye tetramethylrhodamine methyl ester (TMRM) (Molecular Probes, Thermo Fisher Scientific, USA) was used to monitor the mitochondrial membrane potential ( $\Delta\Psi_m$ ) of amastigotes. The cells were washed twice in PBS by centrifugation at 3,000 x g for 10 minutes. They were resuspended at  $5 \times 10^7$  cells/ml in PBS. TMRM was added to each cell

suspension to a final concentration of 5 nM. After a 20-minute incubation at 32°C, the cells were centrifuged at 3,000 x g for 15 minutes and resuspended at  $5 \times 10^7$  cells/min in PBS. For cells treated with the protonophore FCCP (Carbonyl cyanide-4-(trifluoromethoxy)phenylhydrazone), the drug was added to the cells to a final concentration of 0.25 or 2  $\mu$ M; the treated cells were incubated for 10 minutes at 32°C, then stained with TMRM. Each cell suspension was distributed in triplicates of 100  $\mu$ l per well in a black 96-well polypropylene microplate (Greiner bio-one, VWR, Canada). Samples fluorescence was measured with the Infinite F500 filter-based plate reader (Tecan, Switzerland), using the excitation filter 535 +/- 25 nm and the emission filter 590 +/- 20 nm.

## **2.13 Native PAGE**

### **2.13.1 Isolation of crude organellar fractions**

Crude organellar fractions containing mitochondria were isolated by hypotonic lysis of amastigotes, as described elsewhere (Verner et al, 2014).  $10^9$  cells were harvested and washed in PBS by centrifugation at 3,000 x g for 10 minutes at room temperature. The following steps were performed at 4°C. The cell pellet was resuspended in 1.5 mL of NET buffer (150 mM NaCl; 100 mM EDTA; 10 mM Tris-HCl, pH 8) and left on ice for 10 minutes. After a 10-minute centrifugation at 16,000 x g, the cells were resuspended in 1.4 ml of DTE buffer (1 mM Tris-HCl pH 7.9; 1 mM EDTA). The cells swelling was monitored by phase contrast microscopy. When cells began to burst, the lysate was passed twice through a 26G needle and immediately transferred to a new tube containing sucrose to a final concentration of 0.25 M. After centrifugation at 16,000 x g for 10 minutes, the pellet was resuspended in 500  $\mu$ l of STM buffer

(250 mM sucrose; 20 mM Tris-HCl, pH 7.9; 2 mM MgCl<sub>2</sub>) with 10 µg/ml of DNase I and 3 mM MgCl<sub>2</sub>. The suspension was incubated for one hour on ice. The reaction was stopped by addition of an equivalent volume of STE buffer (250 mM sucrose; 20 mM Tris-HCl, pH 7.9; 2 mM EDTA) followed by centrifugation at 16,000 x g for 10 minutes. The organelle-enriched pellet was washed twice with STE buffer then stored at -80°C until analysis.

### **2.13.2 Lysis of the organellar fractions**

To solubilize the mitochondrial protein complexes, the crude organellar pellets were resuspended in STE buffer (250 mM sucrose; 20 mM Tris-HCl, pH 7.9; 2 mM EDTA) and the protein concentration was determined using the Pierce BCA Protein Assay Kit (Thermo Fisher Scientific, USA). The suspensions were centrifuged at 16,000 x g at 4°C for 20 minutes and the pellets were lysed with either dodecyl maltoside or digitonin.

For the lysis with dodecyl maltoside, the pellets were resuspended at 10 mg/ml in solubilisation buffer (750 mM aminocaproic acid; 50 mM Bis-Tris; 0.5 mM EDTA; pH 7) and 10% dodecyl maltoside to a final concentration of 2%. The samples were incubated on ice for one hour then centrifuged at 16,000 x g at 4°C for 30 minutes (Subrtova et al, 2015). The lysates supernatants were collected and their protein concentration measured by BCA assay.

For the solubilization of the protein complexes with digitonin, the organelle-enriched pellets were resuspended in lysis buffer (2 mM aminocaproic acid; 50 mM imidazole-HCl, pH 7; 1 mM EDTA; 50 mM NaCl) and digitonin was added at 4 mg per mg of mitochondrial proteins. Depending on the amount of proteins to load on the gel, the pellets were lysed at 10 or 20 mg/ml. The suspension was incubated on ice for two hours and centrifuged at 16,000 x g for 30 minutes (Subrtova et al, 2015; Wittig et al, 2007). The supernatant was collected and the protein concentration measured by BCA assay.

### **2.13.3 Electrophoresis**

#### ***2.13.3.1 Blue native PAGE***

The separation of the mitochondrial protein complexes by blue native electrophoresis was performed as described elsewhere (Schagger & von Jagow, 1991; Wittig et al, 2006). Coomassie blue loading dye (10x: 5% Coomassie Brilliant Blue G-250 (Biorad, USA) in 0.5 M 6-aminocaproic acid) was added to the crude organellar lysate supernatants to a 1x final concentration. The samples were incubated on ice for 10 minutes and then loaded on 3-12% gradient native gels (Thermo Fisher Scientific, USA) using the Invitrogen XCell SureLock Mini-Cell (Thermo Fisher Scientific, USA). Electrophoresis was done in presence of a cathode buffer containing 50 mM Tricine, 15 mM Bis-Tris-HCl pH 7, 0.02% Coomassie Blue G-250, and an anode buffer containing 50 mM Bis-Tris-HCl pH 7. The gel was run at 4°C, starting at 90 V, 9 mA for an hour, then the voltage was increased to 100 V, until the dye front reached the bottom of the gel (~5 hours).

#### ***2.13.3.2 High resolution clear native PAGE***

Each sample was supplemented with the 5x loading dye (1% Ponceau S in 50% glycerol) to a 1x final concentration and incubated on ice for 10 minutes. As for the blue native PAGE, the samples were loaded on 3-12% gradient native gels in the Invitrogen X-cell SureLock Mini-Cell. Electrophoresis was performed as described elsewhere (Wittig et al, 2007), using an anode buffer made of 25 mM imidazole, pH 7 and a cathode buffer with 50 mM Tricine, 7.5 mM imidazole, pH 7, 0.05% deoxycholate, 0.02% dodecyl maltoside. The electrophoresis was initiated at 90 V (9 mA) until the samples were focused in the gel. The voltage was then increased to 100 V, until the dye front reached the bottom of the gel.

#### **2.13.4 Blue-silver gel staining**

For Coomassie staining of the gel, 10-20 µg of proteins were loaded per lane. After electrophoresis, the gel was incubated overnight in fixative (40% ethanol, 10% acetic acid) with gentle shaking following the method described by Candiano *et al.* (Candiano et al, 2004). After two 5-minute washes in deionised water, the gel was stained for two hours in blue silver stain (12% Coomassie Brilliant Blue G-250 (Biorad, USA), 10% ammonium sulphate (Millipore Sigma, USA), 10% o-phosphoric acid (Thermo Fisher Scientific, USA), 20% Methanol (Thermo Fisher Scientific, USA)). It was then destained with successive washes in deionised water.

#### **2.13.5 In-gel activity staining**

For the visualization of the individual oxidative phosphorylation complexes, following separation of the mitochondrial complexes by hrCN-PAGE, the gel strips were incubated in the appropriate reaction buffer, as described elsewhere (Verner et al, 2014). Samples were loaded on native gel using 40-50 µg of proteins per lane (up to 75 µg for Complex V activity).

For the staining of Complex I, the gel strip was incubated in 100 mM Tris-HCl, pH 7.4, 0.14 mM NADH (β-Nicotinamide adenine dinucleotide) (Millipore Sigma, USA), 1 mg/ml NBT (nitrotetrazolium blue) (Millipore Sigma, USA) in the dark.

Complex II succinate dehydrogenase activity was detected by incubating the native gel in 50 mM sodium phosphate pH 7.4, 84 mM sodium succinate (Millipore Sigma, USA), 0.2 mM phenazine methosulfate (PMS) (Millipore Sigma, USA), 2 mg/ml NBT, 4.5 mM EDTA (Ethylenediaminetetraacetic acid), 10 mM potassium cyanide (KCN) (Millipore Sigma, USA).

Complex IV was stained using a reaction buffer containing 50 mM sodium phosphate pH 7.4, 1 mg/ml diamino benzidine (DAB) (Millipore Sigma, USA), 24 U/ml catalase (Millipore Sigma, USA), 1 mg/ml cytochrome c (Millipore Sigma, USA), 75 mg/ml sucrose.

For the Complex V  $F_1F_0$  ATPase activity staining, the gel was placed in 35 mM Tris-HCl pH 8, 270 mM glycine, 19 mM magnesium sulfate, 0.2% Lead (II) nitrate ( $Pb(NO_3)_2$ ), 8 mM ATP.

The gels were incubated overnight in the appropriate buffers at room temperature with gentle shaking. Except for the Complex V activity, the reactions were stopped by placing the gels in 50% methanol, 10% acetic acid for 15 minutes. The Complex V activity staining was stopped using 50% methanol. The gels were rinsed twice in deionised water and scanned with an Epson Perfection 4990 scanner (Epson, USA).

#### **2.13.6 Western blot**

For Western blot detection, 30  $\mu$ g of proteins from the organellar extract supernatants were loaded per lane. Proteins were transferred to a PVDF membrane by wet transfer in 48 mM Tris-HCl, 39 mM glycine, 20% methanol, pH 9, overnight at 25 V with stirring at 4°C. In order to fix the proteins after transfer, the membrane was left to air-dry for about 20 minutes. It was reactivated by incubation with shaking for 20 seconds in 100% methanol then rinsed twice with deionised water. The membrane was blocked for one hour with agitation in the Odyssey blocking buffer (Licor, USA). Detection was performed by incubation for at least one hour with a primary antibody diluted in blocking buffer at room temperature, followed by a one-hour incubation at room temperature with the Alexa Fluor 680 goat anti-rabbit secondary antibody (Thermo Fisher Scientific, USA) diluted to 0.2  $\mu$ g/ml in blocking buffer. The membrane was washed three times

10 minutes in TBS-T following each antibody incubation. The membrane was then scanned with the Odyssey CLx Imager (Licor, USA). The primary antibodies used are listed in Table 2.2.

**Table 2.2: List of primary antibodies used for Western blot after native PAGE separation of mitochondrial proteins.**

Protein target	Target host	Protein complexes	Host	Source	References
Rieske	<i>L. tarentolae</i>	complex III	Rabbit	Dr A. Zikova	(Gnipova et al, 2015)
COIV	<i>L. tarentolae</i>	complex IV	Rabbit	Dr E. Horakova	(Maslov et al, 2002)
ATPase Tb2	<i>Trypanosoma brucei</i>	complex V	Rabbit	Dr A. Zikova	(Subrtova et al, 2015)
$\beta$ subunit	<i>Trypanosoma brucei</i>	complex V	Rabbit	Dr A. Zikova	(Subrtova et al, 2015)

#### **2.14 Measurement of the enzymatic activities of the mitochondrial oxidative phosphorylation complexes**

Mitochondria-enriched fractions were isolated by hypotonic lysis of amastigotes, as described in Section 2.13.1. To solubilize the mitochondrial protein complexes, the organellar pellet was resuspended in solubilisation buffer (750 mM aminocaproic acid; 50 mM Bis-Tris; 0.5 mM EDTA; pH 7) and 10% dodecyl maltoside to a final concentration of 2%. After a one-hour incubation on ice, the lysate was centrifuged for 30 minutes at 16,000 x g at 4°C and the supernatant was collected. All reactions were set up to a final volume of 1 ml in spectrophotometer cuvettes and absorbances were monitored by spectrophotometer, as described by others (Kirby et al, 2007; Verner et al, 2014).

The NADH dehydrogenase activity of Complex I was assessed in NDH buffer (50 mM potassium phosphate, pH 7.5; 1 mM EDTA, pH 8.5; 0.2 mM KCN), after addition of 5  $\mu$ l of organellar lysate supernatant and 5  $\mu$ l of 20 mM NADH. The reaction was started by addition of

10  $\mu$ l of 2 mM ubiquinone-1 (Coenzyme Q1) and the change in absorbance was monitored every 10 seconds for 3 minutes at 340 nm. Inhibition of the reaction was evaluated with a final concentration of 10  $\mu$ M of rotenone.

For the determination of the succinate dehydrogenase activity of Complex II, 5  $\mu$ l of organellar extract were added to the SDH buffer (25 mM potassium phosphate, pH7.2; 5 mM  $MgCl_2$ ; 20 mM sodium succinate), containing 2  $\mu$ g/ml of antimycin A, 2  $\mu$ g/ml of rotenone, 2 mM potassium cyanide (KCN) and 50  $\mu$ M of 2,6-dichlorophenolindophenol (DCPIP). Following incubation at 32°C for 10 minutes, the baseline activity was monitored every 10 seconds for 3 minutes at 600 nm. The reaction was started with the addition of ubiquinone-1 to a final concentration of 65  $\mu$ M and the absorbance was measured every 10 seconds for 5 minutes at 600 nm. Inhibition of the reaction was assessed in presence of a final concentration of 1 mM of malonate.

Complex III cytochrome c reductase activity was measured after addition of 2  $\mu$ l of organellar extract and 4  $\mu$ l of 10 mM 2,3-dimethoxy-5-methyl-6-dodecyl-1,4-benzoquinol (DBH – decylubiquinol) to the QCR buffer (40 mM sodium phosphate, pH 7.4; 0.5 mM EDTA, pH 8.5; 20 mM sodium malonate; 50  $\mu$ M cytochrome c; 0.005% dodecyl maltoside). The reaction absorbance was evaluated every 5 seconds for 3 minutes at 550 nm. Inhibition of the reaction was performed in presence of antimycin A at a final concentration of 0.3  $\mu$ g/ml. DBH was obtained after reduction of decylubiquinone as described in (Kirby et al, 2007).

The cytochrome c oxidase activity of Complex IV was assayed in the COX buffer (40 mM sodium phosphate, pH 7.4; 0.5 mM EDTA, pH 8.5; 20  $\mu$ M cytochrome c; 30  $\mu$ M sodium ascorbate; 0.005% (w/v) dodecyl maltoside) after addition of 10  $\mu$ l of organellar extract.

Absorbance was measured every 10 seconds for 10 minutes at 550 nm. The reaction was inhibited in presence of 100  $\mu\text{M}$  KCN.

The enzymatic activities for each complex were calculated using the following formula:  
enzyme activity ( $\text{nmol}\cdot\text{min}^{-1}\cdot\text{mg}^{-1}$ ) =  $(\Delta \text{ Absorbance}/\text{min} \times 1,000) / [(\text{extinction coefficient of substrate} \times \text{volume of sample used in ml}) \times (\text{sample protein concentration in mg}\cdot\text{ml}^{-1})]$   
(Spinazzi et al, 2012). The protein concentration in the organellar lysate supernatant was determined with the Pierce BCA Protein Assay Kit (Thermo Fisher Scientific, USA). Complex I NADH dehydrogenase activity was calculated using an extinction coefficient of  $6.2 \text{ mM}^{-1}\cdot\text{cm}^{-1}$  for NADH and expressed as U/mg of total proteins, with a unit (U) of activity representing the amount of enzyme necessary for the conversion of 1 nmol of NADH per minute. Complex II succinate dehydrogenase activity was calculated using an extinction coefficient of  $19.1 \text{ mM}^{-1}\cdot\text{cm}^{-1}$  for DCPIP and expressed as U/mg of total proteins, with 1 U of activity corresponding to the amount of enzyme necessary for the conversion of 1 nmol of DCPIP per minute. Complex III cytochrome c reductase activity was calculated using an extinction coefficient of  $21.1 \text{ mM}^{-1}\cdot\text{cm}^{-1}$  for cytochrome c and expressed as mU/mg of proteins, where 1 U corresponds to the amount of enzyme that reduces 1  $\mu\text{mol}$  of cytochrome c per minute. Complex IV cytochrome c oxidase activity was calculated with an extinction coefficient of  $21.1 \text{ mM}^{-1}\cdot\text{cm}^{-1}$  for cytochrome c and expressed as mU/mg of proteins, where 1 U corresponds to the amount of enzyme that oxidizes 1  $\mu\text{mol}$  of cytochrome c per minute (Horváth et al, 2005).

Complex V ATPase (ATP hydrolysis) activity was evaluated as described elsewhere (Schnauffer et al, 2005). Crude mitochondrial fractions were obtained by digitonin extraction. The cells were harvested at  $3,000 \times g$  for 10 minutes and washed twice in PBS. They were

permeabilized at  $1 \times 10^7$  cells/ml with 0.0125% digitonin in SoTE (0.6 M sorbitol; 20 mM Tris-HCl, pH 7.5; 2 mM EDTA) and incubated for 5 minutes on ice. The crude mitochondrial pellet was collected after centrifugation at 8,000 x g for 15 minutes at 4°C and resuspended in ATPase assay buffer (200 mM KCl; 10 mM Tris-HCl, pH 8.2; 2 mM MgCl<sub>2</sub>). The protein concentration in the mitochondria-enriched pellet was determined with the Pierce BCA Protein Assay Kit (Thermo Fisher Scientific, USA). The assay was performed with 1 mg of proteins in ATPase assay buffer and the reaction was started by the addition of ATP to a final concentration of 5 mM. At 5 and 10 minutes after the start of the reaction, a 95- $\mu$ l aliquot was collected, added to 5  $\mu$ l of 3 M trichloroacetic acid and incubated on ice for 30 minutes. After a 10-minute centrifugation at 16,000 x g for 10 minutes, 90  $\mu$ l of the supernatant were added to 910  $\mu$ l of Sumner Reagent (0.88% (w/v) Iron(II) sulfate heptahydrate [FeSO<sub>4</sub> x 7 H<sub>2</sub>O]; 375 mM sulfuric acid; 0.66% (w/v) ammonium molybdate tetrahydrate [(NH<sub>4</sub>)<sub>6</sub>Mo<sub>7</sub>O<sub>24</sub> x 4 H<sub>2</sub>O]) prepared as described by Law *et al.* (Law et al, 1995) and incubated for 15 minutes at room temperature. The absorbance was measured at 610 nm. Inhibition of the reaction was tested in presence of 10  $\mu$ g/ml (~10  $\mu$ g/mg of proteins) of oligomycin or 1 mM of sodium azide. Standards of inorganic phosphate (made of Na<sub>2</sub>HPO<sub>4</sub>) in the range of 0-200 nmol/ml were set up in parallel in order to determine the amount of free phosphate released in the reaction over time. The enzymatic activity was expressed as U/mg, with 1 U of activity corresponding to the amount of enzyme required for the release of 1 nmol of free phosphate per minute.

## 2.15 Statistical analysis

A Mann-Whitney U test was performed in order to determine any significant differences between the mitochondrial activities measured in *L. mexicana* A600<sup>-/-</sup> amastigotes in comparison to the *L. mexicana* WT amastigotes. Measurements were considered significantly different when a *P*-value <0.05 was obtained.

## 2.16 GST pull-down assay

### 2.16.1 Isolation of amastigotes mitochondria-enriched fractions

Mitochondria-enriched fractions from *L. mexicana* WT amastigotes were isolated by sequential treatment of the cells with increasing concentrations of digitonin, as described elsewhere (Foucher et al, 2006). The cells were collected and centrifuged at 3,000 x g for 10 minutes. They were washed twice with PBS and resuspended to  $2 \times 10^9$  cells/ml in resuspension buffer (145 mM NaCl; 11 mM KCl; 75 mM Tris-HCl, pH 7.4) in the presence of protease inhibitors (10 mM 1,10-Phenanthroline, 10  $\mu$ M E-64, 1 mM PMSF and 1X Roche complete EDTA-free protease inhibitors cocktail). An equivalent volume of digitonin at 20  $\mu$ M in 10% methanol was added and the suspension was incubated at 37°C for 5 minutes. 100  $\mu$ l of 0.3 M sucrose was added per ml of lysate before centrifugation at 16,000 x g for 10 minutes at 4°C. The supernatant, designated Fraction 1, was collected. The pellet was resuspended in the same volume as before of resuspension buffer with protease inhibitors and an equivalent volume of digitonin at 200  $\mu$ M and incubated for 5 minutes at 37°C. After addition of 100  $\mu$ l per ml of 0.3 M sucrose, the lysate was centrifuged. The supernatant, Fraction 2, was saved and the insoluble fraction was resuspended as before in resuspension buffer with protease inhibitors and an

equivalent volume of digitonin at 1 mM. After incubation for 5 minutes at 37°C and centrifugation, the soluble fraction, Fraction 3 was collected while the pellet was treated with 10 mM of digitonin. Fraction 4 was collected as the supernatant. The final pellet, Fraction 5, was resuspended in resuspension buffer with protease inhibitors. The protein concentration of the different fractions was determined using the Pierce BCA Protein Assay Kit (Thermo Fisher Scientific, USA).

### **2.16.2 Pull-down**

The GST and the GST- $\Delta$ N.A600.1 proteins, which production was described above in Section 2.5, were each bound to Glutathione Sepharose 4B beads (GE Healthcare, USA) by incubating 40 pmol of the appropriate protein to 100  $\mu$ l of beads for at least two hours at 4°C with end-to-end rotation. The protein-bound beads were pelleted by centrifugation at 500 x g for 5 minutes. After collection of the supernatant, the beads were washed once with PBS and once with resuspension buffer (75 mM Tris-HCl, pH 7.4; 145 mM NaCl; 11 mM KCl).

After pre-clearing for two hours at 4°C with new Glutathione Sepharose 4B beads, the amastigotes digitonin fractions 3 and 4 (3 mg of proteins) isolated in section 2.16.1, were incubated overnight with the GST or the GST- $\Delta$ N.A600.1 protein-bound Glutathione Sepharose 4B beads at 4°C with end-to-end rotation. The mixture was centrifuged at 500 x g for 5 minutes. The supernatant was collected and the pelleted beads were washed twice with 1 ml of buffer B (20 mM Tris-HCl, pH7.5; 150 mM NaCl; 0.5% NP-40; 1 mM DTT), transferred to a mini-spin column (Thermo Fisher Scientific, USA) and washed once with 1 ml of buffer B and once with cleavage buffer (50 mM Tris-HCl, pH7.5; 150 mM NaCl; 1 mM EDTA, pH 8; 0.05% Triton X-100) containing 2 mM DTT. For each wash, the beads were incubated in the buffer for 5 minutes

with rotation before centrifugation. The pulled down proteins were eluted by incubation of the beads overnight with cleavage buffer (with 2 mM DTT) containing 16 U of PreScission Protease (GE Healthcare, USA) to a final volume of 100  $\mu$ l, at 4°C with end-to-end mixing. The eluates were collected as flowthrough from the mini-spin column after centrifugation at 500 x g for 5 minutes. The pelleted beads were rinsed with 100  $\mu$ l of cleavage buffer, which were added to the eluates. The eluates were incubated for two hours at 4°C with 200  $\mu$ l of new Glutathione Sepharose 4B beads in a new mini-spin column then collected after centrifugation at 500 x g for 5 minutes.

The eluted proteins were precipitated by addition of 1  $\mu$ L of 20 mg/ml glycogen (Invitrogen, USA), 800  $\mu$ L of 100% ethanol and 40  $\mu$ L of 2.5 M of sodium acetate, pH 5 to the 200- $\mu$ L eluates. After a 3-hour incubation at room temperature, the precipitated proteins were pelleted by centrifugation at 16,500 x g for 20 minutes at 4°C and left to air-dry. The dried pellets were stored at -20°C until analysis by mass spectrometry.

## **2.17 Co-immunoprecipitation**

### **2.17.1 Antibody-coupling to magnetic beads**

The anti-A600.1 peptide 2 antibody was coupled to magnetic beads (Dynabeads M-270 Epoxy, Thermo Fisher Scientific, USA), following the manufacturer's instructions. 146  $\mu$ g of the antibody was incubated with 10 mg of the magnetic beads in a final volume of 1 ml. After an overnight incubation at 37°C with end-to-end rotation, the pelleted antibody-coated beads were washed with successive buffers provided in the Dynabeads Antibody Coupling kit (Thermo Fisher Scientific, USA) and were resuspended to a final concentration of 10 mg/ml.

### 2.17.2 Preparation of whole cell lysate

Lysates were prepared from *L. mexicana* WT and *A600*<sup>-/-</sup> amastigotes in parallel. The cells were collected, centrifuged at 3,000 x g for 10 minutes at 4°C and washed twice with PBS. The final cell pellet was resuspended at 1 x 10<sup>9</sup> cells/ml in IP buffer (25 mM Tris, pH8; 100 mM NaCl; 10% glycerol; 0.5% NP-40; 5 mM MgCl<sub>2</sub>) in the presence of protease inhibitors (10 mM 1,10-Phenanthroline, 10 μM E-64, 1 mM PMSF and 1x Roche complete EDTA-free protease inhibitors cocktail). After a one-hour incubation at 4°C with end-to-end rotation, the lysate was centrifuged at 16,000 x g for 20 minutes and the supernatant was collected.

### 2.17.3 Proteins pull-down

Two immunoprecipitations, one with the WT amastigotes and one with the *A600*<sup>-/-</sup> amastigotes as negative control, were performed in parallel. The anti-A600.1 antibody-coated magnetic beads were washed once with elution buffer (0.1 M glycine-HCl, pH 2.5) and twice with the IP buffer. They were then incubated with the cell lysate supernatant from WT or *A600*<sup>-/-</sup> amastigotes for one hour at 4°C with end-to-end rotation. After collection of the unbound fraction, the beads were washed three times with PBS-T (PBS + 0.05% Tween-20) containing increasing concentrations of NaCl (100, 150 then 200 mM). The pulled down proteins were eluted after a 20-minute incubation of the beads with 0.1 M glycine-HCl, pH 2.5 at 4°C with end-to-end rotation. Once collected, the eluates were neutralized by addition of 1/10<sup>th</sup> volume of 1 M Tris-HCl, pH 8.5. The pulled down proteins were precipitated as described in section 2.16.2 and the dried pellets were stored at -20°C until analysis for mass spectrometry.

## 2.18 Mass spectrometry analysis

Samples preparation for mass spectrometry analysis was performed as described previously (Chan et al, 2006). Briefly, the precipitated proteins were resuspended in 5x sample buffer and separated by SDS-PAGE. The protein bands were visualized after blue silver staining of the gel, as described previously (Candiano et al, 2004). Each gel lane was excised, cut into smaller pieces and treated for in-gel trypsin digestion of the proteins. The peptides obtained were eluted from the gel pieces, purified and concentrated using the STop And Go Extraction technique (STAGE tip) (Rappsilber et al, 2003). For each assay, the peptides from different assay conditions were differentially labelled by reductive dimethylation, using formaldehyde isotopologues. For the GST pull-down assay, the digested peptides from the pull-down done using the GST- $\Delta$ N.A600.1 protein were labelled with deuterated formaldehyde ( $CD_2O$ ) (peptides labelled “heavy”), while the negative control sample, the peptides from the pull-down with the GST protein, was labelled with light formaldehyde ( $CH_2O$ ) (peptides labelled “light”). For the immunoprecipitation assays, the peptides isolated from the assay with the *WT* amastigotes were labelled with deuterated formaldehyde and the peptides isolated after immunoprecipitation with the *A600<sup>-/-</sup>* amastigotes, were labelled with light formaldehyde. This differential labeling results in a 4 Da mass shift between the light and heavy labelled peptides and allowed for the two sets of peptides to be distinguished once mixed after labelling.

The combined peptides were analyzed using a quadrupole – time of flight mass spectrometer (Impact II; Bruker Daltonics) on-line coupled to an Easy nano LC 1000 HPLC (Thermo Fisher Scientific, USA) using a Captive spray nanospray ionization source (Bruker Daltonics, USA).

Analysis of the mass spectrometry data was performed using MaxQuant 1.5.1.0. The search was performed against the translated *L. mexicana* genome database available from the Wellcome Trust Sanger Institute

(<http://www.sanger.ac.uk/resources/downloads/protozoa/leishmania-mexicana.html>).

Proteins annotated as hypothetical were searched through Blastp for orthologs and through the TriTrypDB database (<http://tritrypdb.org/tritrypdb/>) for potential annotations by researchers regarding the *L. mexicana* proteins or their *T. brucei* orthologs functions, as this closely related trypanosomatid is more extensively researched than *Leishmania*.

## **Chapter 3: The A600.1 protein is expressed in both promastigotes and amastigotes and localized to the mitochondria of amastigotes**

### **3.1 Introduction**

The unicellular parasite *Leishmania* has a digenetic life cycle; in the sand fly vector, it exists as unflagellated promastigotes that differentiate into amastigotes after transmission to a mammalian host during the bloodmeal of an infected sand fly and phagocytosis. In the mammalian host, the parasite establishes residence in the phagolysosome of macrophages, the predominant cell type infected by *Leishmania*. It is able to escape the immune system and to persist and multiply in the host for long periods of time, resulting in leishmaniasis. Since amastigotes represent the parasite form responsible for the disease, research has been focused on the study of genes preferentially expressed in the amastigote stage of the parasite life cycle, as it is likely that these genes are involved in the parasite survival in the mammalian host and/or in the modulation of the host immune response, resulting in the disease. Elucidating their role may help better understand the pathogenesis of leishmaniasis and provide potential targets for the control of the disease.

As previously reported by our laboratory, suppression-subtraction PCR (SS-PCR) was used to identify genes that are preferentially expressed in *L. mexicana* amastigotes. Among the cDNA fragments found to be upregulated in amastigotes were two fragments belonging to the 3'UTR of a novel gene that was named *A600* (Bellatin et al, 2002). Further characterization found that this gene is a member of a multigene family, containing four tandemly linked genes, that were named *A600.1*, *A600.2*, *A600.3* and *A600.4*, respectively, based on their relative

position from the 5' end of the locus. The most distal gene *A600.4* corresponds to the *A600* gene initially identified by SS-PCR because of the abundance of cDNA fragments of its 3'UTR in amastigotes. Northern blots analysis of the expression of the *A600.1* and of the *A600.4* genes showed that the *A600.1* transcript was slightly upregulated in amastigotes (~1.5-fold) whereas the *A600.4* mRNA expression was about 6-fold more abundant in amastigotes than in promastigotes (Murray, 2005).

Deletion of the *A600* locus by homologous recombination showed that the *A600* genes are required for the successful proliferation of amastigotes; *A600*<sup>-/-</sup> amastigotes fail to proliferate beyond four days, both in culture and in macrophages. The growth defect of the *A600*<sup>-/-</sup> mutants was partially rescued by the re-expression of the *A600.1* gene (Murray et al, 2010).

Sequence analysis of the predicted corresponding amino acid sequences showed that the *A600.1* and *A600.2* genes encoded proteins are 100% identical in sequence. The *A600.3* protein shares 99% sequence identity, while the *A600.4* protein shares only 55% with the *A600.1* and *A600.2* proteins. They were predicted to be transmembrane proteins, with two transmembrane domains in the *A600.1* protein and a single one in the *A600.4* protein. Analysis of the predicted amino acid sequence of the *A600.1* and *A600.4* proteins did not identify the presence of any conserved or functional domains in either protein, which made it difficult to elaborate on their function (Murray et al, 2010).

In order to gain further understanding of the function of the *A600* proteins, this chapter describes the characterization of the endogenous *A600* proteins expression profiles during the *L. mexicana* life cycle and their subcellular localization in amastigotes. To do this, polyclonal anti-*A600.1* and anti-*A600.4* antibodies were generated and tested for their reactivity and specificity for the recombinant and endogenous target proteins.

## 3.2 Results

### 3.2.1 Production of recombinant A600.1 and A600.4 proteins

In order to test the ability of the newly generated anti-A600.1 and anti-A600.4 antibodies to recognize their target proteins, recombinant A600.1 and A600.4 proteins were produced and isolated from BL21(DE3) *E. coli* cells transformed with a pGEX-6P1 vector (GE Healthcare, USA) containing either the *L. mexicana* A600.1 or the A600.4 gene, downstream of the GST gene. Those *E. coli* clones were designated BL21+pGST-A600.1 and BL21+pGST-A600.4, respectively. In the pGEX vector, expression of the GST gene is under the control of the inducible *tac* promoter, which is inhibited by the binding of a repressor protein encoded by the *lacI<sup>q</sup>* gene to the operator region of the promoter. This inhibition is abolished in the presence of IPTG, which binds the *lacI<sup>q</sup>* gene product.

Induction of the GST-A600.1 or GST-A600.4 fusion proteins expression was achieved by addition of IPTG to the bacterial culture, as described in Section 2.5.3 of the Material and Methods. Initially, this induction was performed by incubation of the *E. coli* clones BL21+pGST-A600.1 and BL21+pGST-A600.4 at 37°C, with 0.5 mM IPTG in LB Broth, following the procedure described by Harper and Speicher (Harper & Speicher, 2011). However, under these conditions, most of the GST-A600.1 protein and of the GST-A600.4 protein was present in the insoluble fraction of the bacterial lysate, leading to a very low yield of proteins isolated from the soluble fraction. Modifications to the induction conditions were introduced in order to optimize the production of the fusion proteins in the soluble form, following recommendations described in the *GST Gene Fusion System* handbook (GE Healthcare). The bacteria were grown in 2 x YT medium instead of LB Broth. Protein expression was induced

using 0.3 mM IPTG (instead of 0.5 mM) at room temperature (about 25°C) instead of 37°C and the bacterial lysate was incubated with 1% Triton X-100 for 30 minutes before separation of the soluble and insoluble fractions. These new conditions increased the level of soluble GST fusion proteins which were then isolated by affinity chromatography using Glutathione Sepharose 4B beads. The A600.1 or A600.4 portion of the fusion protein was released using the PreScission protease which recognizes a cleavage site between the GST and the A600.1 or A600.4 moieties of the fusion protein. Both the GST tag and the protease (which is also a GST fusion protein) remained bound to the Glutathione Sepharose beads. Alternatively, to purify the full-length recombinant fusion proteins (GST-A600.1 or GST-A600.4), the fusion protein-bound Glutathione Sepharose 4B beads were incubated with reduced glutathione.

The *A600.1* ORF is predicted to encode a protein of 163 amino acids in length with a molecular mass of 17.8 kDa. The A600.4 protein is predicted to have a length of 93 amino acids and a molecular mass of 10.4 kDa. GST is a 26 kDa protein but the GST protein produced by the parental pGEX vector contains additional amino acids that are coded by the PreScission Protease cleavage site and the vector multiple cloning site, which bring its molecular mass to 29 kDa. Taken together, the predicted molecular mass of the GST-A600.1 fusion protein is 45 kDa and 38 kDa for GST-A600.4. The recombinant A600.1 and A600.4 proteins obtained after cleavage by the PreScission Protease from the GST fusion protein contain eight additional amino acids (two from the PreScission Protease cleavage site and six from the vector cloning site) (Figure 2.1). The presence of those additional amino acids brings the predicted molecular mass of the recombinant A600.1 protein to 18.6 kDa and of the recombinant A600.4 protein to 11.2 kDa.

Analysis of the BL21+pGST-A600.1 bacterial fractions by Western blot using an anti-GST antibody detected a band of 50.6 kDa and smaller and fainter bands between 26 and 43 kDa

(Figure 3.1 a). Since those bands are only detected in the fractions collected after induction of the protein expression (lanes 2-4 and 7) and not in the non-induced fraction (lane 1), it can be concluded that the higher band corresponds to the full-length GST-A600.1 protein, while the lower bands represent different sizes of the fusion protein corresponding to different states of proteolysis. The sample in lane 7 corresponds to the eluate collected after incubation of the Glutathione Sepharose 4B beads with the soluble fraction of the BL21+pGST-A600.1 cells lysate and therefore contains the full-length GST-A600.1 fusion protein. The eluate (lane 5) is the sample collected after incubation of the GST-A600.1-bound Glutathione Sepharose 4B beads with the PreScission protease using a batch method of purification. The detection in this eluate by the anti-GST antibody of the same band of 50.6 kDa as in the other fractions (lanes 2-4) and of another band at 27.5 kDa suggests that some of the fusion protein remained uncleaved and was eluted in presence of the PreScission Protease, along with some of the cleaved GST tag represented by the 27.5 kDa band. However, the amido black staining (Millipore-Sigma, USA) of the Western blot membrane revealed that the major protein present in the eluate is represented by a strong band of around 24 kDa (Figure 3.1 b). Since this band is not detected by the anti-GST antibody, it may correspond to the recombinant A600.1 protein, considering its small size, which is close to though slightly higher than the predicted 18.6-kDa mass of the A600.1 moiety cleaved off from the GST tag. Also, the detection by the anti-GST antibody of a band that appears to correspond to the cleaved GST moiety provides evidence of the effective cleavage of the fusion protein by the PreScission Protease.

Western blot analysis of the bacterial fractions after induction of the BL21+pGST-A600.4 clone detected the highest and strongest band at 41 kDa (lanes 8 and 9). This band is likely to correspond to the full-length GST-A600.4 fusion protein. As with the eluate collected

from the BL21+pGST-A600.1 clone, detection with the anti-GST antibody found the presence in the eluate from the BL21+pGST-A600.4 cells, of a band corresponding to the full-length fusion protein (at 41 kDa) and the cleaved GST tag at 27.5 kDa. However, the major band in this sample is seen at approximately 16 kDa after amido black staining of the Western blot membrane and is not detected by the anti-GST antibody. Its small size suggests that it may correspond to the A600.4 protein.

The presence in the PreScission protease eluates (lanes 5 and 10) of some uncleaved GST fusion protein and some cleaved GST tag may be the result of contamination of the eluates with some beads drawn up during sample collection, following the use of the batch method purification. The full-length GST fusion protein may also correspond to some unbound protein that remained within the beads pellet after removal of the unbound fraction and that was not efficiently removed during the subsequent washing steps. Those proteins were still detected after incubation of these eluates with new Glutathione Sepharose 4B beads. Their presence was not deemed an issue for the use of the eluates in subsequent applications.

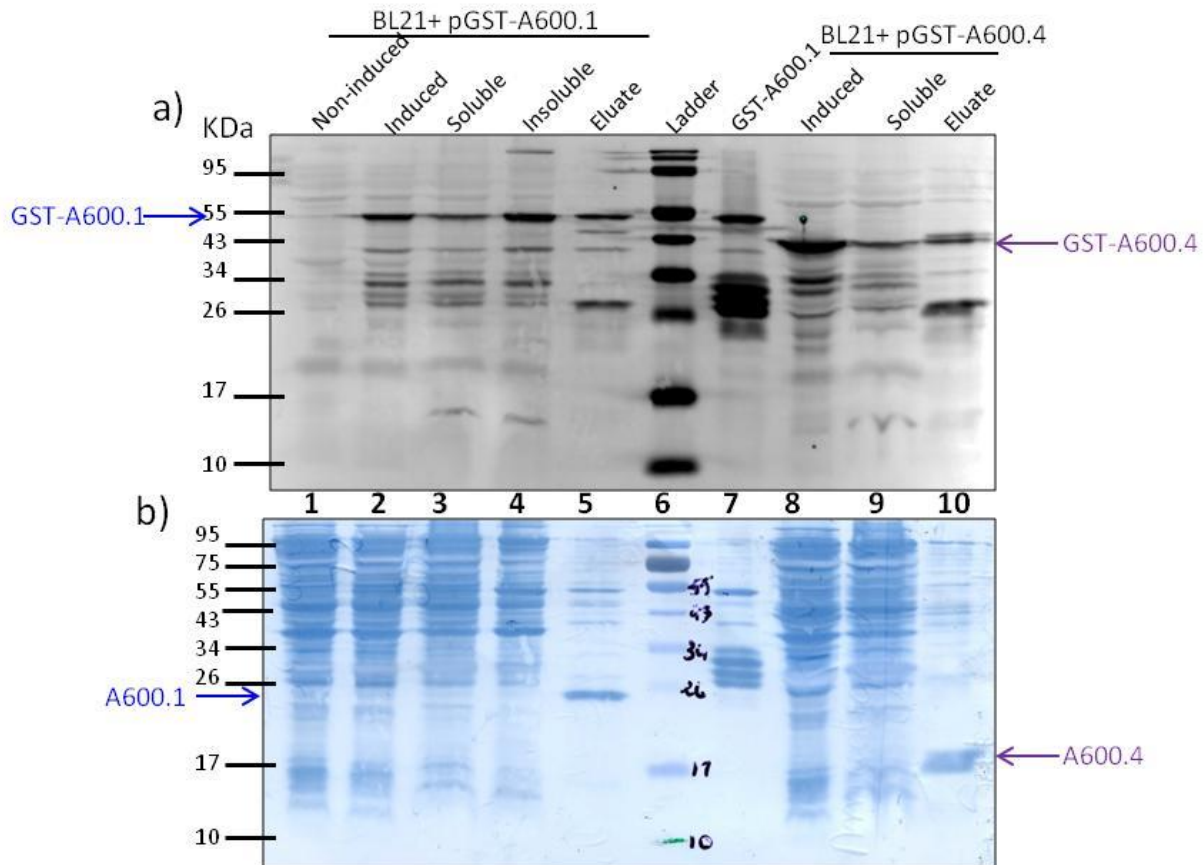


**Figure 3.1: Production and purification of the A600.1 and A600.4 proteins from BL21(de3) *E. coli* clones transformed with the pGEX vector containing the *A600.1* gene (BL21+pGST-A600.1) or the *A600.4* gene (BL21+pGST-A600.4) respectively.**

a) Western Blot analysis of the bacterial fractions of the BL21+pGST-A600.1 and of BL21+pGST-A600.4 clones after induction of the fusion protein expression. The protein samples were separated on a 12% SDS-PAGE and probed with a rabbit anti-GST antibody. b) After scanning with the Odyssey Imager, the membrane used for Western blot was stained with amido black to visualize the total proteins transferred. Non-induced: aliquot of the BL21+pGST-A600.1 culture before addition of IPTG; Induced: aliquot of the bacterial culture 4.5 hours after induction of the fusion protein expression following addition of IPTG; Soluble: supernatant of the induced bacterial lysate after centrifugation; Insoluble: pellet of bacterial lysate after centrifugation; Eluate: eluate collected after incubation of the fusion protein-bound Glutathione Sepharose 4B beads with the PreScission protease. GST-A600.1 (lane 7): eluate collected after elution with reduced glutathione of the Glutathione Sepharose 4B beads incubated with the soluble fraction of the BL21+pGST-A600.1 cell lysate.

### 3.2.2 Characterization of the anti-A600.1 antibodies

The generation of antibodies targeting the *L. mexicana* A600.1 and A600.4 proteins was contracted out to the biotechnology company GenScript. For the production of anti-A600.1

antibodies, two 14-amino acid-long regions of the A600.1 protein sequence were identified using GenScript's trademark antigen design algorithm to use as antigens (Figure 2.2). The two sequences were selected based on criteria such as hydrophilicity, surface exposure, position towards the N-terminus or the C-terminus, secondary structure, the absence of specific sequence motifs and their uniqueness to the A600.1 protein by comparison to the closely related A600.4 protein. The first antigenic peptide, peptide 1, corresponds to the region between amino acids 125 to 138; whereas peptide 2 corresponds to the A600.1 sequence between amino acids 140 and 153. Each antigenic peptide was synthesised and conjugated to the KLH (Keyhole limpet hemocyanin) protein and used to immunize two rabbits. The antibodies generated were purified from the rabbit sera by affinity purification against the respective antigenic peptide.

### ***3.2.2.1 Antibodies reactivity against the recombinant A600.1 protein***

The ability of the isolated antibodies to recognize the target protein was first assayed by ELISA against the recombinant A600.1 and the GST-A600.1 fusion proteins isolated from the BL21+pGST-A600.1 *E. coli* clones (Figure 3.2). The ELISA plates were also coated with the corresponding antigen peptide as positive control and with the recombinant A600.4 protein or GST protein produced from the parental pGEX vector, as negative controls. The reactivities of the affinity purified antibodies were evaluated by assaying the capacity of five-fold serial dilutions of each antibody original solution (antibody 1 stock solution: 2.2 mg/ml; antibody 2 solution: 1.5 mg/ml) to bind to the different antigens. After extensive washing, the bound antibodies were detected using an anti-rabbit antibody conjugated to horseradish peroxidase (HRP). In the presence of hydrogen peroxide, the HRP oxidizes the substrate TMB (3,3',5,5'-Tetramethylbenzidine), leading to the formation of a blue-green color, the intensity of which correlates with the amount of antibody bound to the coated wells.

Using the antibodies reactivity against their respective antigen peptide as reference, both antibodies exhibited a strong reactivity against the recombinant A600.1 and the GST-A600.1 fusion protein. The anti-peptide 1 antibody showed a high reactivity against the A600.1 protein and against the GST-A600.1 protein, with a titer (the antibody amount for which 50% of the maximal signal for antibody binding is observed) of 5.8 ng/ml against A600.1 (corresponding to a 1:375,000 dilution of the antibody stock solution) and of 17.5 ng/ml against GST-A600.1 (corresponding to a 1:125,000 dilution) (Figure 3.2a). The titer of the anti-peptide 2 antibody was similar for both A600.1 and GST-A600.1 (4 ng/ml, corresponding to a dilution of 1:375,000) (Figure 3.2b). By comparison, both antibodies exhibited a low reactivity against the recombinant A600.4 and GST proteins. The anti-peptide 1 antibody was not significantly detected in the negative controls wells (coated with A600.4 or GST) even at the highest concentration tested (2.2 µg/ml). The anti-peptide 2 antibody had no significant reactivity to the negative control proteins. The low reactivity of both antibodies against the GST protein in comparison to the strong binding in the wells containing the GST-A600.1 fusion protein suggests that both antibodies are able to recognize the recombinant A600.1 protein with little reactivity to the closely related A600.4 protein. Overall, these results suggest that those antibodies are likely to recognize the endogenous A600.1 protein and may be used in applications such as Western blot and immunoprecipitation.

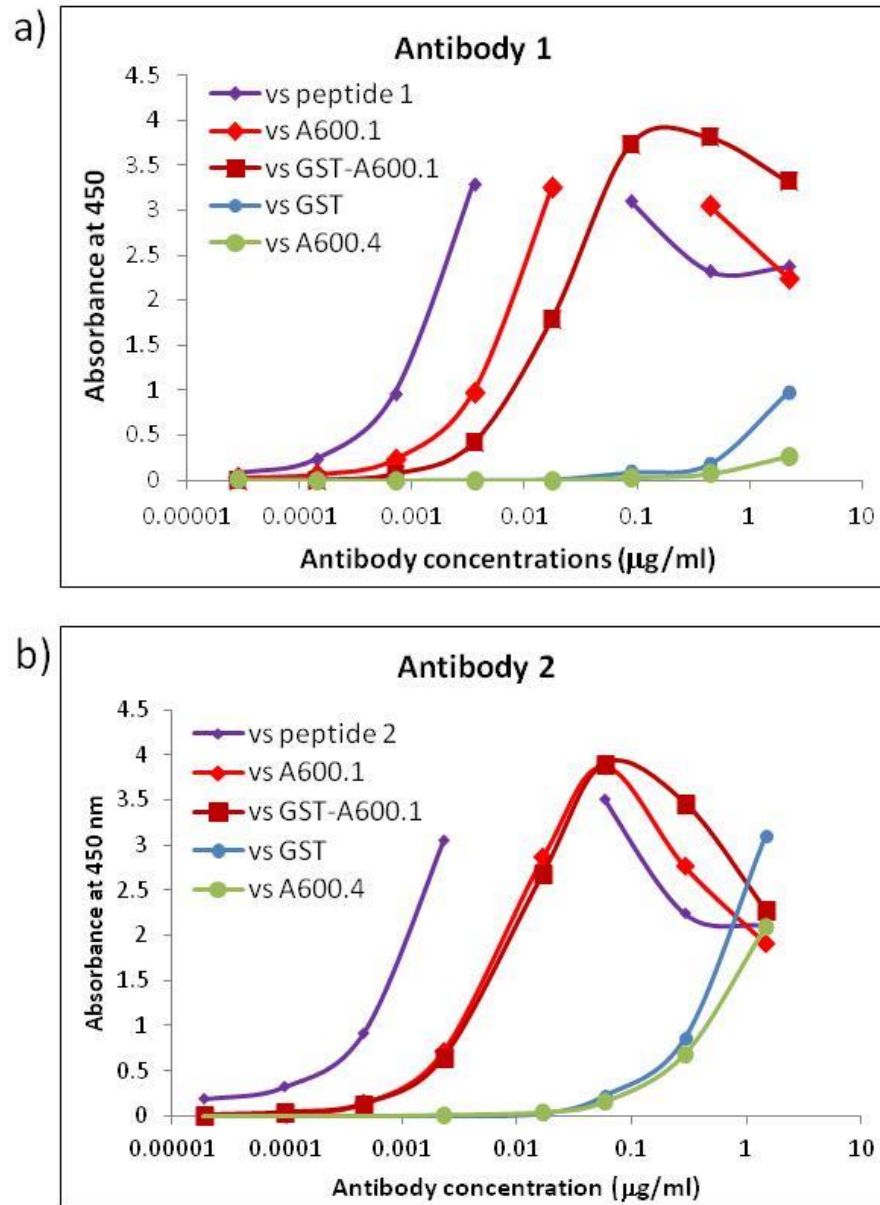


**Figure 3.2: ELISA analysis of the GenScript anti-A600.1 antibodies 1 and 2 specificity for the recombinant A600.1 protein.**

96-well plates were coated with the indicated antigens (antigenic peptide 1 or 2, A600.1, GST-A600.1, GST or A600.4 proteins). Antibody 1 reactivity was assayed at the following concentrations:  $0.028 \times 10^{-3}$ ,  $0.14 \times 10^{-3}$ ,  $0.7 \times 10^{-3}$ ,  $3.5 \times 10^{-3}$ ,  $17.5 \times 10^{-3}$ ,  $0.0874$ ,  $0.437$ ,  $2.185 \mu\text{g/ml}$ . Antibody 2 reactivity was assayed at the following concentrations:  $0.0187 \times 10^{-3}$ ,  $0.0935 \times 10^{-3}$ ,  $0.467 \times 10^{-3}$ ,  $2.3 \times 10^{-3}$ ,  $0.017$ ,  $0.0584$  and  $0.292$  and  $1.461 \mu\text{g/ml}$ . These concentrations correspond to a 1,000-fold followed by five-fold serial dilutions of the antibodies stock solutions, to the highest dilution of 1: 1:78,125,000 (antibody 1 stock solution:  $2.185 \text{ mg/ml}$ ; antibody 2 solution:  $1.461 \text{ mg/ml}$ ).

The primary application for these antibodies is for the Western Blot detection of the *L. mexicana* A600.1 endogenous protein. Therefore, they were first tested for their ability to react against the recombinant A600.1 protein after denaturing SDS-PAGE.

Aliquots of different fractions of the BL21+pGST-A600.1 bacterial lysate were separated by Laemmli SDS-PAGE and analyzed by Western blot with each anti-A600.1 antibody (Figure 3.3). The same banding patterns were obtained with both antibodies, against the different samples. By comparison to the non-induced sample, two strong bands were detected in the induced lysate, that did not appear in either the non-induced lane or the BL21+pGST induced sample; the highest detected band was estimated at 50.5 kDa, similar to the strongest band detected in the same sample by the anti-GST antibody (Figure 3.1), likely to correspond to the full-length GST-A600.1 protein. The two smaller bands estimated at 38 and 18 kDa were likely to correspond to degradation products of the fusion protein. The fact that no major band appears in the non-induced lane (apart for a faint band at 18 kDa) or in the BL21+pGST induced sample suggests that both antibodies do not significantly cross-react with *E. coli* proteins. The signal detected in the BL21+pGST induced sample around 26 kDa was due to the adjacent A600.1 lane that was overloaded. The eluate obtained after cleavage of the GST-A600.1 protein with the PreScission protease exhibited a major band estimated at 23.5 kDa. This band appeared similar to the major band that was detected in this sample at a similar size on the PVDF membrane stained with amido black after Western blot detection of the bacterial fractions with the anti-GST antibody (Figure 3.1). This band was not detected by the anti-GST antibody which suggests that it is likely to correspond to the A600.1 portion of the GST fusion protein. As with the anti-GST antibody, the presence of the two large bands at 50.5 kDa and 38 kDa, respectively, indicates the

presence of uncleaved GST-A600.1 in the eluate; they are however present in much lower proportion than the cleaved A600.1 protein.

Taken together, these results, along with the fact that the main bands do not appear in either the non-induced sample, or in the BL21+pGST induced aliquot suggest that the two anti-A600.1 antibodies recognize the denatured recombinant A600.1 by Western blot and do not cross-react with *E. coli* endogenous proteins.

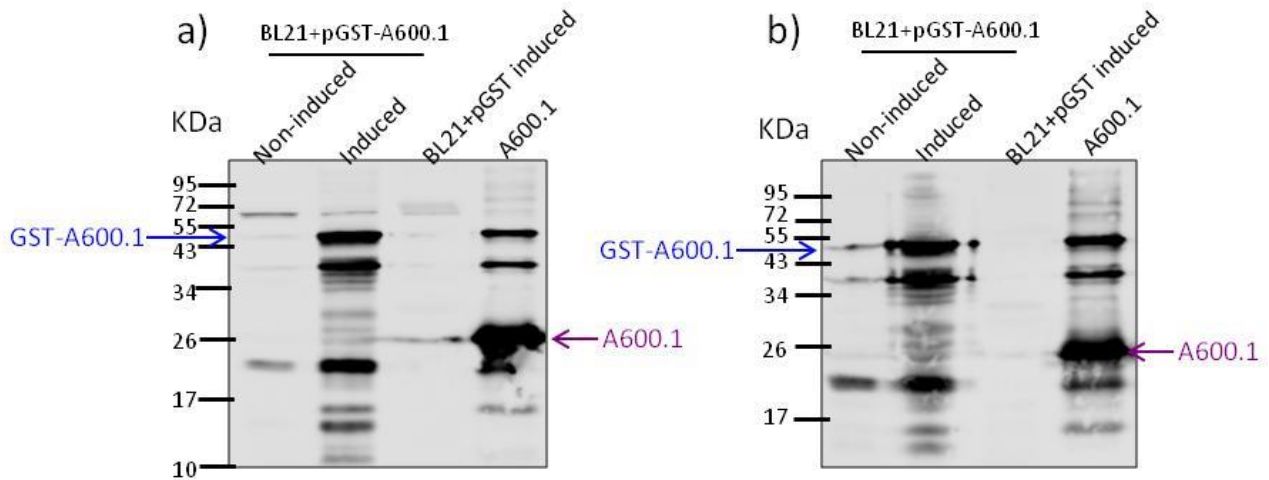


**Figure 3.3: Western Blot analysis of the GenScript anti-A600.1 antibodies 1 and 2 specificity for the recombinant A600.1 protein.**

Aliquots of different fractions of the BL21+pGST-A600.1 bacterial lysate were separated on a 12% Laemmli SDS-PAGE gel. After transfer, the membranes were probed with a 1:10,000 dilution of the antibody 1 (218.5 ng/ml) (a) or antibody 2 (b) (146 ng/ml). The bound antibodies were detected with an anti-rabbit Alexa Fluor 680 goat anti-rabbit antibody diluted at 1:10,000. Membranes were scanned with the Odyssey CLx Imager. Non-induced: aliquot of the bacterial lysate before addition of IPTG. Induced: aliquot of the bacterial lysate five hours after addition of IPTG. BL21+pGST induced: aliquot of the lysate of bacteria transformed with the parental pGEX vector after induction. A600.1: eluate from the GST-A600.1-bound glutathione sepharose beads after incubation with the PreScission Protease.

### 3.2.2.2 Antibodies reactivity against the *L. mexicana* endogenous A600.1 protein

The reactivity and specificity of the anti-A600.1 antibodies against the endogenous A600.1 protein of *L. mexicana* were assayed by Western blot analysis. Whole cell lysates of promastigotes and amastigotes were prepared from the following *L. mexicana* strains of: WT;

*WT+GFP-A600.1* and *A600<sup>-/-</sup>+GFP-A600.1* were used as positive control for the expression of A600.1 in the *WT* cells; *A600<sup>-/-</sup>* cells were used as negative control. The recombinant A600.1 protein obtained after cleavage of the GST-A600.1 protein by the PreScission Protease was loaded as a positive control (Figure 3.4).

When tested at a final concentration of 0.22 µg/ml (corresponding to a 1:10, 0000 dilution of the antibody stock solution), the anti-peptide 1 antibody detected multiple bands in the different lysates (Figure 3.4 a). The *WT+GFP-A600.1* and *A600<sup>-/-</sup>+GFP-A600.1* lysates exhibited a strong band estimated at 52 kDa which is likely to correspond to the GFP-A600.1 fusion protein which has a predicted molecular mass of 45 kDa. Another predominant band detected at 30 kDa also appears in the other lysates, including in the *A600<sup>-/-</sup>* lysates. The presence of this band, as well as two others at 40 and 23 kDa in the *A600<sup>-/-</sup>* lysates, which do not contain any *A600* genes, suggests that at the concentration used, the anti-peptide 1 antibody crossreacts with *L. mexicana* proteins other than A600.1.

By comparison, when tested at a final concentration of 0.15 µg/ml (corresponding to a 1:10, 0000 dilution of the antibodies stock solution), the anti-peptide 2 antibody detected fewer bands in the different lysates (Figure 3.4b). Similarly to the anti-peptide 1 antibody, a band at 52 kDa, likely to correspond to the GFP-A600.1 protein, was found in the *WT+GFP-A600.1* and *A600<sup>-/-</sup>+GFP-A600.1* lysates. Analysis of the wild-type (*WT*) promastigotes and amastigotes lysates reveals a single band at 23.5 kDa at a similar size as the major band detected in the PreScission protease eluate from the BL21+pGST-A600.1 lysate. No band is detected in the *A600<sup>-/-</sup>* negative control lysates (the signal detected in the *A600<sup>-/-</sup>* promastigotes lane is due to a spill of the neighboring A600.1 lane which was overloaded). These results suggest that, when

used at a concentration of 0.15  $\mu\text{g/ml}$ , the anti-peptide 2 antibody recognizes specifically the *L. mexicana* endogenous A600.1 protein and does not crossreact with other *L. mexicana* proteins.

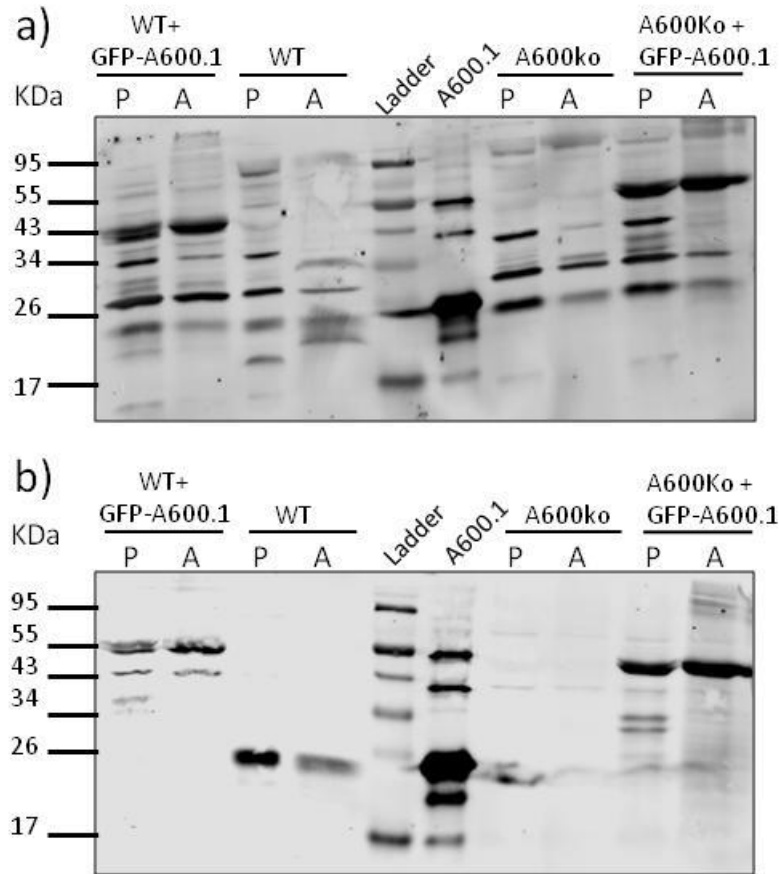


**Figure 3.4: Western Blot analysis of the GenScript anti-A600.1 antibodies 1 and 2 specificity for the endogenous *L. mexicana* A600.1 protein.**

Proteins (30  $\mu\text{g}$ ) from whole cell lysates of promastigotes (P) and amastigotes (A) of the different strains of *L. mexicana* were separated on a 12% denaturing gel, using the Laemmli SDS-PAGE buffer system. After transfer, the membrane was probed with 0.22  $\mu\text{g/ml}$  of antibody 1 (a) or 0.15  $\mu\text{g/ml}$  antibody 2 (b). The bound antibodies were detected with an anti-rabbit Alexa Fluor 680 goat anti-rabbit antibody diluted at 1:10,000. Membranes were scanned with the Odyssey CLx Imager. The A600.1 recombinant protein (0.6  $\mu\text{g}$ ) was used as positive control. WT: *L. mexicana* wild-type; A600ko: *L. mexicana* A600<sup>-/-</sup>; WT+GFP-A600.1 and A600ko+GFP-A600.1: *L. mexicana* WT and A600<sup>-/-</sup> clones transfected with plasmid to express the GFP-A600.1 fusion protein.

To investigate further the specificity of the anti-peptide 1 antibody for the endogenous A600.1 protein and in an attempt to reduce its non-specific interactions with other *L. mexicana* proteins, higher dilutions of the anti-peptide 1 antibody were tested. When the lysates were analysed with the antibody at 0.15 and 0.044 µg/ml (corresponding to dilutions of 1:15,000 and 1:50,000 of the antibody stock solution, respectively), the same banding pattern was observed with both dilutions (Figure 3.5a). Two bands were detected in the *WT* and in the *A600*<sup>-/-</sup> cells: one at 31 kDa, similar to the one seen in all the lysates analysed with the antibody at 0.22 µg/ml (Figure 3.4a), and one at 24 kDa, that appears of a similar size as the major band in the A600.1 eluate. However, this 24 kDa protein is also detected in the *A600*<sup>-/-</sup> cells, which makes it unlikely to correspond to the A600.1 protein. Analysis of the same samples with the anti-peptide 2 antibody at 0.15 µg/ml detected a major band at 25 kDa, in the *WT* promastigotes and amastigotes lysates and in the A600.1 eluate. No band was observed in the *A600*<sup>-/-</sup> cells, which suggests that this 25 kDa band is likely to represent the A600.1 protein (Figure 3.5b). The fainter band at 20 kDa seen in the *WT* samples and in the A600.1 eluate may correspond to a degradation product of the 25 kDa band. This band is occasionally seen in Western blot analysis of *WT* lysates, especially with *WT* amastigotes in which proteolysis appears to occur at a greater extent than in promastigotes, as observed by others (Nugent et al, 2004).

Taken together, these results indicate that the anti-peptide 1 antibody is not specific to the A600.1 protein and therefore is not suitable to use for analysis of the *L. mexicana* endogenous A600.1 protein. On the other hand, the anti-peptide 2 antibody appears to recognize specifically the A600.1 protein and was selected for further characterization of the endogenous protein. It is worth noting that none of the two antibodies reacts against the closely related A600.4 recombinant protein (Figure 3.5).

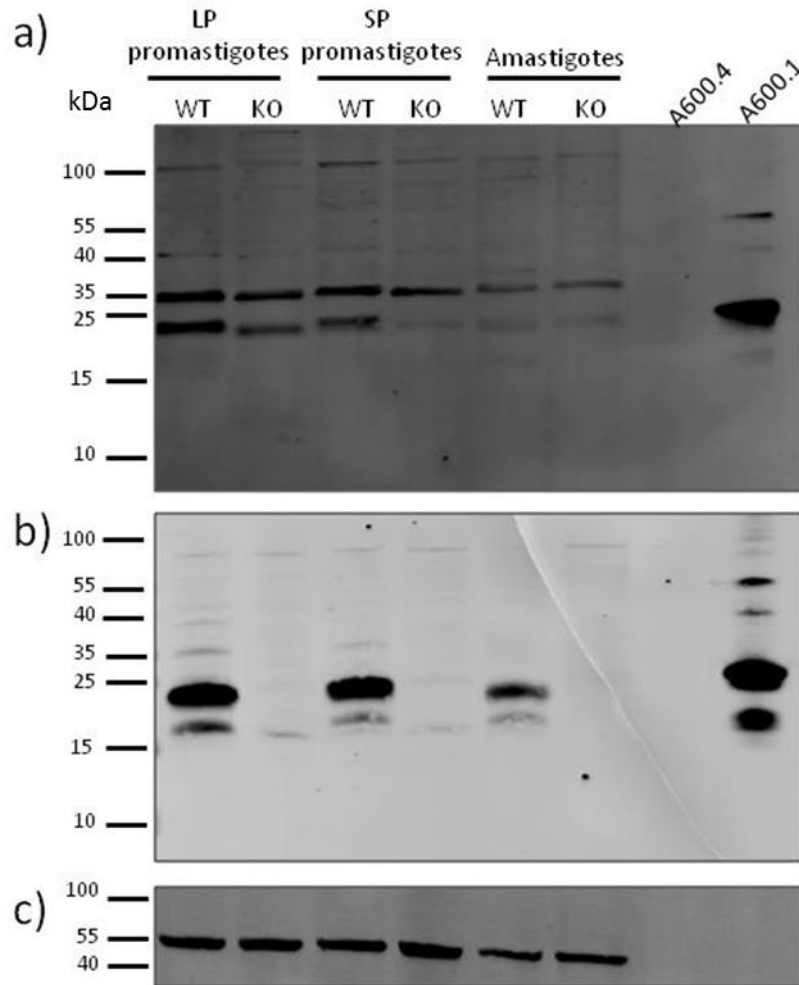


**Figure 3.5: Western Blot testing of the GenScript anti-A600.1 antibody 1 specificity for the endogenous *L. mexicana* A600.1 protein.**

Whole cell lysates from logarithmic (LP) and stationary (SP) promastigotes and from amastigotes of the *L. mexicana* wild-type (WT) and *A600*<sup>-/-</sup> (KO) strains were separated on a 12% denaturing gel, using the Tricine-SDS-PAGE system (30 µg of proteins/well). After transfer, the membrane was probed with a 1:15,000 dilution (0.15 µg/ml) of anti-peptide 1 antibody (a) or a 1:10,000 dilution (0.15 µg/ml) of anti-peptide 2 antibody (b). The bound antibodies were detected with the Alexa Fluor 680 goat anti-rabbit secondary antibody diluted at 1:10,000. Membranes were also probed with a mouse anti-alpha-tubulin antibody (1:2,000 dilution = 0.1 µg/ml) as loading control for the cell lysates (c). Detection of the bound anti-alpha-tubulin antibody was performed with the IRDye 800CW goat anti-mouse secondary antibody. Membranes were scanned with the Odyssey CLx Imager. The recombinant A600.1 and A600.4 proteins (20 ng/well) were used as positive and negative controls respectively.

### **3.2.3 Characterization of the anti-A600.4 antibody**

To raise antibodies against the A600.4 protein, a 14-amino acid-long sequence corresponding to the A600.4 protein region between amino acids 75 and 88 was selected as antigen, following the same procedure as for the generation of the two anti-A600.1 antibodies. This sequence was also chosen for its low degree of identity to the A600.1 protein sequence.

#### ***3.2.3.1 Antibodies reactivity against the recombinant A600.4 protein***

The anti-A600.4 antibody reactivity and specificity for the A600.4 protein was first assayed by ELISA. It was also assayed against the A600.4 antigenic peptide and the GST protein, as positive and negative controls respectively. By comparison to its reactivity against the A600.4 antigenic peptide, the anti-A600.4 antibody exhibited a strong reactivity against the recombinant A600.4 protein, with a titer of 0.7 ng/ml, which corresponds to a 1:625,000 dilution of the antibody stock solution (Figure 3.6). Although a lower reactivity is observed against the GST protein, a significant amount of anti-A600.4 antibody bound to the negative control GST, with a titer of 29.4 ng/ml (corresponding to a dilution of 1:15,000).

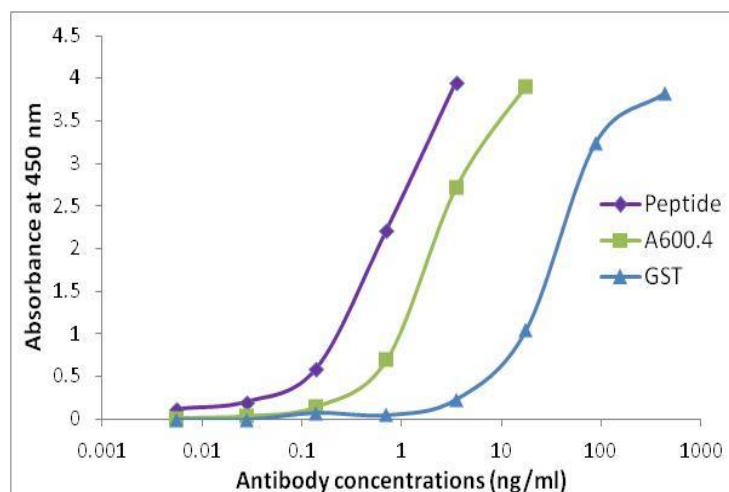


**Figure 3.6: ELISA analysis of the GenScript anti-A600.4 antibody specificity for the A600.4 protein.**

96-well plates were coated with the indicated antigens (antigenic A600.4 peptide, the A600.4 and GST proteins). The antibody reactivity against the indicated antigens was tested at the following concentrations:  $5.6 \times 10^{-3}$ ,  $28 \times 10^{-3}$ , 0.14, 0.71, 3.528, 17.64, 88.2 and 441 ng/ml. These concentrations correspond to a 1,000-fold followed by five-fold serial dilutions of the antibody stock solution at 0.441 mg/ml.

Aliquots of the BL21+pGST and BL21+pGST-A600.4 bacterial lysates were collected before and after induction of protein expression. The soluble fraction of the BL21+pGST-A600.4 lysate was incubated with Glutathione Sepharose 4B beads. The GST-A600.4 protein was isolated after incubation of the beads with the reduced glutathione buffer, whereas the A600.4 protein was isolated after incubation with the PreScission protease. The protein samples were analyzed by Western blot, using the anti-A600.4 peptide antibody at 88.2 ng/ml, corresponding to a 1:5,000 dilution of the antibody stock solution (Figure 3.7). Two similar protein bands were detected in the BL21+pGST-A600.4 induced lysate and in the eluate obtained with the reduced glutathione buffer (containing the purified GST-A600.4 protein). The larger band had an estimated size of 39 kDa and the lower one of 33 kDa. The GST-A600.4 fusion protein is predicted to have a molecular mass of 38 kDa. Since no band was detected in the induced

BL21+pGST lysate or in the non-induced BL21+pGST-A600.4 lysate, it can be concluded that the highest band correspond to the full-length GST-A600.4 fusion protein and the smaller band to a partially degraded GST-A600.4 protein. The eluate collected with the PreScission protease exhibited a single band estimated at 15 kDa. This band appeared to be similar to the major band seen in this sample on the amido black stained PVDF membrane (Figure 3.2) but was not detected by the anti-GST antibody. Since the recombinant A600.4 protein is predicted to have a molecular mass of 11.2 kDa, this band is likely to correspond to the A600.4 portion of the GST-A600.4 fusion protein. The fact that no protein was detected in the induced BL21+pGST lysate nor in the non-induced BL21+pGST-A600.4 lysate suggests that the anti-A600.4 antibody does not cross-react with *E. coli* endogenous proteins.

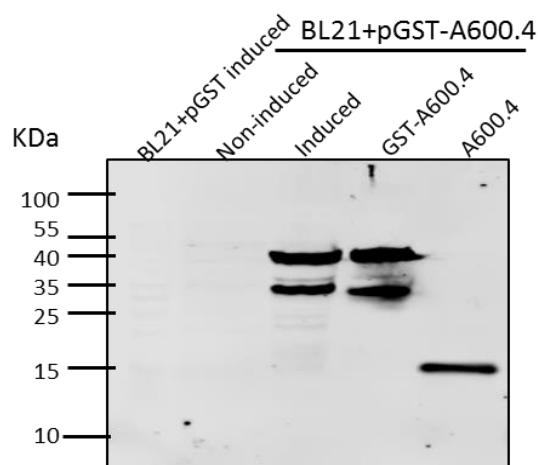


**Figure 3.7: Western Blot analysis of the GenScript anti-A600.4 antibody specificity for the recombinant A600.4 protein produced from *E. coli* clones.**

Aliquots of the bacterial fraction were separated on a 12% Tris-Tricine-SDS gel. After transfer, the membrane was probed with the anti-A600.4 antibody at 88 ng/ml (1:5,000 dilution of the antibody stock solution). The bound antibody was detected with an anti-rabbit Alexa Fluor 680 goat anti-rabbit antibody. Membranes were scanned with the Odyssey CLx Imager. BL21+pGST induced: aliquot of the bacterial lysate of the BL21(de3) *E. coli* clone transformed with the parental pGEX vector after induction of protein expression; non-induced: aliquot of the bacterial lysate of the BL21+pGST-A600.4 *E. coli* clone transformed with the pGEX vector containing the *A600.4* gene, before protein induction; induced: aliquot of the BL21+pGST-A600.4 bacterial lysate after induction; GST-A600.4: eluate collected after elution with reduced glutathione buffer of the Glutathione Sepharose 4B beads incubated with the BL21+pGST-A600.4 lysate.; A600.4: eluate collected after elution of the Glutathione Sepharose 4B beads with the PreScission protease.

### 3.2.3.2 *Antibody reactivity against the L. mexicana A600.4 endogenous protein*

The specificity of the anti-A600.4 antibody for the *L. mexicana* endogenous protein was evaluated by Western blot analysis of *L. mexicana* WT and A600<sup>-/-</sup> whole cell lysates. A single band was detected in the WT promastigotes and amastigotes and in the A600<sup>-/-</sup> SP promastigotes lysates (and more faintly in the A600<sup>-/-</sup> amastigotes) (Figure 3.8). Comparison of Western blot replicates with this antibody found that the band detected in the A600<sup>-/-</sup> lysates consistently migrates at a slightly higher position (21 kDa) than the band observed in the WT lysates (20.5 kDa). It is also observed in the A600<sup>-/-</sup> amastigotes with various intensities. This suggests that the antibody may react with more than one *L. mexicana* protein, one at 20.5 kDa, only present in the WT cells, and one at 21 kDa that would also be present in the A600<sup>-/-</sup> cells. Unlike the anti-A600.1 peptide 2 antibody which recognizes a single band of the same size for the *Leishmania* A6001 and the recombinant proteins, the 20.5 kDa single band detected by the anti-A600.4 antibody in the *L. mexicana* WT cells, has a much higher molecular mass than the 10.4 kDa predicted for the A600.4 endogenous protein and higher than the 15.5 kDa band detected in the A600.4 eluate. Therefore, it is not possible to conclude what protein actually corresponds to this 20.5 kDa band and whether the antibody can recognize the A600.4 endogenous protein.

The detection of a band in the A600<sup>-/-</sup> lysates suggests that this antibody recognizes a *L. mexicana* protein other than A600.4. This and the fact that it cannot be concluded whether the protein detected in the WT cells corresponds to A600.4 make this antibody unsuitable as a tool to study the *L. mexicana* A600.4 endogenous protein.

Adsorption of an aliquot of the polyclonal antibody with a lysate of A600<sup>-/-</sup> amastigotes was performed to try to deplete antibodies that interact with *Leishmania* proteins other than

A600.4. However, the antibody recovered after adsorption did not produce any signal against the samples, including the recombinant protein, suggesting that most of the antibody that could interact with the A600.4 protein was removed from the solution during adsorption (data not shown).

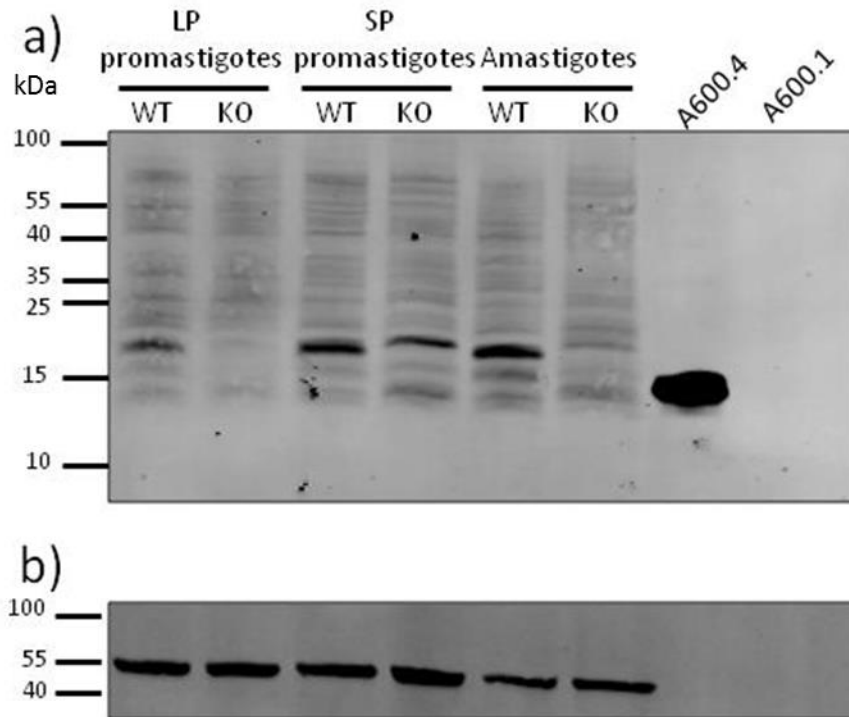


**Figure 3.8: Western Blot analysis of the GenScript anti-A600.4 antibody specificity for the *L. mexicana* endogenous A600.4 protein.**

Proteins (30  $\mu\text{g}$ ) from whole cell lysates of *L. mexicana* wild-type (WT) and *A600*<sup>-/-</sup> (KO) promastigotes and amastigotes were separated on a 12% Tris-Tricine-SDS gel. After transfer, the membrane was probed with the anti-A600.4 antibody at 0.18  $\mu\text{g}/\text{ml}$  (1:2,500 dilution). The bound antibody was detected with an anti-rabbit Alexa Fluor 680 goat anti-rabbit antibody. The membrane was also probed with a mouse anti-alpha-tubulin antibody (1:2,000 dilution = 0.1  $\mu\text{g}/\text{ml}$ ) as loading control for the cell lysates (b). Detection of the bound anti-alpha-tubulin antibody was performed with the IRDye 800CW goat anti-mouse secondary antibody. Membranes were scanned with the Odyssey CLx Imager. A600.4: sample collected after elution with the PreScission protease of the Glutathione Sepharose 4B beads incubated with the BL21+pGST-A600.4 lysate (20 ng/well). A600.1: sample collected after elution with the PreScission protease of the Glutathione Sepharose 4B beads incubated with the BL21+pGST-A600.1 lysate (20 ng/well).

### **3.2.4 Characterization of the A600.1 protein expression profile during the *L. mexicana* life cycle**

Northern blot analysis showed that the *A600.1* gene expression was about 1.5-fold upregulated in amastigotes (Murray, 2005). However, comparison of mRNA levels with the corresponding protein levels showed that mRNA levels do not always reflect the corresponding protein expression profile in promastigotes and amastigotes (Lahav et al, 2011; McNicoll et al, 2006). For this reason, the A600.1 protein expression profile in *L. mexicana* promastigotes and amastigotes was investigated. Since the anti-A600.1 peptide 2 antibody was found to be specific for the A600.1 protein with no cross-reaction with other *L. mexicana* proteins when used in Western blot, this antibody was used for this purpose.

Biochemical comparisons of axenic promastigotes and amastigotes grown in culture to promastigotes isolated from sandflies and lesion-derived amastigotes, respectively have demonstrated the validity of using axenic cultures to replicate the entire *Leishmania* life cycle *in vitro* (Bates, 1994). Logarithmic phase (LP) axenic promastigotes were showed to resemble non-infective procyclic promastigotes that reside in the sandfly mid-gut, whereas stationary phase (SP) axenic promastigotes resemble infective metacyclic promastigotes present in the sandfly salivary glands (Sacks et al, 1985). Differentiation of SP promastigotes into axenic amastigotes can be induced by lowering the pH of the culture medium (from 7 to 5.5) and increasing the temperature (from 26 to 32°C for *L. mexicana*), mimicking the conditions inside the phagolysosome that triggers the differentiation of promastigotes into amastigotes upon transmission from an infected sandfly to a mammalian host. Axenic amastigotes obtained 6 days after induction of promastigotes differentiation have been shown to be similar to amastigotes isolated from lesions (Bates et al, 1992; Zilberstein, 2008).

To determine the expression profile of the A600.1 protein in *L. mexicana* lifecycle, whole cell lysates of *L. mexicana* WT LP and SP promastigotes and axenic amastigotes were prepared by lysing the cells in 5% SDS. LP promastigotes were collected after two days in culture, while SP promastigotes were collected after five days. Amastigotes lysates were collected two days and six days after initiation of promastigotes differentiation. Lysates from *L. mexicana* A600<sup>-/-</sup> promastigotes and amastigotes were also collected to serve as negative controls. To control for protein loading, equivalent amount of proteins per sample were loaded on the gel (30 µg/lane). The samples were analyzed by Western blot, using the anti-A600.1 peptide 2 antibody (Figure 3.9). As seen before (Figure 3.5), the anti-A600.1 antibody 2 recognized a single band, at an estimated size of 23.5 kDa in the WT lysates. The A600.1 protein was detected in both promastigotes and amastigotes samples. No protein was detected in any of the A600<sup>-/-</sup> samples, confirming that the protein found in the WT lysates corresponds to the A600.1 protein. Those results suggest that the A600.1 protein is constitutively expressed at both stages of *L. mexicana* life cycle.

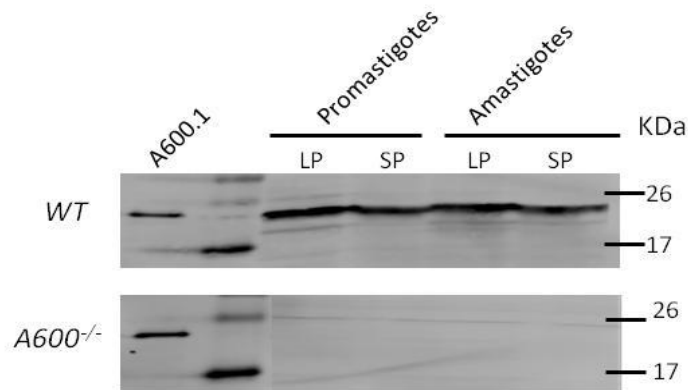


**Figure 3.9: Western Blot analysis of the A600.1 protein expression profile in *L. mexicana* WT and A600<sup>-/-</sup> promastigotes and amastigotes.**

Whole cell lysates of logarithmic phase (LP = day 2) or stationary phase promastigotes (SP = day 5) and amastigotes (SP = day 6) of *L. mexicana* WT and A600<sup>-/-</sup> were collected by lysis in 5% SDS then were separated on a 12% Laemmli SDS-PAGE gel (30 µg of proteins per lane). After transfer, the Western blot membrane was probed with the anti-A600.1 peptide 2 antibody at 0.15 µg/ml. The bound antibody was detected with an anti-rabbit Alexa Fluor 680 goat anti-rabbit antibody. Membranes were scanned with the Odyssey CLx Imager. 5 ng of the recombinant A600.1 protein were loaded as positive control.

### 3.2.5 Subcellular localization of the endogenous A600.1 protein in amastigotes

Several attempts at using the anti-A600.1 peptide 2 antibody to determine the subcellular localization of the endogenous A600.1 protein by immunofluorescence were unsuccessful. No distinctive signal could be detected in the *L. mexicana* WT cells in comparison to the *L. mexicana* A600<sup>-/-</sup> cells. A differential digitonin titration approach was therefore employed instead. This approach consisted of treating the cells with different amounts of digitonin, based on the principle that due to the differences in sterol content, the plasmic and subcellular membranes are differentially disrupted by the non-ionic detergent digitonin. This results in the differential release into the lysate supernatant of proteins from the various cellular compartments, dependent on the amount of digitonin used, as demonstrated using protein markers for each compartment (Rivière et al, 2009; Škodová et al, 2013).

Aliquots of *L. mexicana* WT amastigotes were lysed in presence of different amounts of digitonin and the lysates supernatants were analyzed by Western blot for the detection of different cell compartments proteins. In the initial studies, the digitonin incubation was performed at room temperature, as described elsewhere (Marché et al, 2000; Pilar et al, 2008; Rivière et al, 2009; Wiemer et al, 1995). Under those conditions, no differential disruption of the subcellular membranes were observed as all the different cell compartments markers (cytosolic, glycosomal, mitochondrial) were released in the supernatant at the lowest digitonin concentration. A differential release of those proteins could however be observed when the digitonin lysis was conducted on ice, with only the cytosolic protein present in the supernatant at low digitonin concentrations. Furthermore, proteolysis was found to be an issue during amastigotes lysis, as described elsewhere (Nugent et al, 2004). In comparison to promastigotes, additional protease inhibitors (100  $\mu$ M iodoacetamide, 100  $\mu$ M leupeptin, 1 mM Pefabloc) had to be used with amastigotes to prevent protein degradation.

Western blot analysis of the lysate supernatants indicated that the cytosolic marker, APRT was released at the lowest digitonin concentration (0.06 mg digitonin per mg of protein) (Figure 3.10). Meanwhile, the glycosomal and the endoplasmic reticulum markers, HGPRT and BiP respectively, were released at higher concentrations (> 0.3 mg digitonin per mg of protein). The mitochondrial intermembrane space protein, cytochrome c (cyt c) was used as a marker for the disruption of the mitochondrial outer membrane, in absence of an available antibody against a *Leishmania* mitochondrial outer membrane protein (Niemann et al, 2013). Furthermore, none of the antibodies produced against the mitochondrial outer membrane proteins of the closely related *Trypanosoma brucei* appear to cross-react with their *Leishmania* orthologues (literature search and personal communication with Dr André Schneider from the University of Bern,

Switzerland). The detection of cyt c in the supernatant indicated that the mitochondrial outer membrane was disrupted at similar digitonin concentrations (> 0.3 mg digitonin per mg of protein) as the glycosomal and endoplasmic reticulum membranes, as previously shown in *Trypanosoma brucei* procyclics using the mitochondrial outer membrane protein, VDAC (voltage-dependent anion channel) as a marker (Škodová et al, 2013). The disruption of the mitochondrial inner membrane required much higher amounts of digitonin (>1mg per mg of protein) as shown by the release of the mitochondrial matrix protein, mtHSP70 and the mitochondrial inner membrane protein p27. The co-release of A600.1 with p27 at the highest digitonin concentration strongly suggests a localization of A600.1 to the mitochondrial inner membrane. This result correlates with fluorescence microscopy analysis of *L. mexicana* cells expressing the GFP-A600.1 fusion protein that showed the proximity of the GFP signal to the kinetoplast signal and its co-localization with the mitochondrial marker, MitoTracker (Dr A. Marr, unpublished results).

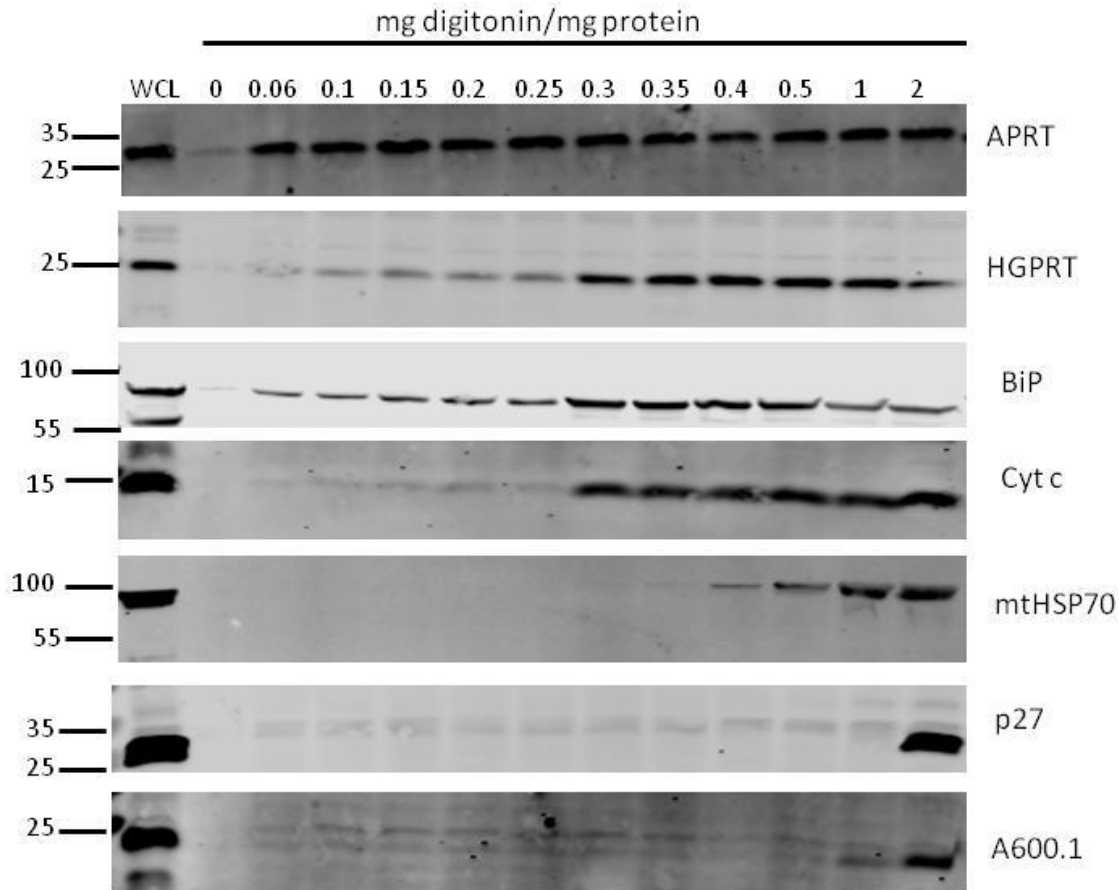


**Figure 3.10: Western Blot analysis of supernatants of *L. mexicana* WT amastigotes lysates after digitonin titration.**

Aliquots of amastigotes (corresponding to 375 mg of proteins) were treated with increasing amounts of digitonin (indicated as mg digitonin per mg of *L. mexicana* proteins). After a five-minute incubation on ice, the lysates were centrifuged at 16,000 x g for 2 min at 4°C and the supernatants collected for analysis. APRT is used as a cytosolic marker, HGPRT as a glycosomal marker, BiP as a marker for the endoplasmic reticulum. Release in the supernatants of the mitochondrial inter membrane space protein, cyt c is an indicator of the disruption of the mitochondrial outer membrane. MtHSP70 is a mitochondrial matrix protein and p27, a protein of the mitochondrial inner membrane.

### 3.2.6 Summary of bioinformatic analysis of the *L. mexicana* A600.1 and A600.4 proteins

Analysis of the *L. mexicana* A600.1 protein sequence with the PSIPRED program (<http://bioinf.cs.ucl.ac.uk/psipred/>) predicted the presence of five  $\alpha$  helical regions, located between amino acids 7-19, 40-63, 80-86, 91-110 and 137-145, and three small  $\beta$  sheets regions, at amino acids 33-36, 129-131 and 156-158 (Figure 3.11a). Three  $\alpha$  helical regions were

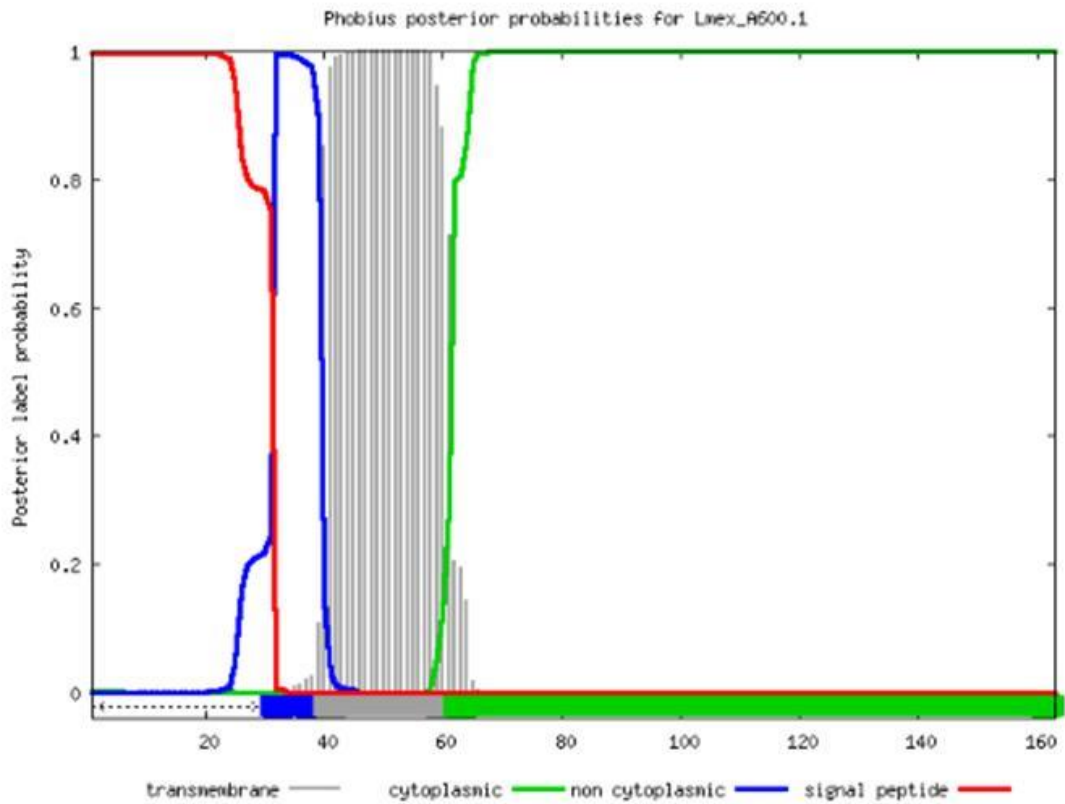




0.431 < cut-off = 0.5) nor in A600.4 (D-score = 0.135) when the “Eukaryotes” was selected as organism group before analysis. When “Bacteria” (Gram-negative or Gram-positive) was selected as the organism group, a signal peptide corresponding to the first 24 amino acids was predicted in the A600.1 protein, with a cleavage site between amino acids 24 and 25.

a)

ID	Lmex_A600.1			
FT	SIGNAL	1	30	
FT	REGION	1	6	N-REGION.
FT	REGION	7	18	H-REGION.
FT	REGION	19	30	C-REGION.
FT	TOPO_DOM	31	39	NON CYTOPLASMIC.
FT	TRANSMEM	40	61	
FT	TOPO_DOM	62	163	CYTOPLASMIC.
	//			



b) ID Lmex\_A600.4  
 FT TOPO\_DOM 1 27 NON CYTOPLASMIC.  
 FT TRANSMEM 28 48  
 FT TOPO\_DOM 49 93 CYTOPLASMIC.  
 //

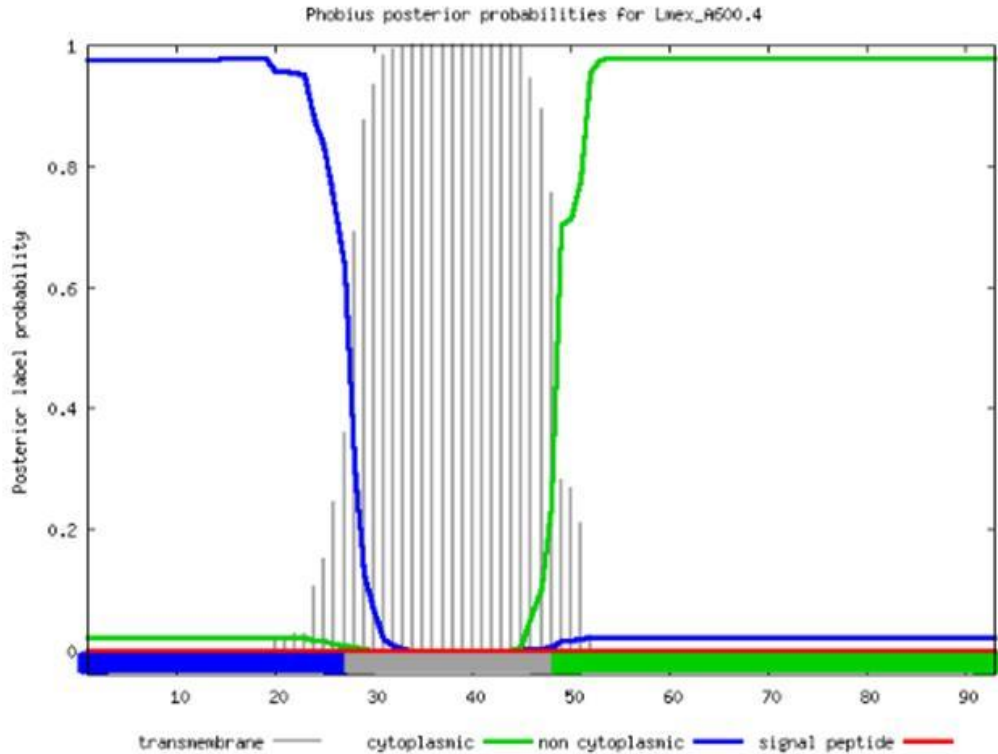


**Figure 3.12: Graphic representation of the topology of the *L. mexicana* A600.1 (a) and A600.4 (b) proteins as predicted by the PHOBIUS program.**

The transmembrane  $\alpha$ -helix predictor program TMHMM predicted (<http://www.cbs.dtu.dk/services/TMHMM/>) two transmembrane  $\alpha$ -helix domains in the A600.1 protein sequence, at amino acids 7-29 and 39-61. Both regions were among the  $\alpha$  helical regions predicted by the PSIPRED program (Figure 3.11a). However, only the second transmembrane domain (residues 40-61) was detected by the Phobius program (Figure 3.12a). One transmembrane  $\alpha$  helical domain was detected in the A600.4 protein sequence, between amino acids 27-48 which is among the three  $\alpha$  helical regions predicted by the PSIPRED program

(Figure 3.11b). The same region was predicted by the Phobius program (Figure 3.12b). Similarly to the Phobius program, the MEMSAT-SVM program (<http://bioinf.cs.ucl.ac.uk/psipred/?memsatsvm=1>) predicted the presence of a signal peptide at the N-terminal end of the A600.1 protein, corresponding to residues 1-31, and one transmembrane  $\alpha$  helix in region 42-61. For the A600.4 protein sequence, a 28-amino acid long signal peptide was predicted at the N-terminal end and one transmembrane domain between amino acids 31 to 48.

The DISOPRED program (<http://bioinf.cs.ucl.ac.uk/psipred/?disopred=1>), which predicts disordered regions predicted the presence of such region at the N-termini (first 15 amino acids), C termini (amino acids 140-193) and the internal region (94-107) of the A600.1 sequence. The same regions were also identified as protein binding sites with confidence scores above 0.6 (Figure 3.13a). Meanwhile, the transmembrane domain-containing region (amino acids 40-80) was predicted as ordered with a confidence score for disorder below 0.1. In the A600.4 protein sequence, the disordered regions were detected at both the N-terminal (amino acids 1-12) and C-terminal ends (amino acids 80-93) and predicted to be both protein binding sites with a confidence score above 0.8 (Figure 3.13b).

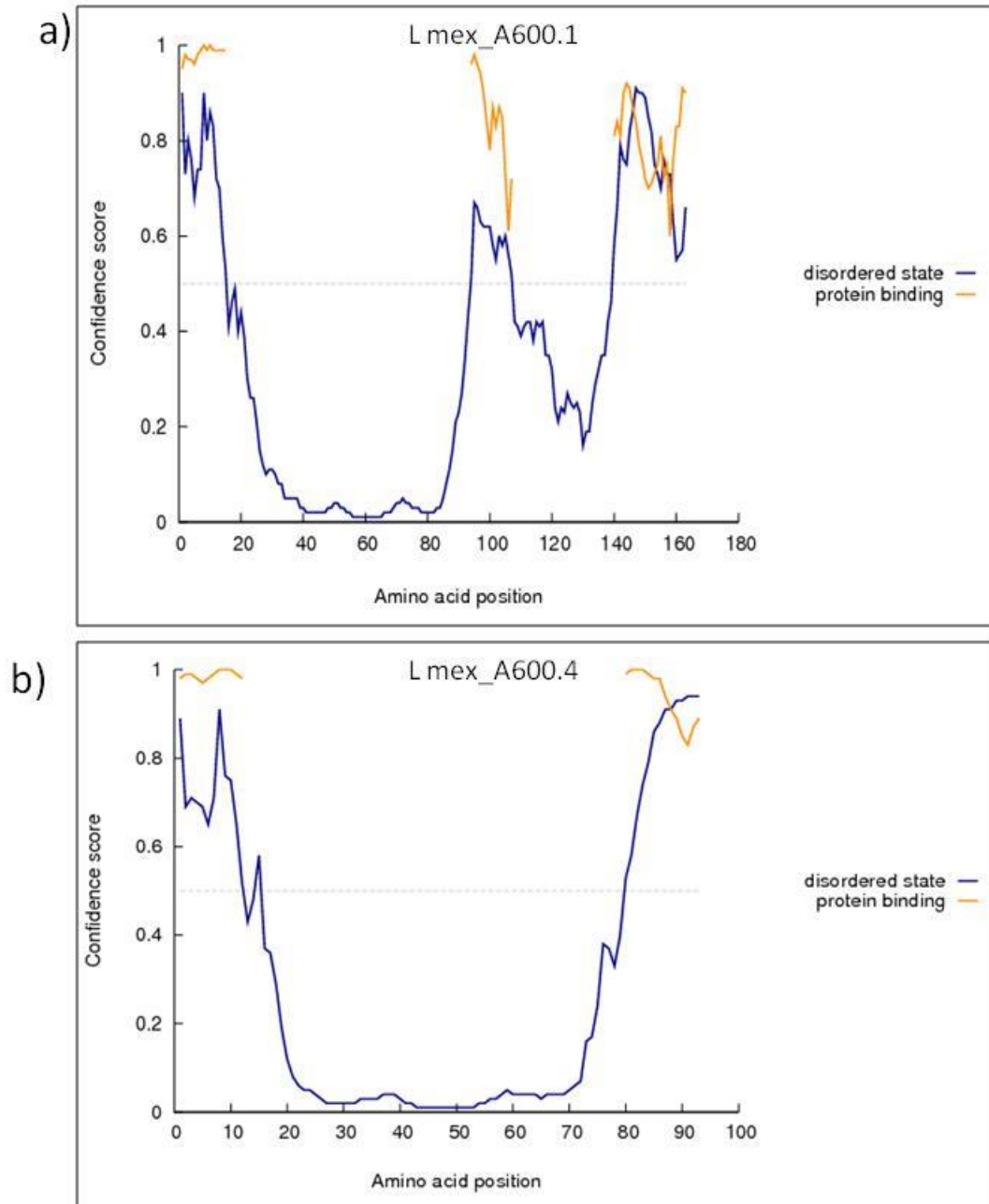


**Figure 3.13: Graphic representation of the intrinsic disorder profile of the *L. mexicana* A600.1 (a) and A600.4 (b) proteins as predicted by the DISOPRED program.**

### 3.3 Discussion

The objective of this chapter was to characterize the *L. mexicana* A600 proteins through analysis of their expression profiles in promastigotes and amastigotes and to elucidate their

subcellular localization, which would provide some information in regards to their function. To do so, antibodies were generated against the A600.1 and A600.4 proteins and their reactivity and specificity for the target A600 protein were tested against both the recombinant and endogenous proteins.

Previously, several attempts had been undertaken to obtain antibodies against the A600 proteins but were unsuccessful. In some cases, the antibody reacted well with the antigen peptide but did not react against the endogenous protein in Western blot. Using the proprietary antigen design program at GenScript, two sequences in the A600.1 protein but only one in the A600.4 protein were identified to use as antigens to immunize rabbits and produce antibodies specific to the *L. mexicana* A600.1 and A600.4 proteins, respectively. Although all three antibodies reacted well against the recombinant target proteins produced in *E. coli*, only one antibody, directed against the A600.1 protein region between amino acids 140 and 153, showed specificity against the *L. mexicana* endogenous protein. The other two antibodies (the anti-A600.1 peptide 1 antibody and the anti-A600.4 antibody) did not appear to recognize specifically the target endogenous proteins in *Leishmania*.

The anti-A600.1 peptide 2 antibody revealed that the A600.1 protein is constitutively expressed between both stages of the parasite. This is in agreement with Northern blots analysis of the *A600.1* gene expression in promastigotes and amastigotes (Murray, 2005). However, considering the high percentage of sequence identity between the A600.1 and the A600.2 and A600.3 proteins (100% and 99%, respectively), it is not possible by Western blot to analyze the expression profile of those proteins separately as the anti-A600.1 antibody is unlikely to distinguish between the three proteins.

Deletion of the *L. mexicana* *A600* locus leads to a proliferation defect of the deletion mutants at the late stage of promastigotes to amastigotes differentiation. Re-expression of the *A600.1* protein in those mutants partially restores proliferation (Murray et al, 2010). Subcellular localization of the *A600.1* protein by digitonin titration of amastigotes suggests that the protein localized to the mitochondria. The fact that the *A600*<sup>-/-</sup> promastigotes development is not affected by the deletion of the *A600* genes, despite the fact that the *A600.1* protein is expressed in that stage of the parasite suggest that the *A600.1* protein is involved in a mitochondrial pathway that is not crucial or can be by-passed in promastigotes but is important at the amastigote stage. This provides further evidence of the greater sensitivity of amastigotes to mitochondria defects. Indeed, while inhibition of the TCA cycle only induced growth arrest in promastigotes with no effect on their viability, it had a cytotoxic effect on amastigotes even with a 100-fold lower amount of inhibitor (McConville & Naderer, 2011; Saunders et al, 2014). Furthermore, similarly to what was observed with the *A600* genes, deletion of genes that affect the levels of certain mitochondrial proteins was found to have more deleterious effects in amastigotes than in promastigotes. The decrease in the levels of the *L. major* LACK protein (the ortholog of the mammalian RACK1 (receptor for activated c kinase 1) protein in *Leishmania*) following deletion of 3 of the 4 copies of the *LACK* gene, resulted in the downregulation of the mitochondrial proteins COX4 and COX6 (subunits of the mitochondria electron transport chain Complex IV). In comparison to *WT* cells and to mutant promastigotes grown at 27°C, *LACK*<sup>-/-</sup> mutant promastigotes grown at amastigote temperatures (35°C) exhibited growth defects both in culture and in macrophages and mitochondrial dysfunction, characterized by low cellular ATP content, a decrease in mitochondrial membrane potential, in oxygen consumption and in Complex IV (cytochrome c oxidase) activity. These defects were all rescued by the episomal expression of

COX4 in those mutants (Cardenas et al, 2015). In a similar fashion, deletion of the *L. donovani* amastigote-specific mitochondrial protein, p27, another Complex IV subunit, which affects amastigotes Complex IV activity and ATP generation by oxidative phosphorylation, was found to be associated with a failure of the parasite to replicate in macrophages and *in vivo* (Dey et al, 2010). *L. amazonensis* promastigotes in which one copy of the essential gene encoding the mitochondrial iron transporter LMIT1 was deleted, exhibited a normal growth in logarithmic phase and no significant mitochondrial defects. In contrast, the low levels of the LMIT1 protein affected amastigotes mitochondrial function and their replication (Mittra et al, 2016). This was manifested by a delay in amastigotes replication following initiation of differentiation from promastigotes, a failure of the parasites to multiply in macrophages, a low mitochondrial membrane potential, low mitochondrial aconitase activity and alterations of the mitochondrial inner membrane ultrastructure. These data indicate a greater dependence of the amastigote stage of the parasite on mitochondrial activity.

Bioinformatic analysis predicted the presence of at least one transmembrane domain in the N-terminal portion of the A600.1 protein. It is possible that A600.1 serves as an anchor for a multi-protein complex to the inner mitochondrial membrane. Due to their sequence identity (55%) and the presence of a central region highly conserved between the two proteins (Figure 2.2), it is possible that the A600.1 and A600.4 proteins have related functions. Therefore, elucidating the function of the A600.1 protein may shed light on the role of the A600.4 protein.

A BLAST search of the *L. mexicana* A600.1 protein revealed the presence of orthologs in other *Leishmania* species and in species of the closely related monoxenous trypanosomatid genus, *Leptomonas*. No ortholog of A600.1 or A600.4 was found in the other medically and veterinary important trypanosomatids, *Trypanosoma brucei* and *Trypanosoma cruzi* or in other

organisms. The value of studying kinetoplastid-specific proteins like the A600 proteins resides in the absence of mammalian homologs which makes them or the pathway they are involved in interesting molecules to investigate as potential targets for drug therapies; the absence of mammalian homologs decreases the likelihood of such therapies to find a target in mammalian cells, therefore decreasing the risk of side effects. Furthermore, these proteins may reveal a novel pathway in *Leishmania*, which may further our understanding of the parasite biology.

## Chapter 4: The *A600* genes and the *Leishmania* mitochondrial metabolism

### 4.1 Introduction

Since the A600.1 protein seems to localize to the mitochondria and *L. mexicana* *A600*<sup>-/-</sup> amastigotes exhibit a growth defect in comparison to the *WT* amastigotes (Murray et al, 2010), it is hypothesized that the deletion of the *A600* genes may affect the mitochondrial metabolism of amastigotes.

Mitochondria generate the majority of the ATP in eukaryotic cells. While promastigotes are able to use glucose as their primary source of carbon, amastigotes are thought to be more dependent on mitochondrial metabolism for survival (McConville & Naderer, 2011; Saunders et al, 2014).

Energy metabolism at the mitochondrial level involves the transport of pyruvate, the end-product of glycolysis into the mitochondria, where it is converted to acetyl-Co-A, and oxidized to CO<sub>2</sub>, via the tricarboxylic acid (TCA) cycle. Electrons from the NADH and succinate products of the TCA cycle are donated to Complex I and Complex II of the respiration chain, respectively, which transfer the electrons to oxygen, via Complexes III and IV. This transport of electrons is coupled to the translocation of protons from the mitochondrial matrix towards the mitochondrial inter membrane space. This results in the generation of a proton gradient across the inner mitochondrial membrane that is utilized by the F<sub>1</sub>F<sub>0</sub> ATP synthase, also referred to as Complex V, to synthesize ATP from ADP and inorganic phosphate. Complexes I, II, III and IV of the respiration chain form with Complex V, the oxidative phosphorylation (OXPHOS) system.

In addition to the synthesis of ATP by oxidative phosphorylation, trypanosomatids possess two additional ATP generation pathways in the mitochondria. ATP can be produced by substrate

phosphorylation, during oxidation of succinyl-CoA to succinate by the succinyl-CoA synthetase (SCoAS) in the TCA cycle and in the acetate: succinate CoA transferase/SCoAS cycle (ASCT cycle) (Bringaud et al, 2006).

Another essential mitochondrial pathway involves the assembly of iron-sulfur clusters, the most ancestral co-factor. Iron-sulfur cluster-containing proteins have diverse functions; many of them are involved in important cellular processes, such as DNA replication and repair, regulation of gene expression, electron transport, TCA cycle and iron homeostasis (Ali & Nozaki, 2013).

The mitochondrion is also the site of fatty acids biosynthesis via a type II fatty acid synthesis pathway and of fatty acid catabolism via  $\beta$ -oxidation (McConville et al, 2008). It also has a role in calcium homeostasis and cell death (Docampo et al, 2014).

Since no known conserved or functional domain could be identified in the A600 protein sequence and in absence of known homologs in other organisms, it was not possible to postulate about their function. To determine whether the A600 proteins may be involved in metabolic pathways, the activities of different mitochondrial pathways between *L. mexicana* WT and *A600*<sup>-/-</sup> amastigotes were analyzed and compared in order to identify the pathways that are affected by the deletion of the *A600* genes. Such pathways may provide some insights regarding the role of the A600 proteins in amastigotes.

## **4.2 Results**

### **4.2.1 Measurement of the ATP levels in *L mexicana* WT and *A600*<sup>-/-</sup> amastigotes**

One of the main functions of the mitochondria is the production of ATP. The cellular levels of ATP in *L. mexicana* WT and *A600*<sup>-/-</sup> amastigotes were measured using a

bioluminescence assay. This assay is based on the oxidation reaction of luciferin by luciferase, a reaction dependent on the presence of ATP and which results in the emission of light in proportion to the amount of ATP present in the sample. The cells were lysed by incubation at 100°C for 5 minutes in TE buffer and mixed with an equal volume of luciferase reagent from the Roche ATP Bioluminescence Assay Kit CLS II (Roche, Germany). The amount of ATP in the lysates was determined by measurement of the bioluminescence in each lysate-luciferase reagent mixture.

The measurement of ATP levels in *A600*<sup>-/-</sup> amastigotes was found to be about 40% lower than in the *WT* amastigotes (Figure 4.1). This may be linked to a decrease in the mitochondrial activities in the *A600*<sup>-/-</sup> amastigotes.

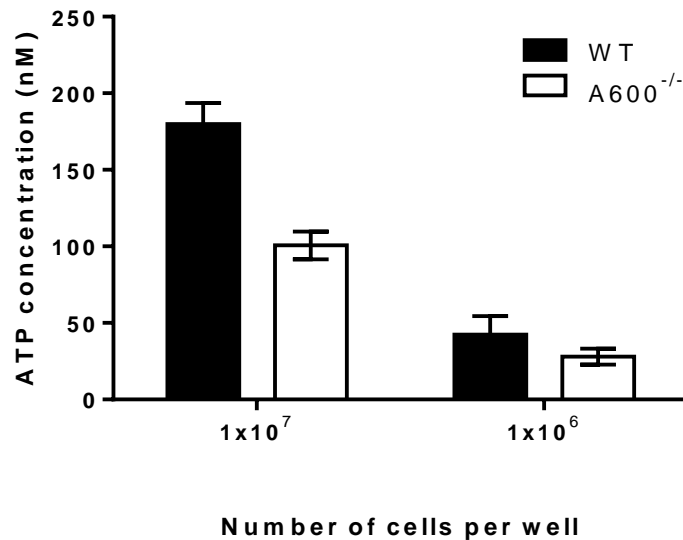


**Figure 4.1: Measurement of ATP concentrations in *L. mexicana* WT and *A600*<sup>-/-</sup> amastigotes.**

50 µl of each ATP standard (10<sup>-11</sup> to 10<sup>-4</sup> M) and *L. mexicana* WT and *A600*<sup>-/-</sup> amastigotes lysates (at 2 x 10<sup>7</sup> and 2 x 10<sup>8</sup> cells/ml) were distributed in triplicates in a 96-well white clear bottom plate and mixed with an equal volume of luciferase reagent. The bioluminescence in each well was measured with a Tecan Infinite 200 Pro luminescence plate reader. The ATP concentrations in the lysates were determined from a log-log plot of the standards bioluminescence.

#### **4.2.2 Comparison of the mitochondrial redox activity of *L. mexicana* WT and *A600*<sup>-/-</sup> amastigotes**

To determine whether the low cellular ATP content measured in the *L. mexicana A600*<sup>-/-</sup> amastigotes was associated with an impairment of the mitochondrial function in those cells, the Alamar Blue assay was employed to evaluate their mitochondrial redox activity. This assay is based on the reduction of the blue, non-fluorescent dye resazurin into resorufin, a pink, highly fluorescent compound. This reduction of the oxidized resazurin is ensured by reductases largely located in the mitochondria, although enzymes of the cytoplasm and glycosome may also be involved (Rampersad, 2012). Therefore, the Alamar Blue assay can be used as an indicator of mitochondrial function (Abu-Amero & Bosley, 2005; Zhang et al, 2004).

The mitochondrial activity was assessed in *L. mexicana* WT and *A600*<sup>-/-</sup> amastigotes collected 4 and 6 days after initiation of promastigotes differentiation into amastigotes. The fluorescence intensity detected in the day 4 and day 6 *A600*<sup>-/-</sup> amastigotes cell suspensions after incubation with the Alamar Blue reagent was equivalent to 64 and 53 % of the fluorescence intensity measured in the day 4 and day 6 WT cell suspensions, respectively. This indicates an impairment of the *A600*<sup>-/-</sup> amastigotes in reducing resazurin, suggesting a defect of the mitochondrial function in amastigotes in the absence of the *A600* genes (Figure 4.2).

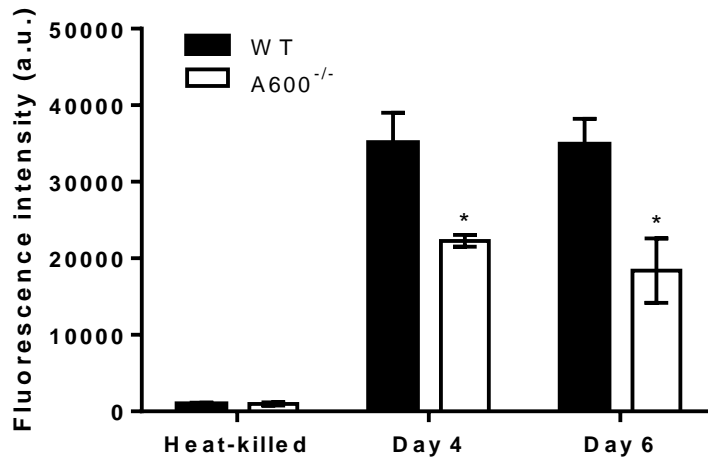


**Figure 4.2: Measurement of the mitochondrial redox activity in *L. mexicana* WT and *A600<sup>-/-</sup>* amastigotes.**

Heat-killed, day 4 and day 6-old amastigotes ( $1 \times 10^6$  cells per well) were incubated with the Alamar Blue reagent in a 96-well plate. After 2.5 hours at 32°C, the samples fluorescence was measured with an excitation wavelength of 550 nm and an emission wavelength of 600 nm. \*:  $P < 0.05$ .

#### 4.2.3 Comparison of the mitochondrial membrane potential $\Delta\Psi_m$ in *L mexicana* WT and *A600<sup>-/-</sup>* amastigotes

To investigate the performance of mitochondria in the *A600<sup>-/-</sup>* amastigotes, the mitochondrial membrane potential of the WT and *A600<sup>-/-</sup>* amastigotes were evaluated. This potential is crucial for the regulation of many mitochondrial activities such as ATP synthesis, ion homeostasis, protein import into the mitochondria and cell death (Gasser et al, 1982; Gottlieb et al, 2003; Gunter & Gunter, 1994; Hauser et al, 1996; Reid et al, 1966).

As electrons are transferred through the electron transport chain of the inner mitochondrial membrane, protons are taken up from the mitochondrial matrix and released to the mitochondrial intermembrane space (Figure 4.3). In a canonical electron transport chain, this movement of protons across the inner mitochondrial membrane is ensured by Complexes I, III and IV which are proton pumps, but Complex II is not involved; this leads to the generation of a

pH gradient and of an electrical gradient or membrane potential designated  $\Delta\Psi_m$ . This gradient is then used by the ATP synthase (Complex V) of the OXPHOS system which contains a channel that allows the reflux of protons back towards the mitochondrial matrix. The energy released by the protons reflux is harnessed for the synthesis of ATP from ADP and inorganic phosphate (Zíková et al, 2016).

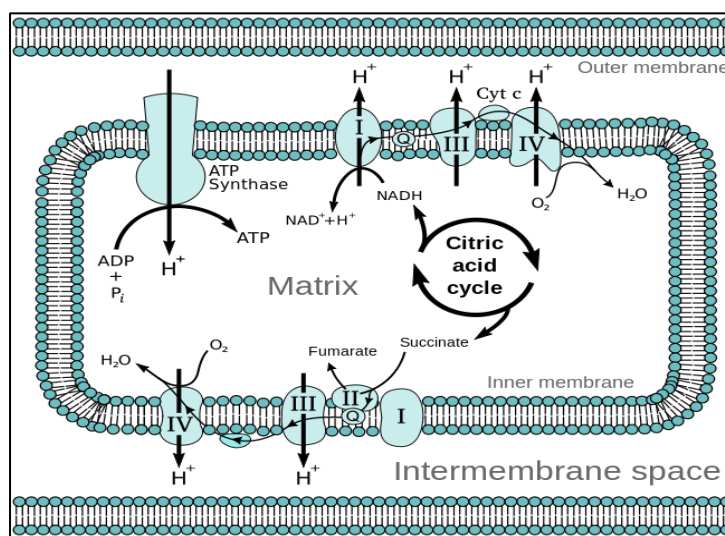


**Figure 4.3: Diagram of the mitochondrial OXPHOS complexes.**

(Retrieved 9 May 2018 from

[https://commons.wikimedia.org/w/index.php?title=File:Mitochondrial\\_electron\\_transport\\_chain%E2%80%9494Etc4.svg&oldid=251534413](https://commons.wikimedia.org/w/index.php?title=File:Mitochondrial_electron_transport_chain%E2%80%9494Etc4.svg&oldid=251534413))

The mitochondrial membrane potential  $\Delta\Psi_m$  can be evaluated using fluorescent dyes, which are cationic lipophilic compounds which accumulate in the mitochondrial matrix in proportion to  $\Delta\Psi_m$ . The higher the  $\Delta\Psi_m$ , the more dye accumulates in the mitochondrial matrix, resulting in a higher fluorescence signal, when the dye is used in a non-quenching mode (ie. below a certain concentration above which dye aggregation occurs leading to fluorescence quenching). Inversely, the lower the  $\Delta\Psi_m$  such as in the presence of substances that depolarize

the membrane, the less dye accumulates in the matrix resulting in a lower mitochondrial fluorescence.

To assess and compare the mitochondrial membrane potential between *WT* and *A600*<sup>-/-</sup> amastigotes, the fluorescent dye TMRM (tetramethylrhodamine methyl ester) was used, as described elsewhere (*Perry et al, 2011*). *L. mexicana WT* and *A600*<sup>-/-</sup> day 6 amastigotes were washed and incubated for 20 minutes in presence of the fluorescent dye TMRM at the non-quenching concentrations of 5 and 10 nM. The cells were centrifuged to remove the excess of dye and resuspended in PBS. Fluorescence was measured using a filter-based fluorescence plate reader, using the excitation filter 535 +/- 25 nm and the emission filter 590 +/- 20 nm. In this assay, since TMRM is used at low concentrations, the majority of the dye accumulates in the mitochondrial matrix leading to a high ratio of mitochondrial fluorescence versus cytosolic fluorescence. In this case, the fluorescence signal measured for the whole cell mainly corresponds to the mitochondrial signal. As controls, some *WT* amastigotes were treated for 10 minutes with FCCP before incubation with TMRM; FCCP is an uncoupling agent that forms protonophores in the inner mitochondrial membrane, allowing the reflux of protons from the mitochondrial intermembrane space back to the mitochondrial matrix, bypassing Complex V, leading to a depolarisation of the inner mitochondrial membrane, hence to a decrease in the  $\Delta\Psi_m$ .

A lower fluorescence signal was obtained with the *A600*<sup>-/-</sup> amastigotes in comparison to the *WT* amastigotes (Figure 4.4). A decrease in the fluorescence signal was also obtained with the *WT* amastigotes treated with FCCP, in a dose-dependent manner, showing that a lower fluorescence signal correlates with a lower mitochondrial membrane potential  $\Delta\Psi_m$ . In correlation with the cellular ATP levels and the mitochondrial redox activity, this result confirms

a decreased mitochondrial activity in the *L. mexicana* *A600*<sup>-/-</sup> amastigotes in comparison to the *WT* amastigotes.

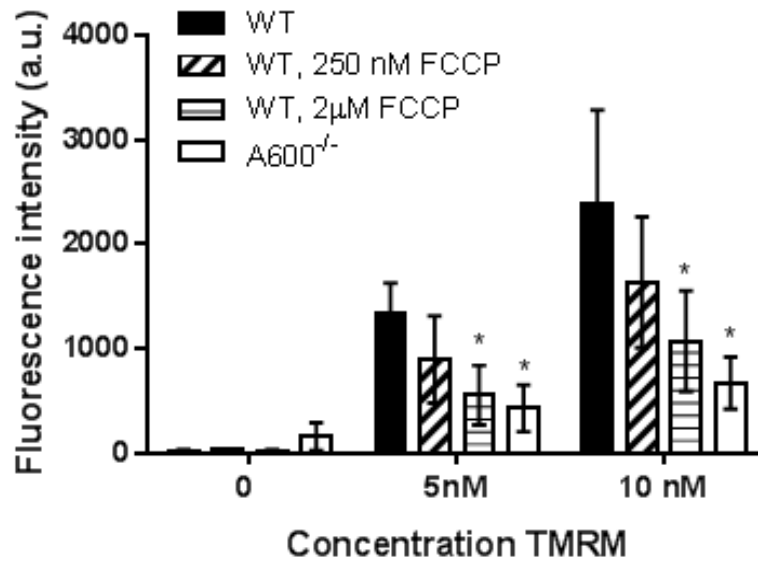


**Figure 4.4: Measurement of mitochondrial membrane potential  $\Delta\Psi_m$  in *L mexicana* *WT* and *A600*<sup>-/-</sup> amastigotes.**

After washing, the day 6 amastigotes were resuspended at  $5 \times 10^7$  cells/ml in PBS and incubated for 20 minutes at 32°C in presence of TMRM at a final concentration of 5 or 10 nM. The whole cell fluorescence was measured by plate reader using an excitation filter of 535 +/- 25 nm and an emission filter of 590 +/- 20 nm. The fluorescence intensity measured corresponds mainly to the amount of fluorescence emitted by the amount of dye accumulated in the mitochondria and therefore correlates to the mitochondrial membrane potential of the cells. \*:  $P < 0.05$ .

#### 4.2.4 Native PAGE analysis of the mitochondrial OXPHOS complexes in *L mexicana* *WT* and *A600*<sup>-/-</sup> amastigotes

Since the mitochondrial membrane potential  $\Delta\Psi_m$  is generated as a result of the electron transport chain activity, a decrease in the  $\Delta\Psi_m$  of amastigotes in absence of the *A600* genes indicates an impairment of the electron transport chain function. Therefore, a native PAGE

approach was first employed to visualize the mitochondrial OXPHOS complexes and determine whether their assembly and/or functionality were affected by the deletion of the *A600* genes.

The native PAGE technique was developed for the separation of membrane proteins and complexes from various biological membranes and cell or tissue homogenates (Schagger et al, 1994; Schagger & von Jagow, 1991; Wittig et al, 2006). It was proved to be a useful tool for the detection of human mitochondrial disorders (Schägger et al, 1996), for the analysis of multi-protein complexes composition (Zikova et al, 2009a), for the identification of protein-protein interactions (Arnold et al, 1998), for in-gel activity assays (Verner et al, 2014; Zerbetto et al, 1997), for immunodetection of proteins or protein complexes (Singha et al, 2012).

#### **4.2.4.1 Optimization of native PAGE conditions**

To visualize the mitochondrial OXPHOS complexes, the blue native PAGE method was first tested with *L. mexicana* WT promastigotes, so that the results could be directly compared to published data which were performed with promastigotes (Verner et al, 2014). Crude mitochondria-enriched fractions were isolated by hypotonic lysis of promastigotes and lysed with dodecyl maltoside at a final concentration of 2%, releasing the mitochondrial protein complexes in the soluble fraction after centrifugation. Coomassie Brilliant Blue G-250 was added to the mitochondrial supernatants to a final concentration of 0.5% and increasing amounts of mitochondrial extracts (10, 25, 50, 75 and 85 µg of proteins) were separated on a 3-12% native gradient gel, as described by Schagger and von Jagow (Schagger & von Jagow, 1991). After electrophoresis, the gels were stained by blue silver staining (Candiano et al, 2004) and one lane containing 85 µg of sample was incubated overnight in Complex V reaction buffer for the detection of this complex in-gel activity.

The same banding pattern was observed in the different lanes, regardless of the amount of proteins loaded per lane (Figure 4.4a). An amount of 10  $\mu\text{g}$  of proteins per lane resulted in the highest resolution of the protein bands with the lowest background. Four major bands were expected to be observed after Coomassie staining of the gel: one around 1MDa representing Complex V dimer, one around 800 kDa corresponding to Complex V monomer, and two around 700 kDa, the upper one being the F1 fraction of Complex V, the lower one Complex IV (personal communication, Dr Alena Zikova, University of South Bohemia, Czech Republic). Instead, only two major bands were seen, estimated at 615 and 673 kDa, respectively, probably corresponding to Complex V F1 fraction and Complex IV (Figure 4.5a). A faint band was detected at 815 kDa which might correspond to the Complex V monomer. Complex V in-gel activity is detected by the formation of white bands in presence of lead(II) nitrate and ATP in the reaction buffer. These white bands correspond to the presence of lead precipitates which formed as a consequence of the low pH induced by the release of free phosphate during ATP hydrolysis by Complex V. The in-gel activity staining of *L. mexicana* WT promastigotes resulted in a major white band estimated at 300 kDa and two very faint bands estimated at 400 and 827 kDa (Figure 4.5b). In-gel activity staining of Complex V of *Leishmania tarentolae* promastigotes or of the closely related *Trypanosoma brucei* procyclic form after native PAGE result in the formation of the three bands of complex V described above as white bands on a dark background, at 1 MDa, 800 and  $\sim$ 700 kDa (Verner et al, 2014; Zikova et al, 2009a). Only the 800 kDa band was detected here but very faintly. The fact that the banding pattern obtained was different than in published results and that no strong high molecular mass band ( $>720$  kDa) could be detected suggest that the complexes isolated in this sample were dissociated.

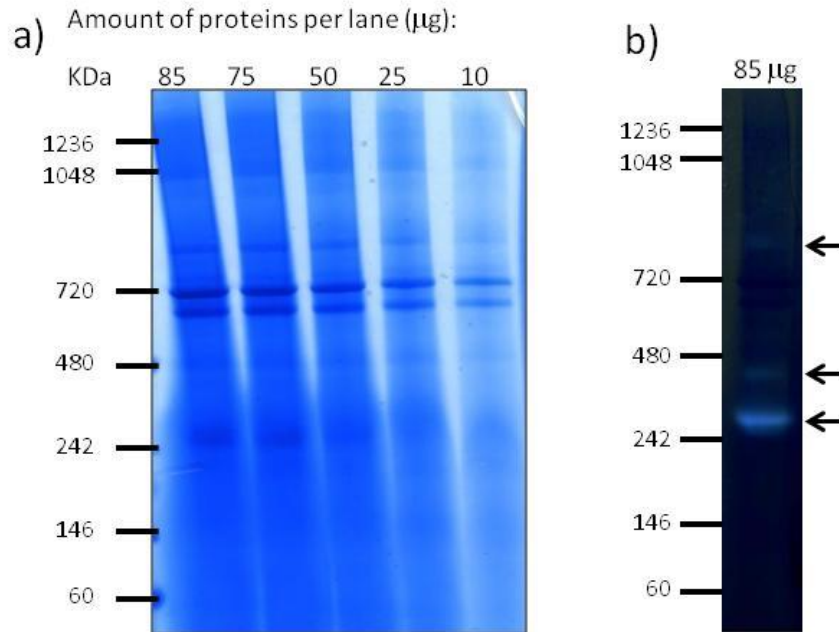


**Figure 4.5: Blue-native PAGE analysis of *L. mexicana* WT promastigote mitochondrial membrane complexes.**

Mitochondria-enriched fractions were lysed with a final concentration of 2% dodecyl maltoside. The indicated amounts of the extracts were separated on a 3-12% native gels at 100 V for 4.5 hours at 4°C. a) Coomassie staining: after electrophoresis, the gel was incubated in fixative overnight and stained in blue silver staining. b) Complex V in-gel activity. 85 µg of proteins were loaded in one lane. After electrophoresis, the lane was cut from the rest of the gel and incubated overnight in Complex V reaction buffer (35 mM Tris-HCl, pH 8; 270 mM glycine, 19 mM MgSO<sub>4</sub>, 0.2% Lead (II) nitrate, 8 mM ATP).

The dissociation of the complexes suggested that the conditions used in the present assay may not preserve the complexes' stability. Different concentrations of detergent were tested for lysing the *L. mexicana* WT promastigotes mitochondria-enriched pellets. Lysis was performed with digitonin at 0.5, 2, 4 or 5 mg/mg of protein or with 1% dodecylmaltoside. Electrophoresis was run using the conditions for high resolution clear native PAGE (hrCN-PAGE) described elsewhere (Wittig et al, 2007), replacing the Coomassie Blue G-250 in the cathode buffer with deoxycholate and dodecyl maltoside. These conditions were described to be milder than the blue native PAGE conditions and therefore may better preserve the physiological assembly of protein complexes. Coomassie staining of the gel after electrophoresis revealed a similar banding pattern

between the different lysates, with the exception of the sample lysed with 0.5 mg digitonin per mg of protein (Figure 4.6a). Digitonin at 0.5 mg per mg of protein appeared insufficient to solubilize the protein complexes from the membranes, as much less proteins were recovered in this sample in comparison to the samples solubilized with higher digitonin concentrations. The mitochondrial extracts obtained after lysis with 2, 4 or 5 mg digitonin per mg of protein or with 1% dodecyl maltoside contained the four major bands described above, estimated at 1,100, 880, 670 and 630 kDa, respectively (Figure 4.6a). This indicates that the conditions used in that assay preserved the integrity of the complexes. Those lysates only differed slightly by the amount of proteins released in the lysate supernatant; higher digitonin concentrations resulted in higher amounts of proteins released.

Complex V activity staining revealed the presence of three white bands in the three digitonin-solubilized mitochondrial samples (2, 4 and 5 mg/mg protein) (Figure 4.6b). The three bands appeared at the predicted sizes for the Complex V dimer (estimated at 1.1 MDa), monomer (~880 kDa) and F1 portion (~700kDa), as described previously (Verner et al, 2014). An additional fainter band was detected at 300 kDa, similar to the one detected previously (Figure 4.5). Some streaking was observed with the dodecyl maltoside lysate which could be due to the presence of insoluble material in the sample or to overloading as observed previously with dodecyl maltoside-solubilised samples (Zikova et al, 2009a). Overall, these new conditions (lysis with digitonin at 2-5mg/mg of protein – hrCN-PAGE) appeared to preserve the association of the mitochondrial respiratory complexes isolated from *L. mexicana* WT promastigotes.

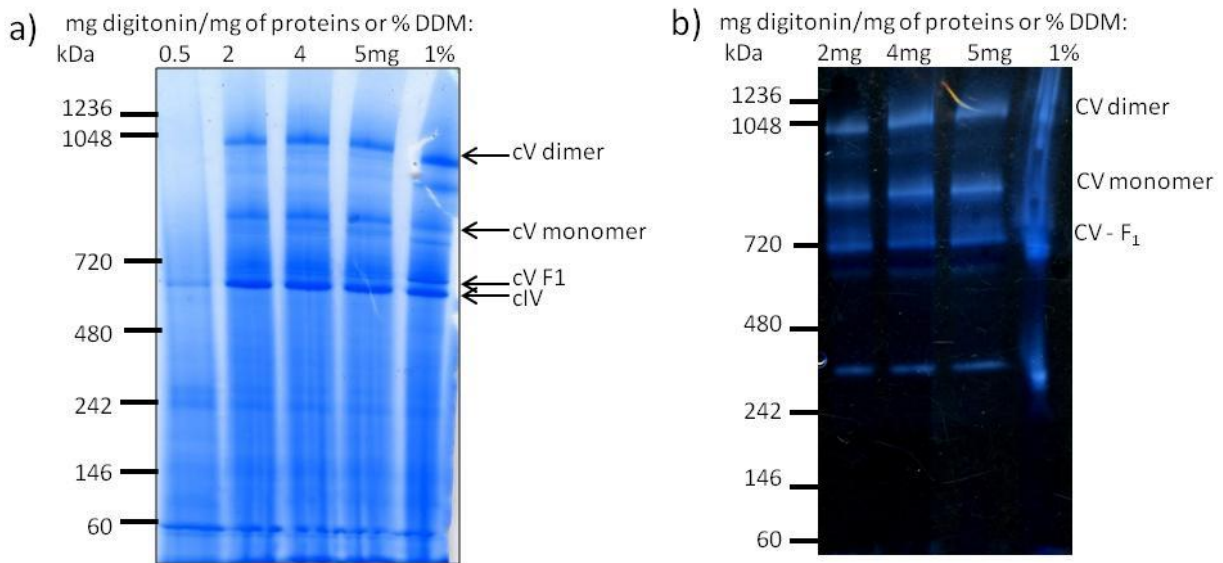


**Figure 4.6: High resolution clear native PAGE analysis of *L. mexicana* WT promastigote mitochondrial OXPHOS complexes.**

Mitochondria-enriched pellets were lysed with either digitonin (0.5-5 mg per mg of proteins) or 1% dodecyl maltoside (DDM). The lysates supernatants were separated on a 3-12% native gel at 100 V for 4.5 hours at 4°C. a) Coomassie staining: 20 µg of proteins from the lysate supernatants were loaded per lane. After electrophoresis, the gel was fixed overnight then stained with blue silver stain. b) Complex V in-gel activity: 40-50 µg of proteins were loaded per lane. After electrophoresis, the gel was incubated overnight in Complex V reaction buffer.

*L. mexicana* WT amastigotes mitochondrial complexes were then analyzed using the hrCN-PAGE conditions. The mitochondria-enriched fractions were lysed with dodecyl maltoside at 0.5, 1 and 2% or with digitonin at 2, 4 and 5 mg/mg of protein. Coomassie staining of the gel of the dodecyl maltoside (1% and 2%) and of the digitonin (4 mg/mg of protein) lysate supernatants revealed four major bands, similar to those observed after Coomassie staining of the digitonin-solubilised mitochondrial complexes of the *L. mexicana* WT promastigotes (Figure 4.6a). Staining of the Complex V in-gel activity resulted in two major bands corresponding to the complex dimer (estimated at 1.1 MDa) and monomer (estimated at 880 kDa) (Figure 4.7b). The 700 kDa band corresponding to the F1 portion was barely detectable in comparison to the promastigotes complexes staining (Figure 4.6b). As with the promastigotes samples, streaking

was observed with the 0.5% and the 1% dodecyl maltoside-solubilised samples, making it difficult to analyse the activity bands in those samples. This streaking seems to be linked to dodecyl maltoside since it was never observed with the digitonin-solubilised samples. Overall, lysis of mitochondrial vesicles with digitonin at 2-5 mg per mg of proteins followed by hrCN-PAGE resulted in separation of the promastigotes and amastigotes mitochondrial respiration complexes without affecting the complexes integrity.

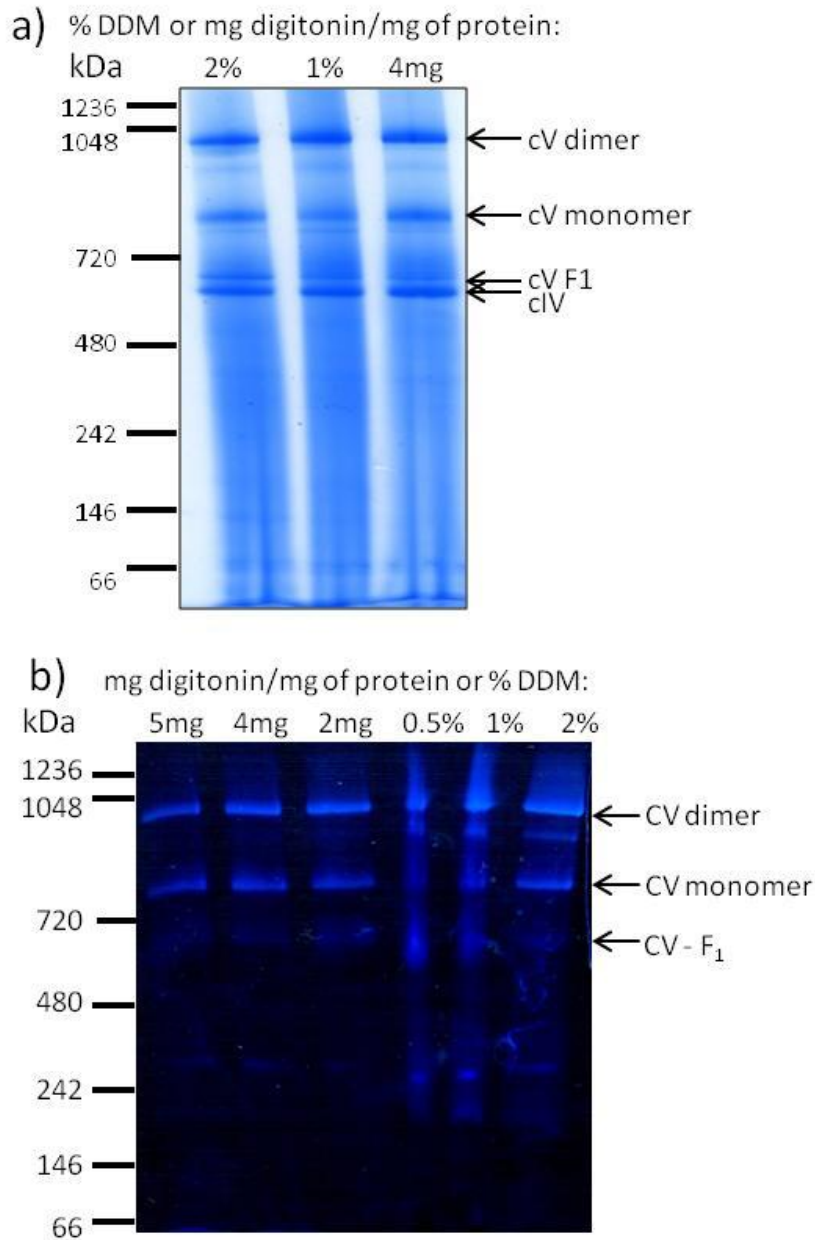


**Figure 4.7: High resolution clear native PAGE analysis of *L. mexicana* WT amastigote mitochondrial complexes.**

Mitochondria-enriched pellets were lysed with the indicated amount of either digitonin or dodecyl maltoside (DDM). The lysates supernatants were separated on a 3-12% native gel at 100 V for 4.5 hours at 4°C. After electrophoresis, the gel was fixed overnight then stained with blue silver stain. a) Coomassie staining: 20 µg of proteins from the lysate supernatants were loaded per lane. b) Complex V in-gel activity: 50 µg of proteins were loaded per lane. After electrophoresis, the gel was incubated overnight in Complex V reaction buffer.

#### 4.2.4.2 Analysis of the *L. mexicana* WT and *A600*<sup>-/-</sup> amastigotes OXPHOS complexes

Having optimized the conditions for the isolation and solubilization of the amastigotes OXPHOS complexes, the same conditions were applied for the isolation and separation of the mitochondrial complexes of the *L. mexicana* WT and *A600*<sup>-/-</sup> amastigotes. After electrophoresis, the gel was incubated overnight in the appropriate reaction buffer for in-gel activity staining of Complexes I, II, IV and V or was incubated for transfer and Western blot detection.

Complex I NADH dehydrogenase in-gel activity is characterized by the formation of a violet precipitate following the transfer of electrons from NADH to nitrotetrazolium blue (NTB). No such precipitate could be observed after overnight incubation of the gel strip containing the WT and *A600*<sup>-/-</sup> amastigotes mitochondrial complexes, suggesting the absence of Complex I activity in both strains (Figure 4.8a). This is in correlation with similar studies that fail to detect Complex I activity in *Leishmania* by native PAGE or SDS-PAGE (Maslov et al, 2002; Nebohacova et al, 2009; Verner et al, 2014).

Complex II activity staining is characterized by the formation of a violet precipitate resulting from the reduction of NTB as final acceptor of electrons from succinate through phenazine methosulfate. Three bands were detected in both lanes (Figure 4.8a), similarly to those detected in *L. tarentolae* promastigotes (Verner et al, 2014). The lower band estimated at 550 kDa appeared similar in size to the band detected after Complex II staining of the closely related *T. brucei* and *T. cruzi* (Acestor et al, 2011; Morales et al, 2009) and appears to migrate at a slightly higher size in the *A600*<sup>-/-</sup> sample. The middle band estimated at 890 kDa appears f similar intensity in both strains, whereas the higher band at 1.1 MDa is very faint in the *A600*<sup>-/-</sup> cells. This data suggests that Complex II is present and active in amastigotes in absence of the *A600* genes.

Since the method described to stain Complex III from bovine heart mitochondria was showed to stain Complex IV (Verner et al, 2014), Complex III was visualized instead by Western blot using an antibody against one of its catalytic subunits, the Rieske iron sulfur protein. A band of approximately 600 kDa was detected in both strains (Figure 4.8b). This band appears to be of similar size as the band detected by the antibody against Complex III apoc 1 subunit in *L. tarentolae* promastigotes (Verner et al, 2014). This result suggests that the complex is present in both strains and that its assembly is not affected by the absence of the A600 proteins.

Complex IV in-gel activity results in the formation of a brown precipitate, following oxidation of cytochrome c and reduction of diamino benzidine. Similar staining was observed between the *WT* and *A600*<sup>-/-</sup> amastigotes, with the main band appearing at ~700 kDa and two weaker bands at 1.1 MDa and 890 kDa, respectively. This is consistent with the Complex IV activity staining obtained with *L. tarentolae* promastigotes (Verner et al, 2014) (Figure 4.8a). Bands of similar sizes as those observed after the in-gel activity staining were detected in both strains following Western blot with an antibody directed against the Complex IV subunit, the COIV protein (Figure 4.8b). These data indicate that Complex IV is assembled and active in the *A600*<sup>-/-</sup> amastigotes.

Similarly to what was found before (Figure 4.7a), the staining of Complex V activity of *WT* amastigotes exhibited two major bands at ~1.1 MDa and ~900 kDa (Figure 4.8a). In comparison, in the *A600*<sup>-/-</sup> samples, the dimer band appeared fainter and some extra bands were detected around the 900 kDa monomer band, which might correspond to different assembly states of the Complex V monomer. The banding pattern obtained for each strain after activity staining was similar to the one observed after Western blot detection of the complex  $\beta$  subunit

(Figure 4.8b), suggesting that Complex V dimer formation may be affected in the absence of the A600 proteins.

Taken together, these data indicate that Complex I is not active in axenic amastigotes. Except for an effect on the Complex V dimerisation, the OXPHOS complexes integrity is maintained in absence of the A600 proteins and the complexes appear to be active in the *L. mexicana* *A600*<sup>-/-</sup> amastigotes.

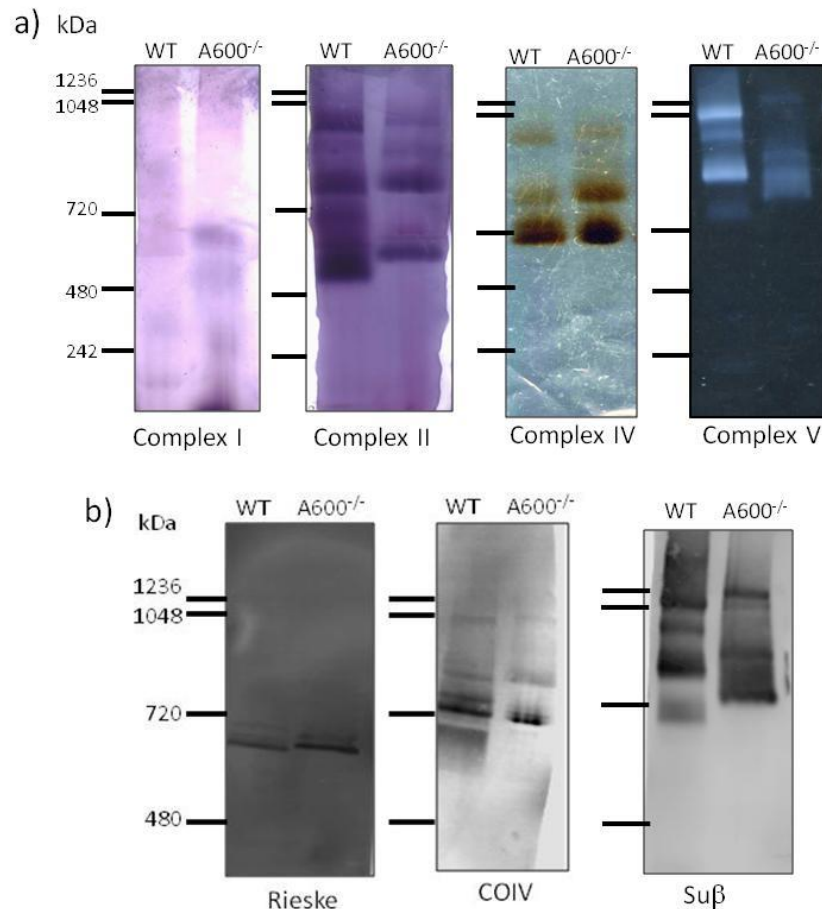


**Figure 4.8: High resolution clear native PAGE analysis of *L mexicana* WT and *A600*<sup>-/-</sup> amastigote mitochondrial OXPHOS complexes.**

The mitochondria-enriched pellets were lysed with 4 mg digitonin per mg of protein. a) In-gel activity staining of Complexes I, II, IV and V. *L mexicana* WT and *A600*<sup>-/-</sup> amastigotes organellar extracts were each loaded at 45 µg of proteins per lane. After electrophoresis, the gel strips were incubated overnight in the appropriate reaction buffer. For detection of Complex I activity: 100 mM Tris-HCl, pH 7.4, 0.14 mM NADH, 1 mg/ml NBT; for Complex II: 50 mM sodium phosphate pH 7.4, 84 mM sodium succinate, 0.2 mM phenazine methosulfate, 2 mg/ml NBT, 4.5 mM EDTA, 10 mM potassium cyanide; for Complex IV: 50 mM sodium phosphate pH 7.4, 1 mg/ml diaminobenzidine, 24 U/ml catalase, 1 mg/ml cytochrome c, 75 mg/ml sucrose; for Complex V: 35 mM Tris pH 8, 270 mM glycine, 19 mM MgSO<sub>4</sub>, 0.2% Lead (II) nitrate, 8 mM ATP. b) Western blot detection of subunit Rieske of Complex III, subunit COIV of Complex IV and subunit β of Complex V. The bound antibodies were detected with an Alexa Fluor 680 goat anti-rabbit secondary antibody.

#### 4.2.5 Comparison of the enzymatic activities of the mitochondrial OXPHOS complexes in *L. mexicana* WT and *A600*<sup>-/-</sup> amastigotes

To investigate further the effect of the absence of the A600 proteins on the OXPHOS pathway, the enzymatic activity of the individual complexes was quantified in *L mexicana* WT and *A600*<sup>-/-</sup> amastigotes, using spectrophotometric assays (Kirby et al, 2007; Verner et al, 2014). For each complex, the enzymatic activity is determined by the variation in absorbance of the reaction overtime following the addition of an electron acceptor, in presence of the complex substrate.

The presence and function of Complex I in *Leishmania*, as in other trypanosomatids, has been a subject of debate (Duarte & Tomas, 2014; Opperdoes & Michels, 2008). Although the genes encoding its subunits have been identified in both the nuclear and mitochondrial genomes, evidence of this complex activity in *Leishmania* remains unclear. In the present experiment, Complex I NADH dehydrogenase activity is assessed by the decrease in absorbance at 340 nm following the transfer of electrons from NADH to ubiquinone. In both the WT and the *A600*<sup>-/-</sup> amastigotes, the decrease of absorbance registered over time following the addition of ubiquinone was minimal in comparison to the blank or negative control reactions (reactions without mitochondrial sample or without substrate), as represented by the slope of the trendline equation in Figures 4.9 a and b which are representative of the variation of absorbance obtained in this assay during the 3 minutes of absorbance measurement with both cell strains. Furthermore, the measured activity appeared insensitive to rotenone inhibition, as the percentage of inhibition obtained was variable, similarly to what was found with *L. tarentolae* promastigotes (Verner et al, 2014) (cf. Appendix B.1). The enzymatic activity obtained here with the WT amastigotes ( $19.6 \pm 5.2$  U/mg) was within the same range as the activity calculated for the *L.*

*tarentolae* promastigotes ( $14 \pm 8$  U/mg). In light of these results, in addition to the absence of NADH dehydrogenase activity detection following in-gel activity staining in native PAGE gels (Figure 4.8a), it is unclear whether the activity measured here is attributable to Complex I, in correlation with previous studies that question the contribution of Complex I to the NADH:Ubiquinone oxido-reductase activity in the closely related *Trypanosoma brucei* (Surve et al, 2012; Verner et al, 2011). Nevertheless, the NADH dehydrogenase activity measured here appeared to be increased in the *A600*<sup>-/-</sup> amastigotes ( $52.4 \pm 22.6$  U/mg) in comparison to the *WT* amastigotes (Figure 4.9c).

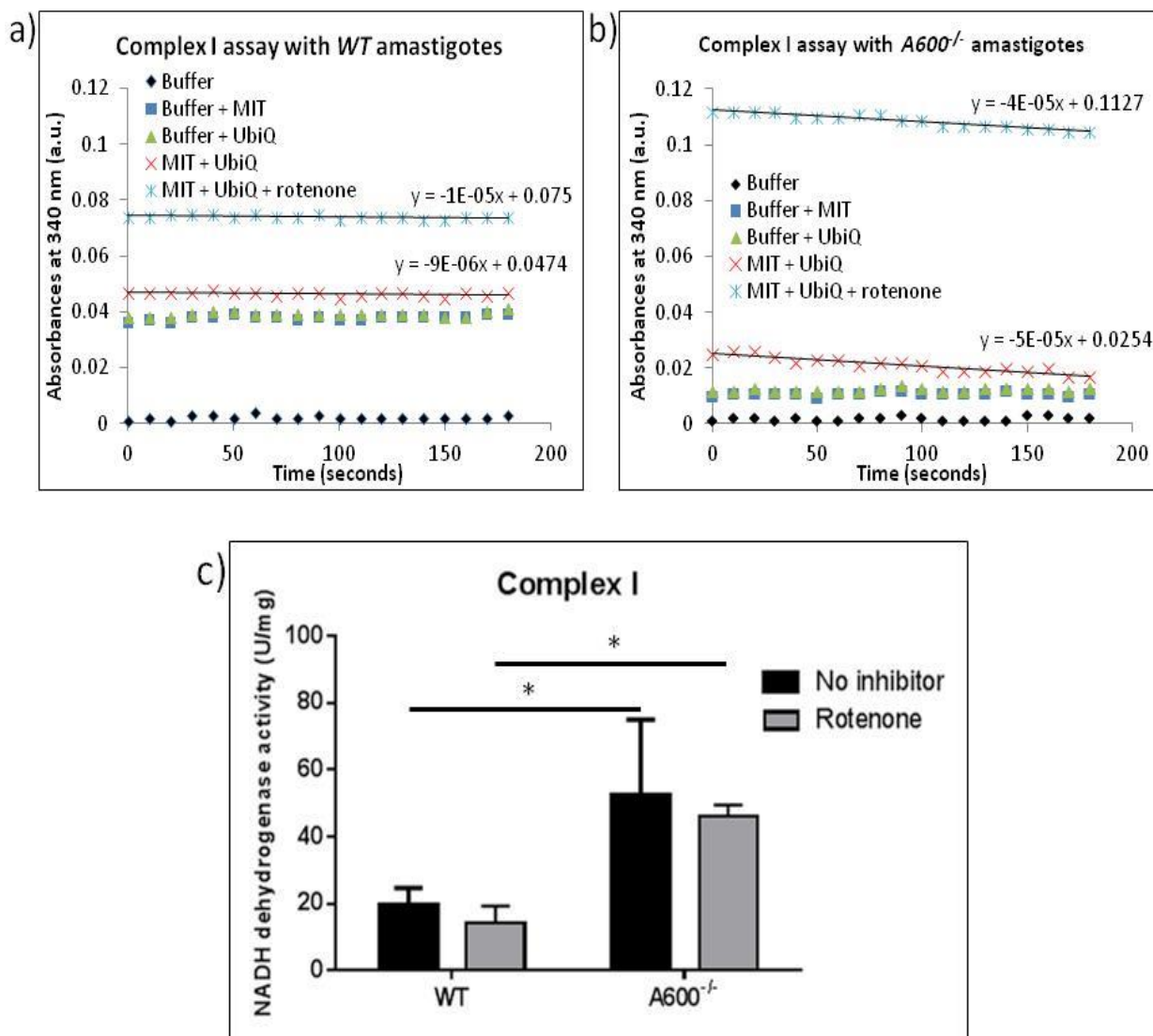


**Figure 4.9: Analysis of Complex I NADH dehydrogenase activity in *L. mexicana* WT and A600<sup>-/-</sup> amastigotes.**

a) Example representative of absorbance variation measured with *L. mexicana* WT amastigotes at 340 nm following addition of ubiquinone. b) Example representative of absorbance variation measured with *L. mexicana* A600<sup>-/-</sup> amastigotes. “Buffer”: cuvette containing the NDH buffer (50 mM potassium phosphate, pH 7.5; 1 mM EDTA, pH 8.5; 0.2 mM KCN) with 0.1 mM NADH. This cuvette was used to blank the spectrophotometer before the absorbance measurement; “Buffer + MIT”: cuvette with NDH buffer with 0.1 mM NADH and 5  $\mu$ l of mitochondria sample; “Buffer + UbiQ”: cuvette with NDH buffer and 0.1 mM NADH with 10  $\mu$ l of 2 mM ubiquinone-1; “MIT + UbiQ”: buffer with 0.1 mM NADH, 5  $\mu$ l of mitochondria sample and 10  $\mu$ l of 2 mM ubiquinone-1; “MIT + UbiQ + rotenone”: buffer with 0.1 mM NADH, 5  $\mu$ l of mitochondria sample, 10  $\mu$ l of 2 mM ubiquinone-1 and 10  $\mu$ l of 1 mM rotenone.  $y$ : equation of the trendlines of the absorbance variation over time in the “MIT + Ubiquinone” and the “MIT + Ubiquinone + rotenone” reactions. c) NADH dehydrogenase activity calculated in *L. mexicana* WT and A600<sup>-/-</sup> amastigotes. 1 unit (U) of enzymatic activity corresponds to the amount of enzyme necessary for the conversion of 1 nmol of NADH per minute. a.u.: arbitrary units. \* $P < 0.05$

Complex II succinate dehydrogenase activity is determined by following the decrease in absorbance at 600 nm caused by the reduction of DCPIP as electrons are transferred from succinate to ubiquinone then from ubiquinol to DCPIP. Comparison of the succinate dehydrogenase activity between the *L. mexicana* WT ( $162.8 \pm 15.4$  U/mg) and the *A600*<sup>-/-</sup> amastigotes ( $193.9 \pm 47.5$  U/mg) found no significant difference in the levels of activity between the two strains (Figure 4.10 c and Table 4.1). In both cases, the activity was inhibited at 80-90% in presence of 1 mM of Complex II inhibitor, malonate (cf. Appendix B.2). This suggests that Complex II is not affected by the deletion of the *A600* genes and that the *A600* proteins may not be involved in this complex activity. Figure 4.10 a and b are representatives of the absorbance variation over time in the different reactions with *WT* and *A600*<sup>-/-</sup> samples. The enzymatic activities calculated for each assay are presented in Appendix B.2 page 225.

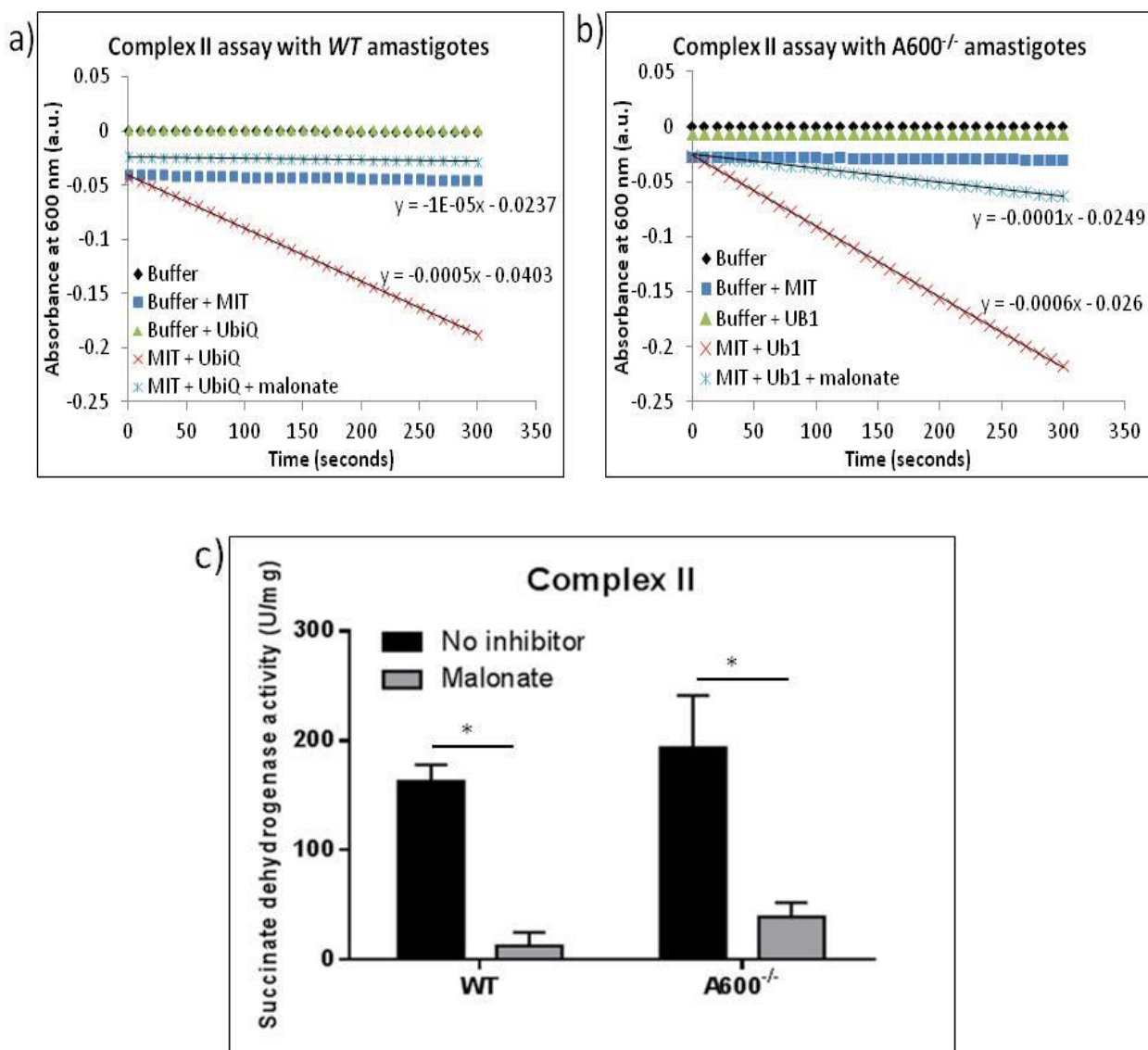


**Figure 4.10: Analysis of the Complex II succinate dehydrogenase activity in *L. mexicana* WT and A600<sup>-/-</sup> amastigotes.**

a) Example of absorbance variation measured with *L. mexicana* WT amastigotes at 600 nm for 5 minutes following addition of ubiquinone. b) Example of absorbance variation measured with *L. mexicana* A600<sup>-/-</sup> amastigotes. “Buffer”: cuvette with SDH buffer only (25 mM potassium phosphate, pH 7.2; 5 mM MgCl<sub>2</sub>; 20 mM sodium succinate with 2 μg/ml antimycin A, 2 μg/ml rotenone, 2 mM KCN and 50 μM DCPIP). This cuvette was used to blank the spectrophotometer; “Buffer + MIT”: SDH buffer with 5 μl of mitochondria sample; “Buffer + UbiQ”: SDH buffer with ubiquinone at 65 μM; “MIT + UbiQ”: SDH buffer with 5 μl of mitochondria sample and 65 μM ubiquinone; “MIT + UbiQ + malonate”: SDH buffer with 5 μl of mitochondria sample, ubiquinone at 65 μM and malonate at 1mM. y: trendline equation for the absorbance variation in the “MIT + UbiQ” and the “MIT + UbiQ + malonate” reactions. c) Succinate dehydrogenase activity calculated in *L. mexicana* WT and A600<sup>-/-</sup> amastigotes. 1 unit (U) of enzymatic activity corresponds to the amount of enzyme necessary for the conversion of 1 nmol of DCPIP per minute. \**P* < 0.05

Complex III cytochrome c reductase activity is assessed by following the increase in absorbance at 550 nm induced by the reduction of cytochrome c, as electrons are transferred from decylubiquinol to the oxidized cytochrome c. The *L. mexicana* *A600*<sup>-/-</sup> amastigotes displayed a significantly lower activity ( $3201.1 \pm 262.5$  mU/mg), representing about 60% of the level of activity in the *WT* amastigotes ( $5213.8 \pm 72$  mU/mg), suggesting that Complex III activity was partially but significantly decreased in absence of the A600 proteins (Figure 4.11c and Table 4.1). This activity was inhibited at around 95% by antimycin A at 0.3  $\mu$ g/ml in both strains. Interestingly, the levels of cytochrome c reductase activity obtained in the *WT* amastigotes were similar to the levels measured elsewhere in *L. tarentolae* promastigotes mitochondrial lysates (Horváth et al, 2000). The enzymatic activities calculated for the individual assays are presented in Appendix B.3 page 226.

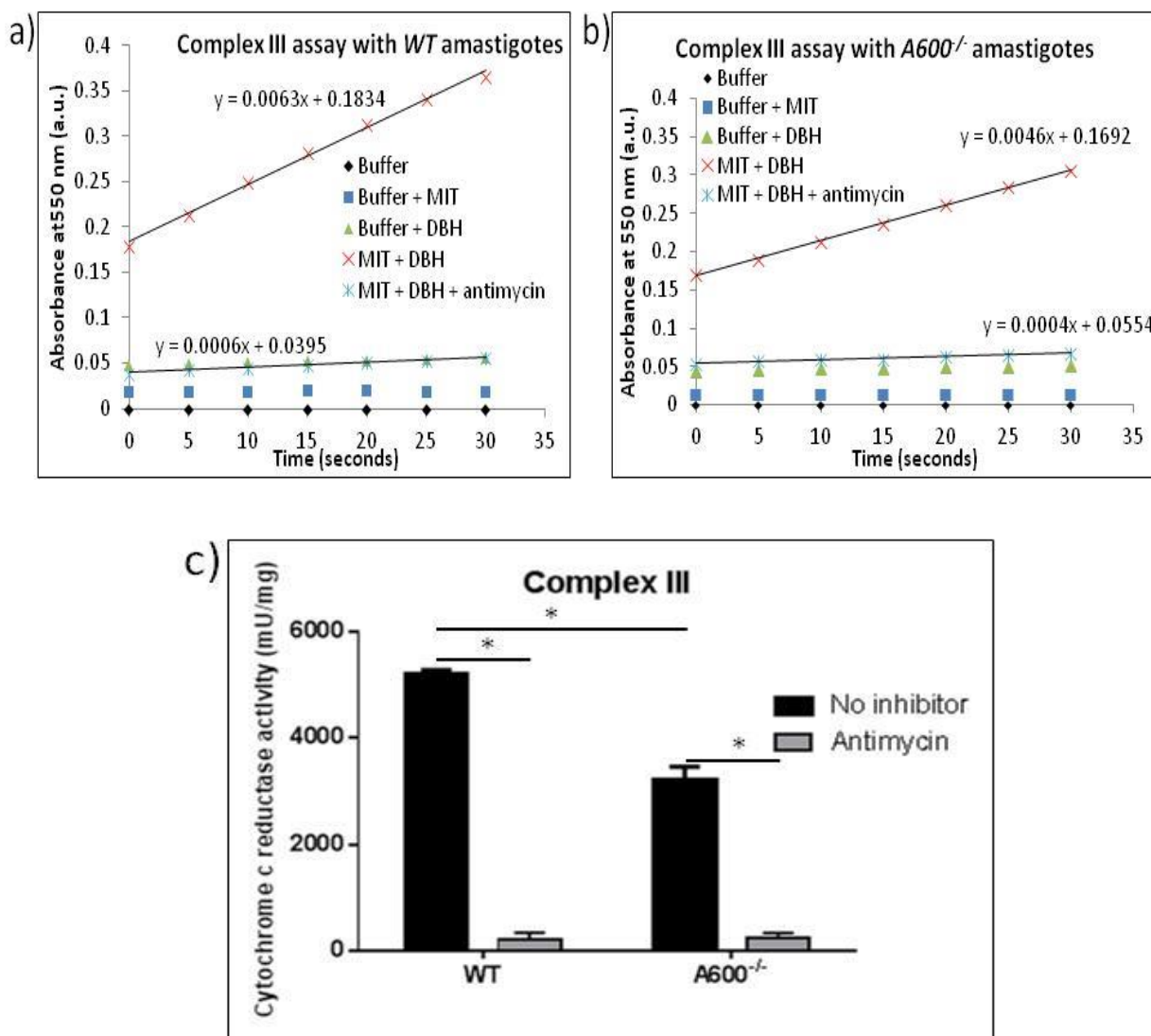


**Figure 4.11: Analysis of the Complex III cytochrome c reductase activity in *L. mexicana* WT and A600<sup>-/-</sup> amastigotes.**

a) Example of absorbance variation over time with *L. mexicana* WT amastigotes at 550 nm following the addition of decylubiquinol. b) Example of absorbance variation measured with A600<sup>-/-</sup> amastigotes. “Buffer”: cuvette containing the QCR buffer (40 mM sodium phosphate, pH 7.4; 0.5 mM EDTA, pH 8.5; 20 mM sodium malonate; 50 μM cytochrome c; 0.005% dodecyl maltoside). This cuvette was used to blank the spectrophotometer; “Buffer + MIT”: cuvette containing the QCR buffer and 2 μl of mitochondria sample; “Buffer + DBH”: cuvette containing the QCR buffer and 40 μM of decylubiquinol (DBH); “MIT + DBH”: cuvette containing the QCR buffer with 2 μl of mitochondria sample and 40 μM of DBH; “MIT + DBH + antimycin”: cuvette containing the QCR buffer with 2 μl of mitochondria sample, 40 μM of DBH and 0.3 μg/ml of antimycin A. y: trendline equation for the absorbance variation in the “MIT + DBH” and the “MIT + DBH + antimycin” reactions. c) Cytochrome c reductase activity calculated in *L. mexicana* WT and A600<sup>-/-</sup> amastigotes. 1 unit (U) of enzymatic activity corresponds to the amount of enzyme necessary for the reduction of 1 μmol of cytochrome c per minute. \**P* < 0.05.

Complex IV cytochrome c oxidase activity is measured by the decrease in absorbance at 550 nm due to the oxidation of cytochrome c. Complex IV activity level was about 60% lower in the *A600*<sup>-/-</sup> amastigotes ( $36 \pm 13.7$  mU/mg) than the level of activity in the *WT* amastigotes ( $87 \pm 26.1$  mU/mg) (Figure 4.12 c and Table 4.1). The activity was nearly completely inhibited in both cell lines in presence of 100  $\mu$ M KCN. The cytochrome c oxidase activity measured in the *A600*<sup>-/-</sup> amastigotes is in the same range as the activity measured in *L. tarentolae* promastigotes (Horváth et al, 2000). The enzymatic activities calculated for the individual assays are presented in Appendix B.4 page 227.

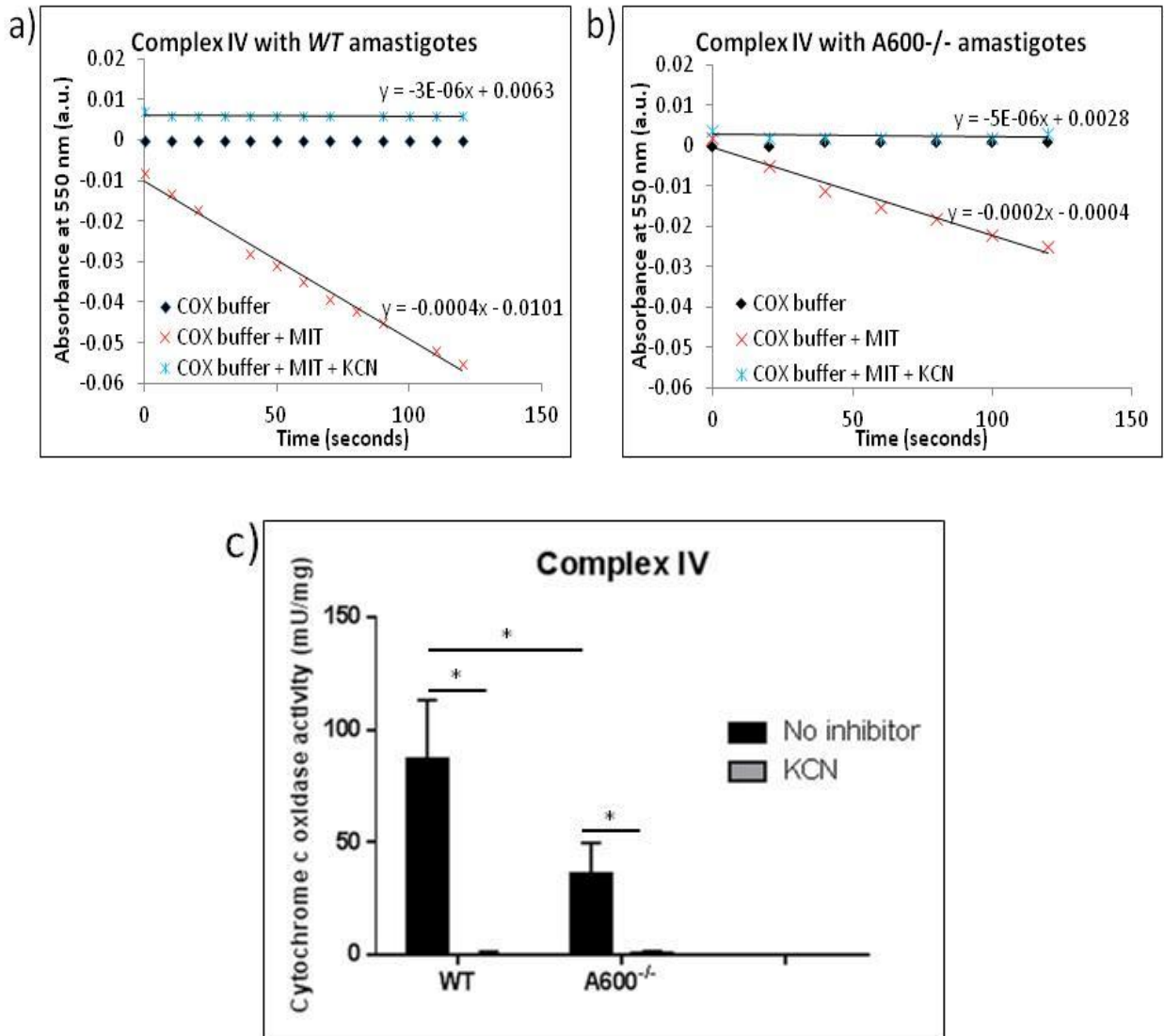


**Figure 4.12: Analysis of Complex IV cytochrome c oxidase activity in *L. mexicana* WT and A600<sup>-/-</sup> amastigotes.**

a) Example of absorbance variation over time at 550 nm with *L. mexicana* WT amastigotes, following the addition of the mitochondria sample. b) Example of absorbance variation over time with *L. mexicana* A600<sup>-/-</sup> amastigotes. “Buffer”: cuvette containing the COX buffer only (40 mM sodium phosphate, pH 7.4; 0.5 mM EDTA, pH 8.5; 20 μM cytochrome c; 30 μM sodium ascorbate; 0.005% (w/v) dodecyl maltoside). This cuvette was used as blank for the spectrophotometer measurements. “Buffer + MIT”: cuvette with the COX buffer and 10 μl of mitochondria sample; “Buffer + MIT + KCN”: cuvette containing the COX buffer with 10 μl of mitochondria sample and 100 μM of KCN.  $y$ : trendline equation for the absorbance variation in the “Buffer + MIT” and the “Buffer + MIT + KCN” reactions. c) Cytochrome c oxidase activity calculated in *L. mexicana* WT and A600<sup>-/-</sup> amastigotes. 1 unit (U) of enzymatic activity corresponds to the amount of enzyme necessary for the oxidation of 1 μmol of cytochrome c per minute. \* $P < 0.05$ .

Complex V functionality was also assessed in order to determine whether the low ATP levels in the *A600*<sup>-/-</sup> amastigotes was linked to a defect in Complex V. This can be achieved by evaluating the complex capability to either synthesize or hydrolyze ATP, activities it can switch between depending on the proton motive force and the ADP/ATP ratio (Suzuki et al, 2003). The ATP hydrolase (ATPase) activity is determined spectrophotometrically by measuring, in presence of ATP, the amount of free phosphate released over time. The complex activity was found to be similar in the two strains, with an activity of  $117 \pm 2.65$  U/mg and  $113.7 \pm 8.9$  U/mg for the *WT* and the *A600*<sup>-/-</sup> amastigotes, respectively (Figure 4.13b and Table 4.1). The enzymatic activities calculated for the individual assays are presented in Appendix B.5 page 227.

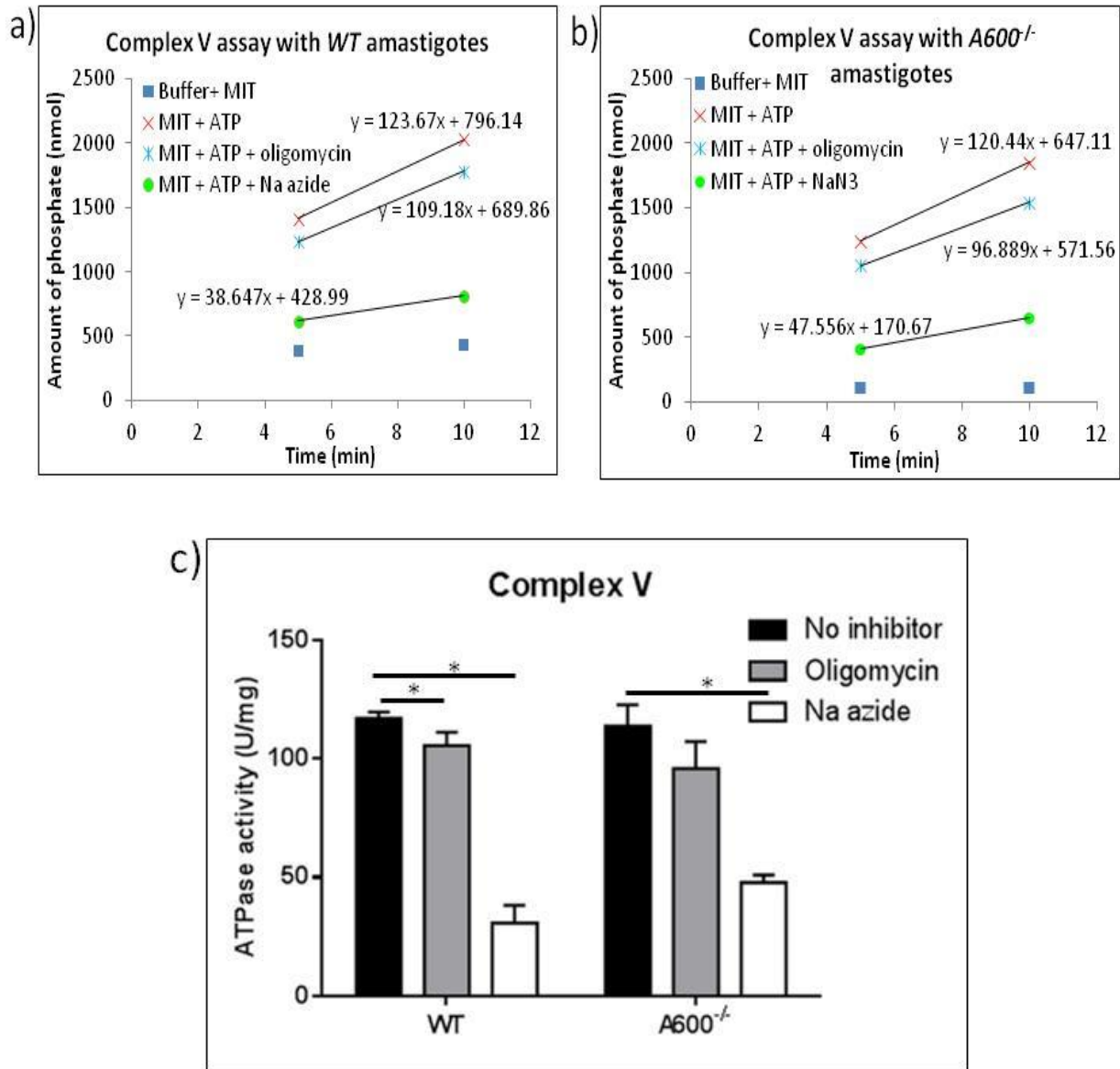


**Figure 4.13: Analysis of Complex V ATPase activity assay in *L mexicana* WT and A600<sup>-/-</sup> amastigotes.**

a) Example of the variation of phosphate in reaction over time with *L mexicana* WT amastigotes, following the addition of ATP. b) Example of the variation of phosphate in reaction with *L mexicana* A600<sup>-/-</sup> amastigotes. “Buffer + MIT”: reaction with ATPase assay buffer (200 mM KCl; 10 mM Tris-HCl, pH 8.2; 2 mM MgCl<sub>2</sub>) and 1 mg of mitochondrial proteins; “MIT + ATP”: reaction with ATPase assay buffer, 1 mg of mitochondrial proteins and 5 mM of ATP. “MIT + ATP + oligomycin”: reaction with ATPase assay buffer, 1 mg of mitochondrial proteins, 5 mM of ATP and 10 μg/ml of oligomycin. “MIT + ATP + NaN<sub>3</sub>”: reaction with TC buffer, 1 mg of mitochondrial proteins, 5 mM of ATP and 1 mM of sodium azide (NaN<sub>3</sub>). *y*: trendline equation for the absorbance variation in the “MIT + ATP”, the “MIT + ATP + oligomycin” and the “MIT + ATP + NaN<sub>3</sub>” reactions. b) ATPase activity calculated in *L mexicana* WT and A600<sup>-/-</sup> amastigotes. 1 unit (U) of enzymatic activity corresponds to the amount of enzyme necessary for the release of 1 nmol of free phosphate per minute. \**P* < 0.05.

**Table 4.1: Enzymatic activities of the mitochondrial electron transport chain complexes.**

		<b>WT</b>	<b>A600<sup>-/-</sup></b>
<b>NADH dehydrogenase</b>			
	No inhibitor	19.6 ± 5.2	52.4 ± 22.6
	Rotenone	22%	17%
<b>Succinate dehydrogenase</b>			
	No inhibitor	162.8 ± 15.4	193.9 ± 47.5
	Malonate	92%	81%
<b>Cytochrome c reductase</b>			
	No inhibitor	5213.8 ± 72	3201.1 ± 262.5
	Antimycin	96%	93%
<b>Cytochrome c oxidase</b>			
	No inhibitor	87 ± 26.1	36 ± 13.7
	KCN	99%	99%
<b>ATPase</b>			
	No inhibitor	117 ± 2.65	113.7 ± 8.9
	Oligomycin	10%	16%
	Sodium azide	74%	58%

The values in rows “No inhibitor” represent the average ± SD of the enzymatic activities of 3 independent assays calculated in absence of inhibitor and are expressed in U/mg of total proteins for the NADH dehydrogenase, succinate dehydrogenase and ATPase activities and in mU/mg for the cytochrome c reductase and oxidase activities. The percentages in the inhibitors rows represent the average of inhibition percentage obtained in presence of the inhibitor in 3 independent assays. The enzymatic activities calculated for each individual assay are presented in Appendix B page 225.

In summary, Complexes III and IV activities were found to be affected by the deletion of the *A600* genes, but not the Complexes II and V, while Complex I seems to be inactive.

### 4.3 Discussion

The subcellular localization of the A600.1 protein suggests that it may be located in the mitochondria, likely as an inner mitochondrial membrane protein as it co-fractionates with the inner mitochondrial membrane protein p27. Therefore, the objective of this chapter was to

determine whether A600.1 may be involved in metabolic pathways by comparing the mitochondrial activities of *L. mexicana* *A600*<sup>-/-</sup> amastigotes to those in *WT* amastigotes.

Amastigotes lacking the A600 proteins exhibited an impaired mitochondrial metabolism, characterized by low cellular ATP levels, a low mitochondrial redox activity and a decrease in the mitochondrial membrane potential  $\Delta\Psi_m$ . An investigation of the enzymatic activity of the OXPHOS complexes revealed, similarly to what was found in *L. tarentolae* promastigotes (Verner et al, 2014), a low rotenone-insensitive NADH dehydrogenase activity in the *WT* amastigotes that appeared to be upregulated in the *A600*<sup>-/-</sup> amastigotes. The insensitivity of this low activity to rotenone, in addition to the absence of NADH dehydrogenase signal in Native PAGE bears the question of whether the activity measured here corresponds to Complex I, similarly to what was observed in the closely related *Trypanosoma brucei*. Indeed, in this organism, deletion of two core subunits of Complex I resulted in only 20% decrease of the NADH:ubiquinone reductase activity in procyclics (the parasite form that resides in the insect midgut) and in no decrease in the bloodstream form despite evidence of the complex presence (Surve et al, 2012; Verner et al, 2011). This leads to the idea that the activity measured here could be due to an alternative NADH dehydrogenase such as NDH2, a single polypeptide enzyme that uses the same electron donor (NADH) and electron acceptor (ubiquinone) as Complex I but does not translocate protons and is insensitive to rotenone (Zíková et al, 2016). However, the NADH dehydrogenase activity measured in *L. tarentolae* promastigotes, which is similar to the activity measured here in the *WT* amastigotes, does not appear to be sensitive either to diphenyl iodonium, an inhibitor of NDH2, although the *ndh2* gene has been identified in *L. tarentolae* genome (Verner et al, 2014). This suggests that another NADH:ubiquinone oxidoreductase enzyme may be present. In line with this proposal is the observation that, although

ablation of the NDH2 protein expression in *T. brucei* procyclics affects the parasite growth and its mitochondrial membrane potential, it had no effect on the level of NADH:ubiquinone oxidoreductase activity (Verner et al, 2013). Therefore, it is unclear which enzyme is responsible for the upregulated NADH dehydrogenase activity observed in the *A600*<sup>-/-</sup> amastigotes. Considering the flexibility of trypanosomatids to adapt to their environment conditions (McConville et al, 2015; Zíková et al, 2016), it can be imagined that the decrease in the OXPHOS pathway activity induced by the absence of the A600 proteins, may have triggered the upregulation of another pathway to ensure the survival of the parasite. Such scenario was observed in the *T. brucei* procyclics where the knock-down of NDH2 resulted in an upregulation of the mitochondrial glycerol-3-phosphate dehydrogenase, which transfers electrons to ubiquinone (Verner et al, 2013). It has also led to the hypothesis that the absence of or low decrease in NADH:ubiquinone oxidoreductase activity in *T. brucei* procyclics following the knock-down of NDH2 protein expression or of Complex I subunits could be due to the upregulation of this other NADH dehydrogenase enzyme. All together, these data suggest that either Complex I is inactive, at least in axenic amastigotes, or that it is involved in activities other than electron transfer as suggested by the identification in the *T. brucei* Complex I of proteins involved in other functions, such as fatty acid synthesis (Acestor et al, 2011).

Complexes II and V activities were not affected by the absence of the A600 proteins, although a decrease in Complex V dimerisation was observed in native PAGE. Complexes III and IV activities were reduced in the *A600*<sup>-/-</sup> amastigotes, falling to 60% and 40% of the levels measured in *WT* amastigotes, respectively, without any obvious effect on their assembly. In the absence of an active Complex I, this defect in Complexes III and IV activities are likely to be the cause of the decrease in the mitochondrial membrane potential  $\Delta\Psi_m$ , which in consequence, may

affect the production level of ATP by oxidative phosphorylation, despite the presence of an active Complex V. Alternatively, the low mitochondrial membrane potential  $\Delta\Psi_m$  could be linked to the low dimerisation of Complex V observed in the *A600*<sup>-/-</sup> amastigotes which can affect the mitochondrial membrane potential, via an effect on the mitochondrial inner membrane architecture, without affecting the complex overall activity (Bornhövd et al, 2006; Subrtova et al, 2015; van der Laan et al, 2016).

Interestingly, the data obtained with the *A600*<sup>-/-</sup> amastigotes mirror results observed in *T. brucei* procyclics following the knock-down of some Complex IV subunits (Gnipova et al, 2012). The separate ablation of the expression of three Complex IV subunits resulted in slower growth of the parasite, a decrease in the mitochondrial membrane potential, in the levels of ATP produced via OXPHOS and in Complex IV activity. While these deletions had no effect on Complex II and V activity or assembly, Complex III activity was decreased for two of these proteins. This data indicate that some Complex IV subunits are involved in interactions with Complex III and affect its function. In yeast and mammalian cell lines, it has been shown that the individual OXPHOS complexes are capable of associating with each other to form supercomplexes, which are proposed to enhance electrons transfer and/or to stabilize the individual complexes. The composition and abundance of these supercomplexes appear to be variable between organisms and tissues, but mainly involve Complexes I (when it is present), III and IV. Under normal physiological conditions, Complexes II and V form homooligomers and do not appear to associate with other complexes (Lobo-Jarne & Ugalde, 2018). The assembly of these individual complexes and their association in supercomplexes involve specific chaperones and assembly factors, following a controlled, multistep process. In *Saccharomyces cerevisiae*, proteins ensuring the interactions between Complexes III and IV have been identified and were

found to share similar attributes with the A600 proteins. Such proteins include the yeast proteins Coi1 and the Hig1 (hypoxia-induced gene 1) proteins, Rcf1 and Rcf2. Like the A600 proteins, they are small proteins with predicted transmembrane domains; Coi1 (cytochrome c oxidase interacting protein 1) is a small protein of 12.4 kDa, with a putative transmembrane domain in its N-terminal region (Singhal et al, 2017). Rcf1 and Rcf2 (respiratory supercomplex factor 1 or 2) are proteins of 18 and 25 kDa, respectively and contain two putative transmembrane domains (Vukotic et al, 2012). All three proteins are embedded in the inner mitochondrial membrane, with their N and C terminal ends (C-terminal region only for Coi1) exposed to the intermembrane space. Similarly to the A600 proteins, they do not contain an N-terminal targeting sequence to the mitochondria. Coi1 is conserved in fungi without apparent homolog in higher eukaryotes. While putative homologs of Rcf1 have been identified in other organisms such as plants, mouse, humans, Rcf2 appears to be a yeast-specific protein. Cells lacking Coi1 or Rcf1 displayed a defect in their mitochondrial respiration characterized by a growth defect when grown on non-fermentable carbon sources, a low mitochondrial membrane potential and a decrease in oxygen consumption (Singhal et al, 2017; Vukotic et al, 2012). Although deletion of Rcf2 alone did not have a significant impact on cells growth, the growth defect was more pronounced in the  $\Delta$ Rcf1/ $\Delta$ Rcf2 double mutant (Strogolova et al, 2012). Investigation of Coi1, Rcf1 or Rcf2 interacting partners identified components of both Complexes III and IV for all three proteins (Singhal et al, 2017; Strogolova et al, 2012; Vukotic et al, 2012). Rcf1 was also identified among Coi1 interacting partners, along with assembly factors for both complexes and Mic60 of the MICOS complex (discussed below). Deletion of either protein appears to affect the formation of supercomplexes III-IV as well as the assembly of Complex IV. At the level of enzymatic activity, Complex IV cytochrome c oxidase activity was

greatly reduced in absence of Coi1 or of both Rcf1 and Rcf2, less so in absence of either Rcf1 or Rcf2. While Complex III cytochrome c reductase activity was not affected by the deletion of either Rcf1 or Rcf2, it was partially reduced in absence of both proteins. The consequence of Coi1 deletion on Complex III activity however was not investigated. These three proteins are proposed to operate as assembly factors for the assembly and/or stabilization of the supercomplex III-IV.

Other proteins which deletions result in similar cell phenotypes as the deletion of the A600 proteins include the subunits of the mitochondrial contact site and cristae organizing system (MICOS). MICOS is a large complex of proteins embedded in the mitochondrial membrane and is highly conserved in most organisms from yeast to humans. It is composed of at least 6 different subunits (7 in vertebrates) and further potential components are under investigation (Schorr & van der Laan, 2018). 5 of the subunit components identified so far are integral membrane proteins and were observed to be particularly enriched in the inner mitochondrial membrane cristae junctions (Pfanner et al, 2014). The presence of this complex in trypanosomatids is yet to be confirmed (Eichenberger, 2018). It appears to be essential in the organization of the inner membrane structure into cristae via the stabilization of cristae junctions and the formation of contact sites with the mitochondrial outer membrane. Deletions of various MICOS subunits result in alterations of the inner mitochondrial membrane architecture, characterized by the loss of cristae junctions, and disruption of some mitochondrial functions, with degrees of severity dependent on the organism. At the level of the respiration, those deletions were found to result in impairment of yeast growth on non-fermentable sources, a decrease in oxygen consumption in mammalian cells, a reduction in the mitochondrial membrane potential and in cellular ATP levels (Anand et al, 2016; Ding et al, 2015; Friedman et al, 2015).

A closer investigation of the state of the OXPHOS complexes found no apparent effect of those deletions on their assembly or on their subunits composition. However, while Complexes II and V activities were not affected, a reduction in activity was observed for Complexes I, III and especially Complex IV (Anand et al, 2016; Friedman et al, 2015; Yang et al, 2015). This indicates that the MICOS complex is required for the optimal function of the assembled Complexes I, III and IV, which may be dependent on the proper organization of the inner mitochondrial membrane. Furthermore, the MICOS and the OXPHOS complexes appear to work in concert for the maintenance of the inner mitochondrial membrane architecture (Friedman et al, 2015). Although the OXPHOS complexes formation and/or activity may be highly dependent on the proper organization of the inner mitochondrial membrane morphology, one cannot exclude an effect of the MICOS complex via other pathways since the MICOS subunits were found to interact with components of other complexes, such as the protein import machineries, VDAC (voltage-dependent anion channel), mitochondrial transcription factors (hence influencing the transcription of mitochondrial genes, some of which encode subunits of the OXPHOS complexes) (van der Laan et al, 2016; Yang et al, 2015). The MICOS complex is yet to be identified in trypanosomatids but its presence in *T. brucei* is under investigation (Eichenberger, 2018).

Analysis of the characteristics of those different proteins function suggests a similar role for the A600 proteins. The A600 proteins could play either a direct role in the regulation of Complexes III and IV activities such as by mediating the interaction between the two complexes, or an indirect role such as by being involved in the organization of the inner mitochondrial membrane structure, which would affect the complexes activities and the dimerisation of Complex V. Interestingly, the cytochrome c reductase activity measured in the *WT* amastigotes

was similar to the activity measured in *L. tarentolae* promastigotes mitochondrial lysates (Horváth et al, 2000). Meanwhile, the cytochrome c oxidase levels found in the *A600*<sup>-/-</sup> amastigotes were in the same range as those measured in *L. tarentolae* promastigotes, an activity that was shown to be upregulated in amastigotes (Dey et al, 2010). This would indicate that the A600 proteins may be involved in the optimization of Complex III activity and the upregulation of Complex IV activity at the amastigote stage. In amastigotes, the flux of the TCA cycle is reduced as its intermediates are siphoned for use by other biosynthetic pathways, such as  $\alpha$ -ketoglutarate that is used for *de novo* synthesis of glutamate and/or glutamine (Saunders et al, 2014). This is likely to impact the flow of substrates such as succinate towards the respiration chain. In order to compensate for this reduction, the A600 proteins may contribute to the optimization of Complexes III and IV activity in amastigotes so as to maintain the synthesis of ATP by oxidative phosphorylation and the mitochondrial membrane potential, essential for mitochondrial activities. This idea is supported by the increase in Complex IV cytochrome c oxidase activity observed in amastigotes and the fact that defects in Complex IV and inhibition of Complex V affect amastigotes survival (Dey et al, 2010; Luque-Ortega et al, 2008; Uboldi et al, 2006; Zikova et al, 2008).

To verify the role of the A600 proteins at the OXPHOS level, ATP production assays were attempted to study the different mitochondrial ATP production pathways and hence assess the performance of other mitochondrial pathways (such as the TCA cycle or the ASCT cycle), as described elsewhere (Schneider et al, 2007). This assay consists in adding specific mitochondrial substrates (depending on the pathway investigated) and ADP to mitochondrial-enriched fractions obtained by digitonin extraction and measuring the subsequent ATP production. The assay was first attempted with *L. mexicana* WT cells but was not successful, as no ATP production was

detected in reactions with mitochondrial substrates by comparison to reactions containing inhibitors. It was later found out that some important details (such as the importance of the pH of the stock solutions used, hence the pH of the reaction) were omitted from the published protocol that may have hindered the success of this assay (Dr Alena Zikova, personal communication).

In conclusion, results in this chapter revealed an impairment of the mitochondrial function in amastigotes in absence of the A600 proteins. Study of the activity of the OXPHOS complexes suggests an involvement of those proteins in the regulation of Complexes III and IV activities that would serve to optimize the OXPHOS pathway function in amastigotes in presence of a decreased flux of the TCA cycle. This role may be fulfilled either directly, by mediating interactions between the two complexes or indirectly via regulation of the inner membrane architecture which is essential for the optimal function of the OXPHOS complexes.

## Chapter 5: Investigation of the potential A600.1 interacting proteins

### 5.1 Introduction

*L. mexicana* A600<sup>-/-</sup> amastigotes growth defect observed *in vitro* and in macrophages was found to correlate with a decrease in the mitochondrial metabolism characterized by a decrease in OXPHOS complexes activities. Differentiation of promastigotes into amastigotes has been shown to be associated with an increased in mitochondrial activities (Rosenzweig et al, 2008b; Saunders et al, 2014). Together, these results support the hypothesis that the A600 proteins may be involved in a mitochondrial pathway that is important for amastigote development.

The *L. mexicana* A600.1 protein is suggested to localize to the mitochondrial inner membrane. This membrane plays an important role in the mitochondrial functions. Contrary to the outer mitochondrial membrane, which is permeable to molecules below 5 kDa, the inner mitochondrial membrane is highly impermeable, including to ions and small molecules, which require the presence of specific carriers (Alberts et al, 2002). The inner membrane contains several protein complexes involved in various mitochondrial pathways, such as the complexes of the electron transport chain and associated proteins, the F<sub>0</sub>F<sub>1</sub> ATP synthase (Complex V), carrier proteins (for ions, small molecules), the protein and the tRNA import machineries and some metabolic enzymes (Acestor et al, 2009).

It is estimated that about 80% of the cellular proteins work in collaboration with other proteins, either as part of a multi-protein complex or through interactions with other proteins (Berggard et al, 2007; Kristensen & Foster, 2013). Surveys of protein-protein interactions such as in *Mycoplasma pneumonia*, *Saccharomyces cerevisiae* and methicillin-resistant *Staphylococcus aureus* found that the number of proteins identified as involved in protein-

protein interactions represented more than 60% of the predicted proteomes (Cherkasov et al, 2011; Gavin et al, 2006; Krogan et al, 2006; Kühner et al, 2009). Therefore, it is hypothesized that the A600.1 and A600.4 proteins may function in concert with other proteins, such as for instance, as anchors of a multi-protein complex. Identification of the A600 potential interacting partners and their functions may allow the determination of the protein complex and/or pathway in which they may be involved. This chapter describes attempts at isolating the potential A600.1 interacting proteins.

## **5.2 Results**

### **5.2.1 Investigation of the A600.1 binding partners by native PAGE**

#### **5.2.1.1 *Detection of the L mexicana A600.1 protein after native PAGE of the L. mexicana WT amastigotes organellar fraction lysates***

##### *i. Detection of A600.1 in the organellar fraction lysates after denaturing SDS-PAGE*

Western blot detection of the A600.1 protein in the *WT* amastigotes crude organellar extracts after separation by hrCN-PAGE and using the anti-A600.1 peptide 2 antibody resulted in an absence of signal. It was thought that the recognition site of the antibody on the A600.1 protein may have been inaccessible to the antibody due to the interaction of the protein with other proteins in whichever complex it might be involved. To verify the presence of A600.1, the organellar extracts obtained from *WT* promastigotes and amastigotes were analyzed by Western blot after denaturing SDS-PAGE. The sample used as positive control corresponds to the pellet from *L. mexicana WT* amastigotes lysed with 25  $\mu$ M of digitonin, left over from a different experiment and previously shown to contain the A600.1 protein by Western blot. Except for a

very faint signal at 23 kDa in the promastigotes whole cell lysate supernatant (WCL SN) (lane 1), no signal was detected in the other fractions (Figure 5.1 - upper panel). The detection of A600.1 in the positive control confirms that the absence of bands in the cell fractions is due to the absence of the A600.1 protein in the samples rather than due to an issue with the antibody or with the proteins transfer.

The same membrane was re-incubated with the anti-Complex V subunit  $\beta$  antibody. With the exception of the two whole cell lysate supernatants (lanes 1 and 6) in which a single band at 58 kDa was detected, likely to correspond to the  $\beta$  subunit which has a predicted size of 56 kDa, multiple bands appeared in the organellar lysate supernatants and pellets (promastigotes: lanes 2 and 3 – amastigotes: lanes 7 and 8) (Figure 5.1 – lower panel). The fact that those bands are of lower sizes than 56 kDa suggest that they correspond to degradation products of the  $\beta$  subunit. These bands were more numerous and of smaller sizes in amastigotes (many bands below 25 kDa versus fewer but larger size bands in promastigotes, mainly between 25 and 55 kDa), suggesting that proteolysis occurred to a greater extent in amastigotes than in promastigotes. The same observation was made by Nugent *et al.* who found proteins degradation to be an issue in the analysis of *L. mexicana* amastigotes protein lysates, but much less in promastigotes preparations (Nugent et al, 2004). The data from the Western blot detection of the  $\beta$  subunit suggest that the A600.1 protein was not detected in either the *WT* promastigotes or the amastigotes fractions due to proteolysis.

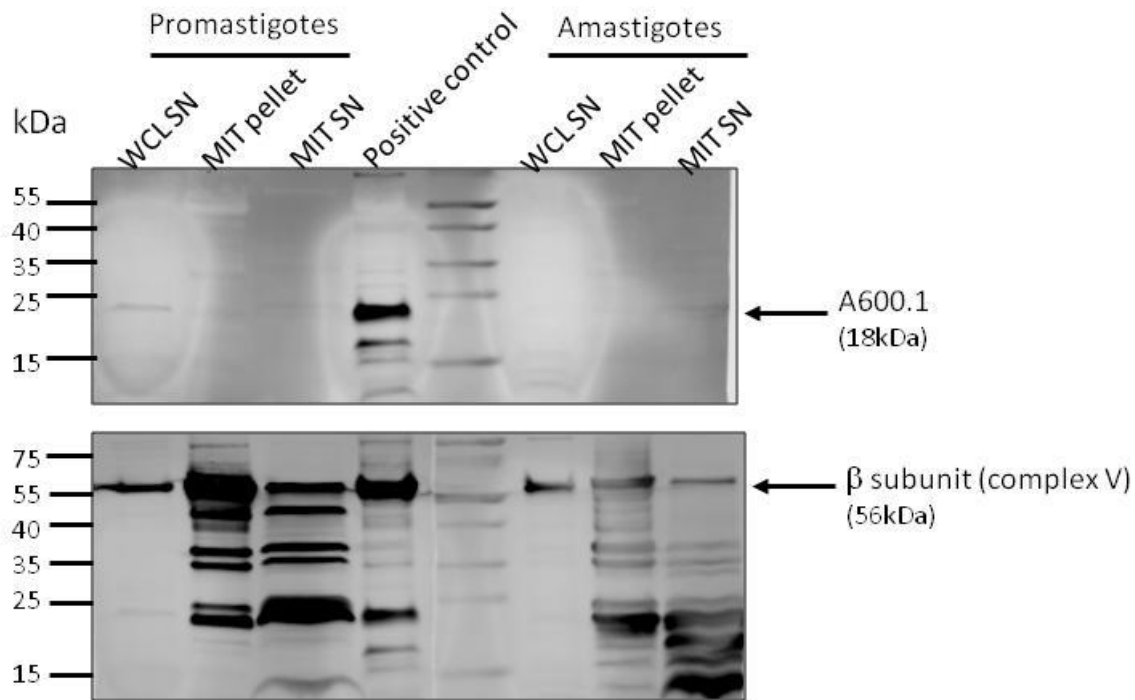


**Figure 5.1: Western blot analysis of SDS-PAGE of *L. mexicana* WT promastigotes and amastigotes fractions after hypotonic cell lysis and mitochondrial digitonin lysis.**

After hypotonic lysis of the promastigotes and amastigotes, the lysate supernatants (WCL SN) were collected and the mitochondria-enriched pellets were lysed with digitonin at 4 mg/mg of protein. The pellets (MIT) lysates were centrifuged at 16,000 x g for 10 minutes. The supernatants (MIT SN) and pellets (MIT pellet) were collected. The samples were separated on a 12% Tris-Tricine gel, loading 30  $\mu$ g of proteins per lane. Detection was performed by incubation with the rabbit anti-A600.1 antibody, followed by incubation with the Alexa Fluor 680 goat anti-rabbit secondary antibody. After scanning, the Western blot membrane was incubated with the rabbit anti- $\beta$  subunit, then with the Alexa Fluor 680 goat anti-rabbit secondary antibody. Positive control: pellet obtained after lysis of *L. mexicana* WT amastigotes with 25  $\mu$ M digitonin.

The organelle-enriched pellets isolation and lysis were repeated in presence of protease inhibitors and the different fractions were analyzed by Western blot for the presence of the A600.1 protein. The DTE and STM buffers, used during isolation of the mitochondria-enriched fraction, and the lysis buffer used for the lysis of the organellar pellets were supplemented with the following protease inhibitors: 10 mM 1,10 Phenanthroline, 10  $\mu$ M E-64, 1 mM PMSF and 1X Roche complete EDTA-free protease inhibitors cocktail. A band at 23 kDa was detected in

all the samples (Figure 5.2). This confirms that the A600.1 protein is effectively solubilized after digitonin treatment of the mitochondria-enriched pellet of promastigotes and amastigotes. It also shows that A600.1 is very susceptible to proteolysis and requires the presence of protease inhibitors to prevent its degradation.

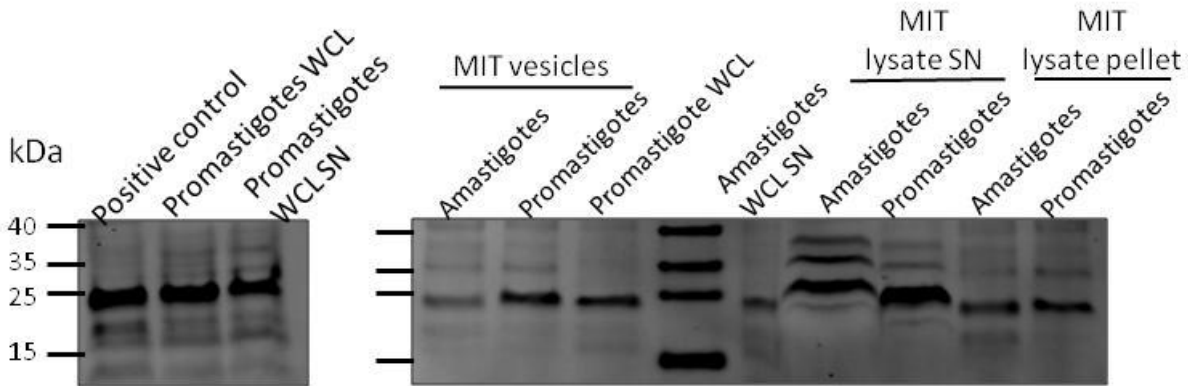


**Figure 5.2: Western blot detection of A600.1 in the *L. mexicana* WT promastigotes and amastigotes fractions isolated in presence of protease inhibitors.**

Protease inhibitors were added to the cells during hypotonic lysis (in DTE buffer), during DNase treatment (in STM buffer) and digitonin lysis of the mitochondria-enriched fractions (4 mg digitonin per mg of protein). The different cells and mitochondrial fractions were separated on a 12% Tris-Tricine gels (30 µg of proteins per lane). After transfer of the proteins to a PVDF membrane, detection was performed with the anti-A600.1 peptide 2 antibody, followed by the Alexa Fluor 680 goat anti-rabbit secondary antibody.

*ii. Detection of A600.1 in the organellar fraction lysates after native PAGE*

Having determined that the A600.1 protein is solubilised in the crude organellar lysate supernatant after digitonin lysis, it was immunodetected by Western blot, after separation on a native gradient gel, to determine whether it co-migrates with known mitochondrial complexes.

*L. mexicana* WT amastigotes were lysed in presence of 1,10 Phenanthroline, PMSF, E-64 and the Roche complete EDTA-free protease inhibitors cocktail. The organellar-enriched fraction was treated with DNase I and later lysed with digitonin in presence of the protease inhibitors. After native PAGE, the proteins were stained by blue silver staining and for the in-gel

activity staining of Complex V. Proteins were also transferred to a PVDF membrane for Western blot detection of the A600.1 protein. As control, one lane of the native gel was loaded with 8  $\mu$ g of recombinant A600.1 protein and stained with blue silver staining.

Detection by Western blot with the anti-A600.1 peptide 2 antibody revealed a band estimated at 300 kDa (Figure 5.3a). Blue silver staining of the gel strip containing the A600.1 recombinant protein detected a band estimated at 90 kDa (Figure 5.3b). This suggests that the band at 300 kDa revealed by Western blot with the anti-A600.1 antibody might correspond to the A600.1 protein present within a homo- or hetero-oligomeric protein complex.

After Coomassie staining of the sample isolated in presence of protease inhibitors, only a band at ~900 kDa was observed, likely corresponding to Complex V monomer (Figure 5.3c); the 1 MDa Complex V dimer band and the bands at ~700 kDa corresponding to Complex V F1 portion and to Complex IV observed in the sample isolated without protease inhibitors were not visible in presence of inhibitors. Complex V in-gel activity staining revealed a band estimated at 950 kDa, similar to the one seen by Coomassie staining (Figure 5.3d). The strongest activity band appeared at ~300 kDa. Interestingly, this band located in the same region as the 300 kDa band detected by the anti-A600.1 antibody. The faintness of the bands corresponding to the OXPHOS complexes in the sample with protease inhibitors detected after Coomassie staining suggested that the complexes assembly was affected in presence of the inhibitors. This idea was reinforced by the absence of the Complex V dimer in-gel activity band at 1 MDa and the fact that the stronger Complex V band activity was detected at 300 kDa.

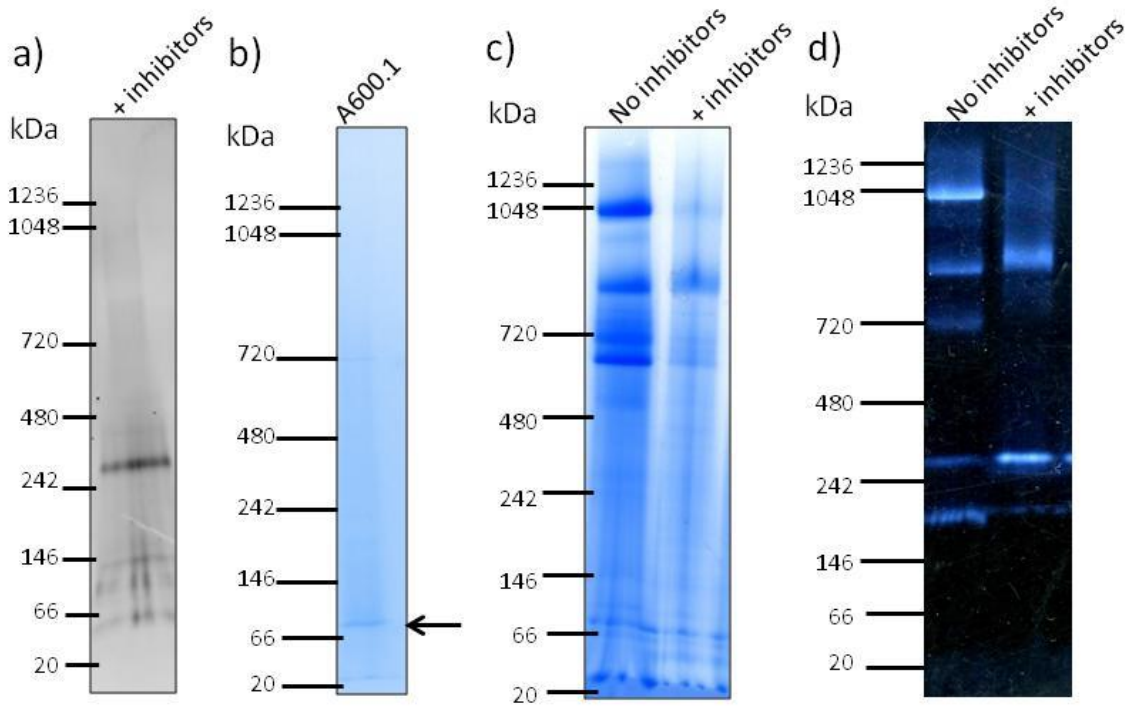


**Figure 5.3: High resolution clear native PAGE of *L. mexicana* WT amastigotes mitochondrial membrane complexes isolated in presence of protease inhibitors**

a), c) and d): mitochondria-enriched fractions were isolated by hypotonic lysis in presence or not of protease inhibitors, then lysed with 4 mg of digitonin per mg of protein in presence or not of inhibitors. The lysate supernatant was separated on a 3-12% native gel at 100 V for 4.5 hours at 4°C. a) Western blot detection of the A600.1 protein after separation of 30 µg of the organellar extract isolated in presence of protease inhibitors. Detection was performed with the anti-A600.1 antibody followed by the Alexa 680 goat anti-rabbit antibody. c) Coomassie blue staining: after electrophoresis using 20 µg of organellar extract, the gel was fixated overnight then stained with blue silver stain. d) Complex V in-gel activity staining: after electrophoresis with 60 µg of organellar extract, the gel was incubated overnight in the Complex V reaction buffer (35 mM Tris pH 8, 270 mM glycine, 19 mM magnesium sulfate, 0.2% Lead (II) nitrate, 8 mM ATP). b) Coomassie blue staining of gel strip containing lane with recombinant A600.1 protein (8 µg).

The *WT* amastigotes organellar lysate obtained in presence of protease inhibitors was also analyzed by Western Blot for the expression of the different OXPHOS complexes using antibodies against some of their subunits. Complex V presence was detected using an antibody against its subunit  $\beta$  (present in the  $F_1$  portion of Complex V) and one against Tb2 (a transmembrane subunit of Complex V  $F_0$  moiety) (Subrtova et al, 2015; Zikova et al, 2009b).

The detection of both proteins resulted in a band estimated at 950 kDa, likely to correspond to the complex monomer (Figure 5.4). In correlation with the Coomassie and in-gel activity staining results (Figure 5.3), the complex dimer band was not detected on either blot. No signal was detected when the membrane was incubated with the antibody against Complex III subunit, the Rieske protein. A very faint band, estimated at 300 kDa was detected with the antibody against the COIV protein of the Complex IV (Figure 5.4). These Western blot results correlate with the data from the in-gel activity and Coomassie staining suggesting that the mitochondrial OXPHOS complexes are dissociated when solubilized in presence of protease inhibitors.

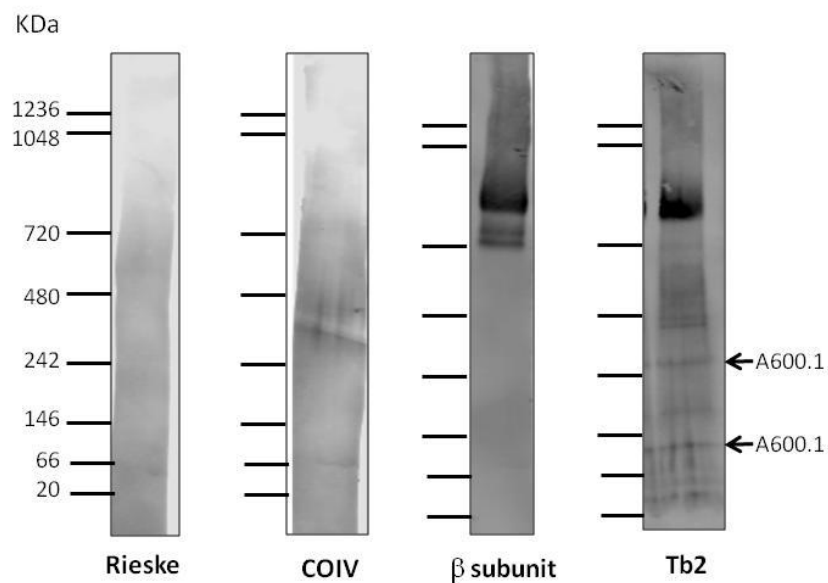


**Figure 5.4: Western blot analysis after high resolution clear native PAGE of *L. mexicana* WT amastigotes organellar lysates isolated in presence of protease inhibitors.**

After electrophoresis on a 3-12% native gel, the organellar lysate proteins (30  $\mu$ g) were transferred to a PVDF membrane. The blots were probed for the detection of the Rieske protein of Complex III, the COIV protein (Complex IV),  $\beta$  subunit or Tb2 subunits of Complex V. The bound antibodies were detected with the Alexa Fluor 680 goat anti-rabbit secondary antibody. The blot used for Tb2 detection was previously probed with the anti-A600.1 antibody and the arrows indicate the bands that were detected by this antibody.

It was suspected that 1,10 Phenanthroline particularly may have an effect on the complexes stability, due to its strong metal ion chelating effects. Therefore, *L. mexicana* WT amastigotes mitochondrial-enriched fractions were isolated and lysed in presence of only 1,10 Phenanthroline at 10 mM. The lysate was analyzed by Coomassie staining after native PAGE (Figure 5.5). By comparison to the lysate obtained without inhibitors, the 1 MDa and 800 kDa protein bands appeared very faint in the lysate with 1,10 Phenanthroline, suggesting a dissociating effect of this inhibitor on the protein complexes.

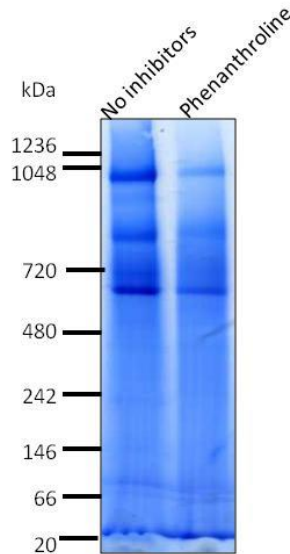


**Figure 5.5: High resolution clear native PAGE analysis of *L. mexicana* WT amastigotes organellar lysate.**

The mitochondria-enriched fractions were isolated and lysed with digitonin in presence (Phenanthroline) or not (No inhibitors) of 10 mM of 1,10 Phenanthroline. 20  $\mu$ g of each lysate was separated on a 3-12% native gel, using the hrCN-PAGE conditions. After electrophoresis, the gel was fixed overnight then stained with blue silver stain.

To test the protease inhibitors requirement to prevent the A600.1 protein degradation, *L. mexicana* WT amastigotes were lysed by hypotonic lysis in the DTE buffer (1 mM Tris-HCl pH 7.9, 1 mM EDTA) containing different combinations of the protease inhibitors. The whole cell lysates were separated on a 12% Tris-Tricine SDS gel and were analyzed by Western blot

using the anti-A600.1 antibody (Figure 4.13). As seen before there was no signal in the *WT* lysate in the absence of inhibitors, nor in the *A600<sup>-/-</sup>* lysate containing the inhibitors. The A600.1 protein was detected in the samples containing a combination of 1,10 Phenanthroline and either E-64 or the Roche cocktail. It was not however detected in the lysates with a combination of 1,10 Phenanthroline and PMSF or with a combination of E-64 and the Roche cocktail. Moreover, none of the inhibitors alone were enough to prevent the protein degradation.

1,10-Phenanthroline is a metalloprotease inhibitor, E-64 a cysteine protease inhibitor, PMSF a reversible serine protease inhibitor, whereas the Roche complete, EDTA-free protease inhibitor cocktail contains serine and cysteine protease inhibitors. These results indicate that the A600.1 protein is the target of combined proteolysis by metalloproteases and cysteine proteases and requires the presence of 1,10 Phenanthroline and either E-64 or the Roche cocktail to prevent its degradation.

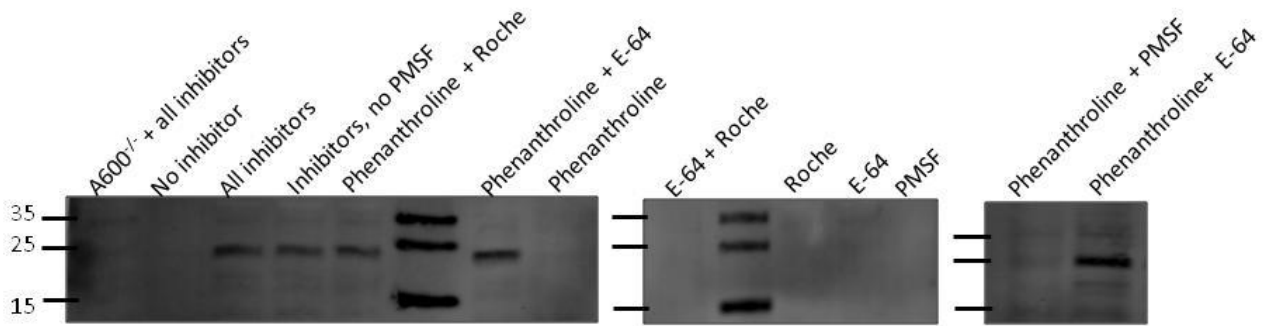


**Figure 5.6: Western blot analysis of *L. mexicana* WT amastigotes whole cell lysates obtained by hypotonic lysis in presence of different combination of protease inhibitors.**

The cells were resuspended at  $7 \times 10^8$  cells/ml in DTE buffer containing different protease inhibitors, as indicated, and passed through a 26 G needle, following the same protocol as for the isolation of mitochondria-enriched fractions by hypotonic lysis. The cell lysates (30  $\mu$ g of proteins) were separated on a 12% Tris-Tricine gel and transferred to a PVDF membrane. The blots were incubated with the anti-A600.1 peptide 2 antibody, then with the Alexa Fluor 680 goat anti-rabbit secondary antibody. “A600<sup>-/-</sup> + all inhibitors”: *L. mexicana* A600<sup>-/-</sup> amastigotes lysed in presence of all four inhibitors. The rest of the samples are lysates of *L. mexicana* WT amastigotes. “No inhibitor”: lysate without inhibitor. “All inhibitors”: lysate with all four inhibitors. “Inhibitors, no PMSF”: lysate with Phenanthroline, E-64, Roche cocktail but no PMSF. “Phenanthroline + Roche”: lysate with Phenanthroline and Roche inhibitors cocktail. “Phenanthroline + E-64”: lysate with Phenanthroline and E-64. “Phenanthroline”: lysate with Phenanthroline only. “E-64 + Roche”: lysate with E-64 and Roche inhibitors cocktail. “Roche”: lysate with Roche inhibitors cocktail only. “E-64”: lysate with E-64 only. “PMSF”: lysate with PMSF only. “Phenanthroline + PMSF”: lysate with Phenanthroline and PMSF.

The interference of 1,10-Phenanthroline with the complexes stability did not permit the analysis of the migration of A600.1 in comparison to the intact respiratory protein complexes. However, the detection of the protein at a higher molecular weight than the recombinant protein after hrCN-PAGE separation of the WT mitochondrial lysates suggests that it is likely to be associated to a protein complex.

### 5.2.1.2 Identification of the co-migrating proteins

The native gel region corresponding to the protein band at 300 kDa detected by the anti-A600.1 antibody was cut out and analyzed by mass spectrometry to identify the proteins it contained, some of which may be A600.1 interacting proteins (Figure 5.3a). The A600.1 protein was not detected among the 109 proteins identified, which could be due to the amount of the

protein present in that region being insufficient for it to be detected by mass spectrometry. However, this approach does not always allow to differentiate among the identified proteins, those that truly interact with the A600.1 protein and those that simply happen to migrate in the same region, as found in (Acestor et al, 2011). The majority of the proteins identified belong to different pathways, which did not allow to extrapolate as to the function or pathways in which the A600.1 protein may be involved and whether it forms oligomers or is in association with other proteins. Interestingly, out of the 30 proteins identified by at least 2 peptides, 10 are annotated or have orthologs annotated as carrier or part of a transporter or channel (highlighted in orange in Table 4.1). An alternative approach such as affinity purification would be more adapted for the isolation and identification of the A600.1 potential interacting partners.

**Table 5.1: List of proteins identified by MS from the 300 kDa native PAGE band detected by Western blot with the anti-A600.1 antibody**

<b>Protein ID</b>	<b>Protein name</b>	<b># of peptides</b>	<b>Seq. cov. [%]</b>
LmxM33.0140 LmxM33.0160	malate dehydrogenase	6	28.8
LmxM28.1200	putative glucose-regulated protein 78	5	13.2
LmxM02.0450	conserved hypothetical protein 84% ID: putative VDAC of <i>L. major</i>	4	15.5
LmxM13.0390 LmxM13.0280	alpha tubulin	3	8.2
LmxM02.0670	putative mitochondrial carrier protein	3	10.5
LmxM36.5460	conserved hypothetical protein 54% ID: 2-hydroxyglutarate dehydrogenase of <i>Trypanosoma grayi</i>	3	10
LmxM36.9987 LmxM20.0100	phosphoglycerate kinase C, glycosomal	3	11.5
LmxM36.2030	chaperonin HSP60, mitochondrial precursor	1	7.4
LmxM27.0760	putative small GTP-binding protein Rab1	2	16.5
LmxM02.0460	conserved hypothetical protein 78% identity with <i>L. panamensis</i> VDAC, putative	2	5.8
LmxM18.1300	conserved hypothetical protein 81% identity with <i>L. panamensis</i> mitochondrial carrier protein, putative	2	6.5
LmxM36.2020	chaperonin HSP60, mitochondrial precursor	1	8.3
LmxM34.4430	putative mitochondrial phosphate transporter	2	8.2
LmxM28.2260	putative glycosomal membrane protein	2	10.8
LmxM06.1100*	conserved hypothetical protein * 36 % ID with hypothetical protein (Tb927.7.5700) of <i>T. brucei</i>	2	10.6
LmxM19.9997 LmxM19.9998 LmxM19.0200	putative ADP,ATP carrier protein 1, mitochondrial precursor	2	6.1
LmxM01.0570	putative tricarboxylate carrier	2	12.3
LmxM26.2000	conserved hypothetical protein 83% ID with <i>L. panamensis</i> methyltransferase	2	5.5
LmxM29.0120	alkyl dihydroxyacetonephosphate synthase	2	5.2
LmxM07.0460	acyl-CoA dehydrogenase, mitochondrial precursor,putative	2	5.8

Protein ID	Protein name	# of peptides	Seq. cov. [%]
LmxM07.0220**	conserved hypothetical protein ** 30% ID: hypothetical protein (Tb927.8.1740) of <i>T. brucei</i>	2	8.5
LmxM01.0490	putative long-chain-fatty-acid-CoA ligase	2	4.7
LmxM11.1000	putative pyruvate phosphate dikinase	2	3.2
LmxM18.0510	putative aconitase	2	3.7
LmxM31.3310	putative dihydrolipoamide dehydrogenase	2	8.4
LmxM30.1280	putative p-glycoprotein e	2	1.6
LmxM30.1290			
LmxM23.0380	ABC transporter-like protein	2	2.4
LmxM29.2900	putative aldehyde dehydrogenase	2	5.8
LmxM33.1330	conserved hypothetical protein 78% ID: putative mitochondrial ATP-dependent chaperone, of <i>Leptomonas pyrrocoris</i>	2	6.7

# of peptides: number of unique peptides identified

Seq. cov. (%): percentage of sequence coverage

ID: identity

VDAC: Voltage-dependent anion channel

\*: LmxM06.1100: annotation in TriTrypdb database on *T. brucei* ortholog (Tb927.7.5700): part of the outer mitochondrial membrane proteome, involved in protein import.

\*\* LmxM07.0220: annotation in TriTrypdb database on *T. brucei* ortholog Tb927.8.1740: identified as interacting partners of Tim17 present in the mitochondrial inner membrane and part of the TIM complex.

## 5.2.2 Identification of the A600.1 binding partners by GST pull-down

In order to isolate and identify the A600.1 interacting proteins, a GST fusion protein containing the C-terminal portion of the A600.1 protein was used as target. Bioinformatic analysis of the amino acid sequence encoded by the *A600.1* gene predicted the presence of two hydrophobic transmembrane domains in the N-terminal region of the protein (Murray et al, 2010). Transfection of *L. mexicana* *A600*<sup>-/-</sup> amastigotes with a plasmid containing the region encoding only for the N-terminal region of the A600.1 protein that contains the two

transmembrane domains (region between amino acids 1-64) but lacks the C-terminal region (amino acids 65-163), failed to rescue the *A600*<sup>-/-</sup> amastigotes growth defect, while transfection with the coding sequence for the full-length protein partially rescued the knock-out phenotype (Charis Segeritz, unpublished results). This indicates that the C-terminal portion (amino acids 65-163) is essential for the protein function.

To avoid the potential isolation of false A600.1 binding proteins through unspecific hydrophobic interactions with the transmembrane domains, a truncated form of the A600.1 protein, designated  $\Delta$ N.A600.1 that lacks the N-terminal region containing those domains (amino acids 1-64), was used as bait.

#### ***5.2.2.1 Testing and optimization of the cleavage of GST- $\Delta$ N.A600.1 by PreScission protease***

The effective cleavage of the GST- $\Delta$ N.A600.1 protein by the PreScission protease was first tested. The cleavage of the  $\Delta$ N.A600.1 moiety from the GST tag following capture on the Glutathione Sepharose 4B beads of the fusion protein and with its binding partners offers an advantage over the elution of the full-length fusion protein by reduced glutathione, in the fact that it reduces the presence in the eluate of false interacting proteins that would bind to the GST moiety (Lin et al, 2014). These potential contaminants may mask the identification of low abundance true interacting proteins and may erroneously be identified as true binding partners. After cleavage,  $\Delta$ N.A600.1 and its potential interacting partners are eluted from the glutathione Sepharose 4B beads, while the GST tag and the PreScission protease (which is also a GST fusion protein) remain on the beads.

To do this, the same amount of GST- $\Delta$ N.A600.1 protein was bound to Glutathione Sepharose 4B beads in three different tubes. After collection of the unbound fraction and

washing, the beads from one tube (sample 1) were eluted with 5X sample buffer to verify the effective binding of GST- $\Delta$ N.A600.1 protein to the beads. The beads from the other two tubes were incubated overnight with 8 U of PreScission protease, as described in the *GST Gene Fusion System Handbook* (GE Healthcare). Eluate from tube 2 was supplemented with 5X sample buffer, while eluate from tube 3 was ethanol precipitated, and the dried protein pellet was resuspended in 5X sample buffer. The beads from the three tubes were resuspended in 5X sample buffer and heated at 95°C for 5 minutes to release in the supernatant any proteins present on the beads. The different samples were then analysed by Western blot using the anti-A600.1 antibody for the detection of the GST fusion protein and/or its  $\Delta$ N.A600.1 moiety obtained after cleavage by the PreScission protease.

A band at 40 kDa, which corresponds to the predicted size of the GST- $\Delta$ N.A600.1 protein, was detected in all the samples (Figure 5.7). This indicates that GST- $\Delta$ N.A600.1 effectively bound to the beads. The presence of a band at 15 kDa in the eluates from tubes 2 and 3, likely to correspond to the  $\Delta$ N.A600.1 portion of the fusion protein (which has a predicted mass of 11.4 kDa) shows that the GST- $\Delta$ N.A600.1 was cleaved by the PreScission protease. However, the faintness of this band, in comparison to the strong band corresponding to the full-length fusion protein in the eluates and the beads supernatants from tubes 2 and 3 suggest that this cleavage was inefficient. Furthermore, the presence of significant amounts of the full-length GST- $\Delta$ N.A600.1 in the eluates indicate that either some unbound GST- $\Delta$ N.A600.1 was not totally washed off after fixation of the protein on the beads and remained in the beads pellet or the protein was displaced from the beads by the PreScission Protease which is also a GST fusion protein.

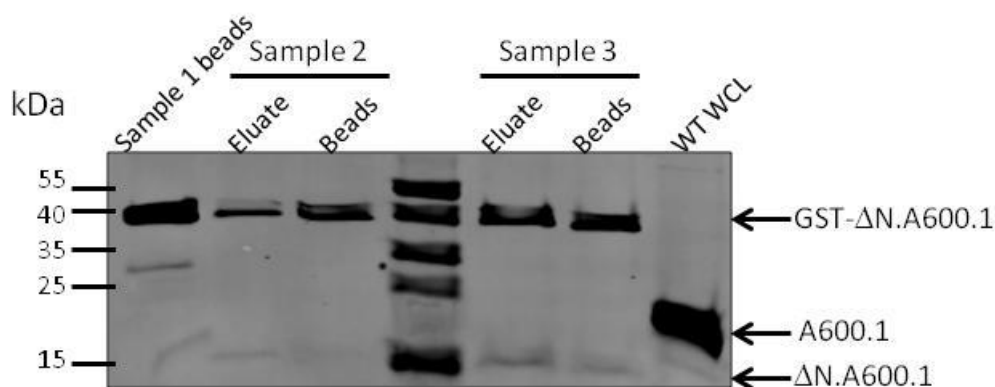


**Figure 5.7: Western blot analysis of GST-ΔN.A600.1-bound Glutathione Sepharose 4B beads after incubation with 8 U of PreScission Protease.**

In 3 tubes, 450  $\mu$ l of PBS containing 40 pmol of GST-ΔN.A600.1 were incubated with 50  $\mu$ l of Glutathione Sepharose 4B beads at 4°C for one hour with rotation. The beads were washed with 500  $\mu$ l of PBS. The beads from sample 1 were resuspended in 50  $\mu$ l of 5X SDS sample buffer (250 mM Tris-HCl pH6.8, 10% SDS, 50% (v/v) glycerol, 0.1% bromophenol blue, 0.1 M DTT) and heated at 95°C for 5 minutes. The beads from samples 2 and 3 were incubated overnight with 100  $\mu$ l of cleavage buffer containing 8 U of PreScission Protease. The protease eluates were collected by centrifugation at 500 x g for 5 minutes (lanes labeled “eluate”). The eluate from sample 3 was precipitated and the protein pellet was resuspended with 25  $\mu$ l of 5X SDS sample buffer. The beads from tubes 2 and 3 were washed with 1 ml of cleavage buffer, resuspended in 50  $\mu$ l of SDS sample buffer and heated at 95°C for 5 minutes (lanes labeled “beads”). Samples were separated on a 12% Tris-Tricine gel and analysed by Western blot with the anti-A600.1 peptide 2 antibody. WT WCL: *L. mexicana* WT whole cell lysate used as positive control.

To improve cleavage of the GST-ΔN.A600.1 protein, the protein-bound beads were incubated with different amounts of the PreScission Protease and the protease cleavage efficiency was assessed and compared based on the presence and intensity of the ΔN.A600.1 15 kDa band in the eluates. Western blot analysis of the eluates with the anti-A600.1 antibody revealed the presence of a strong band at 15 kDa, in the different eluates (Figure 5.8). This suggests that the GST-ΔN.A600.1 protein was effectively cleaved by the PreScission protease. However, an increase in the amount of protease did not appear to greatly increase the amount of cleavage since the intensity of the 15 kDa band was fairly similar in the different eluates, suggesting a similar amount of ΔN.A600.1 protein collected in those samples.

The improvement of the protein cleavage observed here using 8 U of protease in comparison to Figure 5.7 is suspected to be due to the way the protease was added to the beads. Indeed, cleavage was noticed to be most effective when the protease was added after the beads were resuspended in the cleavage buffer rather than resuspending the beads in the buffer already containing the diluted protease.

Some uncleaved GST- $\Delta$ N.A600.1 protein remained present on the beads and some was also eluted. The uncleaved protein present in the eluates might correspond to some unbound protein that remained in the beads pellet despite the extensive washes and contaminated the subsequent eluate. The beads washes and the eluates were collected after pelleting the beads by centrifugation. This method, referred to as the “batch method”, tends to leave a residual volume of solution in the beads pellet after pipetting out the supernatant and this may not allow the complete wash off of unbound GST- $\Delta$ N.A600.1 from the beads before elution (ThermoFisherScientific, 2008).

In the beads treated with 160 U of PreScission Protease, the band corresponding to the uncleaved GST- $\Delta$ N.A600.1 protein appears at a lower size, estimated at 36 kDa, instead of 40 kDa. The migration of the GST- $\Delta$ N.A600.1 protein in this sample might be affected by the presence of the excess of PreScission protease which, with a predicted size of 46 kDa, is expected to migrate in the same region of the SDS-PAGE gel as GST- $\Delta$ N.A600.1.

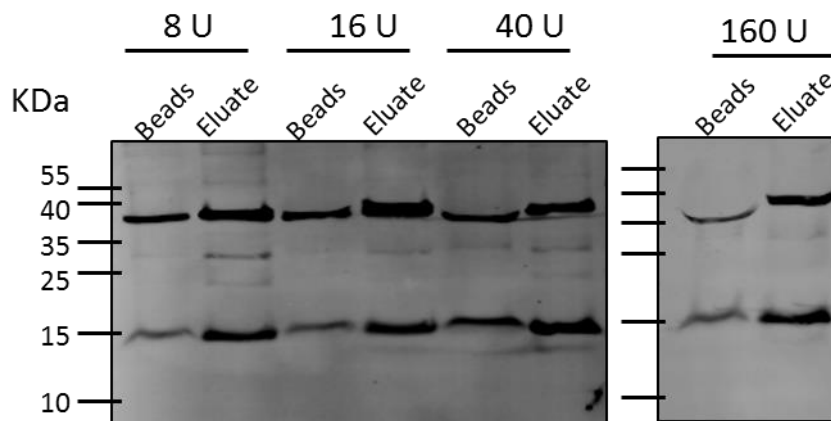


**Figure 5.8: Western blot analysis of GST- $\Delta$ N.A600.1-bound Glutathione Sepharose 4B beads after incubation with different amounts of PreScission Protease.**

Five tubes containing GST- $\Delta$ N.A600.1 protein bound to 50  $\mu$ l of glutathione beads were set up as before. After a one-hour incubation, the beads were washed and incubated overnight with the indicated amounts of PreScission Protease. The eluates were collected by centrifugation and precipitated. The protein pellets and the beads were resuspended in 20  $\mu$ l and 50  $\mu$ l of 5X SDS sample buffer, respectively. The samples were separated on 12% Tris-Tricine gels and analysed by Western blot using the anti-A600.1 antibody.

To reduce the presence of unbound GST- $\Delta$ N.A600.1 in the beads pellet and eliminate the presence of uncleaved GST- $\Delta$ N.A600.1 in the protease eluate, the use of mini-spin columns was tested and compared to the batch method. Five identical tubes were set up in which GST- $\Delta$ N.A600.1 protein was bound to Glutathione Sepharose 4B beads as before.

In sample 1, after washing, the GST- $\Delta$ N.A600.1-bound beads were incubated with the cleavage buffer without the protease and the resulting eluate was collected using the batch method. The eluate and the beads were supplemented with 5X sample buffer and analysed by Western blot with the anti-A600.1 antibody then the anti-GST antibody. In both samples, a band at 40 kDa, likely to correspond to GST- $\Delta$ N.A600.1 was detected by the anti-A600.1 antibody (Figure 5.9 – upper panel). The presence of the fusion protein in the eluate collected in absence of the PreScission protease indicates that the protease was not responsible for the elution of the uncleaved protein (Figure 5.8); its presence is likely due to some residual unbound GST-

$\Delta$ N.A600.1 that remained in the beads pellet after collection of the supernatant following each centrifugation, indicating the inefficiency of the washing steps in removing unbound GST- $\Delta$ N.A600.1 when using the batch method.

In samples 2 and 3, the protein-bound beads were incubated with the PreScission protease as before and the eluate was collected using the batch method. Analysis of those beads supernatant by Western blot with the anti-GST antibody reveals two bands in addition to the 15 and 40 kDa bands detected with the anti-A600.1 antibody (Figure 5.9). One band appeared slightly above the GST- $\Delta$ N.A600.1 40 kDa band, at an estimated size of 48.5 kDa; it is likely to represent the PreScission protease, which is also a GST fusion protein and has a predicted molecular mass of 46 kDa. The second additional band was detected at an estimated size of 25.5 kDa, which may correspond to the GST moiety of the cleaved fusion protein. The faintness of those two bands in the eluate from tube 2 in comparison to their intensity in the beads supernatant suggests that most of the protease and the cleaved GST moiety remained bound to the beads after cleavage while the  $\Delta$ N.A600.1 portion was eluted. The eluate from tube 3 was incubated with new Glutathione Sepharose 4B beads (Beads 2). After collection of the eluate, those beads were resuspended and heated in 5X sample buffer and the supernatant collected. A very faint band at 40 kDa was detected in the beads 2 supernatant using the anti-A600.1 antibody, suggesting that some uncleaved GST- $\Delta$ N.A600.1 were retained on those beads (Figure 5.9 – upper panel). Detection with the anti-GST antibody revealed that they also retain some protease (band at 48.5 kDa) and to a lesser extent some GST (faint band at 25.5 kDa) (Figure 5.9 – lower panel). Analysis of the resulting eluate using the anti-A600.1 antibody showed that it still

contains a significant amount of uncleaved GST- $\Delta$ N.A600.1, in addition to the cleaved  $\Delta$ N.A600.1 moiety at 15 kDa.

Following immobilization of the GST- $\Delta$ N.A600.1 protein in tubes 4 and 5, the beads were transferred to a mini-spin column, washed then incubated overnight with 16 U of PreScission protease. The washes and eluates were collected as flowthrough from the mini-spin columns during centrifugation in a collection tube. In comparison to the beads from tubes 2 and 3, the beads supernatants as well as the eluates from tubes 4 and 5 appeared to contain much less full-length GST- $\Delta$ N.A600.1, as represented by the faintness of the 40 kDa band detected by the anti-A600.1 antibody (Figure 5.9 – upper panel). This suggests that the spin column method was much more efficient for the removal of unbound GST- $\Delta$ N.A600.1 before elution with the protease. It also shows that the full-length GST- $\Delta$ N.A600.1 present in the beads supernatant and the eluates obtained with the batch method (tubes 1-3) mainly correspond to unbound GST- $\Delta$ N.A600.1 inefficiently washed off from the beads before elution, rather than uncleaved GST- $\Delta$ N.A600.1 bound to the beads. Indeed, the intensity of the  $\Delta$ N.A600.1 15 kDa band in eluates 4 and 5 (Figure 5.9 – upper panel) and of the GST 25.5 kDa band (Figure 5.9 – lower panel), in comparison to the faintness of the GST- $\Delta$ N.A600.1 40 kDa band in the corresponding beads supernatant indicates that the majority of the GST fusion protein that remains on the beads after the washes was cleaved by the PreScission protease. Most of the PreScission protease and the GST moiety of the cleaved GST- $\Delta$ N.A600.1 protein were retained by the beads as revealed by the detection of strong bands at 25.5 and 48.5 kDa following analysis of the beads supernatant with the anti-GST antibody (Figure 5.10 – lower panel). Similarly to tube 3, the eluate from tube 5 was re-incubated with new Glutathione Sepharose 4B beads (Beads 2). Detection with the anti-

GST antibody reveals that some PreScission protease remained in the first eluate and were retained by beads 2 but some protease and GST tag remains present in the resulting eluate, though in a low amount in comparison to the  $\Delta$ N.A600.1 moiety.

Taken together, these data indicate that the use of mini-spin columns to wash and elute the beads after fixation of the GST- $\Delta$ N.A600.1 protein efficiently removes any unbound protein from the beads before elution with the PreScission protease. They also showed that cleavage of GST- $\Delta$ N.A600.1 by the protease was very efficient since very little of the full length protein was recovered from the beads and in the eluates after incubation with the PreScission protease, using the mini-spin columns. An additional incubation of the protease eluate with new Glutathione Sepharose beads can help remove some left over protease that was not retained by the beads during elution.

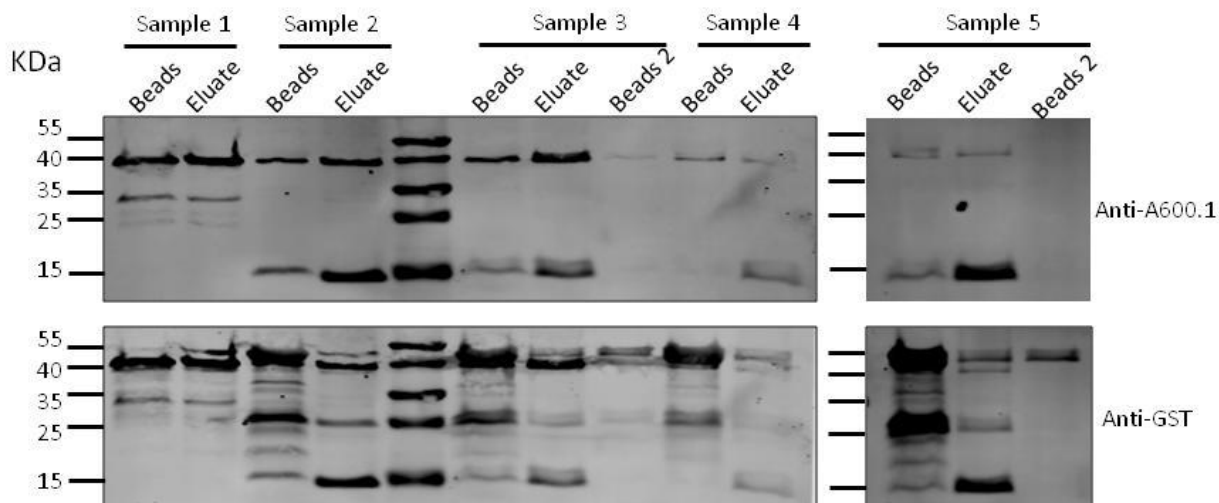


**Figure 5.9: Western blot analysis of GST-ΔN.A600.1-bound Glutathione Sepharose 4B beads after incubation with 16 U of PreScission Protease.**

Five identical tubes were set up in which 40 pmol of GST-ΔN.A600.1 protein were immobilized onto 100  $\mu$ l of Glutathione Sepharose 4B beads. After washing, the beads in tube 1 were incubated overnight with 100  $\mu$ l of cleavage buffer only, whereas the beads in tubes 2 and 3 were incubated with cleavage buffer containing 16 U of PreScission protease. The beads in tubes 4 and 5 were transferred to mini-spin columns for incubation with the protease. The eluates from tubes 1 to 3 were collected by pipetting the supernatants after centrifugation at 500 x g for 5 minutes to pellet the beads. The eluates from tubes 4 and 5 were collected as flowthrough from the mini-spin column by centrifugation at 500 x g for 5 minutes. The eluates from tubes 3 and 5 were incubated for 2 hours with 200  $\mu$ l of new Glutathione Sepharose 4B beads (beads 2). Sample 3 eluate was collected by pipetting the supernatant after centrifugation while sample 5 eluate was collected as the flow through obtained after centrifugation of the mini-spin column. All the eluates were ethanol precipitated and the protein pellets were resuspended in 20  $\mu$ l of 5X SDS sample buffer. The beads (100  $\mu$ l) used to fix the GST-ΔN.A600.1 protein (samples 1-5) and the beads used to incubate the eluates 3 and 5 (lanes labeled “Beads 2”) were resuspended in 100  $\mu$ l and 200  $\mu$ l of 5X SDS sample buffer, respectively. The samples were separated on a 12% Tris-Tricine gel and analyzed by Western blot with the anti-A600.1 antibody (upper panel). Detection was then repeated using the anti-GST antibody (lower panel).

### 5.2.2.2 Isolation of mitochondria-enriched fractions

To reduce the isolation of unspecific binding proteins, the pull-down assay was performed on cell fractions enriched for the A600.1 protein. Such fractions are likely to be also enriched for A600.1 binding partners and can therefore be used as source of potential A600.1 interacting proteins. To identify A600.1 enriched fractions, a digitonin fractionation approach

was employed (Foucher et al, 2006) and the isolated fractions were analysed for the presence of the A600.1 protein.

*L. mexicana* WT amastigotes were treated sequentially with digitonin at 10, 100, 500 and 5,000  $\mu$ M. The soluble fractions collected after each digitonin treatment were designated Fraction 1, Fraction 2, Fraction 3 and Fraction 4, respectively. Fraction 5 corresponds to the final pellet. The fractions were then analyzed by Western blot for the presence of cytosolic and mitochondrial markers as well as for the presence of the A600.1 protein. Similarly to what was showed using the differential digitonin permeabilization approach (Figure 3.10), the cytosolic marker, enolase, were released in the soluble fractions after treatment with low digitonin concentrations, as suggested by its detection in Fractions 1 and 2. The release of the inner mitochondrial membrane protein COIV required higher digitonin concentrations as revealed by its presence in Fractions 3, 4 and 5. This confirms that Fractions 3 and 4 are enriched with mitochondrial proteins (Foucher et al, 2006). The A600.1 protein co-localized with the COIV protein in the fractions 3 and 4, as revealed by its strong detection in these fractions. A pool of fractions 3 and 4 were therefore used for the pull-down assays.

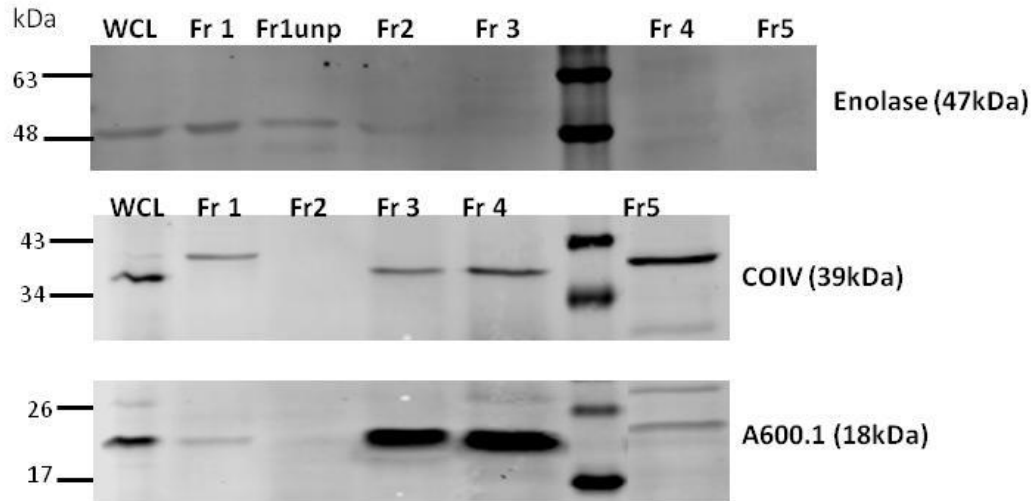


**Figure 5.10: Western Blot analysis of *L. mexicana* WT amastigotes digitonin fractions.**

After collection, the proteins from the soluble fractions (fractions 1 to 4) were precipitated with acetone and resuspended in 5% SDS. Each fraction (30  $\mu$ g of proteins) was separated on a 12% Laemmli (for enolase and COIV detection) or Tris-Tricine (for A600.1 detection) SDS-PAGE gel. After transfer of the proteins to a PVDF membrane, Western blot detection was performed with the following antibodies: rabbit anti-COIV, rabbit anti-enolase or rabbit anti-A600.1 peptide 2. The bound antibody was detected with an Alexa Fluor 680 goat anti-rabbit antibody. Membranes were scanned with the Odyssey CLx Imager. Fr1: fraction ; Fr1unp: fraction 1 before acetone precipitation; Fr2: fraction 2; Fr3: fraction 3; Fr4: fraction 4; Fr5: fraction 5.

### 5.2.2.3 Isolation of the $\Delta$ N.A600.1 interacting proteins

To identify the proteins that interact with A600.1, a pool of mitochondria-enriched fractions 3 and 4 from *L. mexicana* WT amastigotes was incubated with GST- $\Delta$ N.A600.1-bound Glutathione Sepharose 4B beads.  $\Delta$ N.A600.1 and its binding partners were then purified by elution with the PreScission protease. As negative control, a pull-down assay was performed in parallel with amastigotes mitochondria-enriched fractions incubated with GST-bound beads. The eluted proteins were ethanol precipitated and separated by SDS-PAGE. The protein bands were excised from the gel and digested with trypsin. The peptides from the proteins pulled-down with the GST- $\Delta$ N.A600.1 beads were labeled with heavy, deuterated formaldehyde ( $CD_2O$ ), while the peptides from the pull-down with the GST beads were labeled with light formaldehyde ( $CH_2O$ ).

The two sets of peptides were then pooled and analyzed by mass spectrometry. Each assay was performed three times. Proteins were considered as potential  $\Delta N.A600.1$  interacting proteins if they were identified in at least two of the three assays with a heavy versus light ratio (ratio H/L) equivalent or above 1.2. Results are summarized in Table 5.2 and the proteins identified in each pull-down with a heavy versus light ratio equivalent or above 1.2 are listed in Appendix C.

Table 5.2: List of potential ΔN.A600.1 interacting partners

Protein ID	Protein name	Pull-down 1			Pull-down2			Pull-down 3		
		Ratio H/L	Seq. Cov. (%)	# of peptides	Ratio H/L	Seq. cov. (%)	# of peptides	Ratio H/L	Seq. cov. (%)	# of peptides
LmxM22.1460	i/6 autoantigen-like protein	<b>50.09</b>	4.41	1	-	-	-	<b>1.79</b>	24	6
LmxM22.0730	hypothetical protein	<b>8.79</b>	2.4	1	-	-	-	<b>1.88</b>	16	15
LmxM23.0080	hypothetical protein	<b>3.23</b>	2.15	1	<b>1.44</b>	3.3	2	<b>2.51</b>	11	17
LmxM09.1340	histone H2B	<b>3.05</b>	14.95	2	-	-	-	<b>1.59</b>	3	3
LmxM34.3340	6-phosphogluconate dehydrogenase, decarboxylating	<b>1.94</b>	2.09	1	<b>1.17</b>	5	2	-	-	
LmxM09.0100	calmodulin-like protein containing EF hand domain	<b>1.48</b>	9.28	4	-	-	-	<b>1.43</b>	41.9	27
LmxM32.2440	hypothetical protein	-	-	-	<b>1.22</b>	11.2	4	<b>3.35</b>	21.9	11
LmxM05.0380	microtubule-associated protein	-	-	-	<b>1.44</b>	54.2	4	<b>2.24</b>	57.4	8
LmxM22.0050	hypothetical protein	-	-	-	<b>1.24</b>	11.7	4	<b>1.93</b>	10.9	4
LmxM18.1380	pyruvate dehydrogenase E1 component alpha subunit	-	-	-	<b>1.19</b>	44.2	18	<b>1.56</b>	20.6	7
LmxM34.1130 LmxM34.1160 LmxM34.1150	oligosaccharyl transferase-like protein	-	-	-	<b>1.71</b>	8.9	5	<b>1.34</b>	6.3	3

Protein ID	Protein name	Pull-down 1			Pull-down2			Pull-down 3		
		Ratio H/L	Seq. Cov. (%)	# of peptides	Ratio H/L	Seq. cov. (%)	# of peptides	Ratio H/L	Seq. cov. (%)	# of peptides
LmxM16.0550	orotidine-5-phosphate decarboxylase/orotate phosphoribosyltransferase	-	-	-	<b>1.26</b>	27.4	13	<b>1.27</b>	21.4	5
LmxM06.1000	hypothetical protein, conserved	-	-	-	<b>1.26</b>	4.7	1	<b>1.25</b>	4.7	1
LmxM24.0320	fumarate hydratase	-	-	-	<b>1.29</b>	7.7	3	<b>1.22</b>	7.7	3

Ratio H/L: heavy versus light ratio

Seq. cov. (%): percentage of sequence coverage

# of peptides: number of unique peptides identified

Table 5.3: List of potential contaminants

Protein ID	Protein name	Pull-down 1			Pull-down 2			Pull-down 3		
		Ratio H/L	Seq. cov. (%)	# of peptides	Ratio H/L	Seq. cov. (%)	# of peptides	Ratio H/L	Seq. cov. (%)	# of peptides
LmxM32.3150 LmxM19.0390	putative 40S ribosomal protein S13	<b>6.53</b>	5.96	1	-	-	-	<b>1.4</b>	23.8	4
LmxM08.1230	beta tubulin	-	-	-	<b>1.6</b>	47.1	1	<b>1.3</b>	50.5	2
LmxM36.2020	chaperonin HSP60, mitochondrial precursor	<b>5.14</b>	4.24	2	-	-	-	<b>1.4</b>	31.3	3
LmxM18.1370	putative heat shock protein	<b>3.12</b>	1.46	1	-	-	-	<b>1.48</b>	3.2	2

Among the proteins isolated, 19 proteins were identified with a heavy versus light ratio >1.2 in at least 2 assays (Table 5.1 and 5.2). Among the 10 proteins identified with known functions, two are proteins associated with the cytoskeleton LmxM22.1460 (i/6 autoantigen-like protein) and LmxM05.0380 (microtubule-associated protein), three are metabolic enzymes: LmxM34.3340 (6-phosphogluconate dehydrogenase: enzyme of the pentose phosphate pathway), LmxM18.1380 (pyruvate dehydrogenase E1 component alpha-subunit: converts pyruvate into acetyl-CoA in the mitochondria) and LmxM24.0320 (fumarate hydratase: TCA cycle enzyme) and two are involved in biosynthetic pathways: LmxM34.1130 (oligosaccharyl transferase-like protein: involved in protein glycosylation) and LmxM16.0550 (orotidine-5-phosphate decarboxylase/orotate phosphoribosyltransferase: involved in pyrimidine biosynthesis). One of the five proteins annotated as hypothetical proteins was found to share 30% identity over 76% of its sequence with the *T. brucei* protein Tb927.7.2640, annotated as a putative cytoskeleton associated protein.

Among those 19 proteins, only one, LmxM23.0080, annotated as hypothetical was identified in all three assays. Unfortunately, no further information could be obtained about this protein when searching for potential orthologs via Blastp or via the TriTrypDB database where its *T. brucei* and *T. cruzi* orthologs are also annotated as hypothetical proteins.

Four of those 19 proteins were classified as potential contaminants as they correspond to abundant cellular proteins (ribosomal, heat shock proteins, tubulins) that tend to be identified in pull-down assays regardless of the targeted complexes (Table 5.2), based on our experiences and the literature (Foucher et al, 2006; Zikova et al, 2008).

Overall, these results did not allow to conclude whether the A600.1 protein interacts with other proteins or to determine the cellular pathway in which it may be involved as, with the

exception of LmxM23.0080, which function is unknown, no protein was isolated in all three replicates with a heavy to light ratio above 1.2 and the proteins isolated as potential binding partners based on a heavy to light ratio above 1.2, do not belong to the same pathway.

### **5.2.3 Identification of A600.1 binding partners by co-immunoprecipitation**

In parallel to the GST pull-down assays, a co-immunoprecipitation (co-IP) approach was employed to isolate potential A600.1 interacting proteins, using the anti-A600.1 peptide 2 antibody covalently bound to magnetic beads. This technique relies on the ability of the antibody to pull-down the endogenous A600.1 protein from the cell sample. Because of concerns that the mitochondria isolation procedure may disrupt the potential endogenous A600.1-containing complex(es) and/or the endogenous A600.1 protein-protein interactions, the assay was performed using whole cell lysate as source of potential interacting proteins.

#### **5.2.3.1 *Amastigotes lysis method***

The first step was to select a lysis method that would release the A600.1 endogenous protein in the soluble fraction of the cell lysate so that it can be easily immunoprecipitated with the anti-A600.1 antibody. To preserve the native state of the endogenous A600.1 protein and of the protein complex it may interact with, *L. mexicana* WT amastigotes whole cell proteins were extracted using a non-denaturing detergent lysis method, following recommendations in the Dynabeads Co-immunoprecipitation kit instructions manual (Life Technologies) and adapted from (Dey et al, 2010). The method was first tested for the presence of the A600.1 protein in the soluble fraction. *L. mexicana* WT amastigotes were lysed in IP buffer (25 mM Tris-HCl, pH 8; 100 mM NaCl; 10% glycerol; 0.5% NP-40, 5 mM MgCl<sub>2</sub>, 1 mM DTT) in the presence of protease inhibitors (10 mM 1,10 Phenanthroline; 10 μM E-64, 1 mM PMSF and 1x Roche

complete EDTA-free protease inhibitors cocktail). In parallel, some cells were lysed in the more denaturing RIPA buffer (50 mM Tris-HCl, pH 8; 150 mM NaCl; 1% NP-40; 0.5% sodium deoxycholate; 0.1 % SDS) as control, since it had been previously used in our lab to lyse amastigotes and solubilize the A600.1 protein. Western blot analysis of both lysates soluble and insoluble fractions using the anti-A600.1 antibody revealed that after lysis with the IP buffer, the majority of the A600.1 protein was released in the soluble fraction of the amastigotes lysate (Figure 5.11). This shows that the IP buffer is effective at solubilizing the A600.1 protein during lysis of the *WT* amastigotes.

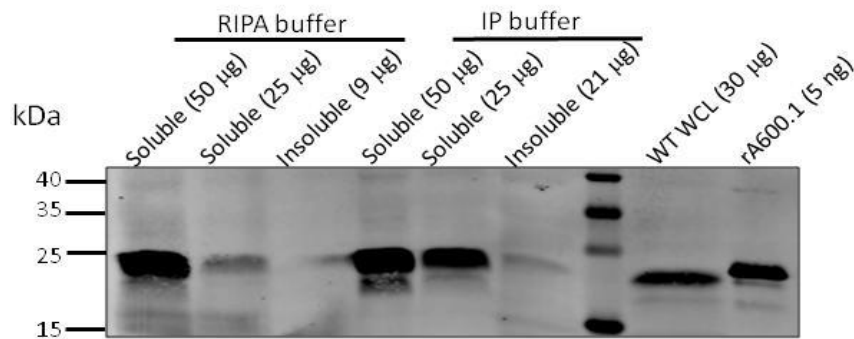


**Figure 5.11: Western blot detection of the A600.1 protein in *L. mexicana* *WT* amastigotes fractions after lysis with RIPA or IP buffer.**

After incubation in the appropriate buffer, the *L. mexicana* *WT* amastigotes lysates were centrifuged at 16,000 x g for 20 minutes. After collection of the supernatants, the pellets were resuspended in half the volume of the lysate in RIPA or IP buffer. The supernatants (soluble fraction) and the resuspended pellets (insoluble fraction) were separated on a 12% Laemmli SDS-PAGE gel (amount of proteins loaded in brackets) then transferred on a PVDF membrane. Detection was performed using the anti-A600.1 peptide 2 antibody, followed by the Alexa Fluor 680 goat anti-rabbit secondary antibody. WT WCL: whole cell lysate of *L. mexicana* *WT* amastigotes. rA600.1: recombinant A600.1 protein produced in *E. coli*.

### 5.2.3.2 *Evaluating the ability of the anti-A600.1 antibody to immunoprecipitate the endogenous A600.1 protein*

The anti-A600.1 peptide 2 antibody was coupled to the Dynabeads magnetic beads following the manufacturer's protocol. The antibody-coupled beads were rinsed with the IP buffer then incubated for one hour with either the *L. mexicana* WT or the *L. mexicana* A600<sup>-/-</sup> amastigotes soluble fraction. After collection of the unbound fraction, the beads were washed twice with PBS and three times with IP buffer. The proteins bound to the antibody-coupled beads were released by resuspending and heating the beads at 95°C in 5X SDS sample buffer.

The Western blot analysis of the beads supernatants (lanes labeled "bound") using the anti-A600.1 antibody revealed the presence of a strong band of an estimated size of 58 kDa, likely to correspond to the IgG heavy chain of the antibody, which has an expected size of 55 kDa. A fainter band estimated at 27 kDa was also detected in those samples, likely to correspond to the antibody light chain (Figure 5.12). The light and heavy chains of the antibody were detected by the anti-rabbit secondary antibody used for detection. The presence of these bands confirms that the anti-A600.1 antibody was effectively bound to the beads. In addition to those two bands, the supernatant from the beads incubated with the *L. mexicana* WT amastigotes lysate contained an extra band estimated at 23 kDa, the position the A600.1 protein migrates to after SDS-PAGE. This band was also detected in the WT amastigotes samples before (sample labeled "soluble") and after incubation (sample labeled "unbound") with the beads but it was not present in the A600<sup>-/-</sup> samples (Figure 5.6), which confirms that this band corresponds to the A600.1 protein. This indicates that the anti-A600.1 antibody can effectively immunoprecipitate the endogenous A600.1 protein from the WT amastigotes soluble fraction.

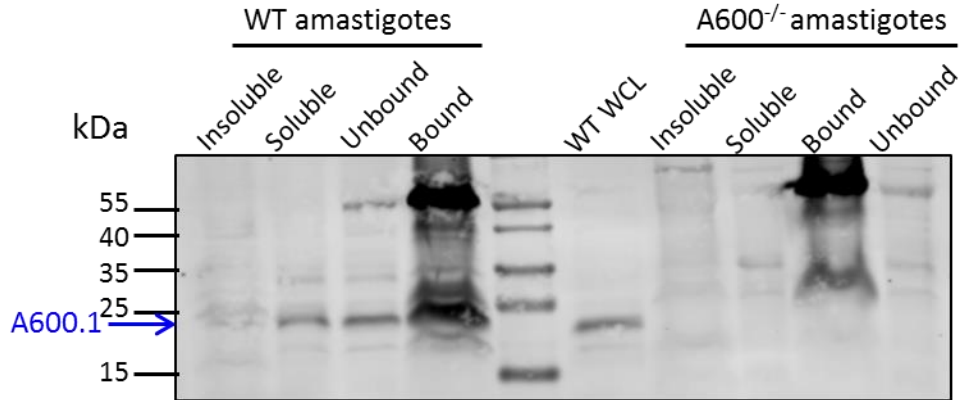


**Figure 5.12: Western blot analysis of *L. mexicana* WT and *A600*<sup>-/-</sup> amastigotes samples before and after incubation with the anti-A600.1-coupled magnetic beads.**

The different fractions were separated on a 12% Tris-Tricine gel then transferred on a PVDF membrane. Detection was performed using the anti-A600.1 peptide 2 antibody, followed by the Alexa Fluor 680 goat anti-rabbit secondary antibody. Insoluble: pellet after lysate centrifugation. Soluble: supernatant after lysate centrifugation. Unbound: lysate supernatant collected after incubation with antibody-coupled beads. Bound: supernatant collected after heating the antibody-coupled beads following incubation with the cell sample. WT WCL: whole cell lysate of *L. mexicana* WT amastigotes.

### 5.2.3.3 *Evaluating the IP and elution conditions on the antibody fixation to the magnetic beads*

Because the presence of the antibody IgG heavy chain was detected in washes and in eluates where it could interfere with the detection of lower abundance specific A600.1 binding proteins, antibody leakage in the washes was monitored after modification of the successive buffers used to wash the beads after antibody coupling and before incubation with the cell lysate. To help wash off any unbound antibody after coupling, Tween-20 was included to a final concentration of 0.05% in the HB and LB buffers provided in the beads kit. To mimic the immunoprecipitation conditions, the beads were incubated for one hour at 4°C in the IP buffer, in which DTT was omitted as it may dissociate IgG heavy and light chains as well as affecting the binding of the antibody to the beads (Life Technologies). The beads were washed three times with PBS-T (PBS + 0.05% Tween-20) containing increasing concentrations of NaCl (100, 150

then 200 mM). To mimic the conditions during the elution step, two elution buffers were tested: 1% SDS and 0.1 M glycine, pH 2.5.

Analysis of the different beads washes by Western blot using the anti-rabbit secondary antibody to detect the presence of the anti-A600.1 antibody IgG indicated the presence of a band of an estimated size of 58 kDa corresponding to the IgG heavy chain, in the different beads washes after coupling and before the one-hour incubation with the IP buffer (Figure 5.13 a and b). However, the fact that this band intensity decreased in the successive washes suggests that this band corresponds to unbound antibody left over after removal of the antibody solution after the overnight incubation which got progressively washed off with the successive washes, rather than some bound antibody uncoupling from the beads. No antibody was detected in the IP buffer wash, suggesting that all unbound antibody had been removed at that point, which would correspond to the step when the antibody-coupled beads would be incubated with the cell lysate (Figure 5.13 b).

In the first elution with 1% SDS, a relatively strong band appeared at 55 kDa, suggesting that this buffer released some bound antibody from the beads (Figure 5.13 c). A similar band but less intense was detected in the first eluate with the low pH glycine buffer suggesting that this buffer also induced some antibody leakage but to a much lesser extent than the 1% SDS. The low pH glycine buffer was therefore selected to test elution of the endogenous A600.1 protein after immunoprecipitation with the anti-A600.1-coupled beads.

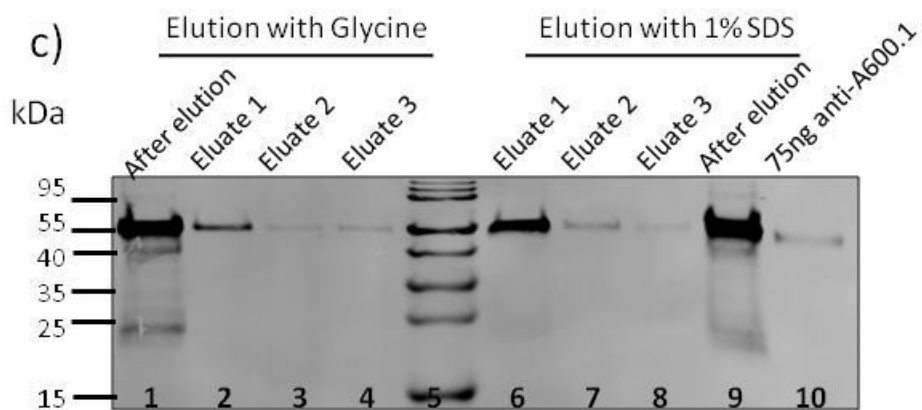
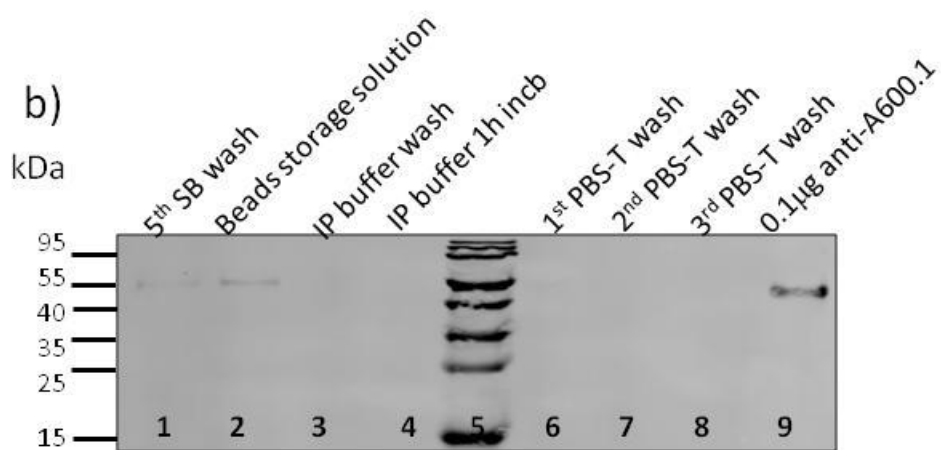
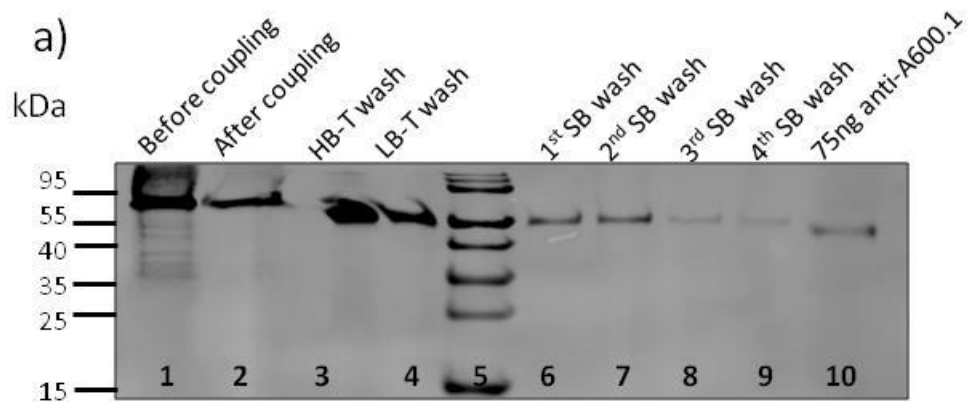


**Figure 5.13: Western blot analysis of washes of the anti-A600.1 antibody-coupled beads.**

The anti-A600.1 antibody solution (Fig a, lane 1 – sample “before coupling”) was incubated with the Dynabeads magnetic beads (15 µg antibody per mg of beads) at 37°C overnight with rotation. After collection of the beads supernatant (Fig a, lane 2 – sample “after coupling”), the antibody-coupled beads were washed successively in the buffers provided in the beads kit (Fig a, lanes 3-9). The beads were resuspended at 10 mg/ml in SB buffer (provided in kit) and stored at 4°C. When ready for use, the storage solution was removed (Fig b, lane 2) and the beads were washed once with IP buffer (Fig b, lane 3) then incubated for one hour at 4°C with rotation with IP buffer as for an IP with cell lysate. After collection of the supernatant (Fig b, lane 4), the beads were washed 3 times with PBS + Tween-20 with increasing concentrations of NaCl (100-200 mM). To mimic the elution of bound proteins after IP, the beads were incubated with 0.1 M glycine, pH 2.5 or 1% SDS (60 µl for 1.5 mg of antibody-coupled beads) 3 times for 10 minutes. After collection, the glycine eluates were neutralized with 1/10<sup>th</sup> of 1 M Tris-HCl, pH 8.5. The beads were then heated for 5 minutes in 60 µl of 5x sample buffer. 50 µl of each sample were separated on a 12% Tris-Tricine gel and transferred on a PVDF membrane. Detection was performed with the Alexa Fluor 680 goat anti-rabbit antibody (Thermo Fisher Scientific, USA). 75-100 µg of anti-A600.1 antibody was loaded as positive control (lane 10 in Figure a and c; lane 9 in Figure b).

**5.2.3.4 Evaluating elution of the endogenous A600.1 protein from the anti-A600.1**

***antibody-coupled beads***

The *L. mexicana* WT and A600<sup>-/-</sup> amastigotes were lysed in IP buffer without DTT and the lysate soluble fractions were incubated with washed anti-A600.1 antibody-coupled beads. The immunoprecipitated proteins were eluted with 0.1 M of glycine, pH 2.5. Analysis of the samples by Western blot using the anti-A600.1 antibody followed by the anti-rabbit antibody, showed that the six eluates contained a 58 kDa band suggesting the presence of the antibody IgG heavy chain in the different eluates (Figure 5.14 a). While no other band was detected in the three eluates from the beads incubated with the A600<sup>-/-</sup> lysate soluble fraction, the first eluate from the beads incubated with the WT lysate contained an extremely strong band at 23 kDa. This band migrated at the same level as the band in the WT lysate samples and in the recombinant A600.1 lane. Its absence in any of the A600<sup>-/-</sup> samples (Figure 5.14 a and b) suggests that this band corresponds to the A600.1 protein. This indicates that the A600.1 endogenous protein was effectively solubilized with the IP buffer and immunoprecipitated by the anti-A600.1 antibody

coupled to the magnetic beads and that the majority of the immunoprecipitated protein was eluted from the beads after a single incubation with 0.1 M glycine, pH 2.5.

Additional protein bands were detected in the eluate 1 from the beads incubated with the *WT* sample. The smallest but intense one migrated just below the A600.1 band and at an estimated size of 17 kDa and seemed to be similar to a small but fainter band detected at the same position in the *WT* lysates before and after incubation with the antibody-coupled beads (Figure 5.14 b). Since it is not detected in the *A600*<sup>-/-</sup> sample, this band might be a degradation product of the A600.1 protein. Two other higher but fainter bands appeared in this *WT* eluate at 39 kDa and 30 kDa, respectively. Those bands could have two origins: they could be degradation products of the antibody IgG heavy chain, although the fact that they are not detected in any of the other eluates makes this explanation unlikely. Another possibility is that those bands might correspond to oligomers of the A600.1 protein that were not totally denatured during heating and were detected due to the concentration of the protein in this sample as suggested by the strong intensity of the A600.1 band at 23 kDa.

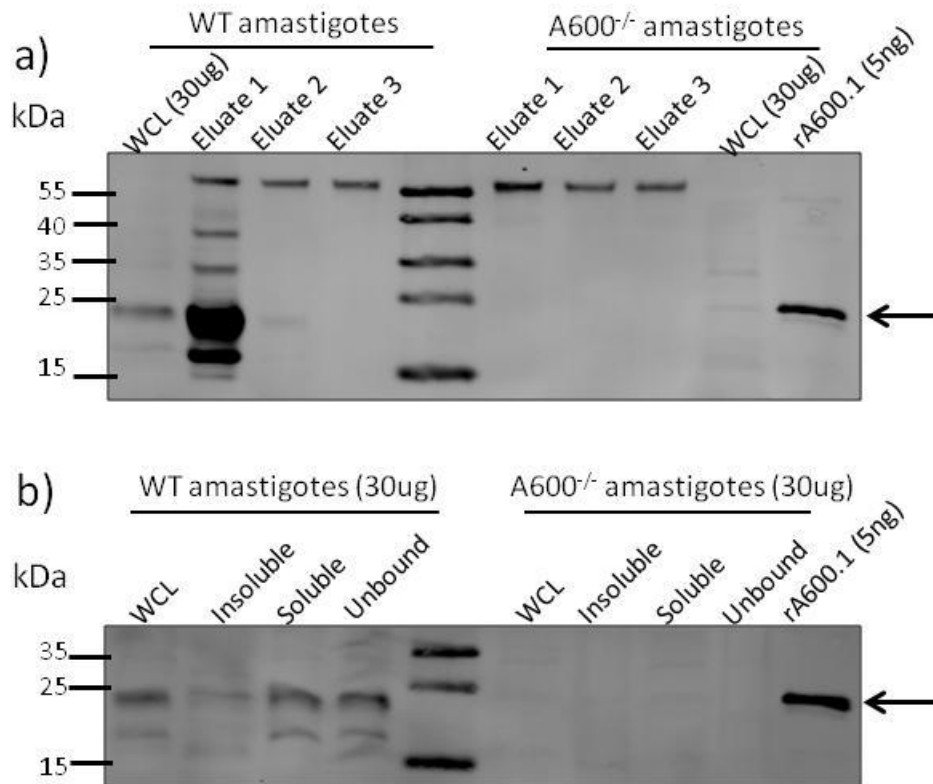


**Figure 5.14: Western blot analysis of *L. mexicana* WT and *A600*<sup>-/-</sup> amastigotes samples after immunoprecipitation with the anti-A600.1 antibody coupled to magnetic beads and elution.**

The indicated amounts of lysates fractions and 60  $\mu$ l of eluates were separated on a 12% Tris-Tricine gel and transferred to a PVDF membrane. Detection was performed with the anti-A600.1 antibody followed by the Alexa Fluor 680 goat anti-rabbit secondary. WCL: whole cell lysate. Insoluble: pellet obtained after centrifugation of whole cell lysate. Soluble: supernatant obtained after lysate centrifugation. Unbound: lysate supernatant collected after incubation with antibody-coupled beads. rA600.1: recombinant A600.1 protein produced from *E. coli*.

### 5.2.3.5 Mass spectrometry analysis of the proteins co-immunoprecipitated by the anti-A600.1 antibody-coupled beads

Since the majority of the A600.1 protein was eluted after the first elution, only the first eluate was analysed by mass spectrometry. The peptides from proteins immunoprecipitated from the *L. mexicana* WT amastigotes lysate were labeled with heavy deuterated formaldehyde (CD<sub>2</sub>O). The peptides from the *L. mexicana* *A600*<sup>-/-</sup> amastigotes IP were labeled with light

formaldehyde (CH<sub>2</sub>O). The two sets of peptides were pooled and analysed together by mass spectrometry.

In the first immunoprecipitation, 16 proteins were identified. Six were classified as contaminants as they corresponded to abundant cellular proteins (tubulins, ribosomal and heat shock proteins) that are often identified in pull-down assays, as explained previously. Five proteins were identified with a heavy versus light ratio above 1.2 and listed in Table 5.3. The protein identified with the highest ratio of 14.4, LmxM33.3640 corresponds to the A600.1 protein, which confirmed that the target protein was effectively immunoprecipitated by the antibody-bound beads and eluted successfully. Other proteins included LmxM25.1170 or 25.1180, the putative  $\beta$  subunit of the ATP synthase (or Complex V), LmxM18.1380, the pyruvate dehydrogenase E1,  $\alpha$  subunit of the multi-enzyme pyruvate dehydrogenase complex that oxidizes pyruvate to acetyl-CoA, and LmxM27.0930, a putative isovaleryl-coA dehydrogenase, which belongs to the family of acyl-coA dehydrogenases, which are involved in fatty acids oxidation. LmxM29.2980, which corresponds to the glycosomal glyceraldehyde 3-phosphate dehydrogenase (gGAPDH) is an enzyme of the glycolysis. Its localization to the glycosome, a specialized organelle that contains, among others, the glycolytic enzymes, makes it an unlikely binding partner of A600.1.

**Table 5.4: List of potential A600.1 binding partners identified by co-IP**

<b>Protein ID</b>	<b>Protein name</b>	<b>Ratio H/L</b>	<b>Sequence coverage (%)</b>	<b># of peptides</b>
LmxM33.3640 LmxM33.3642	A600.1	<b>14.5</b>	7.4	1
LmxM25.1170 LmxM25.1180	putative ATPase beta subunit	<b>1.66</b>	9.5	3
LmxM29.2980	glyceraldehyde 3-phosphate dehydrogenase, glycosomal	<b>1.25</b>	6.1	2
LmxM27.0930	putative isovaleryl-coA dehydrogenase	<b>1.22</b>	3.2	1
LmxM18.1380	putative pyruvate dehydrogenase E1 component alpha subunit	<b>1.196</b>	2.4	1

(Proteins identified with a heavy to light ratio (ratio H/L) above 1.2)

#### **5.2.3.6 Analysis of the proteins co-immunoprecipitated and eluted from the anti-A600.1 antibody-coupled beads by blue silver staining**

When the eluates above from the co-IPs with  $5 \times 10^9$  *L. mexicana* WT and *A600*<sup>-/-</sup> lysates were separated by SDS-PAGE and stained before mass spectrometry analysis, the protein bands were hardly detectable. This may have led to A600.1 interacting proteins present at substoichiometric amounts to go undetected during analysis. Therefore, the assay was repeated using approximately ten times more cells. The eluted proteins were separated on a 12% Tris-Tricine gel which was then stained with blue silver stain. The blue silver staining of the SDS-PAGE of the WT and *A600*<sup>-/-</sup> eluates revealed the presence of bands, though very faint, between 35 kDa and 55 kDa in the WT eluate. Those bands were not seen in the *A600*<sup>-/-</sup> eluate (Figure

5.15). This suggested that these bands may correspond to proteins associated to the A600.1 protein since they were not detected in its absence.

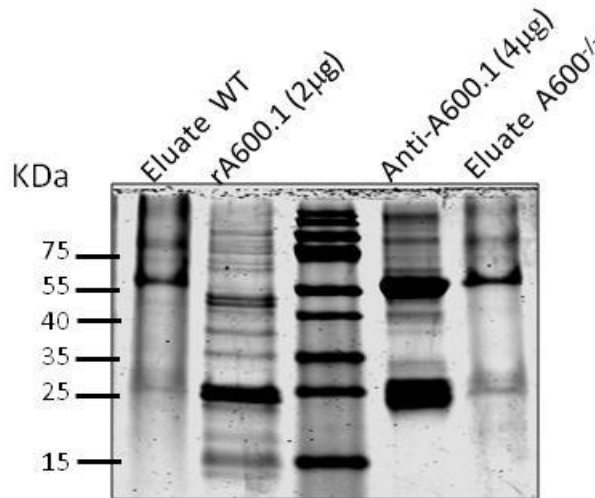


**Figure 5.15: Blue silver staining of SDS-PAGE of co-immunoprecipitated proteins from  $45 \times 10^9$  *L. mexicana* WT and *A600*<sup>-/-</sup> amastigotes lysates.**

Soluble fractions were collected after lysis of  $45 \times 10^9$  *L. mexicana* WT and *A600*<sup>-/-</sup> amastigotes. Each fraction was incubated with 7.5 mg of anti-A600.1 antibody-coupled beads and elution was performed using 500  $\mu$ L of 0.1 M glycine, pH 2.5. The eluates were precipitated and the dried protein pellets were resuspended in 40  $\mu$ L of 5x SDS sample buffer. Samples were separated on a 12% Tris-tricine gel, along with 2  $\mu$ g of recombinant A600.1 (rA600.1) purified from *E. coli* and 4  $\mu$ g of anti-A600.1 antibody as controls. After overnight fixation, the gel was stained with blue silver stain. The destained gel was scanned using the Odyssey CLx Imager.

The proteins immunoprecipitated using the new IP conditions were analyzed by mass spectrometry. Among the 49 proteins identified, 24 proteins were classified as contaminants, as defined previously, since they corresponded to abundant cellular proteins, such as ribosomal (n=21) or heat shock proteins (n=2). 17 of the rest had a heavy versus light ratio above 1.2, among which 5 were annotated as hypothetical (Table 5.4). 5 proteins (or their *T. brucei* orthologs) are annotated as nucleotide binding proteins (LmxM08\_29.2200, LmxM27.2100,

LmxM36.1610 / 36.1620, LmxM06.0460, LmxM19.0200) and only one of those 17 proteins, LmxM29.2980, the glycosomal GAPDH isoenzyme, was also identified in the previous co-IP.

As observed with the pull-down assays results, the proteins identified belong to different cellular pathways, which did not allow to determine the particular pathway in which the A600.1 protein may be involved.

**Table 5.5: List of proteins identified in second co-IP**

<b>Protein ID</b>	<b>Protein name</b>	<b>Ratio H/L</b>	<b>Sequence coverage (%)</b>	<b># of peptides</b>
LmxM08_29.2200	putative GTP-binding protein	<b>28.99</b>	12.9	10
LmxM27.2100	putative RNA-binding protein	<b>11.75</b>	3.3	2
LmxM33.3640	A600.1	<b>11.57</b>	12.9	2
LmxM36.1620 LmxM36.1610	universal minicircle sequence binding protein	<b>10.82</b>	45.2	3
LmxM06.0460	ATP-NAD kinase-like protein	<b>10.41</b>	1.8	2
LmxM29.2980	glyceraldehyde 3-phosphate dehydrogenase, glycosomal	<b>8.35</b>	7.5	2
LmxM15.0410	conserved hypothetical protein	<b>6.86</b>	3.5	2
LmxM07.0380	conserved hypothetical protein	<b>6.2</b>	0.7	2
LmxM33.4620	conserved hypothetical protein	<b>6.1</b>	6.2	4
LmxM19.1010	conserved hypothetical protein	<b>5.9</b>	3.7	2
LmxM16.0780	conserved hypothetical protein	<b>5.01</b>	0.6	2
LmxM36.3530 LmxM30.1900 LmxM30.2030	putative polyubiquitin, partial ubiquitin-fusion protein	<b>4.95</b>	16.2	1
LmxM36.3980	conserved hypothetical protein	<b>4.12</b>	9.1	3
LmxM19.0200	putative ADP, ATP carrier protein 1, mitochondrial precursor	<b>3.5</b>	3.8	2
LmxM28.2510	putative acyl-CoA dehydrogenase	<b>2.12</b>	3.8	2
LmxM23.0950	cytosolic leucyl aminopeptidase	<b>1.98</b>	3.9	2
LmxM17.9995	elongation factor 1-alpha	<b>1.60</b>	7.8	3

Ratio H/L: ratio heavy to light

#### 5.2.4 Summary regarding the identification of potential A600.1 interacting proteins

The proteins immunoprecipitated by the anti-A600.1 antibody were compared to the list of proteins identified in the GST pull-down assays. Proteins that were identified in at least one co-IP and one pull-down assay with a heavy to light ratio above 1.2 are listed in Table 5.6.

**Table 5.6: List of proteins identified in the GST pull-downs and co-IP assays**

Protein ID	Protein name	Ratio >1.2				
		IP1	IP 2	P-d 1	P-d 2	P-d 3
LmxM25.1170 LmxM25.1180	putative ATPase beta subunit	1.66	-	3.39	-	-
LmxM29.2980	glyceraldehyde 3-phosphate dehydrogenase, glycosomal	1.25	8.35	15.01	-	-
LmxM18.1380	putative pyruvate dehydrogenase E1 component alpha subunit	1.2	-	-	1.19	1.57
LmxM27.0930	isovaleryl-coA dehydrogenase, putative	1.22	-	-	1.52	-
LmxM25.1710	putative pyruvate dehydrogenase E1 beta subunit	1.08	-	-	-	2.41
LmxM19.9998 LmxM19.0200 LmxM19.9997	ADP, ATP carrier protein 1, mitochondrial precursor, putative	-	3.5	-	1.40	-
LmxM23.0950	cytosolic leucyl aminopeptidase	-	1.98	-	1.2	-
LmxM23.0080	hypothetical protein	-	-	3.23	1.44	2.5

The numbers indicate the ratio heavy versus light obtained in the pull-down (P-d) or co-immunoprecipitation (IP) assay in which the protein was identified with a ratio heavy versus light >1.2.

Seven proteins were identified; among them, was the glycosomal GAPDH (LmxM29.2980), which presence in the eluates has been discussed previously. Two of the proteins were proteins of the oxidative phosphorylation pathway, the putative ATPase beta subunit (LmxM25.1170; LmxM25.1180) and the putative ADP, ATP carrier protein 1, mitochondrial precursor (LmxM19.0200). Two other proteins were identified as components of the multi-enzyme pyruvate dehydrogenase complex, the putative pyruvate dehydrogenase E1,  $\alpha$  subunit (LmxM18.1380) and putative pyruvate dehydrogenase E1,  $\beta$  subunit (LmxM25.1710), which catalyses the oxidation of pyruvate into acetyl-coA. LmxM27.0930, annotated as isovaleryl-coA dehydrogenase, belongs to the acyl-coA dehydrogenase family, which are enzymes involved in fatty acid oxidation. Another protein, LmxM23.0950 was annotated as cytosolic leucyl aminopeptidase, a protein that was localised to the cytosol of *L. amazonensis* promastigotes (Morty & Morehead, 2002). This cytosolic localization suggests that this protein might not be a true A600.1 interacting protein. Among those proteins, only one, the putative ADP, ATP carrier protein 1 mitochondrial precursor, which was identified in one co-immunoprecipitation and one pull-down assay, was also identified in the native gel band.

Overall, the results of the co-IPs and GST pull-down assays did not allow to conclusively determine the true A600.1 interacting proteins, and therefore the pathway in which the A600.1 protein may be involved, as very few proteins were consistently isolated in the different replicates and the proteins identified had unrelated functions. This suggests that many of the proteins identified are likely to be unspecific interacting proteins and that the cell samples used as source of potential interacting proteins contained abundant unspecific cellular proteins that may have impaired the isolation and/or detection of potentially less abundant specific A600.1 interacting proteins.

### 5.3 Discussion

The mitochondrial localization of the *L. mexicana* A600 proteins and the decrease in mitochondrial metabolism observed in *L. mexicana* A600<sup>-/-</sup> amastigotes suggest that the A600 proteins may be involved in a mitochondrial pathway that is essential for amastigotes development. This chapter describes approaches used to try to identify the pathway or potential protein complex in which those proteins may be involved by investigating the potential A600.1 interacting proteins. This was attempted by using a GST pull-down assay approach, in which the A600.1 protein was added to the cell sample, as an exogenous GST fusion protein and in parallel using a co-immunoprecipitation method, in which the endogenous protein is pulled out from the cell sample along with its binding partners, using the anti-A600.1 peptide 2 antibody.

Very few proteins were found to be consistently isolated in the GST pull-downs and the co-IPs. This low consistency and the fact that the proteins identified (or their *T. brucei* orthologs) are known to be involved in separate protein complexes or pathways made it hard to conclude whether they were true A600.1 interacting proteins and whether the A600.1 protein is actually part of a multi-protein complex. One of the isolated proteins, the glycosomal GAPDH, has been identified in all assays, but with a heavy versus light ratio above 1.2 in only three of them. Two isoforms of this enzyme have been identified in *L. mexicana*, one in the cytosol and one in the glycosome, and share 55% sequence identity (Hannaert et al, 1992). The glycosomal enzyme has been characterized as an enzyme of the glycolysis, whereas the function of its cytosolic counterpart remains to be elucidated. However, the glycosomal localization of the GAPDH isoform identified in the present assays makes it an unlikely interacting partner of the A600.1 protein which is localized in the mitochondria. Moreover, the *T. brucei* glycosomal GAPDH has

been classified as a contaminant of TAP tagged complexes due to its regular presence in different and unrelated TAP-tag assays during purification and determination of the composition of various mitochondrial complexes in *T. brucei* (Zikova et al, 2008). This suggests that this protein is likely a non-specific A600.1 interacting protein. Other proteins identified in different assays with a heavy versus light ratio above 1.2 include two proteins of the oxidative phosphorylation pathway, the putative ATPase  $\beta$  subunit (LmxM25.1170; LmxM25.1180) and the putative ADP, ATP carrier protein 1, mitochondrial precursor (LmxM19.9998; LmxM19.0200; LmxM19.9997). Interestingly, three other proteins identified as components of the ATP synthase complex (Complex V) were isolated in one of the GST pull-down assay replicates, along with the ATPase  $\beta$  subunit with a ratio above 1.2, but they were not identified in the other assays, so could not be conclusively considered potential A600.1 interacting proteins. Furthermore, the *T. brucei* ATPase  $\beta$  subunit was also classified among the frequent contaminants of the *T. brucei* TAP-tagged complexes. Other proteins include LmxM18.1380 (putative pyruvate dehydrogenase E1 component  $\alpha$  subunit) and LmxM25.1710 (putative pyruvate dehydrogenase E1  $\beta$  subunit) which belongs to the pyruvate dehydrogenase complex, a multi-enzyme complex that is responsible for the conversion of pyruvate into acetyl-CoA in the mitochondria. Based on those results, it was not possible to determine the pathway or protein complex(es) in which the A600.1 protein may be involved.

The co-IP assay was performed on whole cell lysates rather than mitochondrial fractions due to concerns that the mitochondria isolation procedure may disrupt the potential A600.1-containing complex(es) and/or A600.1 protein-protein interactions. However, the results obtained suggest that the cell samples used as source of potential interacting proteins may

contain abundant non-specific A600.1 interacting proteins, which presence may have hindered the binding and/or detection of potentially less abundant specific A600.1 binding partners. Indeed, when whole cell lysates were used (present and previous experiments) about 45% of the proteins isolated were ribosomal proteins, which are known contaminants of protein-protein interaction assays due to their abundance in the cells. Furthermore, a mitochondria-localized protein such as A600.1 that is synthesized in the cytosol, has to be transported into the mitochondria across the outer and inner membrane, inserted into the mitochondrial inner membrane and potentially integrated into its final complex (Mokranjac & Neupert, 2009; Osman et al, 2007; Schneider et al, 2008; Tzagoloff et al, 2004). This may involve various transient interactions with different protein machineries (import protein complexes, chaperones, scaffolding proteins) that may be identified by pull-down/IP as true interacting proteins and may lead to consider the A600.1 protein as part of a machinery that it may only transiently interact with rather than being a *bona fide* component of. This may explain the identification of the mtHsp70, a component of the mitochondrial inner membrane TIM23 complex, as a common contaminant in TAP-tag experiments in *T. brucei*. The TIM23 complex ensures the translocation and insertion into the inner mitochondrial membrane of mitochondrial precursor proteins and as part of this complex, mtHsp70 binds to the translocating preprotein and releases it into the mitochondrial matrix (Mokranjac & Neupert, 2009). Therefore, due to the sensitivity of the detection of proteins by mass spectrometry, the identification of true A600.1 interacting proteins may require the use of more refined A600.1-enriched cell fractions as source of potential interacting proteins, to reduce the representation of unspecific abundant proteins and increase the proportion of potentially less abundant A600.1 binding partners. As an example, for the identification of *T. brucei* mitochondrial complexes protein composition, the application of a

tandem affinity purification (TAP) approach was applied in which at least three known components of the complex studied were tagged, in combination with co-IP when an antibody against the complex was available (Acestor et al, 2011; Panigrahi et al, 2008a; Zikova et al, 2008; Zikova et al, 2009a). Each TAP-tagged complex was purified by at least two of three complementary methods, which include additional purification steps of the cell fractions or isolated complexes on Percoll or glycerol gradients before final isolation by affinity purification.

For those reasons and the fact that the type of interactions in which the A600.1 protein may be involved in is unknown, in complementation to the co-IP technique, an *in vivo* system, such as a TAP or a BioID approach, might be a more favorable option. In such system, the protein of interest is expressed in the host cells as a fusion protein. In the TAP approach, the protein is fused to two tags, such as Protein A and calmodulin binding protein, which allows a two-step purification process using an IgG affinity column to which the Protein A tag binds, followed by purification on a calmodulin affinity column of the eluate from the IgG affinity column (Rigaut et al, 1999). In the BioID approach, the target protein is expressed as a BirA fusion protein. The BirA tag corresponds to a bacterial protein ligase that biotinylate proteins in the immediate environment of the fusion protein (interacting proteins or in the same complex) and the biotinylated proteins are isolated by using a streptavidin column (Roux et al, 2012). In those two assays, the expression of the tagged protein of interest in the live cells allows it to be processed in the same way as the endogenous protein, such as undergoing post-translational modifications that may be essential for interactions with its binding partners, localizing to the correct cell compartment where it can be integrated into the potential endogenous complex and/or interact with its physiological targets. Such system allows the purification of endogenous, therefore physiological associations of proteins (Berggard et al, 2007). The TAP technique has

been used successfully in the closely related *T. brucei* for identification of the protein subunits of the electron transport chain complexes (Acestor et al, 2011; Zikova et al, 2009a) or in *L. tarentolae* for the purification of the core complex involved in the editing of mitochondrial RNA (Li et al, 2009). The BioID approach has been successfully applied in *L. mexicana* for the identification of proteins interacting with the flagellar targeting domain of the glucose transporter LmxGT1 which led to the identification of a novel protein KHARON1 involved in the localization of this transporter to the flagellar membrane (Tran et al, 2013). In *T. brucei*, it has allowed the identification of the interacting partners and substrates of the *T. brucei* polo-like kinase, TbPLK, which appears to be involved in the development of a new flagella during cell division (McAllaster et al, 2015).

The advantage of an *in vitro* system such as the GST pull-down is that it can be applicable to quantitative proteomics in which a pull-down control can be performed using the GST protein to identify unspecific interactions (interactions with the GST tag or the beads) in parallel to the pull-down with the GST fusion protein and the peptides obtained from both pull-downs can be mixed and analyzed together by mass spectrometry after differential labeling, as was done in the present experiments. However, such system uses an exogenous bait protein in proportions that may be different to the levels of the endogenous protein, which may lead to artificial or non-specific interactions. Also, this system may rely on the ability of the bait protein to interact spontaneously with its potential binding partners, in a non-physiological and more diluted environment than the cellular compartment the endogenous protein localizes to, without the potential assistance of protein chaperones. Such interactions may require the presence of a binding domain or conserved motif either on the A600.1 protein or on the A600.1 binding proteins (Hu et al, 1992; Mayer et al, 1991; Weng et al, 1993). However, no such domain or

motif has been identified in the A600.1 protein sequence. Also, in this non-physiological configuration, the bait protein may interact with a protein(s) that it never normally encounters in the cell (Phizicky & Fields, 1995). All these considerations may explain why the proteins isolated using the GST pull-down assay approach may not be true A600.1 interacting proteins.

It was thought that the presence of the transmembrane domains on the protein bait used in the GST pull-down assay may induce the isolation of unspecific binding proteins via hydrophobic interactions. Also, the fact that re-expression of the N-terminal region only of A600.1 in *A600*<sup>-/-</sup> cells failed to rescue the knock-out growth defect suggests that the C-terminal region of the protein is essential for the protein function. Therefore, the GST pull-down assay was performed using a GST fusion protein lacking the N-terminal region of the A600.1 protein containing the two predicted transmembrane domains. However, it cannot be excluded that some protein-protein interactions may occur through this region and may have been missed using the GST-ΔN.A600.1 as bait.

In conclusion, the detection of the A600.1 protein after hrCN-PAGE separation of the organelle-enriched lysate suggests that it is present in a homo- or hetero-oligomeric complex. The GST pull-down assay and the co-immunoprecipitation conditions used here did not allow to identify the pathway and/or the protein complex in which it is involved in. Therefore, the identification of the potential A600.1 interacting proteins may require the use of more refined A600.1-enriched subcellular fractions and the use of *in vivo* systems that allow the expression of the protein used as bait in its natural environment, hence its processing, subcellular localization and interaction with potential binding partners under normal physiological conditions before lysing the cells for pull-down.

## Chapter 6: Conclusion

### 6.1 Overall analysis and conclusion of the research

The original aim of my thesis was to elucidate the role of a novel family of proteins in the development of the mammalian stage of *L. mexicana*. The successful generation of a specific anti-A600.1 antibody allowed the analysis of the endogenous protein expression profile and its subcellular localization. The A600.1 protein was found to be constitutively expressed in the different stages of the parasite *in vitro* and possibly localizes to the inner membrane of the mitochondria of amastigotes.

Based on this localization, the mitochondrial metabolic activities of the *A600*<sup>-/-</sup> amastigotes were evaluated by comparison to the activities in the *WT* amastigotes. The absence of the A600 proteins was found to result in an impairment of mitochondrial function in amastigotes, that translated into a low cellular ATP content, a low mitochondrial redox activity and a decrease in the mitochondrial membrane potential  $\Delta\Psi_m$ . Furthermore, analysis of the OXPHOS complexes activities revealed a decrease in the activity of Complexes III and IV and in the dimerisation of Complex V. Complex I appeared to be inactive in amastigotes, indicating that the mitochondrial membrane potential is essentially maintained by the activity of Complexes III and IV.

Analysis of mitochondria-enriched organellar fraction by hrCN-PAGE suggests that the protein is part of a multi-protein complex and a GST pull-down assay and a co-immunoprecipitation approach were used to isolate potential A600.1 binding partners. Significant variations were obtained between replicates and, along with the pull-down of abundant likely unspecific proteins did not allow to determine whether A600.1 is associated to

other proteins or form oligomers and the mitochondrial process in which it may be involved in. My results however show that the co-immunoprecipitation technique applied using our anti-A600.1 antibody can successfully be employed to immunoprecipitate the endogenous protein, and should allow the isolation of any potential binding proteins. However, A600.1-enriched cell fractions are required as source of interacting proteins to minimize the interference of abundant contaminant proteins and increase the representation of potentially less abundant A600.1 binding partners.

Overall, the results generated during my research suggest that the A600 proteins are involved in a mitochondrial process that is essential for the development of the mammalian stage of *Leishmania*. Therefore, I propose that the A600 proteins are involved in a mechanism aimed at optimizing the OXPHOS pathway activity in amastigotes. Indeed, in amastigotes, the TCA cycle flux is decreased due to the depletion of its intermediates that are diverted towards other biosynthesis pathways (Saunders et al, 2014). To maintain their mitochondrial membrane potential, crucial to various mitochondrial activities, and the production of ATP via Complex V, amastigotes may compensate for the subsequent decrease in the flux of electrons towards the electron transport chain by potentiating the activities of its OXPHOS complexes III and IV, the latter having been found to be upregulated in amastigotes (Dey et al, 2010). The A600 proteins may fulfill their role either as part of a complex or via interaction with other proteins to maintain the mitochondrial inner membrane architecture or by mediating interaction between Complexes III and IV, as summarized in Figure 6.1.

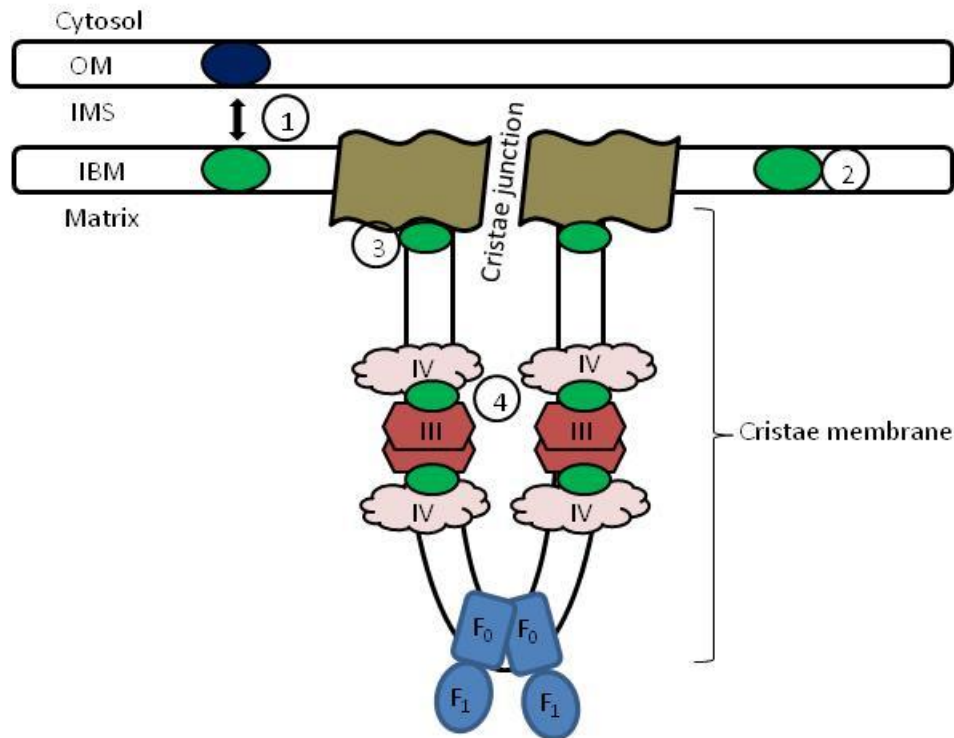


**Figure 6.1: Schematic summarizing the possible functions of A600.1.**

It is proposed that the A600.1 protein (represented in green) may be involved in the mitochondrial inner membrane structure, which is organized in invaginations called cristae that are separated by cristae junctions from the inner boundary membrane (IBM), which juxtaposes the mitochondrial outer membrane (OM). This role could be fulfilled (1) by interaction of the homo- or hetero-oligomeric A600.1-containing complex with an outer mitochondrial membrane protein complex or (2) with the inner membrane phospholipids such as cardiolipin which is essential to the mitochondrial membranes organization and function (Ren et al, 2014) or (3) by interaction with or as part of a MICOS-like complex (the MICOS complex was found to be essential to the formation of cristae junctions in eukaryotes but remains to be identified in trypanosomatids). A600.1 may also be involved in mediating the interaction between Complexes III and IV (4). IMS: inter membrane space; III: Complex III; IV: Complex IV; F<sub>0</sub>: Complex V membrane domain embedded in the mitochondrial inner membrane and which contains the proton channel; F<sub>1</sub>: Complex V hydrophilic domain which contains the catalytic sites and extends into the mitochondrial matrix. This figure was modeled on the schematic representation of the architecture of the mitochondrial inner membrane in (van der Laan et al, 2016).

## 6.2 Contribution to the field

My research identified a novel *Leishmania* mitochondrial protein which presence was previously found to be essential for amastigotes proliferation, and showed that this protein is involved in the optimization of the mitochondrial OXPHOS pathway at the amastigote stage. The

A600 genes are part of the 910 *Leishmania* protein-coding genes (out of a total of around 8,000) that have no orthologs in the two other most studied and closely related trypanosomatids, *T. brucei* and *T. cruzi* (Ivens et al, 2005). This suggests that the A600 proteins may be part of a pathway or complex that is unique to *Leishmania*, a characteristic that could be harnessed in the search for novel therapies against leishmaniasis with low risk of interaction with the host proteins. Furthermore, my research adds to the growing evidence on the dependence of the disease-causing form of *Leishmania* on an increase in the mitochondrial function for survival (Cardenas et al, 2015; Dey et al, 2010; Mitra et al, 2016; Saunders et al, 2014; Uboldi et al, 2006).

Furthermore, most studies published on the characterization of the electron transport chain in *Leishmania* have been realized with promastigotes (Bermúdez et al, 1997; Chen et al, 2001; Horváth et al, 2000; Maslov et al, 1999; Maslov et al, 2002; Nebohacova et al, 2009; Santhamma & Bhaduri, 1995; Verner et al, 2014). They all conclude on the presence of Complexes II, III, IV and V, while the presence of an active Complex I remains debatable. Since the genes encoding Complex I subunits were identified in *L. major* genome, it was suggested that this complex may be active at the amastigote stage (Berriman et al, 2005; Duarte & Tomas, 2014). However, studies on the presence and/or activity of those complexes in amastigotes are scarcer and little is known regarding the composition of their electron transport chain. While deletions of Complex IV subunits were found to affect *L. major* and *L. donovani* amastigotes survival or virulence, suggesting the importance of this complex in amastigotes (Dey et al, 2010; Uboldi et al, 2006), one study concluded on the absence of Complexes I, II and IV in *L. donovani* amastigotes (Chakraborty et al, 2010). Another study from the same group concluded on an absence of function of Complexes II and V but the presence of Complexes I and III

activities in amastigotes (Mondal et al, 2014). My research found that the *L. mexicana* amastigotes OXPHOS pathway contains active Complexes II, III, IV and V, while Complex I appears to be inactive, similarly to what was showed in *L. tarentolae* promastigotes (Verner et al, 2014).

### **6.3 Strengths and limitations of the research**

#### ***Strengths:***

Contrary to some *Leishmania* species such as *L. major*, *L. mexicana* is easily amenable to differentiation into axenic amastigotes *in vitro* from SP promastigotes. This allows the direct study of the biology of the disease-causing form of the parasite in culture, without the need to infect macrophages or animals to obtain amastigotes.

The generation of an anti-A600.1 antibody with specificity for the *L. mexicana* endogenous protein greatly helped our research into the characterization of the protein: it allowed the characterization of the protein expression profile during the parasite life cycle and the determination of its subcellular localization and to follow its distribution after cell lysis.

#### ***Limitations:***

My research on the characterization of the A600.4 protein, which gene expression led to the identification of the *A600* gene family and suggests that it may be upregulated at the amastigote stage, was hampered by a lack of specificity of the antibody for the endogenous protein. The endogenous protein expression profile and its subcellular localization could not be confirmed.

In the absence of putative A600.1 or A600.4 proteins homologs in other organisms and of known functional or conservative domains in their predicted amino acid sequences, the function

of the A600 proteins or the pathway in which they may be involved in could not be postulated upon at the beginning of this research. In addition, there is limited knowledge about *Leishmania* amastigotes biology. The phenotype of the *A600*<sup>-/-</sup> amastigotes suggested that the A600 proteins are likely to be involved in a process that is unique or upregulated in amastigotes in comparison to promastigotes. However, most studies on *Leishmania* are realized with promastigotes and the mechanisms that are activated in amastigotes are often unknown or speculated upon, based on observations made in promastigotes. Therefore, after determining the subcellular localization of the A600.1 protein in the mitochondria, it was not possible to focus my investigation on specific mitochondrial activities or pathways, among the different mitochondrial pathways known to exist in higher eukaryotes, but that often remain to be characterized in *Leishmania* amastigotes.

## **6.4 Possible future directions**

### **6.4.1 Identification of the A600-associated mitochondrial pathway**

To further characterize the mitochondrial pathway and/or protein complex in which the A600 proteins may be involved in amastigotes and to investigate whether other pathways than the OXPHOS system may be affected by their absence, an *in organello* ATP generation assay using mitochondria-enriched fractions may be employed, as described elsewhere (Schneider et al, 2007). My work showed that the ATP levels are decreased in *A600*<sup>-/-</sup> amastigotes. As described in my introduction, there are three sites of ATP production in the mitochondria of trypanosomatids, which are associated to three major mitochondrial pathways: Type I ATP synthesis by the F<sub>1</sub>F<sub>0</sub> ATP synthase (Complex V) is linked to the activity of the electron transport chain; Type II synthesis by the succinyl CoA synthetase is linked to the TCA cycle and Type III synthesis in the ASCT cycle is linked to the generation of acetyl-CoA from pyruvate,

the end product of glycolysis or from the  $\beta$ -oxidation of fatty acids. Each of these ATP generation sites can be assayed separately by addition of specific substrates and inhibitors to the mitochondria-enriched fractions. The production of ATP in response to specific substrates allows to assess the functionality of the associated pathway (electron transport chain, TCA cycle or production of acetyl-CoA). Investigating the functionality of those pathways would allow to verify whether mitochondrial pathways other than the OXPHOS pathway is affected by the absence of the A600 proteins, thus narrowing down the list of potential pathways in which the A600 proteins may be involved in.

This could also be achieved by identification of the potential A600.1 interacting proteins. A TAP (Tandem Affinity Purification)-tag approach in parallel to the co-immunoprecipitation technique using the anti-A600.1 antibody 2 should be employed with A600.1-enriched fractions to isolate and identify potential A600.1 interacting proteins.

#### **6.4.2 Characterization of the A600.4 protein function**

The *A600* gene family was discovered because of the amastigote-preferential expression of the *A600.4* gene. This expression profile in addition to the phenotype of the *A600*<sup>-/-</sup> amastigotes makes the A600.4 protein an interesting target to understand the parasite survival and development in the mammalian stage and to investigate novel avenues for therapies development. The study of the protein in my research was hampered by the lack of specificity of the anti-A600.4 antibody for the endogenous protein. To characterize this protein, *A600.4*<sup>-/-</sup> mutants should be generated and their phenotype compared to *A600*<sup>-/-</sup> cells.

In absence of a specific anti-A600.4 antibody, a Tandem Affinity Purification (TAP) approach can be used to determine the subcellular localization of A600.4 fusion protein in

amastigotes, via immunofluorescence and subcellular fractionation. The technique can also be used to isolate and identify potential A600.4 binding partners.

### **6.4.3 Analysis and comparison of the subunit composition of the OXPHOS complexes of *Leishmania* amastigotes and promastigotes**

To help fill the gap in knowledge regarding the energy metabolism in amastigotes and the functionality of the electron transport chain, the subunit composition of the OXPHOS complexes should be investigated and compared in both promastigotes and amastigotes. This can be achieved by Native PAGE separation of the mitochondrial complexes and analysis of the corresponding bands by mass spectrometry. In parallel, a TAP approach and immunoprecipitation can be employed to isolate each complex and identify their components by mass spectrometry. Deletion mutants of potential stage-specific components of each complex can then be generated to determine their importance in the parasite development. A similar endeavor has been successfully conducted in *T. brucei* procyclic form and data from this study can be used and compared to identify *Leishmania* orthologs (Acestor et al, 2011; Panigrahi et al, 2008b; Subrtova et al, 2015; Zikova et al, 2008; Zikova et al, 2009a). Complexes III and IV composition have also been elucidated in *L. tarentolae* promastigotes after isolation of the respective complexes by chromatography and separation of the respiratory complexes by Blue Native/Tris-tricine-SDS two-dimensional PAGE (Horváth et al, 2000).

Dey *et al.* identified in *L. donovani* a Complex IV subunit that is specific to amastigotes and metacyclics and may contribute to the increase of Complex IV activity in the amastigote stage and to the survival of the parasite *in vivo* (Dey et al, 2010). This suggests that the OXPHOS complexes of the different life stages of *Leishmania* may contain additional accessory subunits that may play a role in the parasite adaptation to different environments. Therefore, identification

of differences in the OXPHOS complexes subunit composition between the two stages and their importance in the parasite survival may provide further understanding of the mechanisms put in place by the parasite to adapt and survive in different environments. In addition, this could also lead to the identification of novel targets for drug therapies and deletion mutants that are associated with attenuation in the virulence of the parasite *in vivo* may be evaluated for their potential as vaccines against leishmaniasis.

## References

- Aagaard-Hansen J, Nombela N, Alvar J (2010) Population movement: a key factor in the epidemiology of neglected tropical diseases. *Tropical Medicine & International Health* **15**: 1281-1288
- Abu-Amero KK, Bosley TM (2005) Detection of mitochondrial respiratory dysfunction in circulating lymphocytes using resazurin. *Archives of Pathology & Laboratory Medicine* **129**: 1295-1298
- Acestor N, Panigrahi AK, Ogata Y, Anupama A, Stuart KD (2009) Protein composition of *Trypanosoma brucei* mitochondrial membranes. *Proteomics* **9**: 5497-5508
- Acestor N, Zikova A, Dalley RA, Anupama A, Panigrahi AK, Stuart KD (2011) *Trypanosoma brucei* mitochondrial respiratome: composition and organization in procyclic form. *Molecular & cellular proteomics : MCP* **10**: M110 006908
- Akerman M, Shaked-Mishan P, Mazareb S, Volpin H, Zilberstein D (2004) Novel motifs in amino acid permease genes from *Leishmania*. *Biochemical and biophysical research communications* **325**: 353-366
- Akopyants NS, Matlib RS, Bukanova EN, Smeds MR, Brownstein BH, Stormo GD, Beverley SM (2004) Expression profiling using random genomic DNA microarrays identifies differentially expressed genes associated with three major developmental stages of the protozoan parasite *Leishmania major*. *Molecular and biochemical parasitology* **136**: 71-86
- Alberola J, Rodríguez A, Francino O, Roura X, Rivas L, Andreu D (2004) Safety and efficacy of antimicrobial peptides against naturally acquired leishmaniasis. *Antimicrobial Agents and Chemotherapy* **48**: 641-643
- Alberts B, Johnson A, Lewis J, Raff M, Roberts K, Walter P (2002) The Mitochondrion. In *Molecular Biology of the Cell*, Fourth edn, pp 769-781. New York: Garland Science
- Ali V, Nozaki T (2013) Iron–sulphur clusters, their biosynthesis, and biological functions in protozoan parasites. In *Advances in Parasitology*, Rollinson D (ed), Vol. 83, pp 1-92. Academic Press
- Alvar J, Vélez ID, Bern C, Herrero M, Desjeux P, Cano J, Jannin J, den Boer M, the WHO control team (2012) Leishmaniasis worldwide and global estimates of its incidence. *PloS one* **7**: e35671
- Anand R, Strecker V, Urbach J, Wittig I, Reichert AS (2016) Mic13 is essential for formation of crista junctions in mammalian cells. *PloS one* **11**: e0160258

Arnold I, Pfeiffer K, Neupert W, Stuart RA, Schägger H (1998) Yeast mitochondrial F1F0-ATP synthase exists as a dimer: identification of three dimer-specific subunits. *The EMBO journal* **17**: 7170-7178

Bangs JD, Uyetake L, Brickman MJ, Balber AE, Boothroyd JC (1993) Molecular cloning and cellular localization of a BiP homologue in *Trypanosoma brucei*. Divergent ER retention signals in a lower eukaryote. *Journal of Cell Science* **105**: 1101-1113

Bates PA (1994) Complete developmental cycle of *Leishmania mexicana* in axenic culture. *Parasitology* **108** ( Pt 1): 1-9

Bates PA, Robertson CD, Tetley L, Coombs GH (1992) Axenic cultivation and characterization of *Leishmania mexicana* amastigote-like forms. *Parasitology* **105** ( Pt 2): 193-202

Bates PA, Tetley L (1993) *Leishmania mexicana*: induction of metacyclogenesis by cultivation of promastigotes at acidic pH. *Experimental parasitology* **76**: 412-423

Bellatin JA, Murray AS, Zhao M, McMaster WR (2002) *Leishmania mexicana*: identification of genes that are preferentially expressed in amastigotes. *Experimental parasitology* **100**: 44-53

Benaim G, Bermudez R, Urbina JA (1990) Ca<sup>2+</sup> transport in isolated mitochondrial vesicles from *Leishmania braziliensis* promastigotes. *Molecular and biochemical parasitology* **39**: 61-68

Beneke T, Madden R, Makin L, Valli J, Sunter J, Gluenz E (2017) A CRISPR Cas9 high-throughput genome editing toolkit for kinetoplastids. *Royal Society Open Science* **4**: 170095

Bente M, Harder S, Wiesgigl M, Heukeshoven J, Gelhaus C, Krause E, Clos J, Bruchhaus I (2003) Developmentally induced changes of the proteome in the protozoan parasite *Leishmania donovani*. *Proteomics* **3**: 1811-1829

Berggard T, Linse S, James P (2007) Methods for the detection and analysis of protein-protein interactions. *Proteomics* **7**: 2833-2842

Berman JD (1997) Human leishmaniasis: clinical, diagnostic and chemotherapeutic developments in the last 10 years. *Clinical infectious diseases* **24**: 684-703

Bermúdez R, Dagger F, D'Aquino JA, Benaim G, Dawidowicz K (1997) Characterization of mitochondrial electron-transfer in *Leishmania mexicana*. *Molecular and biochemical parasitology* **90**: 43-54

Berriman M, Ghedin E, Hertz-Fowler C, Blandin G, Renauld H, Bartholomeu DC, Lennard NJ, Caler E, Hamlin NE, Haas B, Böhme U, Hannick L, Aslett MA, Shallom J, Marcello L, Hou L, Wickstead B, Alsmark UCM, Arrowsmith C, Atkin RJ, Barron AJ, Bringaud F, Brooks K, Carrington M, Cherevach I, Chillingworth T-J, Churcher C, Clark LN, Corton CH, Cronin A,

Davies RM, Doggett J, Djikeng A, Feldblyum T, Field MC, Fraser A, Goodhead I, Hance Z, Harper D, Harris BR, Hauser H, Hostetler J, Ivens A, Jagels K, Johnson D, Johnson J, Jones K, Kerhornou AX, Koo H, Larke N, Landfear S, Larkin C, Leech V, Line A, Lord A, MacLeod A, Mooney PJ, Moule S, Martin DMA, Morgan GW, Mungall K, Norbertczak H, Ormond D, Pai G, Peacock CS, Peterson J, Quail MA, Rabbinowitsch E, Rajandream M-A, Reitter C, Salzberg SL, Sanders M, Schobel S, Sharp S, Simmonds M, Simpson AJ, Tallon L, Turner CMR, Tait A, Tivey AR, Van Aken S, Walker D, Wanless D, Wang S, White B, White O, Whitehead S, Woodward J, Wortman J, Adams MD, Embley TM, Gull K, Ullu E, Barry JD, Fairlamb AH, Opperdoes F, Barrell BG, Donelson JE, Hall N, Fraser CM, Melville SE, El-Sayed NM (2005) The genome of the African trypanosome *Trypanosoma brucei*. *Science* **309**: 416-422

Bochud-Allemann N, Schneider A (2002) Mitochondrial substrate level phosphorylation is essential for growth of procyclic *Trypanosoma brucei*. *The Journal of biological chemistry* **277**: 32849-32854

Bornhövd C, Vogel F, Neupert W, Reichert AS (2006) Mitochondrial membrane potential is dependent on the oligomeric state of F1F0-ATP synthase supracomplexes. *Journal of biological chemistry* **281**: 13990-13998

Bringaud F, Ghedin E, El-Sayed NM, Papadopoulou B (2008) Role of transposable elements in trypanosomatids. *Microbes and infection* **10**: 575-581

Bringaud F, Muller M, Cerqueira GC, Smith M, Rochette A, El-Sayed NM, Papadopoulou B, Ghedin E (2007) Members of a large retroposon family are determinants of post-transcriptional gene expression in *Leishmania*. *PLoS pathogens* **3**: 1291-1307

Bringaud F, Rivière L, Coustou V (2006) Energy metabolism of trypanosomatids: Adaptation to available carbon sources. *Molecular and biochemical parasitology* **149**: 1-9

Brooks DR, Denise H, Westrop GD, Coombs GH, Mottram JC (2001) The stage-regulated expression of *Leishmania mexicana* CPB cysteine proteases is mediated by an intercistronic sequence element. *Journal of biological chemistry* **276**: 47061-47069

Bulet P, Stöcklin R, Menin L (2004) Anti-microbial peptides: from invertebrates to vertebrates. *immunological reviews* **198**: 169-184

Burchmore RJS, Rodriguez-Contreras D, McBride K, Barrett MP, Modi G, Sacks D, Landfear SM (2003) Genetic characterization of glucose transporter function in *Leishmania mexicana*. *Proceedings of the national academy of sciences* **100**: 3901-3906

Candiano G, Bruschi M, Musante L, Santucci L, Ghiggeri GM, Carnemolla B, Orecchia P, Zardi L, Righetti PG (2004) Blue silver: a very sensitive colloidal Coomassie G-250 staining for proteome analysis. *Electrophoresis* **25**: 1327-1333

- Cardenas D, Carter PM, Nation CS, Pizarro JC, Guidry J, Aiyar A, Kelly BL (2015) LACK, a RACK1 ortholog, facilitates cytochrome c oxidase subunit expression to promote *Leishmania major* fitness. *Molecular Microbiology* **96**: 95-109
- Chakraborty B, Biswas S, Mondal S, Bera T (2010) Stage specific developmental changes in the mitochondrial and surface membrane associated redox systems of *Leishmania donovani* promastigote and amastigote. *Biochemistry Biokhimiia* **75**: 494-518
- Chan QWT, Howes CG, Foster LJ (2006) Quantitative comparison of caste differences in honeybee hemolymph. *Molecular & cellular proteomics* **5**: 2252-2262
- Charest H, Matlashewski G (1994) Developmental gene expression in *Leishmania donovani*: differential cloning and analysis of an amastigote-stage-specific gene. *Molecular and cellular biology* **14**: 2975-2984
- Chen M, Bennedsen M, Zhai L, Kharazmi A (2001) Purification and enzymatic activity of an NADH-fumarate reductase and other mitochondrial activities of *Leishmania parasites*. *APMIS : acta pathologica, microbiologica, et immunologica Scandinavica* **109**: 801-808
- Cherkasov A, Hsing M, Zoraghi R, Foster LJ, See RH, Stoyanov N, Jiang J, Kaur S, Lian T, Jackson L, Gong H, Swayze R, Amandoron E, Hormozdiari F, Dao P, Sahinalp C, Santos-Filho O, Axerio-Cilies P, Byler K, McMaster WR, Brunham RC, Finlay BB, Reiner NE (2011) Mapping the protein interaction network in methicillin-resistant *Staphylococcus aureus*. *Journal of proteome research* **10**: 1139-1150
- Cohen-Freue G, Holzer TR, Forney JD, McMaster WR (2007) Global gene expression in *Leishmania*. *International journal for parasitology* **37**: 1077-1086
- Croft SL, Olliaro P (2011) Leishmaniasis chemotherapy - challenges and opportunities. *Clinical microbiology and infection* **17**: 1478-1483
- Cruz A, Coburn CM, Beverley SM (1991) Double targeted gene replacement for creating null mutants. *Proceedings of the National Academy of Sciences of the United States of America* **88**: 7170-7174
- Dabirian S, Taslimi Y, Zahedifard F, Gholami E, Doustdari F, Motamedirad M, Khatami S, Azadmanesh K, Nysten S, Rafati S (2013) Human Neutrophil Peptide-1 (HNP-1): a new anti-leishmanial drug candidate. *PLoS neglected tropical diseases* **7**: e2491
- de Menezes JPB, Sampaio Guedes CE, de Oliveira Almeida Petersen AL, Bittencourt Mothé Fraga D, Sampaio Tavares Veras P (2015) Advances in development of new treatment for leishmaniasis. *BioMed Research International* **2015**: 11

De Pablos LM, Ferreira TR, Walrad PB (2016) Developmental differentiation in *Leishmania* lifecycle progression: post-transcriptional control conducts the orchestra. *Current opinion in microbiology* **34**: 82-89

Debrabant A, Joshi MB, Pimenta PF, Dwyer DM (2004) Generation of *Leishmania donovani* axenic amastigotes: their growth and biological characteristics. *International journal for parasitology* **34**: 205-217

Desjeux P (2004) Leishmaniasis: current situation and new perspectives. *Comparative immunology, microbiology and infectious diseases* **27**: 305-318

Dey R, Meneses C, Salotra P, Kamhawi S, Nakhasi HL, Duncan R (2010) Characterization of a *Leishmania* stage-specific mitochondrial membrane protein that enhances the activity of cytochrome c oxidase and its role in virulence. *Molecular microbiology* **77**: 399-414

Dillon LAL, Suresh R, Okrah K, Corrada Bravo H, Mosser DM, El-Sayed NM (2015) Simultaneous transcriptional profiling of *Leishmania major* and its murine macrophage host cell reveals insights into host-pathogen interactions. *BMC genomics* **16**: 1108

Ding C, Wu Z, Huang L, Wang Y, Xue J, Chen S, Deng Z, Wang L, Song Z, Chen S (2015) Mitofilin and CHCHD6 physically interact with Sam50 to sustain cristae structure. *Scientific Reports* **5**: 16064

do Nascimento Viviane V, Mello Éde O, Carvalho Laís P, de Melo Edésio JT, Carvalho Ade O, Fernandes Katia VS, Gomes Valdirene M (2015) PvD1 defensin, a plant antimicrobial peptide with inhibitory activity against *Leishmania amazonensis*. *Bioscience Reports* **35**

Docampo R, Vercesi AE, Huang G (2014) Mitochondrial calcium transport in trypanosomes. *Molecular and biochemical parasitology* **196**: 108-116

Doudna JA, Charpentier E (2014) The new frontier of genome engineering with CRISPR-Cas9. *Science* **346**

Duarte M, Tomas AM (2014) The mitochondrial complex I of trypanosomatids--an overview of current knowledge. *Journal of bioenergetics and biomembranes* **46**: 299-311

Eichenberger C (2018) Characterization of a putative MICOS complex in *Trypanosoma brucei*. In *35th Annual Swiss Trypanosomatid Meeting*, p 3. Leysin, Switzerland

El-Sayed NM, Myler PJ, Bartholomeu DC, Nilsson D, Aggarwal G, Tran A-N, Ghedin E, Worthey EA, Delcher AL, Blandin G, Westenberger SJ, Caler E, Cerqueira GC, Branche C, Haas B, Anupama A, Arner E, Åslund L, Attipoe P, Bontempi E, Bringaud F, Burton P, Cadag E, Campbell DA, Carrington M, Crabtree J, Darban H, da Silveira JF, de Jong P, Edwards K, Englund PT, Fazelina G, Feldblyum T, Ferella M, Frasch AC, Gull K, Horn D, Hou L, Huang Y, Kindlund E, Klingbeil M, Kluge S, Koo H, Lacerda D, Levin MJ, Lorenzi H, Louie T, Machado

CR, McCulloch R, McKenna A, Mizuno Y, Mottram JC, Nelson S, Ochaya S, Osoegawa K, Pai G, Parsons M, Pentony M, Pettersson U, Pop M, Ramirez JL, Rinta J, Robertson L, Salzberg SL, Sanchez DO, Seyler A, Sharma R, Shetty J, Simpson AJ, Sisk E, Tammi MT, Tarleton R, Teixeira S, Van Aken S, Vogt C, Ward PN, Wickstead B, Wortman J, White O, Fraser CM, Stuart KD, Andersson B (2005) The genome sequence of *Trypanosoma cruzi*, etiologic agent of Chagas disease. *Science* **309**: 409-415

El Fakhry Y, Ouellette M, Papadopoulou B (2002) A proteomic approach to identify developmentally regulated proteins in *Leishmania infantum*. *Proteomics* **2**: 1007-1017

Fernandes AP, Canavaci AM, McCall LI, Matlashewski G (2014) A2 and other visceralizing proteins of *Leishmania*: role in pathogenesis and application for vaccine development. *Subcellular biochemistry* **74**: 77-101

Fernandes MC, Dillon LAL, Belew AT, Bravo HC, Mosser DM, El-Sayed NM (2016) Dual transcriptome profiling of *Leishmania*-infected human macrophages reveals distinct reprogramming signatures. *mBio* **7**

Fiebig M, Kelly S, Gluenz E (2015) Comparative life cycle transcriptomics revises *Leishmania mexicana* genome annotation and links a chromosome duplication with parasitism of Vertebrates. *PLoS pathogens* **11**: e1005186

Flegontov P, Butenko A, Firsov S, Kraeva N, Eliáš M, Field MC, Filatov D, Flegontova O, Gerasimov ES, Hlaváčová J, Ishemgulova A, Jackson AP, Kelly S, Kostygov AY, Logacheva MD, Maslov DA, Oppendoes FR, O'Reilly A, Sádlová J, Ševčíková T, Venkatesh D, Vlček Č, Volf P, Jan V, Záhonová K, Yurchenko V, Lukeš J (2016) Genome of *Leptomonas pyrrhocoris*: a high-quality reference for monoxenous trypanosomatids and new insights into evolution of *Leishmania*. *Scientific reports* **6**: 23704

Foucher AL, Papadopoulou B, Ouellette M (2006) Prefractionation by digitonin extraction increases representation of the cytosolic and intracellular proteome of *Leishmania infantum*. *Journal of proteome research* **5**: 1741-1750

Friedman JR, Mourier A, Yamada J, McCaffery JM, Nunnari J (2015) MICOS coordinates with respiratory complexes and lipids to establish mitochondrial inner membrane architecture. *eLife* **4**: e07739

Gallis HA, Richard HD, William WP (1990) Amphotericin B: 30 years of clinical experience. *Reviews of Infectious Diseases* **12**: 308-329

Gannavaram S, Vedvyas C, Debrabant A (2008) Conservation of the pro-apoptotic nuclease activity of endonuclease G in unicellular trypanosomatid parasites. *Journal of cell science* **121**: 99-109

- Gasser SM, Daum G, Schatz G (1982) Import of proteins into mitochondria. Energy-dependent uptake of precursors by isolated mitochondria. *Journal of biological chemistry* **257**: 13034-13041
- Gavin A-C, Aloy P, Grandi P, Krause R, Boesche M, Marzioch M, Rau C, Jensen LJ, Bastuck S, Dümpelfeld B, Edlmann A, Heurtier M-A, Hoffman V, Hoefert C, Klein K, Hudak M, Michon A-M, Schelder M, Schirle M, Remor M, Rudi T, Hooper S, Bauer A, Bouwmeester T, Casari G, Drewes G, Neubauer G, Rick JM, Kuster B, Bork P, Russell RB, Superti-Furga G (2006) Proteome survey reveals modularity of the yeast cell machinery. *Nature* **440**: 631
- Geraldo MV, Silber AM, Pereira CA, Uliana SRB (2005) Characterisation of a developmentally regulated amino acid transporter gene from *Leishmania amazonensis*. *FEMS Microbiology letters* **242**: 275-280
- Gillespie PM, Beaumier CM, Strych U, Hayward T, Hotez PJ, Bottazzi ME (2016) Status of vaccine research and development of vaccines for leishmaniasis. *Vaccine* **34**: 2992-2995
- Gnipova A, Panicucci B, Paris Z, Verner Z, Horvath A, Lukes J, Zikova A (2012) Disparate phenotypic effects from the knockdown of various *Trypanosoma brucei* cytochrome c oxidase subunits. *Molecular and biochemical parasitology* **184**: 90-98
- Gnipova A, Subrtova K, Panicucci B, Horvath A, Lukes J, Zikova A (2015) The ADP/ATP carrier and its relationship to oxidative phosphorylation in ancestral protist *Trypanosoma brucei*. *Eukaryotic cell* **14**: 297-310
- González-Aseguinolaza G, Almazán F, Rodríguez JF, Marquet A, Larraga V (1997) Cloning of the gp63 surface protease of *Leishmania infantum*: Differential post-translational modifications correlated with different infective forms1. *Biochimica et biophysica acta (BBA) - molecular basis of disease* **1361**: 92-102
- Gossage SM, Rogers ME, Bates PA (2003) Two separate growth phases during the development of *Leishmania* in sand flies: implications for understanding the life cycle. *International journal for parasitology* **33**: 1027-1034
- Gottlieb E, Armour SM, Harris MH, Thompson CB (2003) Mitochondrial membrane potential regulates matrix configuration and cytochrome c release during apoptosis. *Cell death and differentiation* **10**: 709-717
- Guerra DG, Decottignies A, Bakker BM, Michels PAM (2006) The mitochondrial FAD-dependent glycerol-3-phosphate dehydrogenase of Trypanosomatidae and the glycosomal redox balance of insect stages of *Trypanosoma brucei* and *Leishmania spp.* *Molecular and biochemical parasitology* **149**: 155-169
- Gunter KK, Gunter TE (1994) Transport of calcium by mitochondria. *Journal of bioenergetics and biomembranes* **26**: 471-485

Gupta N, Goyal N, Kumar R, Agrawal AK, Seth PK, Rastogi AK (1996) Membrane characterization of amastigote-like forms of *Leishmania donovani*. *Tropical medicine & international health : TM & IH* **1**: 495-502

Haanstra JR, González-Marcano EB, Gualdrón-López M, Michels PAM (2016) Biogenesis, maintenance and dynamics of glycosomes in trypanosomatid parasites. *Biochimica et Biophysica Acta (BBA) - Molecular Cell Research* **1863**: 1038-1048

Haile S, Papadopoulou B (2007) Developmental regulation of gene expression in trypanosomatid parasitic protozoa. *Current opinion in microbiology* **10**: 569-577

Hancock REW, Sahl H-G (2006) Antimicrobial and host-defense peptides as new anti-infective therapeutic strategies. *Nature biotechnology* **24**: 1551-1557

Handler MZ, Patel PA, Kapila R, Al-Qubati Y, Schwartz RA (2015) Cutaneous and mucocutaneous leishmaniasis: Clinical perspectives. *Journal of the American Academy of Dermatology* **73**: 897-908; quiz 909-810

Handman E, Bullen DVR (2002) Interaction of *Leishmania* with the host macrophage. *Trends in parasitology* **18**: 332-334

Hannaert V, Albert MA, Rigden DJ, da Silva Giotto MT, Thiemann O, Garratt RC, Van Roy J, Opperdoes FR, Michels PA (2003) Kinetic characterization, structure modelling studies and crystallization of *Trypanosoma brucei* enolase. *European journal of biochemistry / FEBS* **270**: 3205-3213

Hannaert V, Blaauw M, Kohl L, Allert S, Opperdoes FR, Michels PA (1992) Molecular analysis of the cytosolic and glycosomal glyceraldehyde-3-phosphate dehydrogenase in *Leishmania mexicana*. *Molecular and biochemical parasitology* **55**: 115-126

Harper S, Speicher DW (2011) Purification of proteins fused to glutathione S-transferase. *Methods in molecular biology* **681**: 259-280

Hart DT, Coombs GH (1982) *Leishmania mexicana*: Energy metabolism of amastigotes and promastigotes. *Experimental parasitology* **54**: 397-409

Hauser R, Pypaert M, Hausler T, Horn EK, Schneider A (1996) In vitro import of proteins into mitochondria of *Trypanosoma brucei* and *Leishmania tarentolae*. *Journal of cell science* **109**: 517-523

Holzer TR, McMaster WR, Forney JD (2006) Expression profiling by whole-genome interspecies microarray hybridization reveals differential gene expression in procyclic promastigotes, lesion-derived amastigotes, and axenic amastigotes in *Leishmania mexicana*. *Molecular and biochemical parasitology* **146**: 198-218

Horváth A, Berry EA, Huang L-s, Maslov DA (2000) *Leishmania tarentolae*: A parallel isolation of cytochrome bc1 and cytochrome c oxidase. *Experimental parasitology* **96**: 160-167

Horváth A, Horáková E, Dunajčíková P, Verner Z, Pravdová E, Šlapetová I, Cuninková Lu, Lukeš J (2005) Downregulation of the nuclear-encoded subunits of the complexes III and IV disrupts their respective complexes but not complex I in procyclic *Trypanosoma brucei*. *Molecular microbiology* **58**: 116-130

Hotez PJ, Molyneux DH, Fenwick A, Ottesen E, Ehrlich Sachs S, Sachs JD (2006) Incorporating a rapid-impact package for neglected tropical diseases with programs for HIV/AIDS, tuberculosis, and malaria. *PLOS medicine* **3**: e102

Hu P, Margolis B, Skolnik EY, Lammers R, Ullrich A, Schlessinger J (1992) Interaction of phosphatidylinositol 3-kinase-associated p85 with epidermal growth factor and platelet-derived growth factor receptors. *Molecular and cellular biology* **12**: 981-990

Inbar E, Canepa GE, Carrillo C, Glaser F, Suter Grotemeyer M, Rentsch D, Zilberstein D, Pereira CA (2012) Lysine transporters in human trypanosomatid pathogens. *Amino acids* **42**: 347-360

Ivens AC, Peacock CS, Worthey EA, Murphy L, Aggarwal G, Berriman M, Sisk E, Rajandream M-A, Adlem E, Aert R, Anupama A, Apostolou Z, Attipoe P, Bason N, Bauser C, Beck A, Beverley SM, Bianchetin G, Borzym K, Bothe G, Bruschi CV, Collins M, Cadag E, Ciarloni L, Clayton C, Coulson RMR, Cronin A, Cruz AK, Davies RM, De Gaudenzi J, Dobson DE, Duesterhoeft A, Fazelina G, Fosker N, Frasch AC, Fraser A, Fuchs M, Gabel C, Goble A, Goffeau A, Harris D, Hertz-Fowler C, Hilbert H, Horn D, Huang Y, Klages S, Knights A, Kube M, Larke N, Litvin L, Lord A, Louie T, Marra M, Masuy D, Matthews K, Michaeli S, Mottram JC, Müller-Auer S, Munden H, Nelson S, Norbertczak H, Oliver K, O'Neil S, Pentony M, Pohl TM, Price C, Purnelle B, Quail MA, Rabinowitsch E, Reinhardt R, Rieger M, Rinta J, Robben J, Robertson L, Ruiz JC, Rutter S, Saunders D, Schäfer M, Schein J, Schwartz DC, Seeger K, Seyler A, Sharp S, Shin H, Sivam D, Squares R, Squares S, Tosato V, Vogt C, Volckaert G, Wambutt R, Warren T, Wedler H, Woodward J, Zhou S, Zimmermann W, Smith DF, Blackwell JM, Stuart KD, Barrell B, Myler PJ (2005) The genome of the kinetoplastid parasite, *Leishmania major*. *Science* **309**: 436-442

Jain NK, Mishra V, Mehra NK (2013) Targeted drug delivery to macrophages. *Expert opinion on drug delivery* **10**: 353-367

Jha TK, Sharma VK (1984) Pentamidine-induced diabetes mellitus. *Transactions of the royal society of tropical medicine and hygiene* **78**: 252-253

Jhingran A, Chatterjee M, Madhubala R (2008) Leishmaniasis: Epidemiological trends and diagnosis. In *Leishmania: After The Genome*, Myler PJ, Fasel N (eds), 1, pp 1-14. Caister Academic Press

Kimutai R, Musa AM, Njoroge S, Omollo R, Alves F, Hailu A, Khalil EAG, Diro E, Soipei P, Musa B, Salman K, Ritmeijer K, Chappuis F, Rashid J, Mohammed R, Jameneh A, Makonnen E, Olobo J, Okello L, Sagaki P, Strub N, Ellis S, Alvar J, Balasegaram M, Alirol E, Wasunna M (2017) Safety and effectiveness of sodium stibogluconate and paromomycin combination for the treatment of visceral leishmaniasis in Eastern Africa: results from a pharmacovigilance programme. *Clinical drug investigation*: 1-14

Kirby DM, Thorburn DR, Turnbull DM, Taylor RW (2007) Biochemical assays of respiratory chain complex activity. In *Methods in cell biology* Vol. 80, pp 93-119. Academic Press

Kivens WJ, Hunt SW, 3rd, Mobley JL, Zell T, Dell CL, Bierer BE, Shimizu Y (1998) Identification of a proline-rich sequence in the CD2 cytoplasmic domain critical for regulation of integrin-mediated adhesion and activation of phosphoinositide 3-kinase. *Molecular and cellular biology* **18**: 5291-5307

Kovářová J, Barrett MP (2016) The pentose phosphate pathway in parasitic trypanosomatids. *Trends in parasitology*

Kristensen AR, Foster LJ (2013) High throughput strategies for probing the different organizational levels of protein interaction networks. *Molecular bioSystems* **9**: 2201-2212

Krogan NJ, Cagney G, Yu H, Zhong G, Guo X, Ignatchenko A, Li J, Pu S, Datta N, Tikuisis AP, Punna T, Peregrín-Alvarez JM, Shales M, Zhang X, Davey M, Robinson MD, Paccanaro A, Bray JE, Sheung A, Beattie B, Richards DP, Canadien V, Lalev A, Mena F, Wong P, Starostine A, Canete MM, Vlasblom J, Wu S, Orsi C, Collins SR, Chandran S, Haw R, Rilstone JJ, Gandi K, Thompson NJ, Musso G, St Onge P, Ghanny S, Lam MHY, Butland G, Altaf-Ul AM, Kanaya S, Shilatifard A, O'Shea E, Weissman JS, Ingles CJ, Hughes TR, Parkinson J, Gerstein M, Wodak SJ, Emili A, Greenblatt JF (2006) Global landscape of protein complexes in the yeast *Saccharomyces cerevisiae*. *Nature* **440**: 637

Kühner S, van Noort V, Betts MJ, Leo-Macias A, Batische C, Rode M, Yamada T, Maier T, Bader S, Beltran-Alvarez P, Castaño-Diez D, Chen W-H, Devos D, Güell M, Norambuena T, Racke I, Rybin V, Schmidt A, Yus E, Aebersold R, Herrmann R, Böttcher B, Frangakis AS, Russell RB, Serrano L, Bork P, Gavin A-C (2009) Proteome organization in a genome-reduced bacterium. *Science* **326**: 1235-1240

Kulkarni MM, Barbi J, McMaster WR, Gallo RL, Satoskar AR, McGwire BS (2011) Mammalian antimicrobial peptide influences control of cutaneous *Leishmania* infection. *Cellular microbiology* **13**: 913-923

Laemmli UK (1970) Cleavage of structural proteins during the assembly of the head of bacteriophage T4. *Nature* **227**: 680-685

Lahav T, Sivam D, Volpin H, Ronen M, Tsigankov P, Green A, Holland N, Kuzyk M, Borchers C, Zilberstein D, Myler PJ (2011) Multiple levels of gene regulation mediate differentiation of the intracellular pathogen *Leishmania*. *The FASEB Journal* **25**: 515-525

Law RHP, Manon S, Devenish RJ, Nagley P (1995) ATP synthase from *Saccharomyces cerevisiae*. In *Methods in Enzymology* Vol. 260, pp 133-163. Academic Press

Lee SH, Stephens JL, Englund PT (2007) A fatty-acid synthesis mechanism specialized for parasitism. *Nature reviews Microbiology* **5**: 287-297

Leifso K, Cohen-Freue G, Dogra N, Murray A, McMaster WR (2007) Genomic and proteomic expression analysis of *Leishmania* promastigote and amastigote life stages: the *Leishmania* genome is constitutively expressed. *Molecular biochemical parasitology* **152**: 35-46

Li F, Ge P, Hui WH, Atanasov I, Rogers K, Guo Q, Osato D, Falick AM, Zhou ZH, Simpson L (2009) Structure of the core editing complex (L-complex) involved in uridine insertion/deletion RNA editing in trypanosomatid mitochondria. *Proceedings of the National Academy of Sciences of the United States of America* **106**: 12306-12310

Lin L, P. KN, C. YJ, Alun J, L. SJ (2014) Single-step protease cleavage elution for identification of protein–protein interactions from GST pull-down and mass spectrometry. *Proteomics* **14**: 19-23

Llanes A, Restrepo CM, Vecchio GD, Anguizola FJ, Leonart R (2015) The genome of *Leishmania panamensis*: insights into genomics of the *L. (Viannia)* subgenus. *Scientific reports* **5**: 8550

Lobo-Jarne T, Ugalde C (2018) Respiratory chain supercomplexes: structures, function and biogenesis. *Seminars in cell & developmental biology* **76**: 179-190

Luque-Ortega JR, Hof Wvt, Veerman EC, Saugar JM, Rivas L (2008) Human antimicrobial peptide histatin 5 is a cell-penetrating peptide targeting mitochondrial ATP synthesis in *Leishmania*. *The FASEB journal* **22**: 1817-1828

Lye L-F, Owens K, Shi H, Murta SMF, Vieira AC, Turco SJ, Tschudi C, Ullu E, Beverley SM (2010) Retention and loss of RNA interference pathways in trypanosomatid protozoans. *PLoS pathogens* **6**: e1001161

Marché S, Michels PAM, Opperdoes FR (2000) Comparative study of *Leishmania mexicana* and *Trypanosoma brucei* NAD-dependent glycerol-3-phosphate dehydrogenase. *Molecular and biochemical parasitology* **106**: 83-91

Marchese L, Nascimento J, Damasceno F, Bringaud F, Michels P, Silber A (2018) The uptake and metabolism of amino acids, and their unique role in the biology of pathogenic trypanosomatids. *Pathogens* **7**: 36

- Maroli M, Feliciangeli MD, Bichaud L, Charrel RN, Gradoni L (2013) Phlebotomine sandflies and the spreading of leishmaniasis and other diseases of public health concern. *Medical and veterinary entomology* **27**: 123-147
- Marr AK, Cen S, Hancock REW, McMaster WR (2016) Identification of synthetic and natural host defense peptides with leishmanicidal activity. *Antimicrobial agents and chemotherapy* **60**: 2484-2491
- Marr AK, McGwire BS, McMaster WR (2012) Modes of action of leishmanicidal antimicrobial peptides. *Future microbiology* **7**: 1047-1059
- Martel D, Beneke T, Gluenz E, Sp, #xe4, th GF, Rachidi N (2017) Characterisation of Casein Kinase 1.1 in *Leishmania donovani* using the CRISPR Cas9 toolkit. *BioMed research international* **2017**: 11
- Maslov DA, Nawathean P, Scheel J (1999) Partial kinetoplast-mitochondrial gene organization and expression in the respiratory deficient plant trypanosomatid *Phytomonas serpens*. *Molecular and biochemical parasitology* **99**: 207-221
- Maslov DA, Zikova A, Kyselova I, Lukes J (2002) A putative novel nuclear-encoded subunit of the cytochrome c oxidase complex in trypanosomatids. *Molecular and biochemical parasitology* **125**: 113-125
- Maugeri DA, Cazzulo JJ, Burchmore RJS, Barrett MP, Ogbunude POJ (2003) Pentose phosphate metabolism in *Leishmania mexicana*. *Molecular and biochemical parasitology* **130**: 117-125
- Mayer BJ, Jackson PK, Baltimore D (1991) The noncatalytic src homology region 2 segment of abl tyrosine kinase binds to tyrosine-phosphorylated cellular proteins with high affinity. *Proceedings of the National Academy of Sciences of the United States of America* **88**: 627-631
- McAllaster MR, Ikeda KN, Lozano-Núñez A, Anrather D, Unterwurzacher V, Gossenreiter T, Perry JA, Crickley R, Mercadante CJ, Vaughan S, de Graffenried CL (2015) Proteomic identification of novel cytoskeletal proteins associated with TbPLK, an essential regulator of cell morphogenesis in *Trypanosoma brucei*. *Molecular biology of the Cell* **26**: 3013-3029
- McConville MJ, De Souza DP, Saunders EC, Pyke J, Naderer T, Ellis MA, Sernee MF, Ralton JE, Likic VA (2008) Analysis of the *Leishmania* metabolism. In *Leishmania: After The Genome*, Myler PJ, Fasel N (eds), 5, pp 75-106. Norfolk, UK: Caister Academic Press
- McConville MJ, Naderer T (2011) Metabolic pathways required for the intracellular survival of *Leishmania*. *Annual review of microbiology* **65**: 543-561
- McConville MJ, Saunders EC, Kloehn J, Dagley MJ (2015) *Leishmania* carbon metabolism in the macrophage phagolysosome- feast or famine? *F1000Research* **4**: 938

- McNicoll F, Drummelsmith J, Müller M, Madore É, Boilard N, Ouellette M, Papadopoulou B (2006) A combined proteomic and transcriptomic approach to the study of stage differentiation in *Leishmania infantum*. *Proteomics* **6**: 3567-3581
- McNicoll F, Muller M, Cloutier S, Boilard N, Rochette A, Dube M, Papadopoulou B (2005) Distinct 3'-untranslated region elements regulate stage-specific mRNA accumulation and translation in *Leishmania*. *Journal of biological chemistry* **280**: 35238-35246
- Medina-Acosta E, Cross GA (1993) Rapid isolation of DNA from trypanosomatid protozoa using a simple 'mini-prep' procedure. *Molecular and biochemical parasitology* **59**: 327-329
- Meheus F, Balasegaram M, Olliaro P, Sundar S, Rijal S, Faiz MA, Boelaert M (2010) Cost-effectiveness analysis of combination therapies for visceral leishmaniasis in the Indian subcontinent. *PLoS neglected tropical diseases* **4**: e818
- Meheus F, Boelaert M, Baltussen R, Sundar S (2006) Costs of patient management of visceral leishmaniasis in Muzaffarpur, Bihar, India  
Coûts de la prise en charge de patients à la leishmaniose viscérale à Muzaffarpur en Inde  
Costes del manejo del paciente con Leishmaniasis Visceral en Muzaffarpur, India. *Tropical medicine & international health* **11**: 1715-1724
- Mitra B, Laranjeira-Silva MF, Perrone Bezerra de Menezes J, Jensen J, Michailowsky V, Andrews NW (2016) A trypanosomatid iron transporter that regulates mitochondrial function is required for *Leishmania amazonensis* virulence. *PLoS pathogens* **12**: e1005340
- Mizbani A, Taslimi Y, Zahedifard F, Taheri T, Rafati S (2011) Effect of A2 gene on infectivity of the nonpathogenic parasite *Leishmania tarentolae*. *Parasitology research* **109**: 793-799
- Mokranjac D, Neupert W (2009) Thirty years of protein translocation into mitochondria: unexpectedly complex and still puzzling. *Biochimica et biophysica acta* **1793**: 33-41
- Mondal S, Roy JJ, Bera T (2014) Characterization of mitochondrial bioenergetic functions between two forms of *Leishmania donovani* – a comparative analysis. *Journal of bioenergetics and biomembranes* **46**: 395-402
- Morales J, Mogi T, Mineki S, Takashima E, Mineki R, Hirawake H, Sakamoto K, Omura S, Kita K (2009) Novel mitochondrial complex II isolated from *Trypanosoma cruzi* is composed of 12 peptides including a heterodimeric Ip subunit. *The Journal of biological chemistry* **284**: 7255-7263
- Morty RE, Morehead J (2002) Cloning and characterization of a lLeucyl aminopeptidase from three pathogenic *Leishmania* species. *Journal of Biological Chemistry* **277**: 26057-26065

Murray A (2005) Functional genomics of the A600 locus in *Leishmania mexicana*. PhD Thesis, Medical Genetics, University of British Columbia,

Murray A, Fu C, Habibi G, McMaster WR (2007) Regions in the 3' untranslated region confer stage-specific expression to the *Leishmania mexicana* a600-4 gene. *Molecular and biochemical parasitology* **153**: 125-132

Murray AS, Lynn MA, McMaster WR (2010) The *Leishmania mexicana* A600 genes are functionally required for amastigote replication. *Molecular and biochemical parasitology* **172**: 80-89

Myler PJ, Audleman L, deVos T, Hixson G, Kiser P, Lemley C, Magness C, Rickel E, Sisk E, Sunkin S, Swartzell S, Westlake T, Bastien P, Fu G, Ivens A, Stuart K (1999) *Leishmania major* Friedlin chromosome 1 has an unusual distribution of protein-coding genes. *Proceedings of the National Academy of Sciences* **96**: 2902-2906

Naderer T, Ellis MA, Sernee MF, De Souza DP, Curtis J, Handman E, McConville MJ (2006) Virulence of *Leishmania major* in macrophages and mice requires the gluconeogenic enzyme fructose-1,6-bisphosphatase. *Proceedings of the National Academy of Sciences* **103**: 5502-5507

Naderer T, Heng J, McConville MJ (2010) Evidence that intracellular stages of *Leishmania major* utilize amino sugars as a major carbon source. *PLoS pathogens* **6**: e1001245

Nahar M, Dubey V, Mishra D, Mishra PK, Dube A, Jain NK (2010) *In vitro* evaluation of surface functionalized gelatin nanoparticles for macrophage targeting in the therapy of visceral leishmaniasis. *Journal of drug targeting* **18**: 93-105

Nayak A, Akpunarlieva S, Barrett M, Burchmore R (2018) A defined medium for *Leishmania* culture allows definition of essential amino acids. *Experimental parasitology* **185**: 39-52

Ndjamen B, Kang B-H, Hatsuzawa K, Kima PE (2010) *Leishmania* parasitophorous vacuoles interact continuously with the host cell's endoplasmic reticulum; parasitophorous vacuoles are hybrid compartments. *Cellular microbiology* **12**: 1480-1494

Nebohacova M, Kim CE, Simpson L, Maslov DA (2009) RNA editing and mitochondrial activity in promastigotes and amastigotes of *Leishmania donovani*. *International journal for parasitology* **39**: 635-644

Niemann M, Wiese S, Mani J, Chanfon A, Jackson C, Meisinger C, Warscheid B, Schneider A (2013) Mitochondrial outer membrane proteome of *Trypanosoma brucei* reveals novel factors required to maintain mitochondrial morphology. *Molecular & cellular proteomics* **12**: 515-528

Nugent PG, Karsani SA, Wait R, Tempero J, Smith DF (2004) Proteomic analysis of *Leishmania mexicana* differentiation. *Molecular and biochemical parasitology* **136**: 51-62

- Nühs A, De Rycker M, Manthri S, Comer E, Scherer CA, Schreiber SL, Ioset J-R, Gray DW (2015) Development and validation of a novel *Leishmania donovani* screening cascade for high-throughput screening using a novel axenic assay with high predictivity of leishmanicidal intracellular activity. *PLOS neglected tropical diseases* **9**: e0004094
- Olivier M, Gregory DJ, Forget G (2005) Subversion mechanisms by which *Leishmania* parasites can escape the host immune response: a signaling point of view. *Clinical microbiology reviews* **18**: 293-305
- Opperdoes FR, Coombs GH (2007) Metabolism of *Leishmania*: proven and predicted. *Trends in parasitology* **23**: 149-158
- Opperdoes FR, Michels PA (2008) Complex I of Trypanosomatidae: does it exist? *Trends in parasitology* **24**: 310-317
- Osman C, Wilmes C, Tatsuta T, Langer T (2007) Prohibitins interact genetically with Atp23, a novel processing peptidase and chaperone for the F(1)F(O)-ATP synthase. *Molecular biology of the cell* **18**: 627-635
- Panigrahi AK, Zikova A, Dalley RA, Acestor N, Ogata Y, Anupama A, Myler PJ, Stuart KD (2008a) Mitochondrial complexes in *Trypanosoma brucei*: a novel complex and a unique oxidoreductase complex. *Molecular & cellular proteomics : MCP* **7**: 534-545
- Panigrahi AK, Zíková A, Dalley RA, Acestor N, Ogata Y, Anupama A, Myler PJ, Stuart KD (2008b) Mitochondrial complexes in *Trypanosoma brucei*: a novel complex and a unique oxidoreductase complex. *Molecular & cellular proteomics* **7**: 534-545
- Papadopoulou B, Muller M, Rochette A, McNicoll F, Dumas C, Chow C (2008) Regulation of gene expression in *Leishmania* throughout a complex digenetic life cycle. In *Leishmania: After The Genome*, Myler PJ, Fasel N (eds), 3, pp 29-54. Norfolk, UK: Caister Academic Press
- Peacock CS, Seeger K, Harris D, Murphy L, Ruiz JC, Quail MA, Peters N, Adlem E, Tivey A, Aslett M, Kerhornou A, Ivens A, Fraser A, Rajandream MA, Carver T, Norbertczak H, Chillingworth T, Hance Z, Jagels K, Moule S, Ormond D, Rutter S, Squares R, Whitehead S, Rabinowitsch E, Arrowsmith C, White B, Thurston S, Bringaud F, Baldauf SL, Faulconbridge A, Jeffares D, Depledge DP, Oyola SO, Hilley JD, Brito LO, Tosi LR, Barrell B, Cruz AK, Mottram JC, Smith DF, Berriman M (2007) Comparative genomic analysis of three *Leishmania* species that cause diverse human disease. *Nature genetics* **39**: 839-847
- Perry SW, Norman JP, Barbieri J, Brown EB, Gelbard HA (2011) Mitochondrial membrane potential probes and the proton gradient: a practical usage guide. *BioTechniques* **50**: 98-115
- Pfanner N, van der Laan M, Amati P, Capaldi RA, Caudy AA, Chacinska A, Darshi M, Deckers M, Hoppins S, Icho T, Jakobs S, Ji J, Kozjak-Pavlovic V, Meisinger C, Odgren PR, Park SK, Rehling P, Reichert AS, Sheikh MS, Taylor SS, Tsuchida N, van der Blik AM, van der Klei JJ,

- Weissman JS, Westermann B, Zha J, Neupert W, Nunnari J (2014) Uniform nomenclature for the mitochondrial contact site and cristae organizing system. *The Journal of cell biology* **204**: 1083-1086
- Phizicky EM, Fields S (1995) Protein-protein interactions: methods for detection and analysis. *Microbiological reviews* **59**: 94-123
- Pilar AVC, Madrid KP, Jardim A (2008) Interaction of *Leishmania* PTS2 receptor peroxin 7 with the glycosomal protein import machinery. *Molecular and biochemical parasitology* **158**: 72-81
- Ponte-Sucre A, Gamarro F, Dujardin J-C, Barrett MP, López-Vélez R, García-Hernández R, Pountain AW, Mwenechanya R, Papadopoulos B (2017) Drug resistance and treatment failure in leishmaniasis: A 21st century challenge. *PLoS neglected tropical diseases* **11**: e0006052
- Prajapati VK, Awasthi K, Gautam S, Yadav TP, Rai M, Srivastava ON, Sundar S (2011) Targeted killing of *Leishmania donovani* *in vivo* and *in vitro* with amphotericin B attached to functionalized carbon nanotubes. *Journal of antimicrobial chemotherapy* **66**: 874-879
- Pruthi J, Mehra NK, Jain NK (2012) Macrophages targeting of amphotericin B through mannoseylated multiwalled carbon nanotubes. *Journal of drug targeting* **20**: 593-604
- Quijada L, Soto M, Alonso C, Requena JM (2000) Identification of a putative regulatory element in the 3'-untranslated region that controls expression of HSP70 in *Leishmania infantum*. *Molecular and biochemical parasitology* **110**: 79-91
- Ralton JE, Naderer T, Piraino HL, Bashtannyk TA, Callaghan JM, McConville MJ (2003) Evidence that intracellular  $\beta$ 1-2 mannan is a virulence factor in *Leishmania* parasites. *Journal of biological chemistry* **278**: 40757-40763
- Rampersad SN (2012) Multiple applications of Alamar Blue as an indicator of metabolic function and cellular health in cell viability bioassays. *Sensors (Basel, Switzerland)* **12**: 12347-12360
- Rappsilber J, Ishihama Y, Mann M (2003) Stop and Go extraction tips for matrix-assisted laser desorption/ionization, nanoelectrospray and LC/MS sample pretreatment in proteomics. *Analytical chemistry* **75**: 663-670
- Raymond F, Boisvert S, Roy G, Ritt J-F, Légaré D, Isnard A, Stanke M, Olivier M, Tremblay MJ, Papadopoulos B, Ouellette M, Corbeil J (2012) Genome sequencing of the lizard parasite *Leishmania tarentolae* reveals loss of genes associated to the intracellular stage of human pathogenic species. *Nucleic acids research* **40**: 1131-1147
- Real F, Mortara RA (2012) The diverse and dynamic nature of *Leishmania* parasitophorous vacuoles studied by multidimensional imaging. *PLoS neglected tropical diseases* **6**: e1518

Reid RA, Moyle J, Mitchell P (1966) Synthesis of adenosine triphosphate by a protonmotive force in rat liver mitochondria. *Nature* **212**: 257-258

Reithinger R, Dujardin J-C, Louzir H, Pirmez C, Alexander B, Brooker S (2007) Cutaneous leishmaniasis. *The Lancet infectious diseases* **7**: 581-596

Ren M, Phoon CK, Schlame M (2014) Metabolism and function of mitochondrial cardiolipin. *Progress in lipid research* **55**: 1-16

Ribeiro TG, Chávez-Fumagalli MA, Valadares DG, França JR, Rodrigues LB, Duarte MC, Lage PS, Andrade PHR, Lage DP, Arruda LV, Abánades DR, Costa LE, Martins VT, Tavares CAP, Castilho RO, Coelho EAF, Faraco AAG (2014) Novel targeting using nanoparticles: an approach to the development of an effective anti-leishmanial drug-delivery system. *International journal of nanomedicine* **9**: 877-890

Rigaut G, Shevchenko A, Rutz B, Wilm M, Mann M, Seraphin B (1999) A generic protein purification method for protein complex characterization and proteome exploration. *Nature biotechnology* **17**: 1030-1032

Rijal S, Koirala S, Van der Stuyft P, Boelaert M (2006) The economic burden of visceral leishmaniasis for households in Nepal. *Transactions of the royal society of tropical medicine and hygiene* **100**: 838-841

Rivière L, Moreau P, Allmann S, Hahn M, Biran M, Plazolles N, Franconi J-M, Boshart M, Bringaud F (2009) Acetate produced in the mitochondrion is the essential precursor for lipid biosynthesis in procyclic trypanosomes. *Proceedings of the National Academy of Sciences* **106**: 12694-12699

Rodriguez-Contreras D, Feng X, Keeney KM, Bouwer HGA, Landfear SM (2007) Phenotypic characterization of a glucose transporter null mutant in *Leishmania mexicana*. *Molecular and biochemical parasitology* **153**: 9-18

Rogers MB, Hilley JD, Dickens NJ, Wilkes J, Bates PA, Depledge DP, Harris D, Her Y, Herzyk P, Imamura H, Otto TD, Sanders M, Seeger K, Dujardin JC, Berriman M, Smith DF, Hertz-Fowler C, Mottram JC (2011) Chromosome and gene copy number variation allow major structural change between species and strains of *Leishmania*. *Genome research* **21**: 2129-2142

Rosenzweig D, Smith D, Myler PJ, Olafson RW, Zilberstein D (2008a) Post-translational modification of cellular proteins during *Leishmania donovani* differentiation. *Proteomics* **8**: 1843-1850

Rosenzweig D, Smith D, Opperdoes F, Stern S, Olafson RW, Zilberstein D (2008b) Retooling *Leishmania* metabolism: from sand fly gut to human macrophage. *The FASEB Journal* **22**: 590-602

Roux KJ, Kim DI, Raida M, Burke B (2012) A promiscuous biotin ligase fusion protein identifies proximal and interacting proteins in mammalian cells. *The Journal of cell biology* **196**: 801-810

Sacks D, Lawyer P, Kamhawi S (2008) The biology of *Leishmania*-sandfly interactions. In *Leishmania: After the Genome*, Myler PJ, Fasel N (eds), 10, pp 205-238. Norfolk, UK: Caister Academic Press

Sacks DL (2001) *Leishmania*-sand fly interactions controlling species-specific vector competence. *Cellular microbiology* **3**: 189-196

Sacks DL, Hieny S, Sher A (1985) Identification of cell surface carbohydrate and antigenic changes between noninfective and infective developmental stages of *Leishmania major* promastigotes. *Journal of immunology* **135**: 564-569

Sánchez-Brunete JA, Dea MA, Rama S, Bolás F, Alunda JM, Raposo R, Méndez MT, Torrado-Santiago S, Torrado JJ (2004) Treatment of experimental visceral leishmaniasis with amphotericin B in stable albumin microspheres. *Antimicrobial agents and chemotherapy* **48**: 3246-3252

Santhamma KR, Bhaduri A (1995) Characterization of the respiratory chain of *Leishmania donovani* promastigotes. *Molecular and biochemical parasitology* **75**: 43-53

Saunders EC, De Souza DP, Naderer T, Sernee MF, Ralton JE, Doyle MA, Macrae JI, Chambers JL, Heng J, Nahid A, Likić VA, McConville MJ (2010) Central carbon metabolism of *Leishmania* parasites. *Parasitology* **137**: 1303-1313

Saunders EC, Ng WW, Chambers JM, Ng M, Naderer T, Krömer JO, Likić VA, McConville MJ (2011) Isotopomer profiling of *Leishmania mexicana* promastigotes reveals important roles for succinate fermentation and aspartate uptake in tricarboxylic acid cycle (TCA) anaplerosis, glutamate synthesis and growth. *Journal of biological chemistry* **286**: 27706-27717

Saunders EC, Ng WW, Kloehn J, Chambers JM, Ng M, McConville MJ (2014) Induction of a stringent metabolic response in intracellular stages of *Leishmania mexicana* leads to increased dependence on mitochondrial metabolism. *PLoS pathogens* **10**: e1003888

Saxena A, Lahav T, Holland N, Aggarwal G, Anupama A, Huang Y, Volpin H, Myler PJ, Zilberstein D (2007) Analysis of the *Leishmania donovani* transcriptome reveals an ordered progression of transient and permanent changes in gene expression during differentiation. *Molecular and biochemical parasitology* **152**: 53-65

Schagger H (2006) Tricine-SDS-PAGE. *Nature protocols* **1**: 16-22

Schägger H, Bentlage H, Ruitenbeek W, Pfeiffer K, Rotter S, Rother C, Böttcher-Purkl A, Lodemann E (1996) Electrophoretic separation of multiprotein complexes from blood platelets

and cell lines: Technique for the analysis of diseases with defects in oxidative phosphorylation. *Electrophoresis* **17**: 709-714

Schagger H, Cramer WA, Vonjagow G (1994) Analysis of molecular masses and oligomeric states of protein complexes by Blue Native electrophoresis and isolation of membrane protein complexes by two-dimensional native electrophoresis. *Analytical biochemistry* **217**: 220-230

Schagger H, von Jagow G (1991) Blue native electrophoresis for isolation of membrane protein complexes in enzymatically active form. *Analytical biochemistry* **199**: 223-231

Schnauffer A, Clark-Walker GD, Steinberg AG, Stuart K (2005) The F(1)-ATP synthase complex in bloodstream stage trypanosomes has an unusual and essential function. *The EMBO journal* **24**: 4029-4040

Schneider A, Bouzaidi-Tiali N, Chanez AL, Bulliard L (2007) ATP production in isolated mitochondria of procyclic *Trypanosoma brucei*. *Methods in molecular biology* **372**: 379-387

Schneider A, Bursac D, Lithgow T (2008) The direct route: a simplified pathway for protein import into the mitochondrion of trypanosomes. *Trends in Cell Biology* **18**: 12-18

Schorr S, van der Laan M (2018) Integrative functions of the mitochondrial contact site and cristae organizing system. *Seminars in cell & developmental biology* **76**: 191-200

Shaked-Mishan P, Suter-Grotemeyer M, Yoel-Almagor T, Holland N, Zilberstein D, Rentsch D (2006) A novel high-affinity arginine transporter from the human parasitic protozoan *Leishmania donovani*. *Molecular microbiology* **60**: 30-38

Sharlow ER, Close D, Shun T, Leimgruber S, Reed R, Mustata G, Wipf P, Johnson J, O'Neil M, Grögl M, Magill AJ, Lazo JS (2009) Identification of potent chemotypes targeting *Leishmania major* using a high-throughput, low-stringency, computationally enhanced, small molecule screen. *PLoS neglected tropical diseases* **3**: e540

Shih S, Hwang H-Y, Carter D, Stenberg P, Ullman B (1998) Localization and targeting of the *Leishmania donovani* hypoxanthine-guanine phosphoribosyltransferase to the glycosome. *Journal of biological chemistry* **273**: 1534-1541

Simpson AG, Stevens JR, Lukes J (2006) The evolution and diversity of kinetoplastid flagellates. *Trends in parasitology* **22**: 168-174

Singh N, Kumar M, Singh RK (2012) Leishmaniasis: Current status of available drugs and new potential drug targets. *Asian Pacific journal of tropical medicine* **5**: 485-497

Singh OP, Singh B, Chakravarty J, Sundar S (2016) Current challenges in treatment options for visceral leishmaniasis in India: a public health perspective. *Infectious diseases of poverty* **5**: 19

- Singha UK, Hamilton V, Duncan MR, Weems E, Tripathi MK, Chaudhuri M (2012) Protein translocase of mitochondrial inner membrane in *Trypanosoma brucei*. *Journal of biological chemistry* **287**: 14480-14493
- Singhal RK, Kruse C, Heidler J, Strecker V, Zwicker K, Düsterwald L, Westermann B, Herrmann JM, Wittig I, Rapaport D (2017) Coi1 is a novel assembly factor of the yeast complex III–complex IV supercomplex. *Molecular biology of the cell* **28**: 2609-2622
- Siqueira-Neto JL, Song O-R, Oh H, Sohn J-H, Yang G, Nam J, Jang J, Cechetto J, Lee CB, Moon S, Genovesio A, Chatelain E, Christophe T, Freitas-Junior LH (2010) Antileishmanial high-throughput drug screening reveals drug candidates with new scaffolds. *PLoS neglected tropical diseases* **4**: e675
- Škodová I, Verner Z, Bringaud F, Fabian P, Lukeš J, Horváth A (2013) Characterization of two mitochondrial flavin adenine dinucleotide-dependent glycerol-3-phosphate dehydrogenases in *Trypanosoma brucei*. *Eukaryotic cell* **12**: 1664-1673
- Sloof P, Arts GJ, van den Burg J, van der Spek H, Benne R (1994) RNA editing in mitochondria of cultured trypanosomatids: translatable mRNAs for NADH-dehydrogenase subunits are missing. *Journal of bioenergetics and biomembranes* **26**: 193-203
- Smith DF, Peacock CS, Cruz AK (2007) Comparative genomics: from genotype to disease phenotype in the leishmaniasis. *International journal for parasitology* **37**: 1173-1186
- Smith M, Bringaud F, Papadopoulou B (2009) Organization and evolution of two SIDER retroposon subfamilies and their impact on the *Leishmania* genome. *BMC genomics* **10**: 240
- Sollelis L, Ghorbal M, MacPherson CR, Martins RM, Kuk N, Crobu L, Bastien P, Scherf A, Lopez-Rubio JJ, Sterkers Y (2015) First efficient CRISPR-Cas9-mediated genome editing in *Leishmania* parasites. *Cellular microbiology* **17**: 1405-1412
- Spinazzi M, Casarin A, Pertegato V, Salviati L, Angelini C (2012) Assessment of mitochondrial respiratory chain enzymatic activities on tissues and cultured cells. *Nature protocols* **7**: 1235-1246
- Srivastava S, Shankar P, Mishra J, Singh S (2016) Possibilities and challenges for developing a successful vaccine for leishmaniasis. *Parasites & Vectors* **9**: 1-15
- Strogolova V, Furness A, Robb-McGrath M, Garlich J, Stuart RA (2012) Rcf1 and Rcf2, members of the hypoxia-induced gene 1 protein family, are critical components of the mitochondrial cytochrome b-cytochrome c oxidase supercomplex. *Molecular and cellular biology* **32**: 1363-1373

Subrtova K, Panicucci B, Zikova A (2015) ATPaseTb2, a unique membrane-bound FoF1-ATPase component, is essential in bloodstream and dyskinetoplastic trypanosomes. *PLoS pathogens* **11**: e1004660

Sundar S, Olliaro PL (2007) Miltefosine in the treatment of leishmaniasis: Clinical evidence for informed clinical risk management. *Therapeutics and clinical risk management* **3**: 733-740

Surve S, Heestand M, Panicucci B, Schnauffer A, Parsons M (2012) Enigmatic presence of mitochondrial Complex I in *Trypanosoma brucei* bloodstream forms. *Eukaryotic cell* **11**: 183-193

Suzuki T, Murakami T, Iino R, Suzuki J, Ono S, Shirakihara Y, Yoshida M (2003) F0F1-ATPase/Synthase is geared to the synthesis mode by conformational rearrangement of  $\epsilon$  subunit in response to proton motive force and ADP/ATP balance. *Journal of biological chemistry* **278**: 46840-46846

Thermo Fisher Scientific. (2008) Tech Tip #4: Batch and spin cup methods for affinity purification of proteins.

Thiemann OH, Maslov DA, Simpson L (1994) Disruption of RNA editing in *Leishmania tarentolae* by the loss of minicircle-encoded guide RNA genes. *The EMBO journal* **13**: 5689-5700

Tran KD, Rodriguez-Contreras D, Vieira DP, Yates PA, David L, Beatty W, Elferich J, Landfear SM (2013) KHARON1 mediates flagellar targeting of a glucose transporter in *Leishmania mexicana* and is critical for viability of infectious intracellular amastigotes. *The Journal of biological chemistry* **288**: 22721-22733

Tschoeke DA, Nunes GL, Jardim R, Lima J, Dumaresq ASR, Gomes MR, de Mattos Pereira L, Loureiro DR, Stoco PH, de Matos Guedes HL, de Miranda AB, Ruiz J, Pitaluga A, Silva FP, Probst CM, Dickens NJ, Mottram JC, Grisard EC, Dávila AMR (2014) The comparative genomics and phylogenomics of *Leishmania amazonensis* parasite. *Evolutionary bioinformatics online* **10**: 131-153

Tzagoloff A, Barrientos A, Neupert W, Herrmann JM (2004) Atp10p assists assembly of Atp6p into the F0 unit of the yeast mitochondrial ATPase. *Journal of biological chemistry* **279**: 19775-19780

Uboldi AD, Lueder FB, Walsh P, Spurck T, McFadden GI, Curtis J, Likic VA, Perugini MA, Barson M, Lithgow T, Handman E (2006) A mitochondrial protein affects cell morphology, mitochondrial segregation and virulence in *Leishmania*. *International journal for parasitology* **36**: 1499-1514

Uttaro AD (2014) Acquisition and biosynthesis of saturated and unsaturated fatty acids by trypanosomatids. *Molecular and biochemical parasitology* **196**: 61-70

van der Laan M, Horvath SE, Pfanner N (2016) Mitochondrial contact site and cristae organizing system. *Current opinion in cell biology* **41**: 33-42

Van Hellemond JJ, Opperdoes FR, Tielens AGM (1998) Trypanosomatidae produce acetate via a mitochondrial acetate:succinate CoA transferase. *Proceedings of the National Academy of Sciences* **95**: 3036-3041

Van Hellemond JJ, Tielens AGM (1997) Inhibition of the respiratory chain results in a reversible metabolic arrest in *Leishmania* promastigotes. *Molecular and biochemical parasitology* **85**: 135-138

Verner Z, Cermakova P, Skodova I, Kovacova B, Lukes J, Horvath A (2014) Comparative analysis of respiratory chain and oxidative phosphorylation in *Leishmania tarentolae*, *Crithidia fasciculata*, *Phytomonas serpens* and procyclic stage of *Trypanosoma brucei*. *Molecular and biochemical parasitology* **193**: 55-65

Verner Z, Čermáková P, Škodová I, Kriegová E, Horváth A, Lukeš J (2011) Complex I (NADH:ubiquinone oxidoreductase) is active in but non-essential for procyclic *Trypanosoma brucei*. *Molecular and biochemical parasitology* **175**: 196-200

Verner Z, Skodova I, Polakova S, Durisova-Benkovicova V, Horvath A, Lukes J (2013) Alternative NADH dehydrogenase (NDH2): intermembrane-space-facing counterpart of mitochondrial complex I in the procyclic *Trypanosoma brucei*. *Parasitology* **140**: 328-337

Vukotic M, Oeljeklaus S, Wiese S, Vögtle FN, Meisinger C, Meyer Helmut E, Zieseniss A, Katschinski Doerthe M, Jans Daniel C, Jakobs S, Warscheid B, Rehling P, Deckers M (2012) Rcf1 mediates cytochrome oxidase assembly and respirasome formation, revealing heterogeneity of the enzyme complex. *Cell metabolism* **15**: 336-347

Walker J, Vasquez J-J, Gomez MA, Drummelsmith J, Burchmore R, Girard I, Ouellette M (2006) Identification of developmentally-regulated proteins in *Leishmania panamensis* by proteome profiling of promastigotes and axenic amastigotes. *Molecular and biochemical parasitology* **147**: 64-73

Wasan EK, Gershkovich P, Zhao J, Zhu X, Werbovetz K, Tidwell RR, Clement JG, Thornton SJ, Wasan KM (2010) A novel tropically stable oral amphotericin B formulation (iCo-010) exhibits efficacy against visceral leishmaniasis in a murine model. *PLoS neglected tropical diseases* **4**: e913

Weng Z, Taylor JA, Turner CE, Brugge JS, Seidel-Dugan C (1993) Detection of Src homology 3-binding proteins, including paxillin, in normal and v-Src-transformed Balb/c 3T3 cells. *The Journal of biological chemistry* **268**: 14956-14963

WHO. (2010) Control of the Leishmaniases. *WHO Technical report series*, Geneva, Switzerland.

WHO. (2015) Leishmaniasis. *Investing to overcome the global impact of neglected tropical diseases: Third WHO report on neglected tropical diseases*. WHO/Department of control of neglected tropical diseases, p. 118.

Wiemer EAC, Hannaert V, van den Ijssel PRLA, Van Roy J, Opperdoes FR, Michels PAM (1995) Molecular analysis of glyceraldehyde-3-phosphate dehydrogenase in *Trypanoplasma borelli*: An evolutionary scenario of subcellular compartmentation in Kinetoplastida. *Journal of molecular evolution* **40**: 443-454

Wittig I, Braun HP, Schagger H (2006) Blue native PAGE. *Nature protocols* **1**: 418-428

Wittig I, Karas M, Schagger H (2007) High resolution clear native electrophoresis for in-gel functional assays and fluorescence studies of membrane protein complexes. *Molecular & cellular proteomics : MCP* **6**: 1215-1225

Worthey EA, Martinez-Calvillo S, Schnauffer A, Aggarwal G, Cawthra J, Fazelinia G, Fong C, Fu G, Hassebrock M, Hixson G, Ivens AC, Kiser P, Marsolini F, Rickell E, Salavati R, Sisk E, Sunkin SM, Stuart KD, Myler PJ (2003) *Leishmania major* chromosome 3 contains two long convergent polycistronic gene clusters separated by a tRNA gene. *Nucleic acids research* **31**: 4201-4210

Yang R-F, Sun L-H, Zhang R, Zhang Y, Luo Y-X, Zheng W, Zhang Z-Q, Chen H-Z, Liu D-P (2015) Suppression of Mic60 compromises mitochondrial transcription and oxidative phosphorylation. *Scientific reports* **5**: 7990

Yao S. (2014) FDA approves Impavido to treat tropical disease leishmaniasis. US Food and Drug Administration, Vol. 2016, p. Press Release.

Zakai HA, L. C, Bates PA (1998) In vitro stimulation of metacyclogenesis in *Leishmania braziliensis*, *L. donovani*, *L. major* and *L. mexicana*. *Parasitology* **116**: 305-309

Zarella-Boitz JM, Rager N, Jardim A, Ullman B (2004) Subcellular localization of adenine and xanthine phosphoribosyltransferases in *Leishmania donovani*. *Molecular and biochemical parasitology* **134**: 43-51

Zerbetto E, Vergani L, Dabbeni-Sala F (1997) Quantification of muscle mitochondrial oxidative phosphorylation enzymes via histochemical staining of blue native polyacrylamide gels. *Electrophoresis* **18**: 2059-2064

Zhang HX, Du GH, Zhang JT (2004) Assay of mitochondrial functions by resazurin *in vitro*. *Acta pharmacologica Sinica* **25**: 385-389

Zhang K, Beverley SM (2010) Phospholipid and sphingolipid metabolism in *Leishmania*. *Molecular and biochemical parasitology* **170**: 55

- Zhang W-W, Lypaczewski P, Matlashewski G (2017) Optimized CRISPR-Cas9 genome editing for *Leishmania* and its use to target a multigene family, induce chromosomal translocation, and study DNA break repair mechanisms. *mSphere* **2**
- Zhang W-W, Matlashewski G (2001) Characterization of the A2–A2rel gene cluster in *Leishmania donovani*: involvement of A2 in visceralization during infection. *Molecular microbiology* **39**: 935-948
- Zhang WW, Matlashewski G (1997) Loss of virulence in *Leishmania donovani* deficient in an amastigote-specific protein, A2. *Proceedings of the National Academy of Sciences of the United States of America* **94**: 8807-8811
- Zhang WW, Matlashewski G (2015) CRISPR-Cas9-mediated genome editing in *Leishmania donovani*. *mBio* **6**: e00861
- Zhang WW, Mendez S, Ghosh A, Myler P, Ivens A, Clos J, Sacks DL, Matlashewski G (2003) Comparison of the A2 gene locus in *Leishmania donovani* and *Leishmania major* and its control over cutaneous infection. *The Journal of biological chemistry* **278**: 35508-35515
- Zhang WW, Ramasamy G, McCall LI, Haydock A, Ranasinghe S, Abeygunasekara P, Sirimanna G, Wickremasinghe R, Myler P, Matlashewski G (2014) Genetic analysis of *Leishmania donovani* tropism using a naturally attenuated cutaneous strain. *PLoS pathogens* **10**: e1004244
- Zíková A, Hampl V, Paris Z, Týč J, Lukeš J (2016) Aerobic mitochondria of parasitic protists: Diverse genomes and complex functions. *Molecular and biochemical parasitology* **209**: 46-57
- Zikova A, Panigrahi AK, Uboldi AD, Dalley RA, Handman E, Stuart K (2008) Structural and functional association of *Trypanosoma brucei* MIX protein with cytochrome c oxidase complex. *Eukaryotic cell* **7**: 1994-2003
- Zikova A, Schnauffer A, Dalley RA, Panigrahi AK, Stuart KD (2009a) The F(0)F(1)-ATP synthase complex contains novel subunits and is essential for procyclic *Trypanosoma brucei*. *PLoS pathogens* **5**: e1000436
- Zikova A, Schnauffer A, Dalley RA, Panigrahi AK, Stuart KD (2009b) The F(0)F(1)-ATP synthase complex contains novel subunits and is essential for procyclic *Trypanosoma brucei*. *PLoS pathogens* **5**: e1000436
- Zilberstein D (2008) Physiological and biochemical aspects of *Leishmania* development. In *Leishmania: After The Genome*, Myler PJ, Fasel N (eds), 6, pp 107-122. Norfolk, UK: Caister Academic Press

## Appendices

### Appendix A Nucleotide coding sequence of the *A600* genes

#### A.1 Coding sequence of the *L. mexicana A600.1* gene

```
1      atgccctcta tgctcaacct tgtcccggcg accgcgatcg ctgtggggcg gatagccctc
61     cctgcgggctg cgacgacgac gacgactgcg gtcctctgttc ctgtcaacct caggctgaac
121    atcatcacgg cgggtgctgat tctaggtgtg tcaacttgtgt tgacgctggt gtacaccctg
181    tggaaagcttc tcccgaggat ccgcagtggc gagctctcct tctcgaagtt cgagttcgac
241    tggcgtgcgg agctgctgaa ccagacgccg aagaaggaga aggcgcgccg cgcgacggag
301    aaggctcgcc gtgaggagga gatggcgctc gggtgcaacc gcgacaacga cgagggacgc
361    gtgcagtacg cccacacgca gccgcgggtg gaggtggggc agggcgacgc cgcggctgcc
421    agatcgcagc gcaagggaca gaggcacgtc gaggccgatg tgagcgttgc ggtgacggtg
481    ccccgcgagt ag
```

(The underlined nucleotides correspond to the sequences used to design the forward and reverse primers, respectively for insertion of the gene in the pGEX vector).

#### A.2 Coding sequence of the *L. mexicana A600.4* gene

```
1      atgccctcta tgctcaacct tgtcccggcg gtggagacga cgatgaccgc caccocgatg
61     tatgtcgagg tgaggggtgaa tgccgtgccg ttgatgatgg tctttggtgt ctcaactgtg
121    ctggcgctgg tgtacactct gtggaagctt ctcccagaga tccgcagtgg cgagctctcg
181    tctcgaataa cggaggccaa ctttcgtgcg gggctgctga accggaagct gaagagggag
241    aagggtgcgct cggaggatga ttcactctgcg gacatggtgt aa
```

#### A.3 Coding sequence of the *L. mexicana ΔN.A600.1* gene

```
1      atgccctcta tgctcaacct tgtcccggcg accgcgatcg ctgtggggcg gatagccctc
61     cctgcgggctg cgacgacgac gacgactgcg gtcctctgttc ctgtcaacct caggctgaac
121    atcatcacgg cgggtgctgat tctaggtgtg tcaacttgtgt tgacgctggt gtacaccctg
181    tggaaagcttc tcccgaggat ccgcagtggc gagctctcct tctcgaagtt cgagttcgac
241    tggcgtgcgg agctgctgaa ccagacgccg aagaaggaga aggcgcgccg cgcgacggag
301    aaggctcgcc gtgaggagga gatggcgctc gggtgcaacc gcgacaacga cgagggacgc
361    gtgcagtacg cccacacgca gccgcgggtg gaggtggggc agggcgacgc cgcggctgcc
421    agatcgcagc gcaagggaca gaggcacgtc gaggccgatg tgagcgttgc ggtgacggtg
481    ccccgcgagt ag
```

(The region in grey and italics corresponds to the sequence of the *A600.1* gene coding for the N-terminal portion of the protein that is predicted to contain the two transmembrane domains and not included in the *ΔN.A600.1* gene.)

**Appendix B Comparison of the enzymatic activities of *L. mexicana* WT and A600<sup>-/-</sup> amastigotes**

**B.1 NADH dehydrogenase activity of Complex I in amastigotes**

- in *L. mexicana* WT amastigotes

	<b>1</b>	<b>2</b>	<b>3</b>	<b>Mean</b>	<b>SD</b>
<b>Total activity (nmol/min/mg)</b>	14.7	25	19	<b>19.6</b>	5.2
<b>Rotenone- resistant activity (nmol/min/mg)</b>	14.7	8.8	19	<b>14.2</b>	5.1
<b>% of rotenone-resistant activity</b>	100%	35.2%	100%	<b>78.4%</b>	37%
<b>Rotenone-sensitive activity (nmol/min/mg)</b>	0	16.2	0	<b>5.4</b>	9.4
<b>% of rotenone inhibition</b>	0%	64.8%	0%	<b>21.6%</b>	37%

- in *L. mexicana* A600<sup>-/-</sup> amastigotes

	<b>1</b>	<b>2</b>	<b>3</b>	<b>Mean</b>	<b>SD</b>
<b>Total activity (nmol/min/mg)</b>	77.1	47.4	32.7	<b>52.4</b>	22.6
<b>Rotenone- resistant activity (nmol/min/mg)</b>	46.8	42.2	49.1	<b>46.0</b>	3.5
<b>% of rotenone-resistant activity</b>	60.7%	89.0%	100.0%	<b>83.2%</b>	20%
<b>Rotenone-sensitive activity (nmol/min/mg)</b>	30.3	5.2	0	<b>17.8</b>	17.8
<b>% of rotenone inhibition</b>	39.30%	11.0%	0.0%	<b>16.8%</b>	20%

**B.2 Succinate dehydrogenase activity of Complex II in amastigotes**

- in *L. mexicana* WT amastigotes

	<b>1</b>	<b>2</b>	<b>3</b>	<b>Mean</b>	<b>SD</b>
<b>Total activity (nmol/min/mg)</b>	178.5	162.1	147.8	<b>162.8</b>	15.4
<b>Malonate- resistant activity (nmol/min/mg)</b>	1.3	11.3	25.9	<b>12.8</b>	12.4
<b>% of malonate-resistant activity</b>	0.7%	7.0%	17.5%	<b>7.9%</b>	8%
<b>Malonate-sensitive activity (nmol/min/mg)</b>	177.2	150.8	121.9	<b>150.0</b>	27.7
<b>% of malonate inhibition</b>	99.3%	93.0%	81.7%	<b>92.1%</b>	9%

- in *L. mexicana* A600<sup>-/-</sup> amastigotes

	<b>1</b>	<b>2</b>	<b>3</b>	<b>Mean</b>	<b>SD</b>
<b>Total activity (nmol/min/mg)</b>	143.7	200	238.1	<b>193.9</b>	47.5
<b>Malonate- resistant activity (nmol/min/mg)</b>	27.4	37.2	52.9	<b>39.2</b>	12.9
<b>% of malonate-resistant activity</b>	17.8%	18.6%	22.2%	<b>20.2%</b>	2%
<b>Malonate-sensitive activity (nmol/min/mg)</b>	116.3	162.8	185.2	<b>154.8</b>	35.2
<b>% of malonate inhibition</b>	82.2%	81.4%	77.8%	<b>80.5%</b>	2%

### B.3 Cytochrome c reductase activity of Complex III in amastigotes

- in *L. mexicana* WT amastigotes

	<b>1</b>	<b>2</b>	<b>3</b>	<b>Mean</b>	<b>SD</b>
<b>Total activity (nmol/min/mg)</b>	5170.2	5174.3	5296.9	<b>5213.8</b>	72.0
<b>Antimycin- resistant activity (nmol/min/mg)</b>	287.2	55.6	278.8	<b>207.2</b>	131.4
<b>% of antimycin-resistant activity</b>	5.6%	1.1%	5.3%	<b>4%</b>	3%
<b>Antimycin-sensitive activity (nmol/min/mg)</b>	4883	5118.7	5018.1	<b>5006.6</b>	118.3
<b>% of antimycin inhibition</b>	94.4%	98.9%	94.7%	<b>96%</b>	3%

- in *L. mexicana* A600<sup>-/-</sup> amastigotes

	<b>1</b>	<b>2</b>	<b>3</b>	<b>Mean</b>	<b>SD</b>
<b>Total activity (nmol/min/mg)</b>	2973.7	3488.3	3141.3	<b>3201.1</b>	262.5
<b>Antimycin- resistant activity (nmol/min/mg)</b>	139.4	336.8	218.5	<b>231.6</b>	99.3
<b>% of antimycin-resistant activity</b>	4.7%	9.7%	7.0%	<b>7.1%</b>	3%
<b>Antimycin-sensitive activity (nmol/min/mg)</b>	2834.3	3151.5	2922.8	<b>2969.5</b>	163.7
<b>% of antimycin inhibition</b>	95.3%	90.3%	93.0%	<b>92.9%</b>	3%

#### B.4 Cytochrome c oxidase activity of Complex IV in amastigotes

- in *L. mexicana* WT amastigotes

	1	2	3	Mean	SD
<b>Total activity (nmol/min/mg)</b>	113.5	86.2	61.3	<b>87.0</b>	26.1
<b>KCN- resistant activity (nmol/min/mg)</b>	0	1.8	0	<b>0.6</b>	0.95
<b>% of KCN-resistant activity</b>	0%	2.1%	0.0%	<b>0.7%</b>	1%
<b>KCN-sensitive activity (nmol/min/mg)</b>	113.5	84.4	61.3	<b>86.4</b>	26.2
<b>% of KCN inhibition</b>	100%	97.9%	100%	<b>99.3%</b>	1%

- in *L. mexicana* A600<sup>-/-</sup> amastigotes

	1	2	3	Mean	SD
<b>Total activity (nmol/min/mg)</b>	24.4	32.5	51.2	<b>36.0</b>	13.7
<b>KCN- resistant activity (nmol/min/mg)</b>	0	0	2	<b>0.7</b>	1.2
<b>% of KCN-resistant activity</b>	0%	0%	3.9%	<b>1.3%</b>	2%
<b>KCN-sensitive activity (nmol/min/mg)</b>	24.4	32.5	49.2	<b>35.4</b>	12.6
<b>% of KCN inhibition</b>	100%	100%	96.1%	<b>98.7%</b>	2.3%

#### B.5 ATPase activity of Complex V in amastigotes

- in *L. mexicana* WT amastigotes

	1	2	3	Mean	SD
<b>Total activity (nmol/min/mg)</b>	119.1	114	117.8	<b>117.0</b>	2.7
<b>Oligomycin-resistant activity (nmol/min/mg)</b>	110.2	99.5	107	<b>105.6</b>	5.5
<b>% oligomycin inhibition</b>	7.5%	12.7%	9.2%	<b>9.8%</b>	2.7%
<b>Na azide resistant activity (nmol/min/mg)</b>	24	29	38.9	<b>30.6</b>	7.6
<b>% Na azide inhibition</b>	79.8%	74.6%	67.0%	<b>73.8%</b>	6.4%

- in *L. mexicana* A600<sup>-/-</sup> amastigotes

	<b>1</b>	<b>2</b>	<b>3</b>	<b>Mean</b>	<b>SD</b>
<b>Total activity (nmol/min/mg)</b>	121	116.4	103.8	<b>113.7</b>	8.9
<b>Oligomycin-resistant activity (nmol/min/mg)</b>	97.4	106.3	83.9	<b>95.9</b>	11.3
<b>% oligomycin inhibition</b>	19.5%	8.7%	19.2%	<b>15.8%</b>	6.2%
<b>Na azide resistant activity (nmol/min/mg)</b>	48.1	50.8	44.5	<b>47.80</b>	3.2
<b>% Na azide inhibition</b>	60.3%	56.4%	57.1%	<b>57.9%</b>	2.1%

## Appendix C Mass spectrometry results of the GST pull-down assays

### C.1 Mass spectrometry results from GST pull-down assay 1

Table C.1: List of proteins isolated from GST pull-down assay 1 with a heavy to light ratio above 1.2

Protein ID	Description	Sequence coverage (%)	# of Peptides	Ratio H/L
LmxM19.0720	conserved hypothetical protein	10.07	3	84.804
LmxM22.1460	i/6 autoantigen-like protein	4.41	1	<b>50.092</b>
	GST_A600	2.1	1	<b>20.15</b>
LmxM29.2980	glyceraldehyde 3-phosphate dehydrogenase, glycosomal	20.22	8	<b>15.013</b>
LmxM22.0730	conserved hypothetical protein	2.40	1	<b>8.794</b>
LmxM21.1780	putative 40S ribosomal protein S6	6.43	1	<b>8.292</b>
LmxM05.1040	stomatin-like protein	2.80	1	<b>6.733</b>
LmxM19.0390	putative 40S ribosomal protein S13	5.96	1	<b>6.528</b>
LmxM21.1555*	conserved hypothetical protein*	2.78	1	<b>5.986</b>
LmxM36.2020	chaperonin HSP60, mitochondrial precursor	4.24	2	<b>5.135</b>
LmxM25.1170	putative ATPase beta subunit	9.71	4	<b>3.389</b>
LmxM29.3310	conserved hypothetical protein	2.79	1	<b>3.279</b>
LmxM23.0080	conserved hypothetical protein	2.15	1	<b>3.228</b>
LmxM18.1370	putative heat shock protein	1.46	1	<b>3.120</b>
LmxM09.1340	histone H2B	14.95	2	<b>3.054</b>
LmxM14.1100	putative kinesin K39	3.74	1	<b>2.954</b>
LmxM05.0996	putative ATPase alpha subunit	3.32	2	<b>2.057</b>
LmxM21.1770	putative ATP synthase F1 subunit gamma protein	2.97	1	<b>2.041</b>
LmxM34.3340	putative 6-phosphogluconate dehydrogenase, decarboxylating	2.09	1	<b>1.936</b>
LmxM09.0100	calmodulin-like protein containing EF hand domain	9.28	4	<b>1.484</b>

Ratio H/L: ratio heavy to light

Protein ID: protein identity

\*LmxM21.1555: 71% sequence identity with *T. brucei* protein Tb10.70.7760, isolated as one of the F<sub>1</sub>F<sub>0</sub> ATPase complex (Complex V) subunits

## C.2 Mass spectrometry results from GST pull-down assay 2

Table C.2: List of proteins identified in GST pull-down assay 2 with a H/L ratio above 1.2

Protein ID	Protein name	Sequence coverage [%]	# of peptides	Ratio H/L
LmxM29.0350	putative kinesin	2.6	1	2.61
LmxM22.0990	hypothetical protein	3	2	2.22
LmxM31.1340	cleavage and polyadenylation specificity factor-like protein	2.7	2	2.14
LmxM36.0500	putative DNAJ domain protein	9.6	3	2.02
LmxM22.0180	hypothetical protein	17.4	3	2.01
LmxM27.1300	hypothetical protein	17.8	7	1.97
LmxM05.0390	protein kinase, putative	7.8	3	1.90
LmxM03.0270	hypothetical protein	28.5	4	1.84
LmxM18.0500	hypothetical protein	3.3	1	1.82
LmxM29.0120	alkyl dihydroxyacetonephosphate synthase	4.5	2	1.80
LmxM22.1540	alanyl-tRNA synthetase, putative	5.3	4	1.76
LmxM29.0060	hypothetical protein	12.5	2	1.75
LmxM34.1130 LmxM34.1160 LmxM34.1150 LmxM34.1140	oligosaccharyl transferase-like protein	8.9	5	1.71
LmxM33.2470 LmxM10.0070	ribosomal protein l35a, putative	5.6	1	1.70
LmxM24.2110	3-hydroxy-3-methylglutaryl-CoA synthase, putative (HMGS)	38.9	17	1.69
LmxM08_29.0110	hypothetical protein	0.6	2	1.67
LmxM19.0050 LmxM19.0030 LmxM17.1220	histone H2B	39.3	1	1.65
LmxM36.1690	hypothetical protein	9.4	1	1.64
LmxM21.1710	cytochrome c oxidase subunit VI, putative	21	3	1.63
LmxM01.0060	hypothetical protein	12.4	2	1.62
LmxM18.0670 LmxM18.0680	citrate synthase, putative	8.1	3	1.61

<b>Protein ID</b>	<b>Protein name</b>	<b>Sequence coverage [%]</b>	<b># of peptides</b>	<b>Ratio H/L</b>
LmxM34.1180	NADH-dependent fumarate reductase, putative	4.2	3	<b>1.61</b>
LmxM34.0370	ATP-dependent DEAD-box RNA helicase, putative	24.2	9	<b>1.61</b>
LmxM06.1100	hypothetical protein	8.9	2	<b>1.59</b>
LmxM29.3310	MORN repeat-containing protein 1 (MORN1)	24	8	<b>1.59</b>
LmxM27.0930	isovaleryl-coA dehydrogenase, putative	30.5	13	<b>1.52</b>
LmxM34.3860	T-complex protein 1, eta subunit, putative	8.9	4	<b>1.52</b>
LmxM06.0880	acyl-coenzyme a dehydrogenase, putative	26	7	<b>1.51</b>
LmxM26.1860	Present in the outer mitochondrial membrane proteome 2 (POMP2)	4.2	1	<b>1.51</b>
LmxM26.1540	hypothetical protein	12.1	4	<b>1.50</b>
LmxM09.0520	hypothetical protein	8.2	5	<b>1.49</b>
LmxM33.0610	enoyl-[acyl-carrier-protein] reductase, putative	9.5	2	<b>1.49</b>
LmxM19.9998 LmxM19.0200 LmxM19.9997	ADP,ATP carrier protein 1, mitochondrial precursor, putative	31.2	10	<b>1.49</b>
LmxM36.3570	signal recognition particle receptor like protein, putative	2.6	1	<b>1.47</b>
LmxM27.0300	methylmalonyl-coenzyme a mutase, putative	4.4	2	<b>1.46</b>
LmxM26.1040	hypothetical protein	6.2	2	<b>1.46</b>
LmxM33.4290	nucleolar protein family a, putative	5.2	2	<b>1.46</b>
LmxM33.3230	hypothetical protein	4.2	4	<b>1.45</b>
LmxM23.0080	hypothetical protein	3.3	2	<b>1.44</b>
LmxM05.0380	microtubule-associated protein, putative	54.2	4	<b>1.44</b>
LmxM14.1100 LmxM14.1110 LmxM14.1120	kinesin K39, putative	10.4	3	<b>1.42</b>
LmxM36.5150	hypothetical protein	5	2	<b>1.41</b>

<b>Protein ID</b>	<b>Protein name</b>	<b>Sequence coverage [%]</b>	<b># of peptides</b>	<b>Ratio H/L</b>
LmxM15.1010	glutamate dehydrogenase	30.4	30	<b>1.39</b>
LmxM36.0810	hypothetical protein	3.5	1	<b>1.39</b>
LmxM28.2730	hypothetical protein	13.9	6	<b>1.39</b>
LmxM30.2250	3,2-trans-enoyl-CoA isomerase, mitochondrial precursor, putative	14.3	2	<b>1.37</b>
LmxM28.2910	glutamate dehydrogenase, putative	13.1	3	<b>1.37</b>
LmxM17.0120	hypothetical protein	10.7	3	<b>1.36</b>
LmxM32.3210	beta prime cop protein, putative	3.4	2	<b>1.36</b>
LmxM08_29.1740 LmxM08_29.1730 LmxM08_29.1720	histone H2A, putative	18.2	1	<b>1.35</b>
LmxM29.1040	hypothetical protein	9.2	2	<b>1.35</b>
LmxM31.0450 LmxM19.0060	40S ribosomal protein S2	8	2	<b>1.34</b>
LmxM34.2200	putative RNA-binding protein	55.1	15	<b>1.34</b>
LmxM34.4430	mitochondrial phosphate transporter, putative	15.1	4	<b>1.34</b>
LmxM02.0650	hypothetical protein	15.3	2	<b>1.34</b>
LmxM29.0310	hypothetical protein	3	2	<b>1.33</b>
LmxM29.1510	p1/s1 nuclease	7.9	0	<b>1.33</b>
LmxM36.5930	hypothetical protein	11	2	<b>1.33</b>
LmxM30.0850	hypothetical protein	10.6	2	<b>1.33</b>
LmxM05.1050	hypothetical protein	3.8	2	<b>1.32</b>
LmxM27.0500	calpain-like cysteine peptidase, putative	0.9	4	<b>1.32</b>
LmxM35.2150	Hypothetical protein 82% ID: <i>L. panamensis</i> putative short chain dehydrogenase/reductase	10	3	<b>1.31</b>
LmxM34.9997 LmxM34.1900 LmxM34.1880 LmxM34.9996 LmxM34.9995	putative 60S ribosomal protein L5	9.8	3	<b>1.30</b>
LmxM24.0320	fumarate hydratase, putative	7.7	3	<b>1.29</b>

<b>Protein ID</b>	<b>Protein name</b>	<b>Sequence coverage [%]</b>	<b># of peptides</b>	<b>Ratio H/L</b>
LmxM22.0410	hypothetical protein, conserved	6.5	6	<b>1.29</b>
LmxM18.1300	hypothetical protein, conserved	7.1	2	<b>1.28</b>
LmxM02.0450	hypothetical protein, conserved	22.7	6	<b>1.27</b>
LmxM36.1430 LmxM33.0820 LmxM33.0840	translation elongation factor 1-beta, putative	12.5	2	<b>1.27</b>
LmxM16.0550	orotidine-5-phosphate decarboxylase/ototate phosphoribosyltransferase, putative	27.4	13	<b>1.26</b>
LmxM36.3890	hypothetical protein, conserved	22.3	4	<b>1.26</b>
LmxM06.1000	hypothetical protein, conserved	4.7	1	<b>1.26</b>
LmxM36.5100	hypothetical protein, conserved	9	4	<b>1.25</b>
LmxM26.2650	hypothetical protein, conserved	2.9	1	<b>1.25</b>
LmxM21.1563	choline dehydrogenase, like protein	7.7	2	<b>1.24</b>
LmxM10.0945	Protein of the outer mitochondrial membrane proteome 40 (ATOM12)	29.9	3	<b>1.24</b>
LmxM22.0050	hypothetical protein, conserved	11.7	4	<b>1.24</b>
LmxM07.0340	ATP-dependent DEAD/H RNA helicase, putative	10.4	5	<b>1.24</b>
LmxM19.1530	peptidylprolyl isomerase-like protein	10.6	3	<b>1.22</b>
LmxM32.2440	hypothetical protein, conserved	11.2	4	<b>1.22</b>
LmxM02.0460	Mitochondrial outer membrane protein porin, putative (VDAC)	18.6	6	<b>1.21</b>
LmxM34.1230	short chain dehydrogenase, putative	6.7	1	<b>1.20</b>
LmxM23.0950	cytosolic leucyl aminopeptidase	4.6	2	<b>1.20</b>
LmxM34.4020	Bem46-like serine peptidase	4.1	1	<b>1.20</b>
LmxM18.1380	pyruvate dehydrogenase E1 component alpha subunit, putative	44.2	18	<b>1.19</b>

### C.3 Mass spectrometry results GST pull-down assay 3

Table C.3: List of proteins identified in GST pull-down assay 3 with a H/L ratio above 1.2

Protein ID	Protein name	Sequence coverage (%)	# of peptides	Ratio H/L
LmxM32.2440	hypothetical protein 47% ID: kinesin K39 of <i>Strigomonas culicis</i>	21.9	11	3.35
LmxM04.0050	hypothetical protein	6.3	2	2.76
LmxM23.0080	hypothetical protein	41.1	17	2.51
LmxM34.5070	hypothetical protein	13.7	2	2.49
LmxM25.1710	putative pyruvate dehydrogenase E1 beta subunit	20.6	6	2.41
LmxM12.0060	ribonuclease mar1	9.4	2	2.34
LmxM33.2580	hypothetical protein	17.1	2	2.32
LmxM21.0550	dihydrolipoamide acetyltransferase precursor like protein (pyruvate dehydrogenase complex)	19.3	3	2.31
LmxM08.0860	hypothetical protein	15.9	2	2.29
LmxM05.0380	putative microtubule-associated protein, partial	57.4	8	2.24
LmxM19.1160	hypothetical protein	28.5	14	2.10
LmxM22.0050	hypothetical protein	10.9	4	1.93
LmxM22.0730	hypothetical protein	33.4	15	1.88
LmxM14.1440	hypothetical protein	2.9	3	1.84
LmxM22.1460	i/6 autoantigen-like protein	24	6	1.79
LmxM16.0520	hypothetical protein	4	1	1.76
LmxM21.1300	hypothetical protein	8.9	2	1.75
LmxM36.2660	dihydrolipoamide acetyltransferase precursor, putative (pyruvate dehydrogenase complex)	31.8	9	1.71
LmxM27.1220	hypothetical protein	17.8	7	1.67
LmxM26.0890 LmxM26.0880	putative 40S ribosomal protein S16	12.1	2	1.65
LmxM34.3720	hypothetical protein	8.4	3	1.63
LmxM29.3680	hypothetical protein	23.5	9	1.60
LmxM09.1340	histone H2B	54.2	3	1.60

<b>Protein ID</b>	<b>Protein name</b>	<b>Sequence coverage (%)</b>	<b># of peptides</b>	<b>Ratio H/L</b>
LmxM18.1380	putative pyruvate dehydrogenase E1 component alpha subunit (pyruvate dehydrogenase complex)	20.6	7	<b>1.57</b>
LmxM31.1770	hypothetical protein	10.3	3	<b>1.55</b>
LmxM27.1100	hypothetical protein	3.2	1	<b>1.52</b>
LmxM18.1370	putative heat shock protein	3.2	2	<b>1.48</b>
LmxM19.1060	hypothetical protein	8.5	6	<b>1.47</b>
LmxM28.2420	2-oxoglutarate dehydrogenase, E2 component, dihydrolipoamide succinyltransferase, putative	12.6	4	<b>1.46</b>
LmxM17.0410	hypothetical protein, conserved	3	2	<b>1.45</b>
LmxM04.1160	fructose-1,6-bisphosphatase, cytosolic, putative	16.2	5	<b>1.45</b>
LmxM29.3150	hypothetical protein	13.2	2	<b>1.45</b>
LmxM09.0100	calmodulin-like protein containing EF hand domain calcium-binding messenger protein	41.9	27	<b>1.43</b>
LmxM36.2020	chaperonin HSP60, mitochondrial precursor	31.3	3	<b>1.43</b>
LmxM21.0430	hypothetical protein	6	2	<b>1.40</b>
LmxM32.3150 LmxM19.0390	putative 40S ribosomal protein S13	23.8	4	<b>1.40</b>
LmxM29.3380	PAS-domain containing phosphoglycerate kinase, putative	2.1	2	<b>1.39</b>
LmxM05.0340	hypothetical protein	12.7	2	<b>1.38</b>
LmxM14.1330	hypothetical protein	8.8	3	<b>1.38</b>
LmxM04.0940	uncharacterized protein	6.1	2	<b>1.37</b>
LmxM08_29.1300	hypothetical protein	14.9	3	<b>1.35</b>
LmxM34.1130 LmxM34.1160 LmxM34.1150 LmxM34.1140	oligosaccharyl transferase-like protein	6.3	3	<b>1.34</b>
LmxM29.1510	p1/s1 nuclease	17.7	3	<b>1.34</b>
LmxM24.1440	hypothetical protein	4.5	1	<b>1.33</b>
LmxM28.2430	V-type proton ATPase subunit B, putative	4	2	<b>1.31</b>
LmxM07.0220	hypothetical protein	5.4	2	<b>1.29</b>

<b>Protein ID</b>	<b>Protein name</b>	<b>Sequence coverage (%)</b>	<b># of peptides</b>	<b>Ratio H/L</b>
LmxM25.1620	hypothetical protein	21.4	3	1.27
LmxM16.0550	putative Orotidine 5'phosphate decarboxylase-Orotate phosphoribosyltransferase.	12.5	5	1.27
LmxM36.3740 LmxM18.1400	60S ribosomal protein L34, putative	8.3	2	1.26
LmxM06.1000	hypothetical protein	4.7	1	1.25
LmxM34.5330	isopentenyl-diphosphate delta-isomerase, putative	25.8	8	1.25
LmxM19.1120	proteasome regulatory non-ATP-ase subunit 9, putative (RPN9)	3	1	1.24
LmxM10.0290	isocitrate dehydrogenase [NADP], mitochondrial precursor, putative	11.5	4	1.24
LmxM30.1000	hypothetical protein	1.7	1	1.24
LmxM26.1240	heat shock protein 70-related protein	6.6	3	1.23
LmxM22.1560 LmxM22.1520	40S ribosomal protein L14, putative	18.3	3	1.22
LmxM24.0320	fumarate hydratase, putative	7.7	3	1.22
LmxM26.1960	hypothetical protein	15.4	10	1.20